Zijun Cao · Yu Wang
Dianqing Li

Probabilistic Approaches for Geotechnical Site Characterization and Slope Stability Analysis

ZHEJIANG UNIVERSITY PRESS
浙江大学出版社

Springer

Probabilistic Approaches for Geotechnical Site Characterization and Slope Stability Analysis

Zijun Cao · Yu Wang · Dianqing Li

Probabilistic Approaches for Geotechnical Site Characterization and Slope Stability Analysis

ZHEJIANG UNIVERSITY PRESS
浙江大学出版社

Springer

Zijun Cao
State Key Laboratory of Water Resources and Hydropower Engineering Science
Wuhan University
Wuhan, Hubei
China

Dianqing Li
State Key Laboratory of Water Resources and Hydropower Engineering Science
Wuhan University
Wuhan, Hubei
China

Yu Wang
City University of Hong Kong
Hong Kong
China

ISBN 978-3-662-52912-6 ISBN 978-3-662-52914-0 (eBook)
DOI 10.1007/978-3-662-52914-0

Jointly published with Zhejiang University Press

The print edition is not for sale outside the Mainland of China (*Not for sale in Hong Kong SAR, Macau SAR, and Taiwan, and all countries, except the Mainland of China*).

Library of Congress Control Number: 2016944341

Printed on acid-free paper

This Springer imprint is published by Springer Nature
The registered company is Springer-Verlag GmbH Berlin Heidelberg

Preface

In the last few decades, reliability-based design (RBD) approaches/codes and probabilistic analysis methods, such as probabilistic slope stability analysis with Monte Carlo simulation (MCS), have been developed for geotechnical structures to deal rationally with various uncertainties (e.g., inherent spatial variability of soils and uncertainties arising during geotechnical site characterization) in geotechnical engineering. Applications of the RBD approaches/codes and probabilistic analysis methods in turn call for the needs of probabilistic site characterization, which describes probabilistically soil properties and underground stratigraphy based on both prior knowledge (i.e., site information available prior to the project) and project-specific test results. How to combine systematically prior knowledge and project-specific test results in a probabilistic manner, however, is a challenging task. This problem is further complicated by the inherent spatial variability of soils, uncertainties arising during site characterization and the fact that geotechnical site characterization generally only provides a limited number of project-specific test data.

This book focuses on probabilistic characterization of uncertainties in geotechnical properties and their propagation in slope stability analysis using MCS. Several probabilistic approaches are developed and presented in this book for probabilistic site characterization and reliability analysis of slope stability. These approaches effectively tackle the following unresolved issues in geotechnical risk and reliability, which hamper the applications of probabilistic analysis and design approach in geotechnical practice:

1. How to determine project-specific statistics and probability distributions of geotechnical properties based on both prior knowledge and a limited number of project-specific test data obtained during geotechnical site characterization? (Chaps. 3–6)
2. How to express engineering judgments in a quantitative and transparent manner during geotechnical site characterization? (Chap. 4)

3. How to delineate underground stratigraphy (including number and boundaries of soil layers) probabilistically using a limited number of site observation data? (Chap. 6)
4. How to efficiently incorporate various geotechnical-related uncertainties (e.g., uncertainties in geotechnical properties) into slope stability analysis using MCS? (Chap. 7)
5. How to shed light on the relative contributions of various uncertainties to slope failure probability based on MCS? (Chap. 8)
6. How to make MCS-based probabilistic analysis approach of slope stability accessible to geotechnical practitioners who are usually unfamiliar with probability theory and statistics? (Chaps. 7 and 8)

As far as the authors are aware, this is the first book to revisit geotechnical site characterization from a probabilistic point of view and provide rational tools to probabilistically characterize geotechnical properties and underground stratigraphy using limited information obtained from a specific site. This book also develops efficient MCS approaches for slope stability analysis and implements these approaches in a commonly available spreadsheet environment by a package of worksheets and functions/add-in in Excel. These approaches and the software packages are readily available to geotechnical practitioners and alleviate them from reliability computational algorithms. The authors gratefully acknowledge the financial support by the National Science Fund for Distinguished Young Scholars (Project No. 51225903), the National Natural Science Foundation of China (Project Nos. 51329901, 51409196, 51579190, 51528901), the National Program on Key Research Project (2016YFC0800208), and the Natural Science Foundation of Hubei Province of China (Project No. 2014CFA001).

The authors would like to express my heartfelt gratitude toward many colleagues who give invaluable advice and insightful comments on this book. We would also thank Miss Shuo Zheng for her assistance in word processing of the manuscript and Mr. Fuping Zhang, Mr. Jian He, Mr. Xin Liu, and Ms. Mi Tian for their help on the proofread of the manuscript. Last but not least, the authors' deep gratitude goes to their families for their loving consideration and continuous support to encourage us to finish this book.

Wuhan, China — Zijun Cao
Hong Kong, China — Yu Wang
Wuhan, China — Dianqing Li
March 2016

Contents

List of Principal Symbols and Abbreviations

Symbols

D	Depth
$Data$	Site observation data
E_{PMT}	Young's modulus measured by pressure meter test
E_u	Undrained Young's modulus
F_i	Intermediate failure events in Subset Simulation
$\underline{G}$	Covariance matrix of posterior distribution
H_0 and H_A	Null hypothesis and alternative hypothesis
$\underline{H}$	Hessian matrix
I	Integral term
K	Normalizing constant
$\underline{L}$	Upper triangular matrix obtained by Cholesky decomposition
M_k	The kth model class with k soil layers
M_R	Resisting moment
N	Number of samples in each level of subset simulation
N_L and N_{Lmax}	Number of soil layers and its maximum possible value
N_{SPT}	Standard penetration test N-value
Ock_{Mk}	Ockham factor
P_f	Probability of failure
$P(\cdot)$	Probability or probability density function
$P(\cdot\|\cdot)$	Conditional probability or conditional probability density function
$Prior$	Prior knowledge
$\underline{R}$	Correlation matrix
S_u	Undrained shear strength
T_{cr} and T_L	Thicknesses of a clay crust and lacustrine clay layer

$Var(M_R)$	Variance of resisting moment
X	Random variable
$X_{\max}$ and $X_{\min}$	Maximum and minimum of X
$\overline{X}$	Mean of X
$\underline{X}_d$	A set of random variables representing the design soil property
$\underline{X}_t$	A set of site observation data
Y	Critical response used in subset simulation
$\underline{Z}$	A standard Gaussian vector
Z_H	Hypothesis test statistic for slope failure analysis
a_s	Reference value in the equivalent lottery method
$f(\cdot)$	Mathematical representation of the design soil property
$f(\cdot\|\cdot)$	Proposal probability density function of a Markov Chain
f_{obj}	Objective function
fs	Critical value for defining failure criteria of slope stability
$f_T(\cdot)$ and $f_T^{-1}(\cdot)$	Transformation model and its inverse function
$\underline{h}_{N_L}$	Thickness vector
k and k^*	Number of soil layers and its most probable value
m	The highest subset simulation level
n_f	Number of failure samples generated in Monte Carlo simulation
n_{MC}	Number of samples generated in Monte Carlo simulation
n_{MCMC}	Number of samples generated in Markov Chain Monte Carlo simulation
n_m	Number of uncertain model parameters concerned
n_s	Number of standard penetration test data
n_X	Number of X samples
p	Reference probability in the equivalent lottery method
p_0	Conditional probability used in subset simulation
p_a	Atmospheric pressure
q	Normalized cone tip resistance
q_c	Cone tip resistance
r	Radius of a circular slip surface
r_a	Acceptance ratio
r_n	Correlation coefficient
$\underline{s}_n=[s_{\mu n}, s_{\sigma n}, s_{\lambda n}]$	Posterior standard deviations of model parameters
$s(D)$	Remaining fluctuating component
$t(D)$	Trend function
u	Random number falling within [0, 1]
w_X	Standard deviation of X
$\underline{w}_n=[w_{\mu n}, w_{\sigma n}, w_{\lambda n}]$	Prior standard deviations of model parameters
x	soil property
(x_c, y_c)	Coordinate of the center of a circular critical slip surface

x_d	Design soil property
x_t	Measured soil property
y_i	Intermediate threshold value for defining intermediate failure events
ΔD	Separate distance between two depths
Θ	Uncertain model parameters of random fields
Θ_{PN_L}	Uncertain model parameters of a general probability model
Φ	Standard Gaussian cumulative distribution function
Ω	Sample space
α	Significance level for hypothesis testing
β	Reliability index
γ	Unit weight
ε	Transformation uncertainty
θ	Uncertain system parameter
$\underline{\theta}_n$ and $\underline{\theta}_n^*$	Model parameters of the random field in the nth soil layer and their most probable value
$\overline{\theta}_n=[\overline{\mu}_n, \overline{\sigma}_n, \overline{\lambda}_n]$	Prior mean values of model parameters of the random field in the nth soil layer
$\underline{\theta}_{Pn}$	Model parameters of the general probability model in the nth soil layer
λ	Correlation length
λ_n and λ_n^*	Correlation length of the effective friction angle in the nth soil layer and its most probable value
μ and μ^*	Mean and its estimation
μ_0	Mean of unconditional samples
$\mu_{\max}$ and $\mu_{\min}$	Maximum and minimum of the mean
μ_N and μ_N^*	Mean of the logarithm of undrained Young's modulus and its estimation
μ_n and μ_n^*	Mean of the effective friction angle in the nth soil layer and its most probable value
ξ	The logarithm of the measured soil property
$\underline{\xi}$	A set of cone penetration test data
ρ_{ij}	Correlation coefficient
$\underline{\rho}$	Correlation matrix of uncertain variables
σ and σ^*	Standard deviation and its estimation
$\sigma_{\max}$ and $\sigma_{\min}$	Maximum and minimum of the standard deviation
σ_N and σ_N^*	Standard deviation of the logarithm of undrained Young's modulus and its estimation
σ_n and σ_n^*	Standard deviation of the effective friction angle in the nth soil layer and its most probable value
$\sigma_p^{'}$	Preconsolidation stress
σ_{S_u}	Standard deviation of undrained shear strength

$\sigma_s(D)$ and $\sigma_s(D)_N$	Standard deviations of a soil property and its logarithm
σ'_{vo}	Vertical effective stress
ϕ'	Effective friction angle

Abbreviations

CDF	Cumulative distribution function
CIUC	Consolidated isotropic undrained triaxial compression test
COV	Coefficient of variation
CPT	Cone penetration test
FEM	Finite element method
FHWA	Federal Highway Administration
FORM	First-order reliability method
FOSM	First-order second-moment method
FS	Factor of safety
JGS	Japanese Geotechnical Society
LRFD	Load and resistance factor design
MCMCS	Markov Chain Monte Carlo simulation
MCS	Monte Carlo simulation
MH algorithm	Metropolis–Hastings algorithm
MMH algorithm	Modified Metropolis–Hastings algorithm
MPV	The most probable values of model parameters
MRFD	Multiple resistance factor design
NBC	National Building Code
NGES	National Geotechnical Experimentation Site
PDF	Probability density function
PI	Plasticity index
PMT	Pressure meter test
RBD	Reliability-based design
SLS	Serviceability limit state
SPAF	Subjective probability assessment framework
SPT	Standard penetration test
TAMU	Texas A&M University
UC	Undrained compression test
ULS	Ultimate limit state
UU	Unconsolidated undrained triaxial test
VBA	Visual Basic for Application
VST	Vane shear test

Chapter 1
Introduction

1.1 Background

1.1.1 Uncertainties in Soil Properties

Geotechnical materials are natural materials, and their properties are affected by various factors during their formation process, such as properties of their parent materials, weathering and erosion processes, transportation agents, and conditions of sedimentation (e.g., Vanmarcke 1977; Jaksa 1995; Phoon and Kulhawy 1999a; Baecher and Christian 2003; Mitchell and Soga 2005). Properties of geotechnical materials, therefore, vary spatially, which is usually known as "inherent spatial variability" (e.g., Vanmarcke 1977, 1983). In addition to inherent spatial variability of soils, various uncertainties are also incorporated into the estimated soil properties during geotechnical site characterization (e.g., Christian et al. 1994; Kulhawy 1996; Phoon and Kulhawy 1999a), including measurement errors arising from imperfect test equipments and/or procedural–operator errors, statistical uncertainty resulted from insufficient number of tests, and transformation uncertainty associated with the transformation models that are used to interpret test results. The inherent spatial variability and uncertainties that arise during geotechnical site characterization affect the estimations of soil properties and underground stratigraphy. This subsequently influences the analysis and/or designs of geotechnical structures.

1.1.2 Probabilistic Analysis of Geotechnical Structures

The uncertainties (including inherent spatial variability of soils) in soil properties can be rationally incorporated into geotechnical analysis and/or designs using probability theory and statistics. In the context of probability theory and statistics, the performance of geotechnical structures is assessed probabilistically and is

Z. Cao et al., *Probabilistic Approaches for Geotechnical Site Characterization and Slope Stability Analysis*, DOI 10.1007/978-3-662-52914-0_1

frequently measured by reliability index, β, and probability of failure, P_f, which is defined as the probability of the performance requirements (e.g., requirements of ultimate limit state (ULS) and serviceability limit state (SLS)) not being satisfied.

In the last few decades, several probabilistic analysis methods have been developed to estimate the β and P_f of geotechnical structures, such as the first-order second-moment method (FOSM) (e.g., Tang et al. 1976; Christian et al. 1994; Hassan and Wolff 1999), first-order reliability method (FORM, also referred to as Hasofer-Lind method) (e.g., Low and Tang 1997; Low et al. 1998; Low 2003), and direct Monte Carlo simulation (MCS) method (e.g., El-Ramly et al. 2002; Griffiths and Fenton 2004; El-Ramly et al. 2005). These probabilistic analysis methods use probabilistic estimations (e.g., statistics and probability distributions) of soil properties and underground stratigraphy as input and return β and/or P_f of a pre-defined design of geotechnical structures as output.

Among these probabilistic analysis methods, the direct MCS method is gaining popularity in probabilistic analysis of geotechnical structures because of its robustness and conceptual simplicity. Consider, for example, using direct MCS method to estimate slope failure probability. Direct MCS method takes slope geometry, probabilistic estimations of soil properties and underground stratigraphy, and other necessary information as inputs and generates n_{MC} sets of random samples of uncertain system parameters from their respective prescribed probability distributions. Using a given deterministic model (e.g., limit equilibrium methods) of slope stability analysis and the n_{MC} sets of random samples, n_{MC} possible values of factor of safety (FS) are obtained. Then, statistical analysis is performed to estimate slope failure probability according to a predefined failure criterion (e.g., $FS < 1$). To ensure a desired level of the accuracy of failure probability P_f estimated from direct MCS, a rule-of-thumb criterion is commonly adopted that the number n_{MC} of direct MCS samples should be at least ten times greater than the reciprocal of the probability level of interest, i.e., $n_{MC} > 10/P_f$ (e.g., Robert and Casella 2004; Wang 2011; Wang et al. 2011). As the probability level of interest decreases, the required number of direct MCS samples increases rapidly. Direct MCS, therefore, suffers from a lack of efficiency and resolution at small probability levels that are generally of great interest to geotechnical practitioners (e.g., U.S. Army Corps of Engineers 1997). In addition, as pointed out by Baecher and Christian (2003), direct MCS does not offer insights into relative contributions of various uncertainties to the failure probability.

1.1.3 Reliability-Based Design of Geotechnical Structures

In contrast to probabilistic analysis of geotechnical structures, reliability-based design (RBD) aims to determine an optimal design of geotechnical structures (e.g., Wang 2011, Wang et al. 2011), which satisfies predefined performance requirements (e.g., target degrees of reliability defined by target reliability index or target failure probability). During the past two decades, several RBD codes have been

developed and implemented around the world, such as the Eurocode 7 (BSI 2010) in Europe, the load and resistance factor design (LRFD) or the multiple resistance factor design (MRFD) for foundations (Barker et al. 1991; Phoon et al. 1995; Phoon et al. 2003a, b; Paikowsky et al. 2004; Paikowsky et al. 2010) in the USA, the National Building Code (NBC) for foundations (Becker 1996) in Canada, and the Geocode 21 (i.e., JGS4001 (Japanese Geotechnical Society 2006; Honjo et al. 2010)) in Japan. These RBD codes use the probability theory to address various uncertainties in design practice, such as uncertainties in soil properties. A characteristic (or nominal) value of soil properties is used in the design codes, and it is typically defined as a prespecified percentile (e.g., mean or lower 5 % percentile) of the probability distribution of soil properties.

Note that both the probabilistic analysis methods (e.g., FOSM, FORM, and MCS) and RBD codes (e.g., Eurocode 7, LRFD, MRFD, NBC, and Geocode 21) require probabilistic estimations (e.g., statistics and probability distributions) of soil properties and underground stratigraphy as input. Therefore, applications of these probabilistic analysis methods and RBD codes in turn call for the needs of probabilistic site characterization, which interprets the site characterization results in a probabilistic manner and describes soil properties and underground stratigraphy probabilistically. Such probabilistic site characterization, however, has been a challenging task, as discussed in the next subsection.

1.1.4 Geotechnical Site Characterization

In general, geotechnical site characterization is a multi-step process that consists of desk study, site reconnaissance, in situ investigation, laboratory testing, interpretation of site observation data, and inferring soil properties and underground stratigraphy (Clayton et al. 1995; Mayne et al. 2002). Desk study and site reconnaissance provide prior knowledge about the site (i.e., site information available prior to the project, such as engineering experience and engineering judgments). After desk study and site reconnaissance, project-specific test results (i.e., site observation data) can be obtained from in situ investigation work (e.g., in situ boring and testing) and/or laboratory testing. Then, transformation models (e.g., empirical regressions) between the measured property and the design property are used to interpret site observation data (e.g., Kulhawy and Mayne 1990; Phoon and Kulhawy and Trautmann 1999; Mayne et al. 2002). Based on the interpretation outcomes of site observation data and prior knowledge, geotechnical engineers are responsible for estimating the soil properties and underground stratigraphy. Geotechnical site characterization, therefore, relies on both prior knowledge and site observation data (e.g., Clayton et al. 1995; Mayne et al. 2002; Wang et al. 2010). The prior knowledge and site observation data are not perfect information but are associated with uncertainties to some degree (e.g., Baecher 1983; Christian

et al. 1994; Kulhawy 1996; Vick 2002; Baecher and Christian 2003), such as inherent spatial variability of soils, statistical uncertainty, measurement errors, transformation uncertainty associated with transformation models, and uncertainties of engineers' expertise.

Probability theory and statistics have been applied to characterize these uncertainties (e.g., Lumb 1966; Vanmarcke 1977, 1983; Baecher 1983; Jaksa 1995; Kulhawy and Trautmann 1996; Phoon and Kulhawy 1999a, b; Vick 2002). How these uncertainties propagate during different stages of geotechnical site characterization, however, has not been explicitly explored. This poses a challenge in dealing rationally with the uncertainties in geotechnical site characterization, including inherent spatial variability, statistical uncertainty, measurement errors, and transformation uncertainty. In addition, it remains a challenging task for geotechnical engineers to integrate systematically the prior knowledge and site observation data in a probabilistic manner. This problem is further complicated by the fact that only a limited number of project-specific test results are obtained during geotechnical site characterization. The number of project-specific test results is generally too sparse to generate meaningful statistics (e.g., mean, standard deviation, and the other high-order statistical moments) and probability distributions of soil properties for probabilistic analysis and/or designs of geotechnical structures.

1.2 Objectives

This book addresses the challenges in probabilistic site characterization and probabilistic slope stability analysis with MCS. A probabilistic framework is first developed for geotechnical site characterization, which integrates systematically prior knowledge and project-specific test results to estimate probabilistically soil properties and underground stratigraphy. The probabilistic framework addresses directly and explicitly the inherent spatial variability of soils and accounts rationally for various uncertainties that arise during geotechnical site characterization. These uncertainties (including inherent spatial variability of soils) are then incorporated into slope stability analysis by MCS. An advanced MCS method called "subset simulation" (Au and Beck 2001, 2003) is applied to improve the efficiency and resolution of MCS-based probabilistic slope stability analysis at relatively small probability levels. With the aid of improved efficiency, effects of inherent spatial variability of soil properties and critical slip surface uncertainty on slope failure probability are explored. In addition, the relative contributions of various uncertainties to slope failure probability are assessed using failure samples generated in MCS. The detailed objectives of this book are summarized in the following subsections.

1.2.1 Uncertainty Propagation During Geotechnical Site Characterization

This book starts with revisiting the procedure of geotechnical site characterization from an uncertainty propagation point of view. The propagation of inherent spatial variability of soils, statistical uncertainty, measurement errors, and transformation uncertainty is explored and depicted explicitly during different stages of geotechnical site characterization.

1.2.2 Bayesian Framework for Geotechnical Site Characterization

With an improved understanding of uncertainty propagation during geotechnical site characterization, a Bayesian framework is developed that integrates systematically prior knowledge and project-specific test results for probabilistic characterization of soil properties and underground stratigraphy (i.e., the number and boundaries of soil layers). The Bayesian framework is generally and equally applicable for different types of prior knowledge and different numbers of site observation data. It addresses directly and explicitly the inherent spatial variability of soils and accounts rationally for various uncertainties (i.e., statistical uncertainty, measurement errors, and transformation uncertainty) that arise during geotechnical site characterization.

1.2.3 Prior Knowledge and Prior Distribution

Under the Bayesian framework, the information provided by prior knowledge is quantitatively reflected by prior distribution in a probabilistic manner. When only a typical range of the soil parameter concerned is available as prior knowledge, a uniform distribution that covers the typical range can be taken as the prior distribution of the soil parameter in the Bayesian framework. As prior knowledge improves, a more sophisticated and informative prior distribution can be estimated from the prior knowledge.

Based on a stage cognitive model of engineers' cognitive process, a subjective probability assessment approach is developed to estimate prior distribution from prior knowledge. The subjective probability assessment approach assists engineers in utilizing the prior knowledge in a relatively rational way and expressing quantitatively their engineering judgments in a probabilistic manner. The prior distribution obtained from the subjective probability assessment approach quantifies properly information provided by the prior knowledge and is readily used in the Bayesian framework.

1.2.4 Probabilistic Site Characterization Using Limited Site Observation Data

The Bayesian framework developed in this book is equally applicable for different numbers of site observation data. When project-specific tests (e.g., standard penetration tests (SPTs)) only provide sparse data, the Bayesian framework is further developed as an equivalent sample approach that generates a large number of equivalent samples of the soil property concerned for its probabilistic characterization using both prior knowledge and project-specific test results. The proposed probabilistic approach takes advantage of prior knowledge in a rational way and integrates systematically the prior knowledge and site observation data under the Bayesian framework. It effectively tackles the difficulty in generating meaningful statistics and probability distributions from the usually limited number of site observation data obtained during geotechnical site characterization and provides proper probabilistic characterization of the soil property for probabilistic analysis and/or designs in geotechnical engineering practice.

1.2.5 Probabilistic Site Characterization Using a Large Number of Site Observation Data

When a large number of site observation data can be obtained directly from project-specific tests (e.g., near-continuous measurements during a cone penetration test (CPT)), the inherent spatial variability of soil properties can be explicitly modeled using random field theory. In such a case, a Bayesian approach is developed for probabilistic site characterization using the Bayesian framework proposed in this book together with the random field theory. The proposed Bayesian approach combines probabilistically prior knowledge and site observation data under the Bayesian framework and addresses directly and explicitly the inherent spatial variability of the soil property concerned using the random field theory. It identifies properly the most probable number and boundaries of statistically homogenous soil layers and estimates probabilistically the soil property of interest in each soil layer simultaneously.

1.2.6 Probabilistic Slope Stability Analysis Using Subset Simulation

Inherent spatial variability of soils and various uncertainties that arise during geotechnical site characterization can be properly incorporated into probabilistic slope stability analysis, using MCS. A MCS-based probabilistic slope stability analysis approach is developed that implements subset simulation in a commonly

available spreadsheet environment by a package of worksheets and functions/Add-In in Excel with the aid of Visual Basic for Application (VBA). The Excel spreadsheet software package decouples deliberately the worksheets and functions/Add-In for deterministic slope stability analysis and those for reliability analysis (e.g., uncertainty modeling worksheets and subset simulation Add-In), so that the reliability analysis can proceed as an extension of deterministic analysis in a non-intrusive manner. This allows deterministic analysis of slope stability and reliability analysis to be performed separately by personnel with different expertise and in a parallel fashion. The proposed MCS-based probabilistic slope stability analysis approach improves the efficiency and the resolution at relatively small probability levels. With the aid of improved efficiency, effects of the inherent spatial variability of soil properties and the critical slip surface uncertainty on slope failure probability are explored.

1.2.7 Probabilistic Failure Analysis of Slope Stability

Based on the failure samples generated in MCS, a probabilistic failure analysis approach is developed to assess the relative contributions of various uncertainties to slope failure probability. Subset simulation is, again, employed to improve efficiency of generating failure samples in MCS and resolution of calculating slope failure probability at small failure probability levels. The proposed probabilistic failure analysis approach prioritizes and quantifies the effects of various uncertainties on slope failure probability properly, and it gives results equivalent to those from sensitivity studies on uncertain system parameters and, hence, saves additional computational time and efforts for sensitivity studies.

1.3 Layout of the Book

This book is comprised of nine chapters. In this chapter, the research background and objectives have been presented. Chapter 2 reviews the previous studies on geotechnical site characterization, uncertainties in soil properties, Bayesian approach, and probabilistic slope stability analysis, and summarizes in situ and laboratory test results of a US National Geotechnical Experimentation Site (NGES) at Texas A&M University reported in the literature.

Chapter 3 revisits the procedure of geotechnical site characterization from an uncertainty propagation point of view and develops a Bayesian framework for geotechnical site characterization. Then, Chap. 4 develops a subjective probability assessment approach to estimate the prior distribution from prior knowledge.

Chapter 5 proposes an equivalent sample approach that generates a large number of equivalent samples of the soil property concerned for its probabilistic characterization, in which prior knowledge and limited project-specific test results (e.g.,

SPT results) are integrated systematically under the Bayesian framework proposed in Chap. 3. Using the equivalent sample approach, effects of the number of site observation data and different types of prior knowledge on probabilistic characterization of soil properties are explored.

Chapter 6 develops a Bayesian approach that utilizes both prior knowledge and a relatively large number of project-specific test results (e.g., CPT results) to identify the most probable number and boundaries of statistically homogenous soil layers and to characterize probabilistically the soil property in each layer simultaneously. The Bayesian framework proposed in Chap. 3 is applied again in Chap. 6 to integrate probabilistically prior knowledge and project-specific test results. Using the Bayesian approach, effects of confidence levels of prior knowledge on identification of statistically homogenous soil layers and probabilistic characterization of soil properties are explored.

Chapter 7 develops a MCS-based probabilistic slope stability analysis approach that implements subset simulation in a commonly available spreadsheet environment for improving the efficiency and the resolution at relatively small probability levels. With the aid of improved efficiency, the probabilistic slope stability analysis approach is used to explore the effects of the inherent spatial variability of soil properties and the critical slip surface uncertainty on slope failure probability. Then, Chap. 8 proposes a probabilistic failure analysis approach that makes use of failure samples generated in MCS and analyzes these failure samples to assess the relative contributions of various uncertainties to slope failure probability. Finally, Chap. 9 summarizes the study presented in this book and major conclusions.

References

Au, S.K., and J.L. Beck. 2001. Estimation of small failure probabilities in high dimensions by subset simulation. *Probabilistic Engineering Mechanics* 16(4): 263–277.

Au, S.K., and J.L. Beck. 2003. Subset simulation and its applications to seismic risk based on dynamic analysis. *Journal of Engineering Mechanics* 129(8): 1–17.

Baecher, G.B. 1983. Professional judgment and prior probabilities in engineering risk assessment. In *Proceedings of Fourth International Conference on Application of Statistics and Probability in Soil and Structural Engineering*, 635–650. Universita di Firenze (Italy), Pitagora Editrice.

Baecher, G.B., and J.T. Christian. 2003. *Reliability and statistics in geotechnical engineering*, 605 pp. Hoboken, New Jersey: Wiley.

Barker, R.M., J.M. Duncan, K.B. Rojiani, P.S.K. Ooi, C.K. Tan, and S.G. Kim. 1991. *Manuals for the design of bridge foundations, National Cooperative Highway Research Program (NCHRP) Report 343*. Washington, D.C.: Transportation Research Board, National Research Council.

Becker, D.E. 1996. Limit state design for foundations—part II: development for national building code of Canada. *Canadian Geotechnical Journal* 33(6): 984–1007.

BSI (2010). Eurocode 7: Geotechnical Design—Part 1: General Rules.

Christian, J.T., C.C. Ladd, and G.B. Baecher. 1994. Reliability applied to slope stability analysis. *Journal of Geotechnical Engineering* 120(12): 2180–2207.

Clayton, C.R.I., M.C. Matthews, and N.E. Simons. 1995. *Site investigation*. Cambridge, Mass, USA: Blackwell Science.

El-Ramly, H., N.R. Morgenstern, and D.M. Cruden. 2002. Probabilistic slope stability analysis for practice. *Canadian Geotechnical Journal* 39: 665–683.

El-Ramly, H., N.R. Morgenstern, and D.M. Cruden. 2005. Probabilistic assessment of stability of a cut slope in residual soil. *Geotechnique* 55(1): 77–84.

Griffiths, D.V., and G.A. Fenton. 2004. Probabilistic slope stability analysis by finite elements. *Journal of Geotechnical and Geoenvironmental Engineering* 130(5): 507–518.

Hassan, A.M., and T.F. Wolff. 1999. Search algorithm for minimum reliability index of earth slopes. *Journal of Geotechnical and Geoenvironmental Engineering* 125(4): 301–308.

Honjo, Y., Y. Kikuchi, and M. Shirato. 2010. Development of the design codes grounded on the performance-based design concept in Japan. *Soils and Foundations* 50(6): 983–1000.

Jaksa, M.B. 1995. *The Influence of Spatial Variability on the Geotechnical Design Properties of a Stiff, Overconsolidated Clay*. Ph.D. thesis of the University of Adelaide.

Japanese Geotechnical Society. 2006. *Principles for Foundation Designs Grounded on a Performance-based Design Concept*, JGS 4001–2004.

Kulhawy, F.H. and P.W. Mayne. 1990. *Manual on estimating soil properties for foundation design*, Report EL 6800, 306 pp. Palo Alto: Electric Power Research Inst.

Kulhawy, F.H. 1996. From Casagrande's 'Calculated Risk' to reliability-based design in foundation engineering. *Civil Engineering Practice* 11(2): 43–56.

Kulhawy, F.H. and C.H. Trautmann. 1996. Estimation of in-situ test uncertainty. In *Uncertainty in the Geologic Environment: From theory to practice*, vol. 58(I), 269–286 pp. Geotechnical Special Publication.

Low, B.K. 2003. Practical probabilistic slope stability analysis. In *Proceeding of 12th Panamerican Conference on Soil Mechanics and Geotechnical Engineering and 39th U.S. Rock Mechanics Symposium,* 2777–2784. Cambridge, Massachusetts: M.I.T., Verlag Gluckauf Gmbh Essen, 2003.

Low, B.K., R.B. Gilbert, and S.G. Wright. 1998. Slope reliability analysis using generalized method of slices. *Journal of Geotechnical and Geoenvironmental Engineering* 124(4): 350–362.

Low, B.K., and W.H. Tang. 1997. Reliability analysis of reinforced embankments on soft ground. *Canadian Geotechnical Journal* 34(5): 672–685.

Lumb, P. 1966. The variability of natural soils. *Canadian Geotehcnial Journal* 3(2): 74–97.

Mayne, P.W., B.R. Christopher, and De J. Jong. 2002. *Subsurface investigations–geotechnical site characterization*, No. FHWA NHI-01-031. Washington D.C.: Federal Highway Administration, U.S. Department of Transportation.

Mitchell, J.K., and K. Soga. 2005. *Fundamentals of soil behavior*. Hoboken, New Jersey: Wiley.

Paikowsky, S.G., B. Birgisson, M. MvVay, T. Nguyen, C. Kuo, G. Baecher, B. Ayyub, K. Stenersen, K. O'Malley, L. Chernauskas, and M. O'Neill. 2004. *Load and resistance factor design (LRFD) for deep foundations, national cooperative highway research program (NCHRP) Report 507*. Washington, D.C.: Transportation Research Board National Research Council.

Paikowsky, S.G., M.C. Canniff, K. Lesny, A. Kisse, S. Amatya, and R. Muganga. 2010. *LRFD design and construction of shallow foundations for highway bridge structures, NCHRP Report 651*. Washington, DC: Transportation Research Board.

Phoon, K.K., and F.H. Kulhawy. 1999a. Characterization of geotechnical variability. *Canadian Geotechnical Journal* 36(4): 612–624.

Phoon, K.K., and F.H. Kulhawy. 1999b. Evaluation of geotechnical property variability. *Canadian Geotechnical Journal* 36(4): 625–639.

Phoon, K.K., F.H. Kulhawy, and M.D. Grigoriu. 1995. *Reliability-based design of foundations for transmission line structures, Report TR-105000*. Palo Alto: Electric Power Research Institute.

Phoon, K.K., F.H. Kulhawy, and M.D. Grigoriu. 2003a. Development of a reliability-based design framework for transmission line structure foundations. *Journal of Geotechnical and Geoenvironmental Engineering* 129(9): 798–806.

Phoon, K.K., F.H. Kulhawy, and M.D. Grigoriu. 2003b. Multiple resistance factor design for shallow transmission line structure foundations. *Journal of Geotechnical and Geoenvironmental Engineering* 129(9): 807–818.

Robert, C., and G. Casella. 2004. *Monte carlo statistical methods*. Springer.

Tang, W.H., M.S. Yucemen, and A.H.S. Ang. 1976. Probability based short-term design of slope. *Canadian Geotechnical Journal* 13: 201–215.

U.S. Army Corps of Engineers. 1997. Engineering and design: introduction to probability and reliability methods for use in geotechnical engineering. *Engineer technical letter 1110-2-547*. Washington, DC: Department of the Army.

Vanmarcke, E.H. 1977. Probabilistic modeling of soil profiles. *Journal of Geotechnical Engineering* 103(11): 1127–1246.

Vanmarcke, E.H. 1983. *Random fields: analysis and synthesis*. Cambridge: MIT Press.

Vick, S.G. 2002. *Degrees of belief: Subjective probability and engineering judgment*. Reston, Virginia: ASCE Press.

Wang, Y. 2011. Reliability-based design of spread foundations by Monte Carlo simulations. *Geotechnique* 61(8): 677–685.

Wang, Y., S.K. Au, and F.H. Kulhawy. 2011. Expanded reliability-based design approach for drilled shafts. *Journal of Geotechnical and Geoenvironmental Engineering* 137(2): 140–149.

Wang, Y., S.K. Au, and Z. Cao. 2010. Bayesian approach for probabilistic characterization of sand friction angles. *Engineering Geology* 114(3–4): 354–363.

Chapter 2
Literature Review

2.1 Geotechnical Site Characterization

Geotechnical site characterization aims to delineate underground stratigraphy (including the number and thicknesses or boundaries of soil layers) and to estimate soil properties for geotechnical analysis and/or designs. As shown in Fig. 2.1, it is a multi-step process that can be divided into six stages: desk study, site reconnaissance, in situ investigation, laboratory testing, interpretation of observation data, and inferring soil properties and underground stratigraphy, as discussed in the following four subsections.

2.1.1 Desk Study and Site Reconnaissance

Geotechnical site characterization often starts with desk study to collect the existing information about the specific site, including geological information, geotechnical problems and properties, site topography, groundwater conditions, meteorological conditions, existing construction and services, and previous land use (Clayton et al. 1995; Mayne et al. 2002). The existing information can be obtained from various useful sources, as shown in Table 2.1.

Geological information (e.g., geological history) is available from existing geological records (e.g., geological maps, reports, and publications), regional guides (e.g., Geotechnical Engineering Office 2000 for Hong Kong), air photographs, soil survey maps and records, textbooks, etc. The information of geotechnical problems and parameters (e.g., records of adverse ground conditions, soil classification and properties, and stratigraphy) can be collected from existing geotechnical reports (e.g., Kulhawy and Mayne 1990), peer-reviewed academic journals (e.g., geotechnical journals, engineering geology journals, and civil engineering journals), and previous ground investigation reports at or near the site.

Z. Cao et al., *Probabilistic Approaches for Geotechnical Site Characterization and Slope Stability Analysis*, DOI 10.1007/978-3-662-52914-0_2

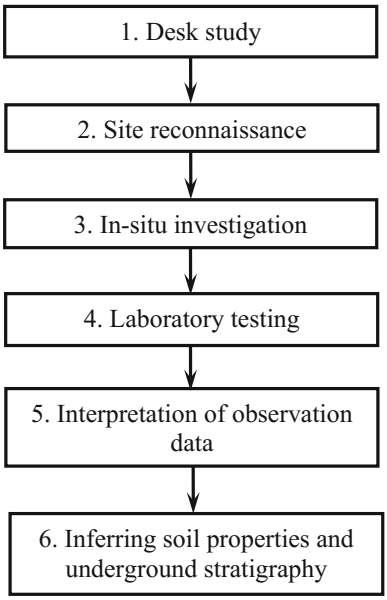

Fig. 2.1 Procedure of geotechnical site characterization (after Clayton et al. 1995; Mayne et al. 2002)

Information on site topography can be gathered from topographical maps and stereo air photographs. Well records, previous ground investigation reports, topographical maps, and air photographs provide information about groundwater conditions of the site (e.g., the groundwater level). Meteorological records provide information on meteorological conditions. Furthermore, information on existing construction and services and previous land use can be collected from topographical maps, air photographs, mining records, etc.

In addition to these sources of existing information, expertise of engineers (i.e., the domain knowledge of engineers, such as knowledge on geology and geotechnical engineering and local experience) also provides useful information for geotechnical site characterization. It is an integration of acquired information (including knowledge from education, information from professional training, and experience from deliberate practice) and engineers' comprehension (Vick 2002). Engineers' expertise is internally organized in knowledge patterns, each of which represents domain knowledge of a certain field or aspect (Vick 2002). The expertise patterns are internally formed when a person grows from an amateur (e.g., student) into a qualified engineer.

After desk study, site reconnaissance is carried out to confirm and supplement the information that is previously collected during desk study. Furthermore, the accesses and work conditions of the site are evaluated at the stage of site reconnaissance.

Table 2.1 Summary of existing information (after Clayton et al. 1995)

Type	Source
Geology	Geological maps
	Geological reports
	Geological publications
	Regional guides
	Air photographs
	Soil survey maps and records
Geotechnical problems and properties	Geotechnical reports
	Academic journals (e.g., geotechnical journals, engineering geology journals, and civil engineering journals)
	Previous ground investigation reports
Site topography	Topographical maps
	Stereo air photographs
Groundwater conditions	Topographical maps
	Air photographs
	Well records
	Previous ground investigation reports
Meteorological conditions	Meteorological records
Existing construction and services	Topographical maps
	Plans held by utilities
	Mining records
	Construction press
Previous land use	Out-of-print topographical maps
	Out-of-print geological maps
	Air photographs
	Airborne remote sensing
	Archaeological society records
	Mining records

2.1.2 In Situ Investigation

In situ investigation work generally includes drilling and sampling, in situ testing, and groundwater investigation (Clayton et al. 1995; Mayne et al. 2002). Herein, four in situ tests are reviewed, including standard penetration test (SPT), cone penetration test (CPT), pressuremeter test (PMT), and vane shear test (VST).

SPT consists of driving a standard thick-walled sampler into ground at the bottom of a borehole through repeated blows of a standard hammer and measuring the number (i.e., SPT *N*-value) of blow counts to advance the sampler to a vertical distance of 300 mm after an initial seating drive of 150 mm (Clayton 1995; Mayne et al. 2002). SPT provides soil samples for soil classification and laboratory tests. It is relatively simple to perform and is suitable for many types of soils. The results

(SPT *N*-values) provided by SPT are, however, highly operator-dependent and are highly variable (e.g., Kulhawy and Trautmann 1996; Mayne et al. 2002).

CPT involves pushing a cylindrical steel probe into the ground at a constant rate and measuring the resistance to the penetration (Lunne 1997; Mayne et al. 2002). CPT generally provides three measurements: cone tip resistance, sleeve friction, and pore water pressure (e.g., piezocone test). During the past several decades, CPT has gained popularity around the world because it is fast and largely operator-independent and provides near-continuous measurements (e.g., Robertson and Campanella 1983a, b; Robertson 1990; Mayne et al. 2002; Phoon et al. 2003; Robertson 2009). However, CPT is not suitable for gravel and boulder deposits and does not allow retrieval of soil samples (e.g., Mayne et al. 2002).

PMT expands a long cylindrical probe radially into surrounding ground to measure the amount of volume of fluid and pressure used to inflate the probe (Mair and Wood 1987; Briaud 1992; Mayne et al. 2002). The measurements subsequently provide the relationship between the pressure and the deformation of soils. PMT has a strong theoretical background and provides a complete stress–strain curve (Mair and Wood 1987; Briaud 1992; Wang and O'Rourke 2007). The procedure of PMT is, however, relatively complicated, and it is quite time-consuming and expensive (Mayne et al. 2002).

VST consists of inserting a four-bladed vane into clay and rotating the device about the vertical axis by applying a torque (Mayne et al. 2002). The measured peak and residual values of the torque are used to calculate undrained shear strength and in situ sensitivity of the clay. The procedure of VST is relatively simple. VST provides a convenient way to evaluate the undrained shear strength for stability analysis of embankment, footing, and excavation in soft clay (Bjerrum 1973; Mesri 1989; Mayne et al. 2002). The undrained shear strength measured by VST, however, needs to be corrected by multiplying it with an empirical correction factor before it is used in calculation (Bjerrum 1973). In addition, application of VST is limited to soft or stiff clay, and the results from VST might be affected by sand lens and seams (Mayne et al. 2002).

2.1.3 Laboratory Testing

After in situ investigation work, soil samples are brought back to laboratory for further testing. The laboratory tests include measuring index properties (e.g., moisture content, specific gravity, unit weight, particle size distribution, Atterberg limits, and moisture–density relationship), strength and stiffness tests (e.g., unconfined compression test, direct shear test, and triaxial tests), permeability tests (e.g., constant head test and falling head test), and consolidation tests (e.g., oedometer test) (Clayton et al. 1995; Mayne et al. 2002). The laboratory tests provide measurements of index properties (e.g., water content, liquid limit, plastic limit, and shrinkage limit), strength and stiffness parameters (e.g., undrained shear strength, effective friction angle, Young's modulus, and shear modulus), coefficient

of permeability, coefficient of compressibility, and preconsolidation stress. Laboratory tests generally result in more accurate measurements than those obtained from in situ tests, but they are usually more time-consuming and expensive than in situ tests (e.g., Mayne et al. 2002).

2.1.4 *Interpretation of Observation Data and Inferring the Site Subsurface Conditions*

In situ and/or laboratory test measurements (i.e., measured property) might not be the soil properties that can be directly used in geotechnical analysis and/or designs (i.e., design property). The design property can be calculated from direct measurements by transformation models (including empirical correlations and/or theoretical relationships) between the measured property and the design property. Many transformation models between geotechnical properties are available in the geotechnical literature (e.g., Kulhawy and Mayne 1990; Phoon and Kulhawy 1999b). For example, Tables 2.2 and 2.3 summarize the availability of transformation models for clays and sands (Kulhawy and Mayne 1990; Phoon and Kulhawy 1999b), respectively.

For clays, both in situ (including SPT, CPT, PMT, and VST tests) and laboratory test results can be used to estimate soil properties on soil classification, consistency, in situ stress state (e.g., preconsolidation stress, overconsolidation ratio, and coefficient of horizontal soil stress), strength (e.g., undrained shear strength), and deformability (e.g., Young's modulus, constrained modulus, and coefficient of consolidation). In addition, laboratory tests of clays also provide measurements to evaluate unit weight, effective friction angle, Poisson's ratio, compression index, coefficient of secondary compression, and coefficient of permeability.

For sands, in situ (including SPT, CPT, and PMT tests) and/or laboratory test results can be used to estimate soil properties on soil classification, in situ stress state (e.g., coefficient of horizontal soil stress), strength (e.g., effective friction angle), deformability (e.g., Poisson's ratio, Young's modulus, compression index, constrained modulus, and subgrade modulus), permeability (e.g., coefficient of permeability), and liquefaction resistance (e.g., cyclic stress ratio). Several transformation models that will be used in this book are given in Appendix 2.1.

Based on the information available prior to the project (including existing information collected from various sources and the expertise of engineers), site observation data obtained from in situ and laboratory tests, and corresponding transformation models, geotechnical engineers estimate the site ground conditions (including soil properties and underground stratigraphy) for geotechnical analysis and/or designs. Finally, geotechnical engineers are responsible for producing a geotechnical site characterization report that records the information about the site and for providing some technical suggestions for geotechnical designs (Mayne et al. 2002).

Table 2.2 Summary of availability of transformation models for clays provided by Kulhawy and Mayne (1990) (after Phoon and Kulhawy 1999b)

Property category	Soil property	Laboratory or theory correlation	In situ test correlation			
			SPT	CPT[c]	PMT	VST
Basic characterization	Classification	✓[a]	×[b]	✓	×	×
	Unit weight	✓	×	×	×	×
	Consistency	×	✓	✓	×	×
In situ stress state	Preconsolidation stress	✓	✓	✓	✓	✓
	Overconsolidation ratio	✓	✓	✓	×	✓
	Coefficient of horizontal soil stress	✓	✓	✓	✓	×
Strength	Effective friction angle	✓	×	×	×	×
	Undrained shear strength	✓	✓	✓	✓	✓
Deformability	Poisson's ratio	✓	×	×	×	×
	Young's modulus	✓	×	×	✓	×
	Compression index	✓	×	×	×	×
	Constrained modulus	✓	✓	✓	×	×
	Coefficient of consolidation	✓	×	✓	×	×
	Coefficient of secondary compression	✓	×	×	×	×
Permeability	Coefficient of permeability	✓	×	×	×	×

[a]✓ = available
[b]× = unavailable
[c]Including piezocone test

2.1.5 Challenges in Geotechnical Site Characterization

Geotechnical site characterization relies on both the information available prior to the project (including the existing information collected from various sources and engineers' expertise) and site observation data (e.g., in situ and laboratory test results). It is a challenging task for geotechnical engineers to integrate systematically and rationally the information from the two sources (i.e., information available prior to the project and site observation data). This problem is further complicated by the fact that only a small portion of geotechnical materials is tested and the number of site observation data is usually limited during geotechnical site

Table 2.3 Summary of availability of transformation models for sands provided by Kulhawy and Mayne (1990) (after Phoon and Kulhawy 1999b)

Property category	Soil property	Laboratory or theory correlation	In situ test correlation		
			SPT	CPT[c]	PMT
Basic characterization	Classification	✓[a]	×[b]	✓	×
	Unit weight	✓	×	×	×
	Relative density	×	✓	✓	×
In situ stress state	Coefficient of horizontal soil stress	✓	×	✓	✓
Strength	Effective friction angle	✓	✓	✓	✓
Deformability	Poisson's ratio	✓	×	×	×
	Young's modulus	✓	✓	×	✓
	Compression index	✓	×	×	×
	Constrained modulus	✓	×	✓	×
	Subgrade modulus	✓	×	×	×
Permeability	Coefficient of permeability	✓	×	×	×
Liquefaction resistance	Cyclic stress ratio	×	✓	✓	×

[a]✓ = available
[b]× = unavailable
[c]Including piezocone test

characterization (Wang et al. 2010). Furthermore, the challenges in geotechnical site characterization become more profound because of the inherent spatial variability of soils and various uncertainties that arise during geotechnical site characterization, as discussed in the next section.

2.2 Uncertainties in Soil Properties

During geotechnical site characterization, various uncertainties are incorporated into the estimated soil properties (e.g., Christian et al. 1994; Kulhawy 1996; Phoon and Kulhawy 1999a; Baecher and Christian 2003), including inherent variability of soil properties, measurement errors, statistical uncertainty, and transformation uncertainty, as discussed in the following four subsections.

2.2.1 Inherent Variability

Geotechnical materials are natural materials, and their properties are affected by various factors during their formation process, such as properties of their parent

materials, weathering and erosion processes, transportation agents, and conditions of sedimentation (Vanmarcke 1977; Jaksa 1995; Phoon and Kulhawy 1999a; Baecher and Christian 2003; Mitchell and Soga 2005). Properties of geotechnical materials, therefore, vary inherently. Such inherent variability is independent of the state of knowledge about geotechnical properties and cannot be reduced as the knowledge improves. Therefore, it is categorized as "aleatory uncertainty" in nature (Baecher and Christian 2003).

Soil properties inherently vary from one location to another location in both horizontal and vertical directions. The soil property at the same elevation is frequently simplified and represented by a single variable (i.e., fully correlated along horizontal direction). Such simplification is usually considered reasonable to some degree for at least two reasons: (1) The soils at the same elevation went through similar geological processes. Therefore, the values of a soil property at different locations, but with the same elevation, are somewhat close to each other, and the correlation of the soil property at different locations in horizontal direction is much stronger than that in vertical direction (e.g., Phoon and Kulhawy 1996, 1999a); (2) such simplification generally leads to conservative designs (e.g., Fenton and Griffith 2007; Klammler et al. 2010). The remaining part of this subsection, therefore, focuses only on spatial variation of soil properties in vertical direction.

Figure 2.2 shows spatial variation of a soil property $x(D)$ along the depth D (i.e., in vertical direction), which can be decomposed into two components: the trend function $t(D)$ of the soil property and the remaining fluctuating component $s(D)$ (Lumb 1966; Vanmarcke 1977 and 1983; DeGroot and Baecher 1993; Phoon and Kulhawy 1999a; Phoon et al. 2003). The soil property can be written as

$$x(D) = t(D) + s(D) \tag{2.1}$$

in which $t(D)$ represents the mean value of $x(D)$ at a given depth; $s(D)$ represents the variation of $x(D)$ at the given depth and has a mean of zero and a standard deviation of $\sigma_s(D)$. Probability theory and statistics have been applied to model the inherent spatial variability of soil properties since 1970s (Lumb 1966 and 1974; Vanmarcke

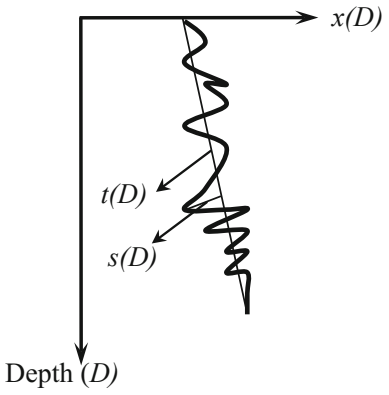

Fig. 2.2 Spatial variability of soil properties along the depth (after Phoon and Kulhawy 1999a)

1977 and 1983; DeGroot and Baecher 1993; Jaksa 1995; Fenton 1999a, b; Wang et al. 2010). Detailed modeling of Eq. (2.1) is further discussed in the following two subsections.

2.2.1.1 Lumb's Formulation

Lumb (1966) proposed three different forms of spatial variation of soil properties along the depth: (1) Both $t(D)$ and standard deviation $\sigma_s(D)$ of $s(D)$ are spatially constant; (2) $t(D)$ varies linearly along the depth, but $\sigma_s(D)$ is spatially constant; and (3) $t(D)$ varies linearly along the depth and $\sigma_s(D)$ increases with the depth. Lumb (1966) examined the spatial variation of soil properties of four soils (i.e., silty sand, clayey silt, sandy clay, and marine clay) and showed that (1) the tangent of effective friction angles of silty sand and clayey silt has spatially constant mean and standard deviation along the depth; (2) the mean of the compression index of sandy clay increases linearly with the depth, while its standard deviation remains constant along the depth; (3) the mean and standard deviation of the undrained shear strength of marine clay increase as the depth increases; and (4) Gaussian distributions are in good agreement with distributions of soil properties of the four soils except for compression index of sandy clay, the distribution of which is close to a lognormal distribution. The mean and standard deviation of soil properties were examined by Lumb (1966), but the correlation of the variation of a soil property at different locations was not considered. By this simplification, the soil property that is normally distributed has the following representation (e.g., Lumb 1966)

$$x(D) = t(D) + \sigma_s(D)z \tag{2.2}$$

in which z is a standard Gaussian random variable. If the soil property is lognormally distributed, it can be written as (e.g., Ang and Tang 2007; Au et al. 2010)

$$x(D) = \exp(t(D)_N + \sigma(D)_N z) \tag{2.3}$$

in which $t(D)_N$ and $\sigma_s(D)_N$ are the mean and standard deviation of the logarithm $\ln(x(D))$ of $x(D)$.

2.2.1.2 Random Field Theory

Vanmarcke (1977 and 1983) developed the random field theory to characterize the spatial variability of geotechnical materials, by which the correlation of a soil property at different locations (i.e., autocorrelation) is taken into account rationally. In the context of random field theory, a soil property within a statistically homogenous soil layer is described by a series of random variables with the same mean and standard deviation, and the autocorrelation among these random variables depends on the correlation length (also sometimes known as "scale of fluctuation")

(Vanmarcke 1977 and 1983; Fenton and Griffiths 2008). The correlation length is a separation distance, within which the soil property shows a relatively strong correlation from point to point. In the space domain, a soil property that is normally distributed can be written as (Ang and Tang 1984; Fenton and Griffiths 2008; Wang et al. 2010)

$$\underline{x}(\underline{D}) = \mu \underline{l} + \sigma \underline{L}^T \underline{Z} \tag{2.4}$$

in which $\underline{x}(\underline{D})$ is a vector of the soil property of interest at different n_D depths; $\underline{D}$ is a depth vector; μ and σ are, respectively, the mean and standard deviation of the soil property, which are spatially constant; $\underline{l}$ is a vector with n_D components that are all equal to one; $\underline{Z}$ is a standard Gaussian vector with n_D components; and $\underline{L}$ is a n_D by n_D upper triangular matrix obtained by Cholesky decomposition of the correlation matrix $\underline{R}$ satisfying

$$\underline{R} = \underline{L}^T \underline{L} \tag{2.5}$$

in which the (i, j)th entry is the correlation coefficient (i.e., ρ_{ij}) of the soil property at the ith and jth depths and is calculated from a correlation function f_ρ, which is a function of the correlation length and describes the correlation of the variation of a soil property at different locations. For a given correlation structure (or correlation function), a random field is uniquely determined by the mean, standard deviation, and correlation length. Based on a set of measurements (e.g., cone tip resistance measured by a CPT test), the mean, standard deviation, and correlation length of the measured properties can be estimated (e.g., Vanmarcke 1977; Jaksa 1995; Fenton 1999b). Note that applying random field theory to describe (or model) the inherent spatial variability of soil properties involves two important issues: the statistical homogeneity (or stationarity) and the correlation function, which are discussed in the following two subsections, respectively.

2.2.1.3 Statistical Homogeneity and Data Transformation

Generally speaking, statistical homogeneity (or stationarity) means that the mean and standard deviation of the soil property of interest are spatially constant, and the autocorrelation only depends on the separate distance between two locations rather than the absolute positions (e.g., Vanmarcke 1983; Fenton 1999a, b). Statistical homogeneity is a significant prerequisite for conventional statistical analysis (e.g., calculating mean and standard deviation) on a set of observation data. If the observation data are not stationary, data transformation techniques can be used to transform the observed data into stationary data, such as detrending techniques for non-constant trend component and variance transformation techniques (e.g., logarithmic transformation and the Box–Cox transformation) for non-constant standard deviation (e.g., Jaksa 1995).

Detrending techniques, such as regression analysis and normalization method (e.g., Jaksa 1995; Phoon et al. 2003), are widely used to remove the obvious trend component. Regression analysis gives the best fit of a predefined trend function based on the observation data. To some degree, the choice of the trend function is a decision on how much of the spatial variability in observation data is considered as a deterministic function, and correspondingly, the residual component in the measurements is considered statistically and is modeled as a random process (i.e., a random field in space domain) (Baecher 1987). The trend function can be linear or polynomial, but, as pointed out by Lumb (1974), there are rarely sufficient data to estimate any form more complicated than a linear trend in routine site characterization. The normalization method can also be used to remove the trend in direct measurements for many geotechnical properties. For example, normalization by the effective overburden stress accounts for the effect of confinement that generally increases with the depth (Wroth 1984; Houlsby 1988; Robertson 1990, 2009; Phoon et al. 2003). Note that normalization by the effective overburden stress requires information on soil unit weights and groundwater conditions, which might not be available.

The adequacy of detrending is of great significance for the assumption of stationarity. This can be examined by many methods, such as visual inspection of the autocovariance function (e.g., Box and Jenkins 1970; Jaksa 1995), the run test (e.g., Alonso and Krizek 1975; Campanella et al. 1987), Kendall's τ tests (e.g., Ravi 1992), and Bartlett's test (e.g., Phoon et al. 2003). It is also worthwhile to point out that the detrending process leads to a decrease in the estimated correlation length (e.g., Phoon et al. 2003), because the detrending process removes the large-scale fluctuation in nature (Fenton 1999a).

2.2.1.4 Correlation Function and Correlation Length

The correlation between the variations of a soil property at different locations can be characterized by a correlation function. In general, there are two types of correlation functions: the finite-scale model, in which the correlation dies out rapidly as the separate distance is greater than the correlation length, and the fractal model, in which the correlation remains significant over a very large distance (Fenton 1999a). Although Fenton (1999b) examined 143 sets of CPT data and concluded that the correlation of soil properties follows the fractal model in nature, the finite-scale model is commonly used in the analysis of geotechnical data (e.g., Lumb 1974; Vanmarcke 1977; DeGroot and Baecher 1993; Jaksa 1995; Phoon et al. 2003).

The major advantage of the finite-scale model is that usually only one model parameter, i.e., correlation length, needs to be determined. In addition, Fenton (1999a) also noted that for a given site, there may be little difference between a properly selected finite-scale model and a real fractal model over a finite domain. Equation (2.6) gives four commonly used finite-scale models for the analysis of geotechnical data (Vanmarcke 1977)

$$f_\rho = \begin{cases} \exp\left(-\frac{2|\Delta D|}{\lambda}\right) & \text{(a)} \\ \exp\left[-\pi\left(\frac{\Delta D}{\lambda}\right)^2\right] & \text{(b)} \\ \left(1+\frac{4|\Delta D|}{\lambda}\right)\exp\left(-\frac{4|\Delta D|}{\lambda}\right) & \text{(c)} \\ \exp\left(-\frac{|\Delta D|}{\lambda}\right)\cos\left(\frac{\Delta D}{\lambda}\right) & \text{(d)} \end{cases} \tag{2.6}$$

in which ΔD is the separate distance between two depths; λ is the correlation length. The correlation length can be estimated by choosing a theoretical correlation model given by Eq. (2.6) to fit the empirical autocorrelation function estimated from observation data (e.g., Jaksa 1995) or by maximum-likelihood methods (e.g., DeGroot and Baecher 1993; Fenton 1999a, b). Because the available observation data for a specific site are usually limited, choosing an appropriate correlation function and determining the correlation length are challenging tasks for a specific site. Fenton (1999a) argued that the correlation model developed for one site is applicable for another site that has similar geological conditions. Among the four finite-scale models in Eq. (2.6), the single exponential correlation function given by Eq. (2.6a) is most widely used in analysis of soil data (e.g., Lumb 1974; DeGroot and Baecher 1993; Lacasse and Nadim 1996; Phoon et al. 2003; Wang et al. 2010). Phoon et al. (2003) observed that, among the four models in Eq. (2.6), the single exponential correlation function (i.e., Eq. (2.6a)) leads to the most stringent criteria for the identification of stationarity using Bartlett statistics.

The statistically homogenous soil layers and correlation functions of soil properties are usually determined using in situ and laboratory test data (i.e., measured soil properties) (e.g., Fenton 1999b; Phoon et al. 2003). Phoon et al. (1995) and Phoon and Kulhawy (1999a) summarized the inherent spatial variability of many soil properties (including both measured and design soil properties), some of which are shown in Table 2.4. Research is, however, relatively limited that addresses directly inherent spatial variability of design soil properties (e.g., effective friction angle) using random field theory.

2.2.2 *Measurement Errors*

Measurement errors are unavoidable during in situ and laboratory tests (Christian et al. 1994; Kulhawy 1996). As pointed out by Kulhawy (1996) and Kulhawy and Trautmann (1996), measurement errors arise from three sources: equipment errors (e.g., inaccuracies of the measuring devices and variations in equipment geometries and systems used for routine testing), procedural–operator errors (e.g., limitations in existing test standards and how these standards are followed by operators), and random testing error (i.e., the remaining scatter in measurements that is not assignable to specific testing parameters and is not caused by inherent variability of soils). The total measurement error can be estimated from the square root of the sum

Table 2.4 Summary of inherent spatial variability of soil properties (After Phoon and Kulhawy 1999a)

Test type	Soil type	Soil property	Mean		Coefficient of variation (%)		Correlation length in vertical direction (m)	
			Range	Average	Range	Average	Range	Average
Strength test	Clay	Undrained shear strength (UC)[a]	6–412 kPa	100 kPa	6–56	33	0.8–6.1	2.5
		Undrained shear strength (UU)[b]	15–363 kPa	276	11–49	22		
		Undrained shear strength (CIUC)[c]	130–713 kPa	405	18–42	32		
	Sand	Effective friction angle	35°–41°	37.6°	5–11	9	N/A	N/A
		Tangent of effective friction angle	0.65–0.92	0.744	5–14	9	N/A	N/A
CPT	Clay	Cone tip resistance	0.5–2.1 MPa	1.6 MPa	5–40	27	0.1–2.2	0.9
		Corrected cone tip resistance	0.4–2.6 MPa	1.3 MPa	2–17	8	0.2–0.5	0.3
	Sand	Cone tip resistance	0.4–29.2 MPa	4.1 MPa	10–81	38	0.1–2.2	0.9
SPT	Clay	SPT *N*-value	7–63	32	37–57	44	N/A	2.4
	Sand	SPT *N*-value	7–74	35	19–62	54	N/A	N/A
PMT	Clay	Limit pressure	0.4–2.8 MPa	10.1	10–32	15	N/A	N/A
	Sand	Limit pressure	1.6–3.6 MPa	2.3 MPa	23–50	40	N/A	N/A
		Young's modulus from pressuremeter tests	5.2–15.6 MPa	9.0 MPa	28–68	42	N/A	N/A
VST	Clay	Undrained shear strength (VST)[d]	6–375 kPa	105 kPa	4–44	24	2.0–6.2	3.8

[a]Undrained compression test
[b]Unconsolidated undrained triaxial test
[c]Consolidated isotropic undrained triaxial compression test
[d]Vane shear test

of the equipment, procedural–operator, and random testing errors (Orchant et al. 1988; Kulhawy and Trautmann 1996). Phoon et al. (1995) summarized the measurement errors of several laboratory tests, including strength tests (e.g., triaxial test, laboratory vane shear test, direct shear test, and Atterberg limit tests). In addition, Kulhawy and Trautmann (1996) summarized the measurement errors of several in situ tests (e.g., SPT, CPT, PMT, and VST) and estimated the total measurement errors of these in situ tests. The total measurement errors of SPT, CPT, PMT, and VST range from 15 % to 45 %, from 5 % to 25 %, from 10 % to 25 %, and from 10 % to 20 %, respectively. Note that these values can be used only as approximate guidelines for estimating measurement errors because they are evaluated based on limited available data and the evaluation relies on subjective judgments (Kulhawy and Trautmann 1996).

It is also worthwhile to note that measurement errors arise from a lack of knowledge about test equipments and procedures, and they are, therefore, categorized as "epistemic uncertainty" in nature (Baecher and Christian 2003). As the knowledge on test equipments and procedures improves, the measurement errors can be reduced. In addition, both measurement errors and inherent variability of soils contribute to the scatter of observation data. It is, however, difficult to discern the fluctuation resulted from inherent variability and that arising from measurement errors.

2.2.3 *Statistical Uncertainty*

As mentioned in Sect. 2.1.5 "Challenges in geotechnical site characterization," the number of project-specific test results is usually limited during geotechnical site characterization (Nawari and Liang 2000; Baecher and Christian 2003; Wang et al. 2010). Different sets of test results with a relatively small sample size might result in significantly different statistics of soil properties. In other words, statistics of soil properties estimated from limited test results are uncertain. Such uncertainty is known as "statistical uncertainty" (Christian et al. 1994; Kulhawy 1996; Baecher and Christian 2003). Statistical uncertainty arises from insufficient observation data and is commonly considered to be included in measurement errors (Kulhawy 1996). It decreases as the observation data increases and is categorized as "epistemic uncertainty" in nature (Baecher and Christian 2003).

2.2.4 *Transformation Uncertainties*

Design soil property that is directly used in design can be estimated from in situ and laboratory test results (i.e., measured property) by transformation models, such as

Table 2.5 Four transformation models and their uncertainties (After Phoon and Kulhawy 1999b)

Soil type	Design property	Measured property	Relationships[b, c, d]	Uncertainty σ_ε
Clay	Undrained shear strength (UU)[a], $S_{u,\mathrm{UU}}$	SPT N-value	$\log\left(\frac{S_{u,\mathrm{UU}}}{p_a}\right) = \log(0.29) + 0.72\,\log(N_{\mathrm{SPT}}) + \varepsilon$	0.15
	Undrained shear strength (VST), $S_{u,\mathrm{VST}}$	Plasticity index (PI)	$\frac{S_{u,VST}}{\sigma'_p} = (0.11 + 0.0037PI)(1+\varepsilon)$	0.25
	Young's modulus measured by pressuremeter test E_{PMT}	SPT N-value	$\log\left(\frac{E_{\mathrm{PMT}}}{p_a}\right) = \log(19.3) + 0.63\,\log(N_{\mathrm{SPT}}) + \varepsilon$	0.37
Sand	Effective friction angle, ϕ'(°)	Cone tip resistance q_c	$\phi' = 17.6 + 11.0\log\left(\frac{q_c/p_a}{\sqrt{\sigma'_{v0}/p_a}}\right) + \varepsilon$	2.8°

[a]Unconsolidated undrained triaxial test
[b]p_a is the atmospheric pressure
[c]σ'_p is preconsolidation stress
[d]σ'_{vo} is vertical effective stress

empirical and theoretical correlations between the measured property and design property (e.g., Kulhawy and Mayne 1990; Phoon and Kulhawy 1999b). Empirical correlations are often obtained from empirical data fitting, and hence, they are associated with some uncertainties because of data scatter and inaccuracy of the best fit (e.g., Kulhawy and Mayne 1990; Phoon and Kulhawy 1999b). Theoretical correlations are also associated with some uncertainties due to idealizations and simplifications in the theory (Phoon and Kulhawy 1999b). The uncertainties associated with the transformation model are collectively referred to as "transformation uncertainty" ε. Transformation uncertainty can be modeled as a random variable with a mean of zero and standard deviation of σ_ε that indicates the magnitude of the transformation uncertainty and reflects the degrees-of-belief on the corresponding transformation model (Phoon and Kulhawy 1999b). Phoon et al. (1995) and Phoon and Kulhawy (1999b) summarized the transformation uncertainty of several commonly used transformation models, four of which are shown in Table 2.5.

Transformation uncertainty arises from a lack of knowledge about the relationship between the measured property and the design property, and it is therefore categorized as "epistemic uncertainty" and can be reduced as the knowledge about the relationship improves (e.g., Baecher and Christian 2003; Zhang et al. 2004).

2.2.5 *Uncertainty Propagation*

The inherent variability and various epistemic uncertainties (including measurement errors, statistical uncertainty, and transformation uncertainty) that arise during site characterization are incorporated into estimated design properties, as shown in Fig. 2.3. The total variability (including inherent variability, measurement errors, statistical uncertainty, and transformation uncertainty) of estimated design properties can be estimated by a second-moment approach developed by Phoon et al. (1995) and Phoon and Kulhawy (1999a, b). When the epistemic uncertainties (i.e., measurement errors, statistical uncertainty, and transformation uncertainties) are large, the total variability of estimated design soil properties is large. This generally leads to conservative designs by reliability-based design (RBD) approaches (e.g., Phoon et al. 1995). As the knowledge improves, the epistemic uncertainties are reduced and the total variability of estimated design soil properties is reduced. The conservatism in designs resulted from RBD approaches then is reduced. This is reasonable in the sense that the design should be less conservative as the knowledge on soil properties accumulates.

It is, however, worthwhile to point out that the epistemic uncertainties that arise from insufficient knowledge do not contribute to the actual response of geotechnical structures. In contrast, the inherent variability of soils affects significantly the actual response of geotechnical structures (e.g., Phoon et al. 1995; Fenton and Griffiths 2002 and 2003; Fenton et al. 2005; Hicks 2005; Klammler et al. 2010). To understand probabilistically the actual response of geotechnical structures, it is meaningful to characterize explicitly the inherent variability of design soil properties for RBD. Research is, however, rare that addresses directly and explicitly the inherent variability of design soil properties using probability theory.

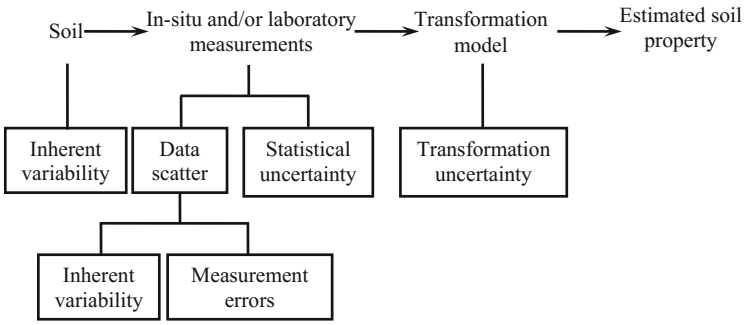

Fig. 2.3 Uncertainties in estimated soil properties (after Phoon and Kulhawy 1999a)

2.3 Bayesian Approach

Bayesian approach provides a formal framework to integrate systematically information from different sources, such as observation data and knowledge available prior to collecting the observation data (i.e., prior knowledge) (e.g., Ang and Tang 2007; Sivia and Skilling 2006). It can be used to estimate probability distributions of model parameters of a system based on prior knowledge and observation data and to update the probability of an event using new information obtained (Baecher and Christian 2003).

2.3.1 Bayesian Mathematical Framework

Let $\Theta = [\theta_1, \theta_2, \ldots, \theta_{n_m}]$ denote a set of random variables that represent the n_m uncertain model parameters of a model $M(\Theta)$ of the system concerned. Under a Bayesian framework, the updated distribution $P(\Theta|Data)$ of model parameters Θ is written as (e.g., Ang and Tang 2007; Wang et al. 2010)

$$P(\Theta|Data) = KP(Data|\Theta)P(\Theta) \tag{2.7}$$

in which *Data* is the observation data; $K = 1/P(Data)$ is a normalizing constant that is independent of model parameters; $P(\Theta)$ is the prior distribution of model parameters that reflects prior knowledge on model parameters in the absence of observation data; and $P(Data|\Theta)$ is the likelihood function that reflects the model fit with observation data.

2.3.2 Prior Distribution

In general, there are two types of prior distribution: uninformative prior distribution and informative prior distribution (Siu and Kelly 1998; Baecher and Christian 2003), as discussed in the following two subsections.

2.3.2.1 Uninformative Prior Distribution

Uninformative prior distributions suggest that there is no prevailing prior knowledge on the possible values of model parameters and all possible values of model parameters are considered equally likely (Jeffreys 1983; Baecher and Christian 2003). For mutually independent model parameters, the prior distribution $P(\Theta)$ is further written as

$$P(\Theta) = \prod_{i=1}^{n_m} P(\theta_i) \tag{2.8}$$

in which $P(\theta_i), i = 1, 2, \ldots, n_m$ is the prior distribution of the model parameter θ_i. Equation (2.9) gives three commonly used uninformative prior distributions of θ_i.

$$P(\theta_i) = \begin{cases} 1/(\theta_{i,\max} - \theta_{i,\min}) & \text{for} \quad \theta_i \in [\theta_{i,\min}, \theta_{i,\max}] \quad \text{(a)} \\ \text{constant} & \text{for} \quad \theta_i \in [-\infty, +\infty] \quad \text{(b)} \\ 1/\theta_i & \text{for} \quad \theta_i \in [0, +\infty) \quad \text{(c)} \end{cases} \tag{2.9}$$

Equation (2.9a) gives an uninformative prior distribution of θ_i with a range from the minimum $\theta_{i,\min}$ to the maximum $\theta_{i,\max}$. This prior distribution is particularly useful when a reasonable range of θ_i is available. Equation (2.9b) gives an uninformative prior distribution of θ_i that ranges from negative infinity to positive infinity. Both Eq. (2.9a) and (2.9b) have been criticized because they are not invariant to transformation of variables (Jeffreys 1983; Siu and Kelly 1998; Baecher and Christian 2003). It is also noted that the integral on Eq. (2.9b) is infinite, which is improper since the integral on a probability density function (PDF) should be unity (Baecher and Christian 2003). In addition, Eq. (2.9b) has two singularities at both endpoints.

Equation (2.9c) gives an uninformative prior distribution of θ_i which ranges from zero to positive infinity and is uniform in a log scale (i.e., $\log(\theta_i)$ is uniformly distributed). Equation (2.9c) is also known as "Jeffreys prior," and it is invariant to power and scale transformation of variables (Jeffreys 1983; Sivia and Skilling 2006). Note that Eq. (2.9c) also has a singularity at $\theta_i = 0$.

Uninformative prior distributions are widely used for the cases with a large number of observation data (e.g., Beck and Yuen 2004; Zhang 2011), in which the observation data tend to dominate the results of Bayesian approach so that the effect of prior knowledge is not so important. Research is, however, rare that explores systematically the effect of uninformative prior knowledge (e.g., Eq. (2.9a)) when the observation data are relatively limited, e.g., geotechnical site characterization.

2.3.2.2 Informative Prior Distribution

Informative prior distribution can be estimated from prior knowledge about model parameters, and it reflects the degrees-of-belief (or confidence level) of prior knowledge on model parameters. When limited prior knowledge on θ_i (e.g., the mean and standard deviation of the system parameter θ_i of interest) is available and it is testable (i.e., it can be determined whether or not there is a probability distribution consistent with the prior knowledge), the maximum entropy method can be used to obtain the prior distribution from the prior knowledge (e.g., Siu and Kelly 1998; Sivia and Skilling 2006). Within the maximum entropy method, the

information entropy H_I is used as a measure of uncertainty of the prior PDF $P(\theta_i)$ of θ_i, and it is defined as (Shannon and Weaver 1949)

$$H_I = -\int P(\theta_i)\ln[P(\theta_i)]\mathrm{d}\theta_i, \quad i = 1, 2, \ldots, n_m, \tag{2.10}$$

Then, the prior PDF $P(\theta_i)$ of θ_i is obtained by maximizing the information entropy H_I subject to constraints of the testable information provided by prior knowledge and normalization (e.g., Sivia and Skilling 2006). The principle of maximum entropy provides a reasonable approach for generating prior distribution based on limited prior knowledge that specifies some probability constraints.

When previous data are available, statistical analysis can be used to estimate prior distribution of model parameters, such as calculating the mean and standard deviation and maximum-likelihood function and fitting previous data with specified distributions by regression analysis (Berger 1985; Maritz and Lwin 1989; Carlin and Louis 1996; Siu and Kelly 1998). Such statistical analysis is a pragmatic approach for constructing prior distributions using previous data. It generally takes the previous data from various sources as the evidence with equal weight. This is, however, not well justified because the quality (or credibility) of data from different sources may be significantly different. In addition, it is difficult to incorporate systematically subjective judgments in the statistical analysis, which is often an essential component of prior knowledge, e.g., engineering judgments in geotechnical engineering.

Subjective probability provides an operational tool to measure the degrees-of-belief of engineers' opinions and to express quantitatively their engineering judgments (e.g., Baecher 1983; Vick 2002; Garthwaite et al. 2005; Silva et al. 2008). Subjective probability assessment methods are, therefore, another useful approach to construct informative prior distributions (Clemen 1996; Siu and Kelly 1998). They are usually developed based on cognitive models, in which a series of cognitive activities of the cognitive process are divided into several stages (e.g., Beach et al. 1986; Koriat et al. 1980; Smith et al. 1991; Vick 2002). For example, Fig. 2.4 shows a stage cognitive model that consists of four stages (Vick 2002): identification of the problem, search for relevant information and determination of possible outcomes, assessment of uncertainties associated with the possible outcomes, and quantification of uncertainties in the numerical probability metric. During subjective probability assessment, various cognitive heuristics are involved, such as availability heuristic, anchoring and adjustment heuristic, and representativeness heuristic (Tversky and Kahneman 1974; Vick 2002). These heuristics are generally useful tools that help the assessor make decisions in a probabilistic manner, but they might, simultaneously, lead to some cognitive biases, as discussed in what follows.

According to the availability heuristic, the likelihood of an event is estimated by the ease with which similar events are recalled (Garthwaite et al. 2005). The event with relatively high probability is easy to be recalled. Conversely, an event with small probability is often difficult to be retrieved from memory. The availability

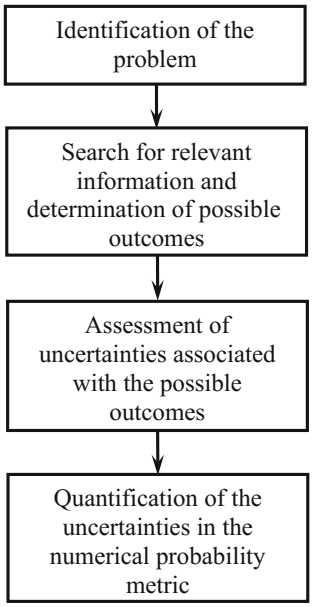

Fig. 2.4 A stage cognitive model (after Vick 2002)

heuristic is often a useful indicator for assessing the probability of an event, but it can also lead to availability bias because of missing some information that is relatively difficult to be acquired (Clemen 1996; Garthwaite et al. 2005). In addition, the availability heuristic possibly results in hindsight bias because of the inclination to exaggerate the likelihood of occurrence of an event after it occurs and confirmation bias due to the inclination to ignore disconfirming evidence during searching for information in memory (Vick 2002).

The assessor sometimes estimates the probability of an event by choosing an initial probability value roughly, which is known as "anchor," and adjusts the probability value according to knowledge about the event of interest to obtain the final probability value. This is referred to as "anchoring and adjustment heuristic." This heuristic helps the assessor overcome cognitive limitation of human information processing capacity (Vick 2002; Garthwaite et al. 2005). Insufficient adjustment, however, might occur, so that the probability estimated from the heuristic might be biased toward the anchor. This subsequently leads to overconfidence bias (Vick 2002).

The representativeness heuristic evaluates the probability of an event by the extent to which the event is similar to some other events belonging to a particular category (Clemen 1996; Vick 2002). The probability of the event concerned belonging to the category increases as the similarity between the event of interest and other related events of the category increases. In general, the representativeness heuristic is a useful tool to estimate probability based on prior knowledge. Several cognitive biases, however, sometimes arise from it because the base rate of the

event concerned is ignored and there is the insensitivity to sample size of the category (Garthwaite et al. 2005).

In addition to cognitive biases, the outcomes (e.g., prior distribution herein) obtained from subjective probability assessment methods are also influenced by cognitive limitations, such as limited capacity of processing information that might lead to ignorance of useful information, limited good calibration range of subjective probability (e.g., from 0.2 to 0.8 by Fischhoff et al. 1977), and limited cognitive discrimination range of subjective probability (e.g., from 0.01 to 0.99 by Hogarth 1975; Fischhoff et al. 1977; Vick 1997 and 2002). Because of the cognitive biases and limitations, outcomes of subjective probability assessment might deviate from the actual beliefs of the assessor and be inconsistent with basic probability axioms (Vick 2002). To enable meaningful and coherent outcomes, subjective probability assessment often requires formally organized external procedures (Vick 2002; Baecher and Christian 2003). It is sometimes difficult to satisfy such a requirement due to the limitation of resources in geotechnical site characterization, particularly for projects with medium or relatively small sizes.

2.3.2.3 Confidence Level of Prior Knowledge

The standard deviation or coefficient of variation (COV) of the prior distribution indicates the degrees-of-belief (or confidence level) of the prior knowledge about model parameters. When the COV is relatively small, the confidence level of the prior knowledge on model parameters is relatively high, and the prior knowledge is relatively informative. As the COV increases, the confidence level of prior knowledge on model parameters decreases, and the prior knowledge becomes more and more uninformative. Siu and Kelly (1998) also noted that informative prior knowledge is likely to have significant impact on the results of Bayesian approach when observation data are relatively limited.

2.3.3 Likelihood Function

Constructing a likelihood function requires a model $M(\Theta)$ that represents the system concerned and describes how the observation data are generated from the system. Within the model $M(\Theta)$, model parameters Θ can be generally divided into two types: Θ_S representing the unknown input parameter of the model used to describe behaviors of the system and Θ_U representing modeling errors associated with the model. The uncertainties in Θ_S and the modeling errors Θ_U result in uncertainties in predications of the model. The goodness of fit of model predications with the observation data for a given set of model parameters is defined by the likelihood function. Based on the applications of the Bayesian approach, the likelihood function can be developed in three ways:

(1) Consider the uncertainties in input parameters Θ_S only when developing the likelihood function. For example, Jung et al. (2008) and Cetin and Ozan (2009) developed the likelihood functions considering uncertainties in input parameters of empirical models of soil classification. Yan et al. (2009) constructed the likelihood function for selecting the most appropriate regression model between the compression index and various other soil properties (e.g., liquid limit, plastic index) with the consideration of uncertainties of regression models.

(2) Consider modeling errors Θ_U only when developing the likelihood function. For example, Zhang et al. (2004) derived the likelihood function for reducing modeling errors associated with the empirical transformation model between the SPT *N*-values and undrained shear strength. Zhang et al. (2009) developed the likelihood function for characterization of modeling errors associated with deterministic models of slope stability analysis. Zhang et al. (2010a, b) constructed the likelihood function for probabilistic back analysis of slope stability with the consideration of modeling errors associated with deterministic models of slope stability analysis. In addition, Ching et al. (2010) derived the likelihood function for reducing uncertainties in estimated soil properties with the consideration of modeling errors associated with empirical transformation models.

(3) Consider both uncertainties in input parameters Θ_S and modeling errors Θ_U when developing the likelihood function. Wang et al. (2010) and Cao et al. (2011) developed the likelihood function for probabilistic characterization of soil properties based on random field theory, in which both uncertainties in model parameters of the random field and modeling errors associated with the transformation model were considered. The Bayesian approach developed by Wang et al. (2010) and Cao et al. (2011) provides proper probabilistic characterization of soil properties using both prior knowledge and limited site observation data (i.e., CPT data). Their approach, however, only applies to a single and predefined statistically homogenous soil layer and provides no information on the number or thicknesses/boundaries of statistically homogenous soil layers.

2.3.4 Posterior Distribution

The posterior distribution in Eq. (2.7) is a joint distribution of model parameters. To obtain the posterior marginal PDF of one model parameter, integration on the posterior distribution over the space of the other model parameters is required. Since the posterior distribution might be very complicated, analytical integration is often infeasible. Numerical integration may be performed using a multidimensional grid over the space of other model parameters, but it must be performed repeatedly for a number of values of the model parameters concerned so as to yield

information about the whole marginal distribution of the model parameter. The computational complexity has been recognized as one key limitation of the Bayesian approach (e.g., Zhang et al. 2009; Wang et al. 2010). Traditionally, conjugated prior distributions (e.g., Siu and Kelly 1998; Baecher and Christian 2003) have been used to bypass the computational problems, but this nevertheless introduces artificial limitations to the choice of prior distribution.

Laplace asymptotic approach (Bleistein and Handelsman 1986) has been widely used in Bayesian system identification to bypass the computational complexity when a relatively large number of observation data are available (e.g., Papadimitriou et al. 1997; Beck and Katafygiotis 1998; Katafygiotis and Beck 1998; Katafygiotis et al. 1998; Wang et al. 2010). By Laplace asymptotic approach, the posterior distribution is approximate to a joint Gaussian PDF, in which the mean vector is equal to the most probable values (MPV) of model parameters. Under this approximation, the determination of posterior mean values of model parameters is reduced to finding the MPV by numerically minimizing the objective function $f_{\text{obj}} = -\ln[P(\Theta|Data)]$. The covariance matrix of the posterior distribution is provided by the inverse of the Hessian matrix of $f_{\text{obj}} = -\ln[P(\Theta|Data)]$. Note that Laplace asymptotic approach generally requires a relatively large number of observation data so that the posterior distribution peaks sharply and the MPV of model parameters are identified with relative ease by the optimization procedure (i.e., minimizing the objective function $f_{\text{obj}} = -\ln[P(\Theta|Data)]$). Wang et al. (2010) have successfully applied the Laplace asymptotic approach to obtain the posterior distribution of random field model parameters using CPT data and showed that the results obtained from the Laplace asymptotic approach are in good agreement with those obtained from numerical integration. This indicates that CPT tests provide sufficient data for Laplace asymptotic approach to identify the MPV of random field model parameters.

2.3.5 *Updating the Probability of an Event*

Bayesian approach can also be used to update the probability of an event A using the new evidence B on A. The updated probability $P(A|B)$ of A given the new evidence B is written as (e.g., Siu and Kelly 1998; Ang and Tang 2007)

$$P(A|B) = P(B|A)P(A)/P(B) \tag{2.11}$$

in which $P(A)$ is the probability of A prior to the collection of the new evidence B; $P(B)$ is the probability of the new evidence B, which is independent of A; and $P(B|A)$ reflects the information on A provided by the new evidence B. Equation (2.11) has been applied to calibration of estimated failure probability in liquefaction evaluation (e.g., Juang et al. 1999) or slope reliability assessment (e.g., Cheung and Tang 2005), probabilistic assessment of soil–structure interaction (e.g., Schuster et al. 2008), and model class selection (e.g., Beck and Yuen 2004; Yan

et al. 2009; Yuen 2010). For example, in model class selection, A represents a model class and B represents the new evidence (e.g., observation data). Using Eq. (2.11), the plausibility (or occurrence probability) of the model class A given the new evidence B is determined.

2.4 National Geotechnical Experimentation Site (NGES) at Texas A&M University

To provide well-characterized reference sites for the development and evaluation of geotechnical design and construction methods and in situ testing methods, five US National Geotechnical Experimentation Sites (NGES) were established by US Federal Highway Administration (FHWA) (Dimillio and Prince 1993; Benoit 2000). Extensive in situ and laboratory test results obtained from NGES are available in the geotechnical literature (e.g., Briaud 2000; Benoit 2000). The test results obtained from the NGES at Texas A&M University (TAMU) are used to illustrate the probabilistic approaches for geotechnical site characterization developed in this book. The NGES at TAMU is therefore introduced briefly below.

The NGES at TAMU is underlain by Pleistocene fluvial and overbank deposits and Eocene-aged Spiller Member of the Crockett Formation and includes a clay site and a sand site (Briaud 2000). Figure 2.5a, b shows the stratigraphy of the clay site and sand site, respectively. As shown in Fig. 2.5a, the clay site is comprised of a top stiff clay layer extending from the ground surface to 5.5 m deep, a thin sand layer from the depth of 5.5 m to the depth of 6.5 m, another stiff clay layer down to 12.5 m deep, and a hard clay layer thereafter. The groundwater level at the clay site

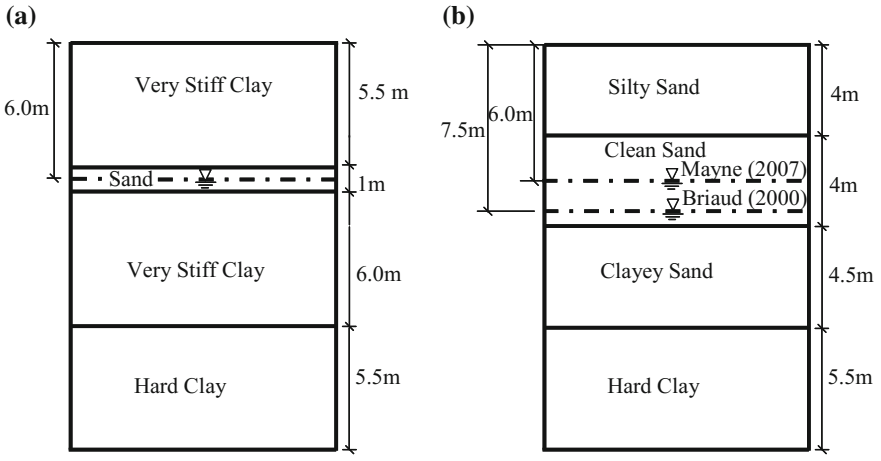

Fig. 2.5 Soil profiles of the clay site and sand site of NGES at Texas A&M University (after Briaud 2000). **a** Clay site. **b** Sand site

is about 6.0 m deep (Briaud 2000). As shown in Fig. 2.5b, the sand site is underlain by a silty sand layer extending from the ground surface to 4.0 m deep, a clean sand layer from the depth of 4.0 m to the depth of 8.0 m, a clayey sand layer from 8.0 m deep to 12.5 m deep, and a hard clay layer thereafter. The groundwater level at the sand site is around 7.5 m deep by Briaud (2000) (or about 6.0 m deep by Mayne 2007). Briaud (2000) summarized results of in situ tests (including SPT, CPT, and PMT) and laboratory tests performed in the clay site and sand site, and Mayne (2007) reported an additional set of CPT test results obtained from the sand site.

Table 2.6 provides the average soil properties of different soil layers of the clay site and sand site reported by Briaud (2000), including water content, particle size distribution, natural unit weight, Atterberg limits, strength (i.e., undrained shear strength, effective stress cohesion, and effective friction angle), coefficient of

Table 2.6 Summary of soil properties of NGES at Texas A&M University (After Briaud 2000)

Soil property	Clay site				Sand site			
Soil type	Very stiff clay[a]	Sand	Very stiff clay[b]	Hard clay	Silty sand	Clean sand	Clayey sand	Hard clay
Water content (%)	24.4	N/A	24.5	26.4	12	17	25	26
Percent of grains (by weight) smaller than 0.075 mm (%)	N/A	N/A	N/A	N/A	17.4	4	30	N/A
Mean grain size (mm)	N/A	N/A	N/A	N/A	0.2	0.25	0.075	N/A
Natural unit weight (kN/m^3)	19.6	N/A	19.5	18.9	20	17	18.3	20
Plastic limit (%)	20.9	N/A	22	22.7	N/A	N/A	22	20
Liquid limit (%)	53.7	N/A	60	56	N/A	N/A	41	61
Undrained shear strength (kPa)	110	N/A	140	160	N/A	N/A	N/A	235
Effective stress cohesion (kPa)	13	N/A	57	N/A	N/A	N/A	N/A	N/A
Effective friction angle (°)	20	N/A	26.5	N/A	34	31	N/A	N/A
Coefficient of permeability (m/year)	0.0005	N/A	0.00007	N/A	0.05	N/A	N/A	N/A
SPT *N*-value (bl/0.3 m)	12	N/A	32	N/A	15	19	22	55
Cone tip resistance (MPa)	2.0	N/A	6.0	N/A	7.0	9.0	10.0	N/A
Young's modulus measured by pressuremeter test (MPa)	15.0	N/A	35.0	230.0	9.0	9.0	33.0	N/A
Limit pressure (MPa)	0.75	N/A	2.2	6.5	0.8	1.0	1.9	N/A

[a]The top soil layer at the clay site
[b]The third soil layer at the clay site

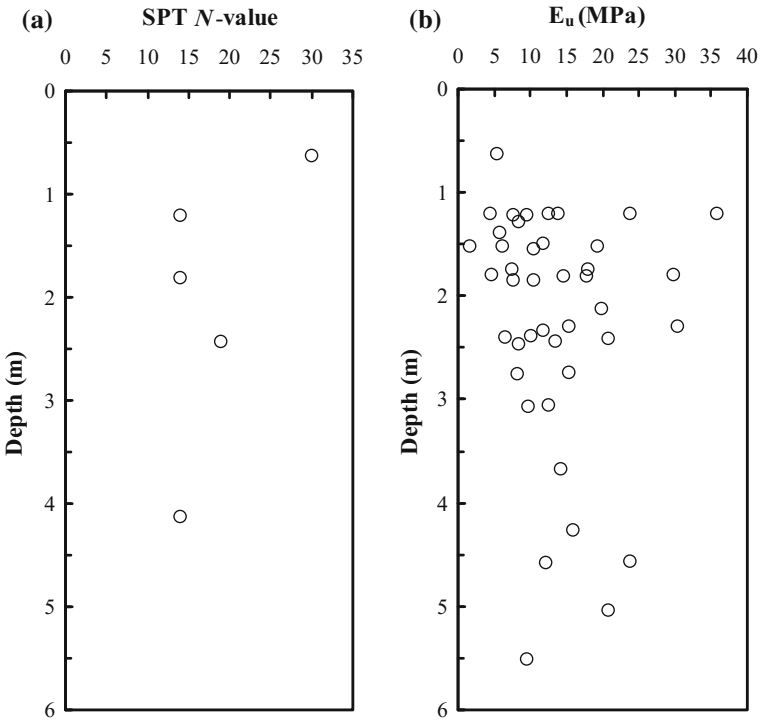

Fig. 2.6 Standard penetration test (SPT) *N*-value and undrained Young's modulus measured by pressuremeter tests at the clay site of the NGES at Texas A&M University. **a** SPT *N*-values. **b** Undrained Young' modulus. (after Briaud 2000)

permeability, SPT *N*-values, cone tip resistance, and Young's modulus and limit pressure measured by pressuremeter tests. Figure 2.6a shows 5 SPT *N*-values versus depth obtained from the SPT tests performed within the top stiff clay layer (Briaud 2000). Pressuremeter tests were also carried out in the top clay layer (Briaud 2000). Figure 2.6b shows in total 42 measurements of the undrained Young's modulus E_u from pressuremeter tests performed at different depths in the top clay layer (Briaud 2000). The SPT *N*-values and undrained Young's modulus E_u obtained from the clay site are used to illustrate and validate the probabilistic approach developed in Chap. 5 of this book.

In addition, Akkaya and Vanmarcke (2003) summarized inherent spatial variability of soil properties at the NGES, and they concluded that (1) for the clay site (see Fig. 2.5a), the mean value, coefficient of variation, and correlation length of cone tip resistance range from 0.14 MPa to 0.27 MPa, from 50 % to 82 %, and from 3.3 m to 9.0 m, respectively, and their respective mean values are 0.2 MPa, 65 %, and 5.4 m; (2) for the sand site (see Fig. 2.5b), the mean value, coefficient of variation, and correlation length of cone tip resistance range from 7.0 MPa to 9.0 MPa, from 30 % to 76 %, and from 1.6 m to 6.4 m, respectively, and their

respective mean values are 8.4 MPa, 50 %, and 3.3 m. Note that the average cone tip resistance (i.e., from 7.0 to 9.0 MPa) of the sand site compares favorably with that reported by Briaud (2000) (see Table 2.6), while the average cone tip resistance (e.g., from 0.14 to 0.27 MPa) of the clay site is much less than that reported by Briaud (2000) (see Table 2.6).

2.5 Probabilistic Slope Stability Analysis

Various uncertainties exist in slope engineering, such as inherent spatial variability of soil properties, uncertainties in subsurface stratigraphy, and modeling errors associated with geotechnical models. Probability theory and statistics provide a rational vehicle to account for these uncertainties in slope stability analysis. In the context of probability theory and statistics, reliability of slope stability is frequently measured by a "reliability index" (β) or slope failure probability (P_f), which is defined as the probability that the minimum factor of safety (FS) is less than unity (i.e., $P_f = P(FS < 1)$). For reference, Table 2.7 lists β and P_f for representative geotechnical components and systems and their expected performance levels. The value of β commonly ranges from 1 to 5, corresponding to P_f varying from about 0.16 to 3×10^{-7}. Geotechnical designs require a β-value of at least 2 (i.e., $P_f < 0.023$) for an expected performance level better than "poor." Relatively small P_f (information on the tail of probability distribution) is of great interest to geotechnical practitioners. The reliability index β and slope failure probability P_f can be estimated by various solution methods, such as the first-order second-moment method (FOSM) (e.g., Tang et al. 1976; Christian et al. 1994; Hassan and Wolff 1999), first-order reliability method (FORM, also referred to as Hasofer–Lind method) (e.g., Low and Tang 1997; Low et al. 1998; Low 2003), direct Monte Carlo simulation (MCS) method (e.g., El-Ramly et al. 2002; Griffiths and Fenton 2004; El-Ramly et al. 2005), and subset simulation (e.g., Au 2001; Au and Beck 2001 and 2003; Au et al. 2009, 2010; Wang et al. 2009). These methods are briefly reviewed in the following subsections.

Table 2.7 Relationship between reliability index (β) and probability of failure (P_f) (after U.S. Army Corps of Engineers 1997)

Reliability index β	Probability of failure $P_f = \Phi(-\beta)^a$	Expected performance level
1.0	0.16	Hazardous
1.5	0.07	Unsatisfactory
2.0	0.023	Poor
2.5	0.006	Below average
3.0	0.001	Above average
4.0	0.00003	Good
5.0	0.0000003	High

[a] $\Phi(\odot)$ = Standard normal cumulative distribution function

2.5.1 First-Order Second-Moment Method (FOSM)

Let $g(\underline{x})$ denote the performance function (or deterministic model) of slope stability used to calculate FS of slope stability, in which $\underline{x} = [x_1, x_2, \ldots, x_k]$ is a set of random variables representing uncertain model parameters in the performance function. Consider, for example, that FS is normally distributed. By FOSM, the reliability index β is calculated as (e.g., Cornell 1969; Ang and Tang 1984; Baecher and Christian 2003)

$$\beta = \frac{\mu_{FS} - 1}{\sigma_{FS}} \tag{2.12}$$

in which μ_{FS} and σ_{FS} are the mean and standard deviation of FS, respectively. μ_{FS} is the value of $g(\underline{x})$ calculated at mean values μ_i, i = 1, 2, …, k of random variables x_i, i = 1, 2, …, k, i.e., $\mu_{FS} = g(\mu_1, \mu_2, \ldots, \mu_k)$, and σ_{FS} is calculated as

$$\sigma_{FS} = \sqrt{\sum_{i=1}^{k} \sigma_i^2 \left(\frac{\partial g}{\partial x_i}\right)^2 + \sum_{i=1}^{k} \sum_{j \neq i}^{k} \rho_{ij} \sigma_i \sigma_j \frac{\partial g}{\partial x_i} \frac{\partial g}{\partial x_j}} \tag{2.13}$$

in which σ_i, i = 1, 2, …, k are standard deviations of random variables x_i, i = 1, 2, …, k, respectively; $\frac{\partial g}{\partial x_i}$, i = 1, 2, …, k are partial derivatives of the performance function with respect to x_i, i = 1, 2, …, k, respectively; ρ_{ij} is the correlation coefficient between two different uncertain parameters x_i and x_j, where $i \neq j$. Then, the slope failure probability P_f is calculated as $1 - \Phi(\beta)$, in which Φ is the cumulative distribution function of a standard Gaussian random variable (e.g., Baecher and Christian 2003).

FOSM is a relatively simple approach for performing probabilistic slope stability analysis. It, however, requires an analytical model of slope stability analysis, which is differentiable for all uncertain variables (i.e., x_i, i = 1, 2, …, k) involved in the model. In addition, FOSM usually uses a predefined critical slip surface of slope failure and does not account for uncertainties of the critical slip surface.

2.5.2 First-Order Reliability Method (FORM)

By FORM, the reliability index β is interpreted as a measure of the distance between the peak of the multivariate distribution of the uncertain variables (e.g., the joint distribution of $\underline{x} = [x_1, x_2, \ldots, x_k]$) and the critical point on the failure boundary in a dimensionless space. It is calculated as (e.g., Hasofer and Lind 1974; Ang and Tang 1984; Low and Tang 1997; Baecher and Christian 2003)

$$\beta = \min_{x_i \in \Omega_F} \sqrt{\left[\frac{\underline{x} - \underline{\mu}}{\underline{\sigma}}\right]^T \underline{\rho}^{-1} \left[\frac{\underline{x} - \underline{\mu}}{\underline{\sigma}}\right]} \tag{2.14}$$

in which Ω_F represents the failure domain; $\underline{\mu}$ is a mean vector of uncertain variables, i.e., $\underline{\mu} = [\mu_1, \mu_2, \ldots, \mu_k]$; $\underline{\sigma}$ is a standard deviation vector of uncertain variables, i.e., $\underline{\sigma} = [\sigma_1, \sigma_2, \ldots, \sigma_k]$; and $\underline{\rho}$ is the correlation matrix of uncertain variables. Note that the equivalent mean values and standard deviations of random variables should be used in Eq. (2.14) when uncertain variables are not normally distributed (Ang and Tang 1984).

Equation (2.14) has been implemented in a spreadsheet environment with the aid of the built-in optimization tool "Solver" for probabilistic slope stability analysis by Low and Tang (1997), Low et al. (1998), and Low (2003). Center coordinates and radius of circular slip surfaces were also considered as additional optimization variables by Low (2003) so that variation of potential critical slip surfaces was implicitly factored in the analysis. However, because of the limitation of the optimization tool used, FORM tends to overestimate β and underestimate P_f (Wang et al. 2009).

2.5.3 Direct Monte Carlo Simulation (Direct MCS)

MCS is a numerical process of repeatedly calculating a mathematical or empirical operator, in which the variables within the operator are random or contain uncertainties with prescribed probability distributions (e.g., Ang and Tang 2007; Wang 2011; Wang et al. 2011). The numerical result from each repetition of the numerical process is considered as a sample of the true solution of the operator, analogous to an observed sample from a physical experiment. Consider, for example, probabilistic slope stability analysis in which the mathematical operator (i.e., the performance function $g(\underline{x})$) involves calculation of the factor of safety, FS, and judgment of occurrence of failure (i.e., $FS < 1$). The direct MCS starts with the characterization of probability distributions of uncertainties concerned, as well as the slope geometry and other necessary information, followed by the generation of n_{MC} sets of random samples according to the prescribed probability distributions. Using the deterministic model $g(\underline{x})$ and the n_{MC} sets of random samples, n_{MC} possible values of FS are obtained. Then, statistical analysis is performed to estimate P_f or β, with the slope failure defined as $FS < 1$ (e.g., Baecher and Christian 2003).

Monte Carlo simulation (MCS) is gaining popularity in the reliability analysis of slope stability due to its robustness and conceptual simplicity. It can be performed together with various types of deterministic models, such as limit equilibrium

methods (e.g., El-Ramly et al. 2002, 2005, and 2006), finite element method (e.g., Griffiths and Fenton 2004; Xu and Low 2006; Griffiths et al. 2009; Hicks and Spencer 2010), and response surface method (e.g., Xu and Low 2006). It, however, suffers from a lack of efficiency and resolution at small probability levels and does not offer insights into the relative contributions of uncertainties to the failure probability (Baecher and Christian 2003).

2.5.4 Subset Simulation

Recently, an advanced Monte Carlo simulation called "subset simulation" has been applied to probabilistic slope stability analysis to improve the efficiency and resolution of the MCS (Au et al. 2009; Wang et al. 2009; Au et al. 2010). Subset simulation makes use of conditional probability and Markov Chain Monte Carlo Simulation (MCMCS) method to efficiently compute small tail probability (Au 2001; Au and Beck 2001 and 2003). It expresses a small probability event as a sequence of intermediate events $\{F_1, F_2, \ldots, F_m\}$ with larger conditional probability and employs specially designed Markov Chains to generate conditional samples of these intermediate events until the final target failure region is achieved. For the slope stability problem, let $Y = 1/FS$ be the critical response (Au et al. 2009; Wang et al. 2009; Au et al. 2010). The probability of $Y = 1/FS$ being larger than a given value y (i.e., $P(Y = 1/FS > y)$) is of interest, and let $0 < y_1 < y_2 < \cdots < y_{m-1} < y_m = y$ be an increasing sequence of intermediate threshold values. The sequence of intermediate events $\{F_1, F_2, \ldots, F_m\}$ are chosen as $F_i = \{Y > y_i, i = 1, 2, \ldots, m\}$ for these intermediate threshold values. By sequentially conditioning on the event $\{F_i, i = 1, 2, \ldots, m\}$, the failure probability can be written as

$$P_f = P(F_m) = P(F_1) \prod_{i=2}^{m} P(F_i|F_{i-1}) \tag{2.15}$$

where $P(F_1)$ is equal to $P(Y > y_1)$ and $P(F_i|F_{i-1})$ is equal to $\{P(Y > y_i|Y > y_{i-1}): i = 2, \ldots, m\}$. In implementations, $y_1, y_2, \ldots y_m$ are generated adaptively using information from simulated samples so that the sample estimate of $P(F_1)$ and $\{P(F_i|F_{i-1}): i = 2, \ldots, m\}$ always corresponds to a common specified value of conditional probability p_0 ($p_0 = 0.1$ is found to be a good choice) (Au 2001; Au and Beck 2001 and 2003; Au et al. 2010). The efficient generation of conditional samples is pivotal in the success of subset simulation, and it is made possible through the machinery of MCMCS (e.g., Beck and Au 2002; Robert and Casella 2004). The procedures of subset simulation and MCMCS are described in the following two subsections, respectively.

2.5.4.1 Subset Simulation Procedure

Subset simulation starts with direct MCS, in which N MCS samples are generated. The Y values of the N samples are calculated and ranked in an ascending order. The $(1 - p_0)N$th value in the ascending list of Y values is chosen as y_1, and hence, the sample estimate for $P(F_1) = P(Y > y_1)$ is always p_0. In other words, there are p_0N samples with $F_1 = Y > y_1$ among the samples generated by direct MCS. Then, starting from the p_0N samples with $F_1 = Y > y_1$, MCMCS is used to simulate $(1 - p_0)N$ additional conditional samples given $F_1 = Y > y_1$, so that there are a total of N samples with $F_1 = Y > y_1$. The Y values of the N samples with $F_1 = Y > y_1$ are ranked again in an ascending order, and the $(1 - p_0)N$th value in the ascending list of Y values is chosen as y_2, which defines the $F_2 = Y > y_2$. Note that the sample estimate for $P(F_2|F_1) = P(Y > y_2|Y > y_1)$ is also equal to p_0. Similarly, there are p_0N samples with $F_2 = Y > y_2$ and these samples provide "seeds" for the application of MCMCS to simulate additional $(1 - p_0)N$ conditional samples with $F_2 = Y > y_2$ so that there are N conditional samples with $F_2 = Y > y_2$. The procedure is repeated m times until the probability space of interest (i.e., the sample domain with $Y > y_m$) is achieved. Note that the subset simulation procedures contain $m + 1$ steps, including one direct MCS to generate unconditional samples and m steps of MCMCS to simulate conditional samples. The $m + 1$ steps of simulations are referred to as "$m + 1$ levels" in subset simulation (Au and Beck 2001 and 2003; Au et al. 2010), and in total, these $m + 1$ levels of simulations generate $N + m(1 - p_0)N$ samples.

2.5.4.2 Markov Chain Monte Carlo Simulation (MCMCS)

MCMCS method is a numerical process that simulates a sequence of samples of random variables $\underline{x}$ as a Markov Chain with the joint PDF of random variables as the Markov Chain's limiting stationary distribution (e.g., Beck and Au 2002; Robert and Casella 2004). It provides a feasible way to generate n_{MCMC} samples from an arbitrary PDF, particularly when the PDF is complicated and is difficult to express analytically and explicitly. There are several MCMCS methods, such as Metropolis algorithm (Metropolis et al. 1953), original Metropolis–Hastings (MH) algorithm (Hastings 1970), and modified Metropolis–Hastings (MMH) algorithm (Au 2001; Au and Beck 2001 and 2003). For example, the original MH algorithm is described below.

Consider, for example, random variables $\underline{x} = [x_1, x_2, \ldots, x_k]$ with a prescribed joint PDF $P(\underline{x})$. In MH algorithm, the Markov Chain starts with an initial state $\underline{x}_1$ that is predefined by the user (e.g., conditional failure samples generated in the previous subset simulation level). Then, the ith state of the $\underline{x}$ Markov Chain, $\underline{x}_i$, $i = 2, 3, \ldots, n_{\mathrm{MCMC}}$, (e.g., $\underline{x}_2$ for the second state) is generated from its previous state $\underline{x}_{i-1}$ (e.g., the initial state $\underline{x}_1$ for $\underline{x}_2$). A candidate sample $\underline{x}_i^*$, $i = 2, 3, \ldots, n_{\mathrm{MCMC}}$, for the ith state is generated from the proposal PDF $f(\underline{x}_i^*|\underline{x}_{i-1})$ (e.g., a normal distribution or uniform distribution centered at the previous state $\underline{x}_{i-1}$). The candidate sample $\underline{x}_i^*$

is, however, not necessarily to be accepted as the ith state of the $\underline{x}$ Markov Chain (i.e., $\underline{x}_i$). The chance to accept the candidate sample $\underline{x}_i^*$ as the $\underline{x}_i$ depends on the "acceptance ratio," r_a, which is calculated as

$$r_a = \frac{P(\underline{x}_i^*)}{P(\underline{x}_{i-1})} \times \frac{f(\underline{x}_{i-1}|\underline{x}_i^*)}{f(\underline{x}_i^*|\underline{x}_{i-1})} \quad \text{for} \quad i = 2, 3, \ldots, n_{\text{MCMC}} \tag{2.16}$$

in which $P(\underline{x}_i^*)$ and $P(\underline{x}_{i-1})$ are PDF values of $\underline{x}_i^*$ and $\underline{x}_{i-1}$, respectively; $f(\underline{x}_i^*|\underline{x}_{i-1})$ is the conditional PDF value of $\underline{x}_i^*$ given $\underline{x}_{i-1}$; $f(\underline{x}_{i-1}|\underline{x}_i^*)$ is the conditional PDF value of $\underline{x}_{i-1}$ given $\underline{x}_i^*$. Using PDF of $\underline{x}$ and the predefined proposal PDF, the acceptance ratio of $\underline{x}_i^*$ is obtained from Eq. (2.16). When r_a is greater than unity, the candidate sample $\underline{x}_i^*$ is accepted as the ith state of the $\underline{x}$ Markov Chain (i.e., $\underline{x}_i$). When r_a falls within [0, 1], the probability to accept $\underline{x}_i^*$ as $\underline{x}_i$ is r_a.

In implementation, a random number u is generated from a uniform distribution with a range from zero to one. If u is less than r_a, $\underline{x}_i^*$ is accepted as $\underline{x}_i$, i.e., $\underline{x}_i = \underline{x}_i^*$. Otherwise, $\underline{x}_i^*$ is rejected, and $\underline{x}_i$ is taken as the previous state $\underline{x}_{i-1}$, i.e., $\underline{x}_i = \underline{x}_{i-1}$. For example, the r_a value for the candidate sample $\underline{x}_2^*$ is calculated from Eq. (2.16) using $\underline{x}_1$ and $\underline{x}_2^*$, and the second state $\underline{x}_2$ is then determined accordingly by comparing the values of r_a and u. Starting from the initial state $\underline{x}_1$, the procedure described above is repeated $n_{\text{MCMC}} - 1$ times to generate $n_{\text{MCMC}} - 1$ samples of $\underline{x}$, i.e., $\underline{x}_i, i = 2, 3, \ldots, n_{\text{MCMC}}$. This leads to a Markov Chain that is comprised of n_{MCMC} $\underline{x}$ samples (including the initial sample).

The original MH algorithm reduces to the Metropolis algorithm when the proposal PDF is symmetric, i.e., $f(\underline{x}_i^*|\underline{x}_{i-1}) = f(\underline{x}_{i-1}|\underline{x}_i^*)$. Both the Metropolis algorithm and the original MH algorithm are not applicable for high-dimensional problems because the acceptance ratio becomes exponentially small as the dimension k increases and most of candidate samples are rejected (Au 2001; Au and Beck 2001). The MMH algorithm was proposed for high-dimensional problems by Au (2001) and Au and Beck (2003). In MMH algorithm, the random vector $\underline{x}$ with k independent components is simulated by generating the candidate sample of $\underline{x}$ component by component, so that the acceptance ratio of individual component of the candidate sample of $\underline{x}$ does not decrease to zero when the dimension increases (Au 2001). In this book, MCMCS method is applied in both subset simulation (see Chaps. 7 and 8) and the probabilistic approach developed for site characterization (see Chap. 5).

Appendix 2.1: Several Empirical Correlations Reported by Kulhawy and Mayne (1990)

This appendix summarizes several empirical correlations reported by Kulhawy and Mayne (1990). Table 2.8 shows empirical correlations between standard penetration test (SPT) N-value and effective friction angle of sands, the relative density of

Table 2.8 Relationship between SPT *N*-value and effective friction angle of sand (after Kulhawy and Mayne 1990)

SPT *N*-value	Relative density	Approximate effective friction angle ϕ'(°)	
		a	b
0–4	Very loose	<28	<30
4–10	Loose	28–30	30–35
10–30	Medium	30–36	35–40
30–50	Dense	36–40	40–45
>50	Very dense	>41	>45

[a]After Peck et al. (1974)
[b]After Meyerhof (1956)

which ranges from very loose to very dense. When the SPT *N*-value is less than 4, the effective friction angle is less than 28° by Peck et al. (1974) or less than 30° by Meyerhof (1956). The effective friction angle increases as the SPT *N*-value increases. When the SPT *N*-value is greater than 50, the effective friction angle is greater than 41° by Peck et al. (1974) or greater than 45° by Meyerhof (1956).

Table 2.9 gives an empirical correlation between cone tip resistance measured by cone penetration test (CPT) and effective friction angle of sands, the relative density of which ranges from very loose to very dense. As the cone tip resistance increases from less than 2.0 MPa to larger than 20 MPa, the effective friction angle increases from less than 30° to larger than 45°.

Table 2.10 summarizes the minimum and maximum of the typical dry unit weight of sands, including silty sand, clean sand, micaceous sand, and silty sand and gravel. The minimum and maximum of the dry unit weight range from 13.6 kN/m^3 to 14.0 kN/m^3 and from 20.0 kN/m^3 to 22.9 kN/m^3, respectively.

Table 2.11 summarizes typical effective friction angles of sands. Typical effective friction angles of loose and dense uniform sands with round grains are 27.5° and 34.0°, respectively. Typical effective friction angles of loose and dense well-graded sands with angular grains are 33.0° and 45.0°, respectively. Typical effective friction angles of loose and dense sandy gravels are 35.0° and 50.0°, respectively. In addition, typical effective friction angles of loose and dense silty

Table 2.9 Relationship between cone tip resistance q_c and effective friction angle of sand (after Kulhawy and Mayne 1990)

Normalized cone tip resistance $q_{c1}p_a^b$	Relative density	Approximate effective friction angle ϕ' (°)[a]
<20	Very loose	<30
20–40	Loose	30–35
40–120	Medium	35–40
120–200	Dense	40–45
>200	Very dense	>45

[a]After Meyerhof (1956)
[b]p_a is the standard atmospheric pressure

Table 2.10 Typical soil unit weight of sand (after Kulhawy and Mayne 1990)

Soil type	Dry unit weight (kN/m^3)[a]	
	Minimum	Maximum
Silty sand	13.6	20.0
Clean, fine to coarse sand	13.3	21.7
Micaceous sand	12.0	18.8
Silty sand and gravel	14.0	22.9

[a]After Hough (1969)

Table 2.11 Typical values of effective friction angle of sand (after Kulhawy and Mayne 1990)

Soil type	Effective friction angle ϕ'(°)[a]	
	Loose	Dense
Sand, round grains, uniform	27.5	34.0
Sand, angular grains, well graded	33.0	45.0
Sandy gravels	35.0	50.0
Silty sand	27.0–33.0	30.0–34.0
Inorganic silt	27.0–30.0	30.0–34.0

[a]After Terzaghi and Peck (1967)

sands range from 27.0° to 33.0° and from 30.0° to 34.0°, respectively. For loose and dense inorganic silts, their typical effective friction angles range from 27.0° to 30.0° and from 30.0° to 34.0°, respectively.

Figure 2.7 shows variation of effective friction angle of soils as a function of dry unit weight, relative density, and soil type. The effective friction angle increases as the dry unit weight and relative density increase. Figure 2.8 shows an empirical correlation between cone tip resistance q_c measured by CPT and the effective friction angle ϕ' of sands, which is a semilog regression equation

$$\phi' = 17.6 + 11.0 \log\left(\frac{q_c/p_a}{\sqrt{\sigma'_{v0}/p_a}}\right) \tag{2.17}$$

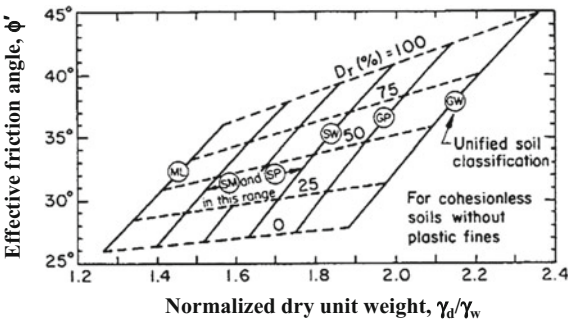

Fig. 2.7 Relationship between the normalized dry unit weight and effective friction angle (after Kulhawy and Mayne 1990)

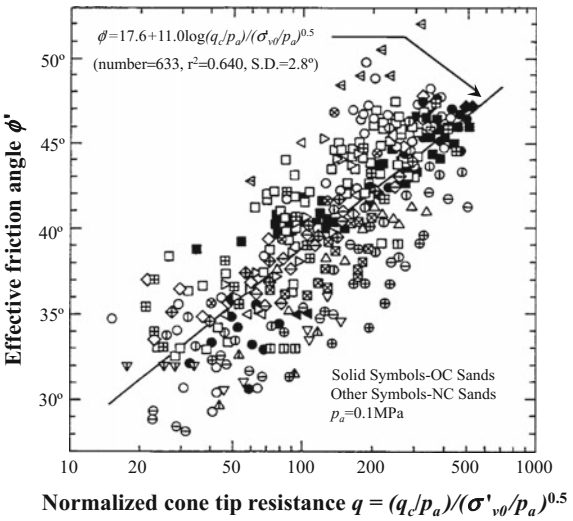

Fig. 2.8 Regression between normalized cone tip resistance and effective friction angle (after Kulhawy and Mayne 1990 and Wang et al. 2010)

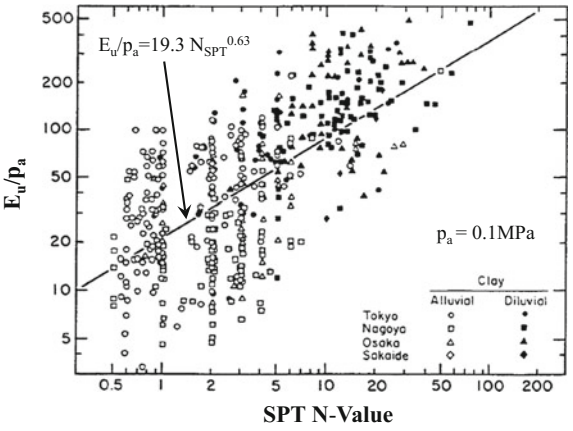

Fig. 2.9 Regression between SPT *N*-value and undrained Young's modulus of clay (after Ohya et al. 1982; Kulhawy and Mayne 1990; Phoon and Kulhawy 1999b and Wang and Cao 2013)

in which σ'_{v0} and p_a are vertical effective stress and standard atmospheric pressure (i.e., 0.1 MPa), respectively. Figure 2.9 shows an empirical correlation between SPT *N*-value (i.e., N_{SPT}) and undrained Young's modulus E_u of clay, and it is written as

$$E_u/p_a = 19.3N_{SPT}^{0.63} \tag{2.18}$$

In Eq. (2.18), the undrained Young's modulus E_u of clay is measured by pressuremeter tests.

References

Akkaya, A.D., and E.H. Vanmarcke. 2003. Estimation of spatial correlation of soil parameters based on data from the Texas A&M University NGES. In *Probabilistic site characterization at the national geotechnical experimentation sites*, Geotechnical Special Publication No. 121, 29–40.

Alonso, E.E., and R.J. Krizek. 1975. Stochastic formulation of soil properties. In *Proceedings of 2nd international conference on applications of statistics and probability in soil and structure engineering*, 9–32. Auchen, Germany.

Ang, A.H.S., and W.H. Tang. 2007. *Probability concepts in engineering: Emphasis on applications to civil and environmental engineering*. New York: Wiley.

Ang, A.H.S., and W.H. Tang. 1984. *Probability concepts in engineering planning and design*, vol. II. New York: Wiley.

Au, S.K. 2001. *On the solution of first excursion probability by simulation with applications to probabilistic seismic performance assessment*. Ph.D. thesis. California, USA: California Institute of Technology.

Au, S.K., and J.L. Beck. 2001. Estimation of small failure probabilities in high dimensions by subset simulation. *Probabilistic Engineering Mechanics* 16(4): 263–277.

Au, S.K., and J.L. Beck. 2003. Subset simulation and its applications to seismic risk based on dynamic analysis. *Journal of Engineering Mechanics* 129(8): 1–17.

Au, S.K., Z. Cao, and Y. Wang. 2010. Implementing advanced Monte Carlo simulation under spreadsheet environment. *Structural Safety* 32(5): 281–292.

Au, S.K., Y. Wang, and Z. Cao. 2009. Reliability analysis of slope stability by advanced simulation with spreadsheet. In *Proceedings of the second international symposium on geotechnical safety and risk*, 275–280. Gifu, Japan, June 2009.

Baecher, G.B. 1983. Professional judgment and prior probabilities in engineering risk assessment. In *Proceedings of fourth international conference on application of statistics and probability in soil and structural engineering*, 635–650. Universita di Firenze (Italy), Pitagora Editrice.

Baecher, G.B. 1987. *Statistical analysis of geotechnical data*. Report No. GL-87-1. Vicksburg, VA: U.S. Army Engineer Waterways Experiment Station.

Baecher, G.B., and J.T. Christian. 2003. *Reliability and statistics in geotechnical engineering*, 605 pp. Hoboken, New Jersey: Wiley.

Beach, L., V. Barnes, and J. Christensen-Szalanski. 1986. Beyond heuristics and biases: A contingency model of judgmental forecasting. *Journal of Forecasting* 5(3): 143–157.

Beck, J.L., and S.K. Au. 2002. Bayesian updating of structural models and reliability using Markov chain Monte Carlo simulation. *Journal of Engineering Mechanics* 128(4): 380–391.

Beck, J.L., and L.S. Katafygiotis. 1998. Updating models and their uncertainties. I: Bayesian statistical framework. *Journal of Engineering Mechanics* 124(4): 455–461.

Beck, J.L., and K.V. Yuen. 2004. Model selection using response measurements: Bayesian probabilistic approach. *Journal of Engineering Mechanics* 130(2): 192–203.

Benoit, J. 2000. The United States National Geotechnical Experimentation Sites program: The first decades. In *National geotechnical experimentation sites*, Geotechnical Special Publication No. 93, 1–25.

Berger, J.O. 1985. *Statistical decision theory and Bayesian analysis*. Springer.

Bjerrum, L. 1973. Problems of soil mechanics and constructions on soft clays. In *Proceedings of 8th international conference on soil mechanics and foundation engineering*, Moscow, Vol. 3, 111–159.

Bleisten, N., and R. Handelsman. 1986. *Asymptotic expansions of integrals*. New York: Dover.

Box, G.E.P., and G.M. Jenkins. 1970. *Time series analysis: Forecasting and control*, 553 pp. San Fransisco: Holden-Day.

Briaud, J.L. 2000. The National Geotechnical Experimentation Sites at Texas A&M University: Clay and sand. A summary. In *National geotechnical experimentation sites*, Geotechnical Special Publication No. 93: 26–51.

Briaud, J.L. 1992. *The pressuremeter*. London, UK: Taylor & Francis.
Campanella, R.G., D.S. Wickremesinghe, and P.K. Robertson. 1987. Statistical treatment of cone penetrometer test data. In *Proceedings of 5th international conference on applications of statistics and probability in soil and structure engineering*, Vancouver, 1011–1019.
Cao, Z., Y. Wang, and S.K. Au. 2011. CPT-Based probabilistic characterization of effective friction angle of sand. In *Geotechnical risk assessment and management*, Geotechnical Special Publication No. 224, 403–410.
Carlin, B.P., and T.A. Louis. 1996. *Bayes and Empirical Bayes methods for data analysis*. London: Chapman and Hall.
Cetin, K.O., and C. Ozan. 2009. CPT-Based probabilistic soil characterization and classification. *Journal of Geotechnical and Geoenvironmental Engineering* 135(1): 84–107.
Cheung, R.W.M., and W.H. Tang. 2005. Realistic assessment of slope reliability for effective landslide hazard management. *Geotechnique* 55(1): 85–94.
Ching, J., K.K. Phoon, and Y.C. Chen. 2010. Reducing shear strength uncertainties in clays by multivariate correlations. *Canadian Geotechnical Journal* 47(1): 16–33.
Christian, J.T., C.C. Ladd, and G.B. Baecher. 1994. Reliability applied to slope stability analysis. *Journal of Geotechnical Engineering* 120(12): 2180–2207.
Clayton, C.R.I. 1995. *The Standard Penetration Test (SPT): Methods and use*. Report 143. UK: Construction Industry Research and Information Association.
Clayton, C.R.I., M.C. Matthews, and N.E. Simons. 1995. *Site investigation*. Cambridge, Mass., USA: Blackwell Science.
Clemen, R.T. 1996. *Making hard decisions: An introduction to decision analysis*. Pacific Grove: Duxbury Press.
Cornell, C.A. 1969. A probability-based structural code. *Journal of the American Concrete Institute* 66(12): 974–985.
DeGroot, D.J., and G.B. Baecher. 1993. Estimating autocovariance of in situ soil properties. *Journal of the Geotechnical Engineering Division* 119(GT1): 147–166.
DiMillio, A.F., and G. Prince. 1993. *National Geotechnical Experimentation Sites*.
El-Ramly, H., N.R. Morgenstern, and D.M. Cruden. 2002. Probabilistic slope stability analysis for practice. *Canadian Geotechnical Journal* 39: 665–683.
El-Ramly, H., N.R. Morgenstern, and D.M. Cruden. 2005. Probabilistic assessment of stability of a cut slope in residual soil. *Geotechnique* 55(1): 77–84.
El-Ramly, H., N.R. Morgenstern, and D.M. Cruden. 2006. Lodalen slide: A probabilistic assessment. *Canadian Geotechnical Journal* 43(9): 956–968.
Fenton, G. 1999a. Estimation for stochastic soil models. *Journal of Geotechnical and Geoenvironmental Engineering* 125(6): 470–485.
Fenton, G. 1999b. Random field modeling of CPT data. *Journal of Geotechnical and Geoenvironmental Engineering* 125(6): 486–498.
Fenton, G., and D.V. Griffiths. 2008. *Risk assessment in geotechnical engineering*. Hoboken, New Jersey: Wiley.
Fenton, G.A., and D.V. Griffiths. 2007. Reliability-based deep foundation design. In *Probabilistic applications in geotechnical engineering*, Geotechnical Special Publication No. 170, 1–12.
Fenton, G.A., and D.V. Griffiths. 2003. Bearing capacity prediction of spatially random c-ϕ soils. *Canadian Geotechnical Journal* 40(1): 54–65.
Fenton, G.A., and D.V. Griffiths. 2002. Probabilistic foundation settlement on spatially random soil. *Journal of Geotechnical and Geoenvironmental Engineering* 128(5): 381–390.
Fenton, G.A., D.V. Griffiths, and M.B. Williams. 2005. Reliability of traditional retaining wall design. *Geotechnique* 55(1): 55–62.
Fischhoff, B., P. Slovic, and S. Lichtenstein. 1977. Knowing with certainty: The appropriateness of extreme confidence. *Journal of Experimental Psychology: Human Perception and Performance* 3(4): 552–564.
Garthwaite, P.H., J.B. Kadane, and A.O. Hagan. 2005. Statistical methods for eliciting probability distributions. *Journal of the American Statistical Association* 100(470): 680–700.
Geotechnical Engineering Office. 2000. *Geoguide 2: Guide to site investigation*. Hong Kong.

Griffiths, D.V., and G.A. Fenton. 2004. Probabilistic slope stability analysis by finite elements. *Journal of Geotechnical and Geoenvironmental Engineering* 130(5): 507–518.

Griffiths, D.V., J. Huang, and G.A. Fenton. 2009. Influence of spatial variability on slope reliability using 2-d random fields. *Journal of Geotechnical and Geoenvironmental Engineering* 135(10): 1367–1378.

Hassan, A.M., and T.F. Wolff. 1999. Search algorithm for minimum reliability index of earth slopes. *Journal of Geotechnical and Geoenvironmental Engineering* 125(4): 301–308.

Hasofer, A.M., and N.C. Lind. 1974. Exact and invariant second-moment code format. *Journal of the Engineering Mechanical Division* 100(EM1): 111–121.

Hastings, W.K. 1970. Monte Carlo sampling methods using Markov chains and their applications. *Biometrika* 57: 97–109.

Hicks, M.A. 2005. Risk and variability in geotechnical engineering. *Geotechnique* 55(1): 1–2.

Hicks, M.A., and W.A. Spencer. 2010. Influence of heterogeneity on the reliability and failure of a long 3D slope. *Computers and Geotechnics* 37: 948–955.

Hogarth, R.M. 1975. Cognitive processes and the assessment of subjective probability distributions. *Journal of the American Statistical Association* 70(350): 271–289.

Hough, B.K. 1969. *Basic soils engineering*, 634 pp. New York: Ronald Press.

Houlsby, G. 1988. *Discussion session contribution*. Birmingham: Penetration Testing in the U.K.

Jaksa, M.B. 1995. *The influence of spatial variability on the geotechnical design properties of a stiff, overconsolidated clay*. Ph.D. thesis. University of Adelaide.

Jeffreys, H. 1983. *Theory of probability*. Oxford, New York: Oxford University Press.

Juang, C.H., D.V. Rosowsky, and W.H. Tang. 1999. Reliability-based method for assessing liquefaction potential of soils. *Journal of Geotechnical and Geoenvironmental Engineering* 125(8): 684–689.

Jung, B.C., P. Gardoni, and G. Biscontin. 2008. Probabilistic soil identification based on cone penetration tests. *Geotechnique* 58(7): 591–603.

Katafygiotis, L.S., C. Papadimitriou, and H.F. Lam. 1998. A probabilistic approach to structural model updating. *Soil Dynamics Earthquake Engineering* 17(7–8): 495–507.

Katafygiotis, L.S., and J.L. Beck. 1998. Updating models and their uncertainties: Model identifiability. *Journal of Engineering Mechanics* 124(4): 463–467.

Klammler, H., M. McVay, D. Horhota, and P. Lai. 2010. Influence of spatially variable side friction on single drilled shaft resistance and LRFD resistance factors. *Journal of Geotechnical and Geoenvironmental Engineering* 138(8): 1114–1123.

Koriat, A., S. Lichtenstein, and B. Fischhoff. 1980. Reasons for confidence. *Journal of Experimental Psychology: Human Learning and Memory* 6(2): 107–118.

Kulhawy, F.H., and P.W. Mayne. 1990. *Manual on estimating soil properties for foundation design*, 306 pp. Report EL 6800. Palo Alto: Electric Power Research Institute.

Kulhawy, F.H. 1996. From Casagrande's 'Calculated Risk' to reliability-based design in foundation engineering. *Civil Engineering Practice* 11(2): 43–56.

Kulhawy, F.H., and C.H. Trautmann. 1996. Estimation of in-situ test uncertainty. In *Uncertainty in the geologic environment: From theory to practice*, Geotechnical Special Publication, 58(I): 269–286.

Lacasse, S., and F. Nadim. 1996. Uncertainties in characterizing soil properties. In *Uncertainty in the geologic environment: From theory to practice*, Geotechnical Special Publication, 58(I): 49–75.

Low, B.K. 2003. Practical probabilistic slope stability analysis. In *Proceeding of 12th Panamerican conference on soil mechanics and geotechnical engineering and 39th U.S. rock mechanics symposium*, 2777–2784. Cambridge, Massachusetts: M.I.T. Verlag Gluckauf Gmbh Essen.

Low, B.K., R.B. Gilbert, and S.G. Wright. 1998. Slope reliability analysis using generalized method of slices. *Journal of Geotechnical and Geoenvironmental Engineering* 124(4): 350–362.

Low, B.K., and W.H. Tang. 1997. Reliability analysis of reinforced embankments on soft ground. *Canadian Geotechnical Journal* 34(5): 672–685.

Lumb, P. 1974. Application of statistics in soil mechanics. In *Soil Mechanics—New Horizons*, Chapter 3, ed. Lee, I.K., 44–111. New York.

Lumb, P. 1966. The variability of natural soils. *Canadian Geotehcnial Journal* 3(2): 74–97.

Lunne, T., P.K. Robertson, and J.J.M. Powell. 1997. *Cone penetration testing in geotechnical practice*, 317 pp. London, U.K.: Blackie-Academic Publishing.

Mair, R.J., and D.M. Wood. 1987. *Pressuremeter testing: Methods and interpretation*. London: Ciria.

Maritz, J.S., and T. Lwin. 1989. *Empirical Bayes methods*. London: Chapman and Hall.

Mayne, P.W. 2007. *Cone penetration testing: A synthesis of highway practice*, National Cooperative Highway Research Program (NCHRP) Synthesis 368. Washington, D.C.: Transportation Research Board.

Mayne, P.W., B. Christopher, and J. DeJong. 2002. *Subsurface investigations—geotechnical site characterization*, No. FHWA NHI-01-031. Washington, D.C.: Federal Highway Administration, U.S. Department of Transportation.

Meyerhof, G.G. 1956. Penetration tests and bearing capacity of cohesionless soils. *Journal of the Soil Mechanics and Foundations Division* 82(SM1): 1–19.

Mesri, G. 1989. Stability analysis with the simple and advanced $\phi = 0$ method for a failed dike. *Discussion Soils and Foundations* 23(4): 133–137.

Metropolis, N., A. Rosenbluth, M. Rosenbluth, and A. Teller. 1953. Equations of state calculations by fast computing machines. *Journal of Chemical Physics* 21(6): 1087–1092.

Mitchell, J.K., and K. Soga. 2005. *Fundamentals of soil behavior*. Hoboken, New Jersey: Wiley.

Nawari, N.O., and R. Liang. 2000. Reliability of measured geotechnical properties. In *Performance confirmation of constructed geotechnical facilities*, Geotechnical Special Publication No. 94, 322–335.

Ohya, S., T. Imai, and M. Matsubara. 1982. Relationships between N value by SPT and LLT pressuremeter results. In *Proceedings of 2nd European symposium on penetration testing*, Vol. 1, 125–130. Amsterdam.

Orchant, C.J., F.H. Kulhawy, and C.H. Trautmann. 1988. *Reliability-based design of foundations for transmission line structures*: *Critical evaluation of in-situ test methods*. Report TR-5507(2). Palo Alto: Electric Power Research Institute.

Papadimitriou, C., J.L. Beck, and L.S. Katafygiotis. 1997. Asymptotic expansions for reliability and moments of uncertain systems. *Journal of Engineering Mechanics* 123(12): 1219–1229.

Peck, R.B., W.E. Hansen, and T.H. Thornburn. 1974. *Foundation engineering*, 514 pp. New York: Wiley.

Phoon, K.K., and F.H. Kulhawy. 1999a. Characterization of geotechnical variability. *Canadian Geotechnical Journal* 36(4): 612–624.

Phoon, K.K., and F.H. Kulhawy. 1999b. Evaluation of geotechnical property variability. *Canadian Geotechnical Journal* 36(4): 625–639.

Phoon, K.K., and F.H. Kulhawy. 1996. On quantifying inherent soil variability. In *Uncertainty in the geologic environment: From theory to practice*, Geotechnical Special Publication No. 58 (I): 326–340.

Phoon, K.K., F.H. Kulhawy, and M.D. Grigoriu. 1995. *Reliability-based design of foundations for transmission line structures*. Report TR-105000. Palo Alto: Electric Power Research Institute.

Phoon, K.K., S.T. Quek, and P. An. 2003. Identification of statistically homogeneous soil layers using modified Bartlett statistics. *Journal of Geotechnical and Geoenviornmental Engineering* 129(7): 649–659.

Ravi, V. 1992. Statistical modeling of spatial variability of undrained strength. *Canadian Geotechnical Journal* 29: 721–729.

Robert, C., and G. Casella. 2004. *Monte Carlo statistical methods*. Springer.

Robertson, P.K. 2009. Interpretation of cone penetration tests—a unified approach. *Canadian Geotechnical Journal* 46: 1337–1355.

Robertson, P.K. 1990. Soil classification using the cone penetration test. *Canadian Geotechnical Journal* 27(1): 151–158.

Robertson, P.K., and R.G. Campanella. 1983a. Interpretation of cone penetration tests. Part I: Sand. *Canadian Geotechnical Journal* 20(4): 718–733.

Robertson, P.K., and R.G. Campanella. 1983b. Interpretation of cone penetration tests. Part II: Clay. *Canadian Geotechnical Journal* 20(4): 734–745.

Schuster, M.J., C.H. Juang, M.J.S. Roth, and D.V. Rosowsky. 2008. Reliability analysis of building serviceability problems caused by excavation. *Geotechnique* 58(9): 743–749.

Shannon, C.E., and W. Weaver. 1949. *The mathematical theory of communication*. Urbana, IL: University of Illinois Press.

Silva, F., T.W. Lambe, and W.A. Marr. 2008. Probability and risk of slope failure. *Journal of Geotechnical and Geoenvironmental Engineering* 134(12): 1691–1699.

Siu, N.O., and D.L. Kelly. 1998. Bayesian parameter estimation in probabilistic risk assessment. *Reliability Engineering and System Safety* 62(1–2): 89–116.

Sivia, D.S., and J. Skilling. 2006. *Data analysis: A Bayesian tutorial*. New York: Oxford University Press.

Smith, G.F., P.G. Benson, and S.P. Curley. 1991. Belief, knowledge, and uncertainty: A cognitive perspective on subjective probability. *Organizational Behavior and Human Decision Processes* 48(2): 291–321.

Tang, W.H., M.S. Yucemen, and A.H.S. Ang. 1976. Probability based short-term design of slope. *Canadian Geotechnical Journal* 13: 201–215.

Terzaghi, K., and R.B. Peck. 1967. *Soil mechanics in engineering practice*, 729 pp. New York: Wiley.

Tversky, A., and D. Kahneman. 1974. Judgment under uncertainty: Heuristics and biases. *Science* 185: 1124–1131.

U.S. Army Corps of Engineers. 1997. Engineering and design: introduction to probability and reliability methods for use in geotechnical engineering. *Engineer Technical Letter 1110-2-547*. Washington, D.C.: Department of the Army.

Vanmarcke, E.H. 1977. Probabilistic modeling of soil profiles. *Journal of Geotechnical Engineering* 103(11): 1127–1246.

Vanmarcke, E.H. 1983. *Random fields: Analysis and synthesis*. Cambridge: MIT Press.

Vick, S.G. 2002. *Degrees of belief: Subjective probability and engineering judgment*. Reston, Virginia: ASCE Press.

Vick, S.G. 1997. Dam safety risk assessment: New directions. *Water Power and Dam Construction* 49(6).

Wang, Y. 2011. Reliability-based design of spread foundations by Monte Carlo simulations. *Geotechnique* 61(8): 677–685.

Wang, Y., S.K. Au, and F.H. Kulhawy. 2011. Expanded reliability-based design approach for drilled shafts. *Journal of Geotechnical and Geoenvironmental Engineering* 137(2): 140–149.

Wang, Y., S.K. Au, and Z. Cao. 2010. Bayesian approach for probabilistic characterization of sand friction angles. *Engineering Geology* 114(3–4): 354–363.

Wang, Y., and Z. Cao. 2013. Probabilistic characterization of Young's modulus of soil using equivalent samples. *Engineering Geology* 159(12): 106–118.

Wang, Y., Z. Cao, S.K. Au, and Q. Wang. 2009. Reliability analysis of a benchmark problem for slope stability. In *Proceedings of the second international symposium on geotechnical safety and risk*, 89–93. Gifu Japan, June 2009.

Wang, Y., and T.D. O'Rourke. 2007. Interpretation of secant shear modulus degradation characteristics from pressuremeter tests. *Journal of Geotechnical and Geoenvironmental Engineering* 133(12): 1556–1566.

Wroth, C.P. 1984. The interpretation of in-situ soil tests. *Geotechnique* 34(4): 449–489.

Xu, B., and B.K. Low. 2006. Probabilistic stability analyses of embankments based on Finite-Element Method. *Journal of Geotechnical and Geoenvironmental Engineering* 132(11): 1444–1454.

Yan, W.M., K.V. Yuen, and G.L. Yoon. 2009. Bayesian probabilistic approach for the correlations of compression index for marine clays. *Journal of Geotechnical and Geoenvironmental Engineering* 135(12): 1932–1940.

Yuen, K.V. 2010. Recent development of Bayesian model class selection and applications in civil engineering. *Structural Safety* 32(5): 338–346.

Zhang, F. 2011. *Bayesian ambient modal identification incorporating multiple setups*. Ph.D. thesis. Hong Kong: City University of Hong Kong.

Zhang, J., W.H. Tang, and L.M. Zhang. 2010a. Efficient probabilistic back-analysis of slope stability model parameters. *Journal of Geotechnical and Geoenvironmental Engineering* 136 (1): 99–109.

Zhang, J., L.M. Zhang, and W.H. Tang. 2009. Bayesian framework for characterizing geotechnical model uncertainty. *Journal of Geotechnical and Geoenvironmental Engineering* 135(7): 932–940.

Zhang, L.L., J. Zhang, L.M. Zhang, and W.H. Tang. 2010b. Back analysis of slope failure with Markov chain Monte Carlo simulation. *Computers and Geotechnics* 37(7–8): 905–912.

Zhang, L.M., W.H. Tang, L.L. Zhang, and J.G. Zheng. 2004. Reducing uncertainty of prediction from empirical correlations. *Journal of Geotechnical and Geoenvironmental Engineering* 130 (5): 526–534.

Chapter 3
Bayesian Framework for Geotechnical Site Characterization

3.1 Introduction

Geotechnical site characterization is a multi-step process that aims to delineate underground stratigraphy (i.e., the number and boundaries of soil layers) and to estimate soil properties for geotechnical analysis and/or designs (e.g., Clayton et al. 1995; Mayne et al. 2002). It relies on both prior knowledge (i.e., the site information available prior to the project) and site observation data (i.e., project-specific test results). How to combine systematically prior knowledge and site observation data, however, remains a challenging task for geotechnical engineers (Wang et al. 2010). This problem is further complicated by various uncertainties incorporated in prior knowledge and site observation data and the fact that only a limited number of project-specific test results are obtained during geotechnical site characterization.

To address these challenges, this chapter develops a Bayesian framework for geotechnical site characterization, which combines systematically prior knowledge and project-specific test results and deals rationally with the inherent spatial variability of soils and various uncertainties (e.g., statistical uncertainty, measurement errors, and transformation uncertainty associated with the transformation model) arising during site characterization in a probabilistic manner. It starts with description of uncertainty propagation during geotechnical site characterization, followed by probabilistic modeling of inherent spatial variability of soils and transformation uncertainty and development of the Bayesian framework. Based on the Bayesian framework, the soil property and boundaries of statistically homogenous soil layers are characterized probabilistically, and a Bayesian model class selection method is developed to determine the most probable number of statistically homogenous soil layers.

Z. Cao et al., *Probabilistic Approaches for Geotechnical Site Characterization and Slope Stability Analysis*, DOI 10.1007/978-3-662-52914-0_3

3.2 Uncertainty Propagation During Geotechnical Site Characterization

Figure 3.1 shows schematically the procedure of geotechnical site characterization together with inherent spatial variability of soils and uncertainties arising during site characterization. Geotechnical site characterization often starts with desk study and site reconnaissance, which provide prior knowledge about the site, including existing information collected from various sources (see Table 2.1) and engineers' expertise (e.g., Clayton et al. 1995; Mayne et al. 2002). The prior knowledge is not perfect information but is associated with some uncertainties (e.g., Baecher 1983; Vick 2002), such as inherent spatial variability and measurement errors incorporated in existing data, subjective uncertainties of engineers' expertise, and so forth.

After desk study and site reconnaissance, in situ investigation work (e.g., in situ boring and testing) and laboratory testing can be performed to provide project-specific test results, i.e., site observation data. The site observation data fluctuates because of inherent spatial variability of soils that are formed and existed long before the project, measurement errors arising from imperfect test equipments and/or procedural–operator errors, and statistical uncertainty resulted from insufficient tests (e.g., Vanmarcke 1977; Christian et al. 1994; Kulhawy 1996; Phoon and Kulhawy 1999a; Baecher and Christian 2003). In addition, the measured soil property is not necessary to be the soil property that can be directly used in geotechnical analysis and/or designs (i.e., the design soil property x_d). The design soil property x_d can be estimated from in situ and laboratory test results (i.e., site

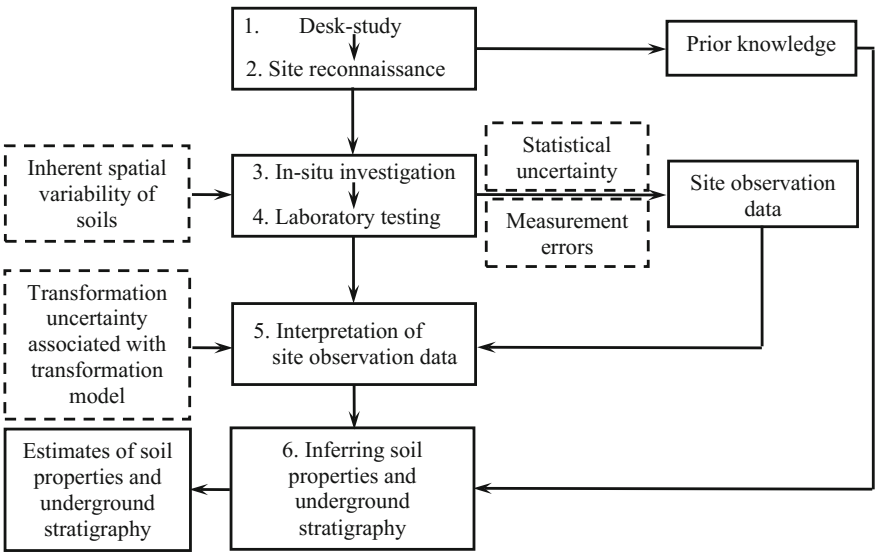

Fig. 3.1 Geotechnical site characterization and uncertainty propagation (After Wang et al. 2016)

observation data of the measured soil property x_t) by a transformation model between x_d and x_t. It is well recognized that the transformation model is associated with uncertainties (i.e., transformation uncertainty or modeling error) because of insufficient knowledge about the relationship between x_d and x_t (e.g., Phoon and Kulhawy 1999b; Baecher and Christian 2003). Transformation uncertainty is incorporated into the interpretation outcomes of the site observation data as well as the inherent spatial variability of soils and statistical uncertainty and measurement errors associated with the site observation data, as shown in Fig. 3.1.

Geotechnical engineers then utilize both the interpretation outcomes of site observation data and prior knowledge to infer the ground conditions (including soil properties and underground stratigraphy) for geotechnical analysis and/or designs. The estimations of soil properties and underground stratigraphy are, therefore, affected by uncertainties in prior knowledge and uncertainties (i.e., inherent spatial variability of soils, statistical uncertainty and measurement errors associated with site observation data, and transformation uncertainty) in the interpretation outcomes of the site observation data. Note that statistical uncertainty and measurement errors are usually combined with site observation data (see Fig. 3.1). They can, therefore, be taken into account through site observation data, as discussed in Sect. 3.4 "Bayesian Framework." In the next section, probability theory is applied to modeling the inherent spatial variability of the design soil property, x_d and the transformation uncertainty associated with the transformation model.

3.3 Uncertainty Modeling

3.3.1 Inherent Spatial Variability

Probability models, e.g., random variables and random fields (e.g., Lumb 1966; Vanmarcke 1977, 1983; Wang et al. 2010; Cao et al. 2011), are applied in this book to characterize inherent spatial variability of a design soil property x_d in a soil profile containing N_L statistically homogenous soil layers. The number N_L in the first part of this chapter (i.e., before Sect. 3.6 "The Most Probable Number of Soil Layers") is considered as a given value. It is then determined among several possible values by a Bayesian model class selection method proposed in Sect. 3.6.

Let $\underline{X}_d = \left[\underline{x}_{d1}, \underline{x}_{d2}, \ldots \underline{x}_{dN_L}\right]^T$ denote a set of random variables representing x_d at different locations in the soil profile with N_L soil layers, in which $\underline{x}_{dn} = [x_{d1}, x_{d2}, \ldots, x_{dk_n}], n = 1, 2, \ldots, N_L$, are k_n random variables representing x_d within the nth soil layer. Note that the value of k_n depends on the adopted probabilistic model and can vary from 1 to a certain positive integer. When $k_n > 1$, $\underline{x}_{dn} = [x_{d1}, x_{d2}, \ldots, x_{dk_n}]$ are a series of random variables representing x_d at k_n different locations within the nth soil layer, i.e., a random field of x_d in the nth soil layer. When $k_n = 1$, the design soil property x_d within the nth soil layer is represented by one random variable, and the inherent variability of x_d in the nth soil layer

is characterized by the probability distribution of the random variable. In the context of probability theory, the probability distribution of $\underline{X}_d$ (i.e., random variables and random fields) depends on several model parameters (e.g., statistics of random variables) $\Theta_{PN_L} = \left[\underline{\theta}_{P1}, \underline{\theta}_{P2}, \ldots, \underline{\theta}_{PN_L}\right]$, where $\underline{\theta}_{Pn}, n = 1, 2, \ldots, N_L$, is the vector of model parameters of the nth soil layer. Note that Θ_{PN_L} (or $\underline{\theta}_{Pn}, n = 1, 2, \ldots, N_L$) is generally comprised of model parameters that are used to describe the inherent spatial variability of x_d (e.g., the mean, standard deviation, and correlation length) and to delineate the boundaries of statistically homogenous soil layers (e.g., thicknesses of soil layers).

3.3.2 *Transformation Uncertainty*

The design soil property x_d can be estimated from project-specific test results of the measured property x_t by a transformation model between them (e.g., Kulhawy and Mayne 1990; Phoon and Kulhawy 1999b; Mayne et al. 2002). Consider, for example, a transformation model as follows

$$x_d = f_T(x_t; \varepsilon_T) \tag{3.1}$$

in which $f_T(\cdot; \varepsilon_T)$ represents the transformation model between x_d and x_t; ε_T is a random variable representing the transformation uncertainty or modeling error.

Let $\underline{X}_t = \left[\underline{x}_{t1}, \underline{x}_{t2}, \ldots, \underline{x}_{tN_L}\right]^T$ denote a set of values of x_t measured at different locations in the soil profile with N_L soil layers, in which $\underline{x}_{tn} = [x_{t1}, x_{t2}, \ldots, x_{tk_n}] n = 1, 2, \ldots, N_L$, are k_n values of x_t measured within the nth soil layer. For the nth soil layer, x_{ti}, $i = 1, 2, \ldots, k_n$, are corresponding to x_{di}, $i = 1, 2, \ldots, k_n$ by Eq. (3.1), respectively. Such a relationship can be generalized to all components in $\underline{X}_t$ and $\underline{X}_d$. Since the probability distribution of $\underline{X}_d$ relies on model parameters $\Theta_{PN_L} = [\underline{\theta}_{P1}, \underline{\theta}_{P2}, \ldots, \underline{\theta}_{PN_L}]$, the probability distribution of $\underline{X}_t$ also depends on Θ_{PN_L}. Knowledge of model parameters Θ_{PN_L} is required to completely define the probability distribution of $\underline{X}_t$. The next section presents a Bayesian framework for updating the knowledge of model parameters Θ_{PN_L} using prior knowledge and site observation data $\underline{X}_t$.

3.4 Bayesian Framework

Figure 3.2 shows schematically the Bayesian framework developed in this chapter. Under the Bayesian framework, the updated knowledge (i.e., posterior knowledge) of model parameters Θ_{PN_L} is reflected by their joint posterior distributions (e.g., Ang and Tang 2007; Wang et al. 2010; Cao et al. 2011)

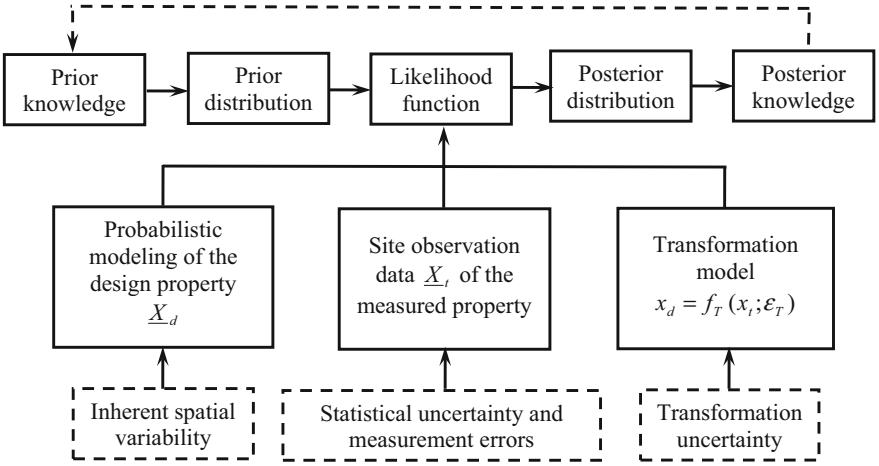

Fig. 3.2 Illustration of the Bayesian framework (After Wang et al. 2016)

$$P(\Theta_{PN_L}|\underline{X}_t, N_L) = K_{N_L} P(\underline{X}_t|\Theta_{PN_L}, N_L) P(\Theta_{PN_L}|N_L) \tag{3.2}$$

in which $K_{N_L} = 1/P(\underline{X}_t|N_L)$ is a normalizing constant for a given number N_L of soil layers; $P(\underline{X}_t|\Theta_{PN_L}, N_L)$ is the likelihood function that reflects the model fit with site observation data $\underline{X}_t$ within the N_L soil layers; $P(\Theta_{PN_L}|N_L)$ is the prior distribution of model parameters of the N_L soil layers.

The likelihood function $P(\underline{X}_t|\Theta_{PN_L}, N_L)$ is the probability density function (PDF) of $\underline{X}_t$ for a given set of model parameters Θ_{PN_L} (i.e., for a given model). It quantifies probabilistically the information on Θ_{PN_L} provided by site observation data $\underline{X}_t$. As shown in Fig. 3.2, derivation of the likelihood function depends on the probabilistic model $\underline{X}_d$ of inherent spatial variability of the design soil property x_d and the transformation model. The inherent spatial variability of x_d and transformation uncertainty associated with the transformation model are explicitly addressed by the probabilistic model $\underline{X}_d$ and the random variable ε'_T, respectively. In addition, statistical uncertainty and measurement errors are also incorporated into the Bayesian framework through site observation data $\underline{X}_t$ (see Fig. 3.2).

The prior distribution $P(\Theta_{PN_L}|N_L)$ is the PDF of Θ_{PN_L} according to the prior knowledge, and it reflects probabilistically prior knowledge about Θ_{PN_L} in the absence of data. It can be estimated from prior knowledge using subjective probability assessment methods (e.g., Siu and Kelly 1998; Vick 2002; Garthwaite et al. 2005). When there is no prevailing knowledge on Θ_{PN_L}, an uninformative prior distribution (e.g., uniform distribution) can be applied in the Bayesian framework.

The posterior distribution $P(\Theta_{PN_L}|\underline{X}_t, N_L)$ is a joint distribution of model parameters Θ_{PN_L} and reflects the posterior knowledge on Θ_{PN_L}. As mentioned before, Θ_{PN_L} (or $\underline{\theta}_{Pn}, n = 1, 2, \ldots, N_L$) includes model parameters that are used to describe the inherent spatial variability of x_d and to delineate the boundaries of N_L

statistically homogenous soil layers. Therefore, the posterior distribution $P(\Theta_{PN_L}|\underline{X}_t, N_L)$ characterizes probabilistically both the design soil property x_d and the boundaries of the N_L soil layers.

3.5 Probability Distribution of the Design Soil Property

For a given set of prior knowledge and site observation data, there are many sets of possible values of model parameters Θ_{Pn} (or $\underline{\theta}_{Pn}, n = 1, 2, \ldots, N_L$). Each set of Θ_{Pn} has its corresponding plausibility, which is defined by the posterior distribution $P(\Theta_{PN_L}|\underline{X}_t, N_L)$ given by Eq. (3.2). For the nth soil layer, the posterior distribution $P(\underline{\theta}_{Pn}|\underline{X}_t, N_L)$, n = 1, 2, …, N_L, of model parameters $\underline{\theta}_{Pn}$ of the soil layer can be obtained from integration on $P(\Theta_{PN_L}|\underline{X}_t, N_L)$ over the space of model parameters of the other soil layers.

Using the Theorem of Total Probability, the joint PDF of the design soil property $\underline{x}_{dn} = [x_{d1}, x_{d2}, \ldots, x_{dk_n}]$ within the nth statistically homogenous soil layer is then expressed as

$$P(\underline{x}_{dn}|\underline{X}_t, N_L) = \int P(\underline{x}_{dn}|\underline{\theta}_{Pn}) P(\underline{\theta}_{Pn}|\underline{X}_t, N_L) d\underline{\theta}_{Pn}, \quad n = 1, 2, \ldots, N_L \tag{3.3}$$

in which $P(\underline{x}_{dn}|\underline{\theta}_{Pn})$, n = 1, 2, …, N_L, is the conditional joint PDF of $\underline{x}_{dn}$ for a given set of model parameters $\underline{\theta}_{Pn}$ of the nth statistically homogenous soil layer, which depends on the probabilistic model adopted to model the inherent variability of x_d.

3.6 The Most Probable Number of Soil Layers

3.6.1 Bayesian Model Class Selection Method

The number N_L of statistically homogenous soil layers is considered as a given value in the previous sections. This section considers the number of statistically homogenous layers as a variable k and utilizes a Bayesian model class selection method (Beck and Yuen 2004; Yan et al. 2009; Yuen 2010) to determine the most probable value k^* (or the most probable model class) among a pool of candidate model classes. A model class herein is referred to a family of stratification models that share the same number (e.g., k) of statistically homogenous soil layers but have different model parameters Θ_{PN_L}. Let N_{Lmax} denote the maximum possible number of soil layers tested. Then, the model class number k is a positive integer varying from 1 to N_{Lmax}. Subsequently, there are N_{Lmax} candidate model classes M_k, k = 1, 2, …, N_{Lmax}, and the kth model class M_k has k statistically homogenous layers. The most probable model class M_k^* is the one that has the maximum plausibility (or occurrence probability), among all candidate model classes, for a given set of site

observation data $\underline{X}_t$. The most probable layer number k^*, therefore, can be determined by comparing the conditional probabilities $P(M_k|\underline{X}_t)$ for all candidate model classes (i.e., $k = 1, 2, \ldots, N_{\text{Lmax}}$) and selecting the one with the maximum value of $P(M_k|\underline{X}_t)$.

According to Bayes' theorem, $P(M_k|\underline{X}_t)$ is written as (Beck and Yuen 2004; Yan et al. 2009; Yuen 2010)

$$P(M_k|\underline{X}_t) = P(\underline{X}_t|M_k)P(M_k)/P(\underline{X}_t), k = 1, 2, \ldots, N_{\text{Lmax}} \tag{3.4}$$

where $P(\underline{X}_t)$ is the PDF of $\underline{X}_t$, and it is constant and independent of M_k; $P(\underline{X}_t|M_k)$ is the conditional PDF of $\underline{X}_t$ for a given model class M_k; $P(M_k)$ is the prior probability of model class M_k. $P(\underline{X}_t|M_k)$ is frequently referred to as the "evidence" for the model class M_k provided by site observation data $\underline{X}_t$, and it increases as the plausibility of $\underline{X}_t$ conditional on M_k increases. Calculation of $P(\underline{X}_t|M_k)$, $P(M_k)$, and $P(\underline{X}_t)$ is discussed in the following three subsections.

3.6.2 Calculation of the Evidence

By the Theorem of Total Probability (e.g., Ang and Tang 2007), the evidence $P(\underline{X}_t|M_k)$ for model class M_k can be expressed as

$$P(\underline{X}_t|M_k) = \int P(\underline{X}_t|\Theta_{Pk}, M_k)P(\Theta_{Pk}|M_k)d\Theta_{Pk}, k = 1, 2, \ldots, N_{Lmax} \tag{3.5}$$

in which $P(\underline{X}_t|\Theta_{Pk},M_k)$ is the likelihood function of M_k; $P(\Theta_{Pk}|M_k)$ is the prior distribution of model parameters Θ_{Pk} of M_k. The likelihood function and prior distribution developed in Sect. 3.4 "Bayesian Framework" for a soil profile given N_L soil layers can be applied directly in Eq. (3.5) by setting $N_L = k$.

3.6.3 Calculation of Prior Probability

The prior probability $P(M_k)$ reflects the prior knowledge on the number of soil layers and can be estimated from the prior knowledge. In the case of no prevailing prior knowledge on the number of soil layers (i.e., uniformly distributed prior), the N_{Lmax} candidate model classes have the same prior probability, and hence, $P(M_k)$ can be taken as a constant $1/N_{\text{Lmax}}$. Then, based on Eq. (3.4), $P(M_k|\underline{X}_t)$ is proportional to the evidence $P(\underline{X}_t|M_k)$ for the model class M_k. Since the most probable model class M_k^* corresponds to the maximum value of $P(M_k|\underline{X}_t)$, it also has the maximum value of $P(\underline{X}_t|M_k)$. In other words, the most probable model class M_k^* can be selected by comparing the values of $P(\underline{X}_t|M_k)$ among N_{Lmax} candidate model classes.

3.6.4 Calculation of Probability Density Function of Site Observation Data

After $P(\underline{X}_t|M_k)$ and $P(M_k)$ are obtained for each model class, $P(\underline{X}_t)$ can be calculated by the Theorem of Total Probability (e.g., Ang and Tang 2007), and it is written as

$$P(\underline{X}_t) = \sum_{k=1}^{N_{Lmax}} P(\underline{X}_t|M_k)P(M_k) \tag{3.6}$$

The conditional probability $P(M_k|\underline{X}_t)$ of model class M_k for a given set of site observation data $\underline{X}_t$ is then calculated using Eqs. (3.4) to (3.6) together with the prior probability $P(M_k)$. The calculation is repeated N_{Lmax} times for the N_{Lmax} candidate model classes, and the values of $P(M_k|\underline{X}_t)$ for the N_{Lmax} model classes are obtained. By comparing these $P(M_k|\underline{X}_t)$ values, the most probable model class M_k^* and the most probable number k^* of statistically homogenous soil layers are determined. In addition, it is also worthwhile to note that $P(M_k|\underline{X}_t)$ is proportional to $P(\underline{X}_t|M_k)P(M_k)$ for the model class M_k by Eq. (3.4) because $P(\underline{X}_t)$ is a normalizing constant and is independent of M_k. Therefore, the most probable model class M_k^* can also be determined by comparing the values of $P(\underline{X}_t|M_k)P(M_k)$ of N_{Lmax} candidate model classes. By this means, the calculation of $P(\underline{X}_t)$ can be avoided when determining the most probable model class M_k^* and the most probable number k^* of statistically homogenous soil layers.

3.7 Summary and Conclusions

This chapter revisited the procedure of geotechnical site characterization from an uncertainty propagation point of view. The propagation of inherent spatial variability of soils, statistical uncertainty, measurement errors, and transformation uncertainty was depicted explicitly during different stages of geotechnical site characterization (see Fig. 3.1). Then, a Bayesian framework was developed for geotechnical site characterization, which integrates systematically prior knowledge and site observation data to characterize probabilistically the design soil property and boundaries of statistically homogenous soil layers. The Bayesian framework addresses directly and explicitly the inherent spatial variability of the design soil property and accounts rationally for various uncertainties (i.e., statistical uncertainty, measurement errors, and transformation uncertainty) that arise during geotechnical site characterization. Based on the Bayesian framework, the most probable number of statistically homogenous soil layers is then determined through a Bayesian model class selection method.

It is also worthwhile to note that posterior knowledge provided by the Bayesian framework reflects the state of knowledge on soil properties based on prior knowledge and the site observation data. The posterior knowledge can be taken as the prior knowledge to update the knowledge of soil properties again when new site observation data are obtained from further in situ and laboratory testing, as shown by the dashed line in Fig. 3.2. The knowledge on soil properties therefore can be updated in a row and be accumulated progressively as site observation data increases.

References

Ang, A.H.S., and W.H. Tang. 2007. *Probability concepts in engineering: emphasis on applications to civil and environmental engineering*. New York: John Wiley and Sons.

Baecher, G.B. 1983. Professional judgment and prior probabilities in engineering risk assessment. In *Proceedings of Fourth International Conference on Application of Statistics and Probability in Soil and Structural Engineering*. Universita di Firenze (Italy), Pitagora Editrice, 635−650.

Baecher, G.B., and J.T. Christian. 2003. *Reliability and statistics in geotechnical engineering*. Hoboken, New Jersey: John Wiley & Sons. 605p.

Beck, J.L., and K.V. Yuen. 2004. Model selection using response measurements: Bayesian probabilistic approach. *Journal of Engineering Mechanics* 130(2): 192–203.

Cao, Z., Y. Wang, and S.K. Au. 2011. CPT-Based probabilistic characterization of effective friction angle of sand. In *Geotechnical Risk Assessment and Management*, *Geotechnical Special Publication No. 224*, pp. 403–410.

Christian, J.T., C.C. Ladd, and G.B. Baecher. 1994. Reliability applied to slope stability analysis. *Journal of Geotechnical Engineering* 120(12): 2180–2207.

Clayton, C.R.I., M.C. Matthews, and N.E. Simons. 1995. *Site investigation*. Cambridge, Mass., USA: Blackwell Science.

Garthwaite, P.H., J.B. Kadane, and A.O. Hagan. 2005. Statistical methods for eliciting probability distributions. *Journal of the American Statistical Association* 100(470): 680–700.

Kulhawy, F.H., and P.W. Mayne. 1990. *Manual on Estimating Soil Properties for Foundation Design, Report EL 6800*. Palo Alto: Electric Power Research Inst. 306p.

Kulhawy, F.H. 1996. From Casagrande's 'Calculated Risk' to reliability-based design in foundation engineering. *Civil Engineering Practice* 11(2): 43–56.

Lumb, P. 1966. The variability of natural soils. *Canadian Geotechnical Journal* 3(2): 74–97.

Mayne, P.W., B.R. Christopher, and J. DeJong. 2002. *Subsurface Investigations—Geotechnical Site Characterization, No. FHWA NHI-01-031, Federal Highway Administration, U. S. Department of Transportation, Washington D.C.*

Phoon, K.K., and F.H. Kulhawy. 1999a. Characterization of geotechnical variability. *Canadian Geotechnical Journal* 36(4): 612–624.

Phoon, K.K., and F.H. Kulhawy. 1999b. Evaluation of geotechnical property variability. *Canadian Geotechnical Journal* 36(4): 625–639.

Siu, N.O., and D.L. Kelly. 1998. Bayesian parameter estimation in probabilistic risk assessment. *Reliability Engineering and System Safety* 62(1–2): 89–116.

Vanmarcke, E.H. 1977. Probabilistic modeling of soil profiles. *Journal of Geotechnical Engineering* 103(11): 1127–1246.

Vanmarcke, E.H. 1983. *Random fields: analysis and synthesis*. Cambridge: MIT Press.

Vick, S.G. 2002. *Degrees of belief: Subjective probability and engineering judgment*. Reston, Virginia: ASCE Press.

Wang, Y., S.K. Au, and Z. Cao. 2010. Bayesian approach for probabilistic characterization of sand friction angles. *Engineering Geology* 114(3–4): 354–363.

Wang, Y., Z. Cao, and D. Li. 2016. Bayesian perspective on geotechnical variability and site characterization. *Engineering Geology* 203: 117–125.

Yan, W.M., K.V. Yuen, and G.L. Yoon. 2009. Bayesian probabilistic approach for the correlations of compression index for marine clays. *Journal of Geotechnical and Geoenvironmental Engineering* 135(12): 1932–1940.

Yuen, K.V. 2010. Recent development of Bayesian model class selection and applications in civil engineering. *Structural Safety* 32(5): 338–346.

Chapter 4
Quantification of Prior Knowledge Through Subjective Probability Assessment

4.1 Introduction

Prior distribution is an essential component of the Bayesian framework developed in the previous chapter, and it reflects the prior knowledge (including the existing information collected from various sources and engineers' expertise) obtained during preliminary stages (e.g., desk study or site reconnaissance) of geotechnical site characterization. When only a typical range of a soil parameter concerned is available as the prior knowledge, a uniform prior distribution of the soil parameter that covers the typical range can be used in the Bayesian framework. As the information provided by prior knowledge improves, a more sophisticated and informative prior distribution can be estimated from prior knowledge. Based on the prior knowledge obtained from desk study and/or site reconnaissance, a subjective probability assessment framework (SPAF) is proposed in this chapter to assist engineers in quantifying the information provided by prior knowledge and estimating the prior distribution from prior knowledge.

This chapter starts with brief description of uncertainties in prior knowledge, followed by development of the SPAF based on a stage cognitive model of engineers' cognitive process. Each stage of the cognitive process is implemented in the proposed SPAF, and several suggestions are provided for each stage to assist engineers in utilizing prior knowledge in a relatively rational way and reducing effects of cognitive biases and limitations mentioned in Chap. 2. The proposed SPAF is applied to characterize probabilistically the sand effective friction angle at a US National Geotechnical Experimentation Site (NGES) at Texas A&M University, and it is illustrated under two scenarios: one with sparse prior knowledge and the other with a reasonable amount of prior knowledge.

Z. Cao et al., *Probabilistic Approaches for Geotechnical Site Characterization and Slope Stability Analysis*, DOI 10.1007/978-3-662-52914-0_4

4.2 Uncertainties in Prior Knowledge

Prior knowledge includes the existing information (e.g., geological information, geotechnical problems and properties, and groundwater conditions) about a specific site collected from various sources (see Table 2.1 in Chap. 2) during desk study and site reconnaissance and engineers' expertise (Clayton et al. 1995; Mayne et al. 2002). The collected information contains various uncertainties, such as inherent variability of soil properties, measurement errors, statistical uncertainty incorporated in historical data, and transformation uncertainty associated with regression models used to interpret the historical data. In addition, the quantity and quality of the expertise of an individual engineer depend on various external factors (e.g., educational background and career experience) and internal factors (e.g., personal attributes and individual cognitive process) (Vick 2002). Variations of such external and internal factors lead to uncertainties in engineers' expertise. Because of uncertainties in the existing information and engineers' expertise, estimates of soil properties and their statistics from prior knowledge are uncertain results rather than cut-and-dried conclusions. Such uncertain estimates are, therefore, referred to as "prior uncertain estimates" in this book.

The plausibility of prior uncertain estimates reflects the confidence level (or degrees-of-belief) of prior knowledge on such estimates, and it can be evaluated intuitively and qualitatively through engineering judgments (including various cognitive heuristics discussed in Chap. 2, such as availability heuristic, representative heuristic, and anchoring and adjustment heuristic). Because of various cognitive biases and limitations (see Chap. 2), outcomes from such intuitive and qualitative evaluations might deviate from the actual beliefs of engineers and be inconsistent with basic probability axioms (Vick 2002). The next section presents a subjective probability assessment framework (SPAF), in which subjective probability is applied to quantify the plausibility of prior uncertain estimates of statistics $\boldsymbol{\Theta} = [\theta_1, \theta_2, \ldots, \theta_{n_m}]$ (e.g., the mean, standard deviation, and correlation length) of the soil property x concerned and to express engineering judgments on x and its statistics $\boldsymbol{\Theta}$ in a probabilistic manner. By this means, the plausibility of prior uncertain estimates of $\boldsymbol{\Theta}$ is quantified by the probability distribution of $\boldsymbol{\Theta}$, which can be taken as the prior distribution of $\boldsymbol{\Theta}$ in the Bayesian framework developed in Chap. 3.

4.3 Subjective Probability Assessment Framework (SPAF)

Engineers formulate subjective probability through a series of internal cognitive activities (i.e., cognitive process). These cognitive activities can be divided into several stages and be described by a stage cognitive model. Consider, for example, the stage cognitive model presented by Vick (2002), as shown in Fig. 4.1. Based on the stage cognitive model, a subjective probability assessment framework (SPAF) is developed in this section, which is shown in Fig. 4.1.

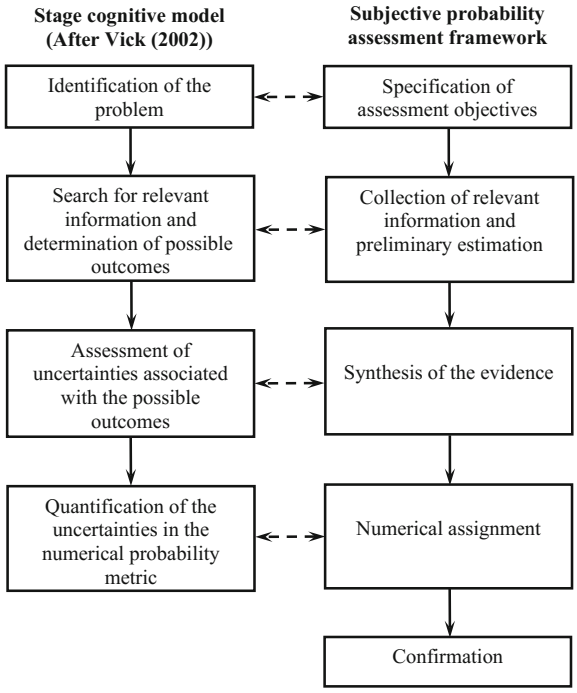

Fig. 4.1 Subjective probability assessment framework (SPAF) (After Cao et al. 2016)

The SPAF starts with specification of assessment objectives (e.g., determining the soil property x and its statistics Θ of interest), followed by collection of relevant information and making prior uncertain estimates on the assessment objectives. A piece of relevant information, a prior uncertain estimate obtained from this piece of relevant information, and the correlations between the relevant information and the prior uncertain estimate are collectively referred to as "a piece of evidence" in this chapter, as shown in Fig. 4.2. The third step (i.e., synthesis of the evidence) deals cautiously with the evidence collected in the second step. In this step, uncertainties associated with each evidence are evaluated, and engineering judgments are formulated internally based on the evidence. After that, the fourth step (i.e., numerical assignment) is to express the engineering judgments through numerical values (i.e., subjective probability values and probability distributions of Θ). The final step (i.e., confirmation) aims to check whether or not the outcomes (e.g., probability distributions of Θ) obtained from the SPAF are consistent with probability axioms and reality and reflect engineers' actual beliefs on assessment objectives.

It is worthwhile to point out that the first four steps of the proposed SPAF correspond to the four stages of the cognitive model of engineers' cognitive process (see Fig. 4.1), respectively. This allows engineers to formulate the subjective probability (or engineering judgments) on assessment objectives by following their

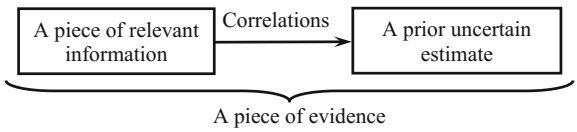

Fig. 4.2 Illustration of the evidence (After Cao et al. 2016)

cognitive process naturally. These five steps of the SPAF are introduced in detail in the following five sections, respectively. Several suggestions are also provided for each step of the SPAF to assist engineers in utilizing prior knowledge in a relatively rational way and reducing effects of cognitive biases and limitations (e.g., availability bias, representativeness bias, insufficient adjustment, and limited capacity of processing information) (see Chap. 2).

4.4 Specification of Assessment Objectives

If assessment objectives are misunderstood, inappropriate information might be collected and utilized in subjective probability assessment. This subsequently results in various cognitive biases (e.g., availability bias and insufficient adjustment) in subjective probability assessment. Therefore, it is of great significance to define and understand assessment objectives clearly at the beginning of the subjective probability assessment. Several suggestions are provided herein to assist engineers in specifying and understanding the assessment objectives properly, such as

(1) Write down the soil property x of interest and define a general assessment objective. For example, the general assessment objective can be "probabilistic characterization of the soil property x";
(2) Decompose the general objective into several sub-objectives. Each sub-objectives is corresponding to a statistic $\theta_i, i = 1, 2, \ldots, n_m$, of x. The statistics $\Theta = [\theta_1, \theta_2, \ldots, \theta_{n_m}]$ of interest depend on the probability theory that is applied to model the inherent variability of x in the Bayesian framework developed in Chap. 3. For example, when using random field theory to model inherent spatial variability of x within a statistically homogenous soil layer, the statistics of interest are model parameters of the random field, i.e., mean μ, standard deviation σ, and correlation length λ of x. In other words, Θ consists of three random variables: μ, σ, and λ, i.e., $\Theta = [\mu, \sigma, \lambda]$. Hence, the sub-objectives can be defined as "evaluating probability of the mean μ of x," "evaluating probability of the standard deviation σ of x," and "evaluating probability of the correlation length λ of x";
(3) Identify probability terms (including statistics of x) that engineers are not familiar with. For engineers, training in probability theory and statistics is usually limited to basic information during their early years of education (El-Ramly et al. 2002). They might be unfamiliar with some probability terms, e.g., correlation length λ. These probability terms should be written down;

(4) Try to understand physically probability terms that engineers are not familiar with. Physical interpretation of probability terms helps engineers understand these terms with relative ease. For example, the correlation length λ of x is a separate distance in which the soil property x shows relatively strong correlation from point to point (Vanmarcke 1977, 1983). By this definition, the correlation length is understood with relative ease.

Decomposition of the general assessment objective and physical interpretations of probabilistic terms assist engineers in clearly understanding the assessment objectives. This helps engineers collect properly information related to the assessment objectives (including the general assessment objective and sub-objectives), as discussed in the next section.

4.5 Collection of Relevant Information and Preliminary Estimation

The next step is to assemble the relevant information on assessment objectives from the prior knowledge (i.e., the collected existing information and engineers' expertise). A piece of relevant information might result in several prior uncertain estimates of the soil property x and/or its statistics Θ using available correlations (e.g., empirical regressions or theoretical correlations) or intuitive inference. Subsequently, it provides several pieces of evidence on assessment objectives. Evidence can be divided into two types: supportive evidence and disconfirming evidence (Vick 2002). Supportive evidence provides information that is consistent with the preconceived view of the assessor (e.g., engineers) about the soil property x, while disconfirming evidence contradicts with the preconceived view of the assessor. Examination of relevant information in prior knowledge eventually provides an evidence list. A relatively comprehensive evidence list includes both supportive evidence and disconfirming evidence collected from the existing information and engineers' expertise. It helps engineers reduce the availability bias arising from missing some useful evidence, the representativeness bias resulted from overemphasis on one particular type of information, and the confirmation bias due to overlooking disconfirming evidence (Vick 2002). Several suggestions are provided to assist engineers in acquiring a relatively comprehensive evidence list from prior knowledge.

As shown in Table 2.1 in Chap. 2, there are seven types of existing information, i.e., geological information, geotechnical problems and properties, site topography, groundwater conditions, meteorological conditions, existing construction and services, and previous land use. Engineers are suggested to cautiously search for relevant information and/or evidence in each type of existing information and the corresponding expertise. For each type of existing information, this can be performed through the following three steps:

(1) Identify the possible sources (including sources of the existing information (see Table 2.1) and engineers' expertise) of relevant information pertaining to this type of existing information;
(2) Assemble the relevant information from each possible source, and write it down;
(3) Evaluate the correlations between each piece of relevant information and the soil property x and its statistics $\Theta = [\mu, \sigma, \lambda]$, and write down the possible outcomes (i.e., prior uncertain estimates). Prior uncertain estimates of x and its statistics Θ can be obtained from the relevant information by correlations (including empirical and theoretical relationships and/or intuitive inference) and/or by conventional statistical equations. The mean and standard deviation of a random variable X (e.g., x or $\theta_i, i = 1, 2, \ldots, n_m$) can be calculated as (e.g., Baecher and Christian 2003)

$$\overline{X} = \frac{\sum_{i=1}^{n_X} X_i}{n_X} \tag{4.1}$$

$$w_X = \frac{\sum_{i=1}^{n_X} (X_i - \overline{X})^2}{n_X - 1} \tag{4.2}$$

in which $\overline{X}$ = the mean of X; w_X = the standard deviation of X; X_i, i = 1, 2, … n_x, are samples of X; n_x is the number of samples of X. When only a range of X from the minimum $X_{\min}$ to the maximum $X_{\max}$ is available, the mean value $\overline{X}$ and standard deviation w_X can be estimated as (e.g., Duncan 2000; Baecher and Christian 2003)

$$\overline{X} = \frac{X_{\max} + X_{\min}}{2} \tag{4.3}$$

$$w_X = \frac{X_{\max} - X_{\min}}{6} \tag{4.4}$$

Outcomes of the three steps are suggested to be written down clearly, including the types, sources, contents of relevant information, the prior uncertain estimates of x and Θ, and the correlations used to obtain the prior uncertain estimates. After that, an evidence list is obtained. Diligent attempts to search for relevant information and/or evidence in prior knowledge lead to a relatively comprehensive evidence list, which helps engineers reduce effects of cognitive biases (Vick 2002). In addition, writing down the relevant information and/or evidence in a list allows engineers to carefully think about each piece of relevant information and/or evidence. This helps engineers overcome the limitation of human information-processing capacity (Vick 2002).

4.6 Synthesis of the Evidence

Engineers utilize the collected evidence to formulate internally engineering judgments on the soil property x and its statistics Θ. The evidence has two essential cognitive properties: strength and weight (Griffin and Tversky 1992; Vick 2002). The strength means the forcefulness or extremeness (i.e., how convincingly or persuasively the evidence argues for a proposition) of the evidence; and the weight indicates the quality (i.e., how reliable it is) and quantity (i.e., how much of it) of the evidence (Griffin and Tversky 1992; Vick 2002). Because of the limitation of information-processing capacity, engineers consider the two properties of the evidence separately and tend to focus more on the strength of the evidence and to underestimate the effect of the weight (Vick 2002). This, sometimes, makes engineers overly confident of strong but unreliable evidence and underemphasize (or ignore) the relatively weak evidence with high weight (e.g., good quality and large quantity), and subsequently leads to overconfidence bias, representativeness bias, and insufficient adjustment (Vick 2002). To reduce effects of the cognitive biases, there is a need to properly balance the effects of strength and weight of the evidence and to synthesize the evidence further for subjective probability assessment. This can, for example, be carried out through the following four steps: (1) evaluating the strength of the evidence; (2) evaluating the weight of the evidence; (3) assembling the evidence and statistical analysis; and (4) reassembling the relevant evidence for each sub-objective, as discussed in the following four subsections, respectively.

4.6.1 Evaluation of the Strength of Evidence

A piece of evidence consists of a piece of relevant information, a prior uncertain estimate, and correlations between the relevant information and the estimate (see Fig. 4.2). The prior uncertain estimate in the evidence can be obtained from theoretical and/or empirical correlations or be inferred intuitively according to the expertise of engineers. Correlations in the evidence can be, therefore, categorized into two types: theoretical/empirical correlation and intuitive inference. Based on the type of correlations used in the evidence, the strength of the evidence can be divided into three levels: weak, moderate, and strong. If only the intuitive inference is used in the evidence, the strength of the evidence is weak. If only theoretical/empirical correlations (e.g., theories of probability and soil mechanics, empirical regressions) are used in the evidence, the strength of the evidence is strong. When both intuitive inference and theoretical/empirical correlations are required to obtain the prior uncertain estimate in the evidence and they are used sequentially, the strength of the evidence is moderate. In addition, when the relevant information is completely equivalent to the prior uncertain estimate and there is no need of correlations, the relevant information totally supports the prior uncertain estimate in the evidence. In such cases, the strength of the evidence is strong.

After the strength of all the evidence in the evidence list is obtained, engineers are suggested to check the strength intuitively. This can be implemented by intuitively evaluating how convincingly the relevant information supports the corresponding prior uncertain estimate according to the correlations used in the evidence. The intuitive evaluation outcomes can also be categorized into three possible levels: highly, moderately, and lowly persuasive, which are corresponding to strong, moderate, and weak strength, respectively. If the strength of a piece of evidence obtained from intuitive judgment is inconsistent with the strength of the evidence obtained previously, engineers are suggested to cautiously think about the inconsistency and try to find out the reasons for the inconsistency. The strength of evidence, sometimes, needs to be properly adjusted according to the causes that lead to the inconsistency.

4.6.2 Evaluation of the Weight of Evidence

The weight of the evidence depends on several factors, including the source of the relevant information, quantity of the relevant information (e.g., the number of existing in-situ test data), and accuracy of the analysis method used to obtain the prior uncertain estimate in the evidence. The weight of the evidence can be evaluated according to the three factors. This can, for example, be performed in two steps:

(1) Evaluate the weight of the relevant information based on its source. The relevant information might have been collected from four types of sources: official publications (e.g., geotechnical reports, peer-reviewed academic journals, textbooks, and geological maps) on the site concerned, official publications on another site, informal sources on the site concerned, and informal sources on another site. By the source of the relevant information, the weight of relevant information can be divided into three levels: high, moderate, and low. Relevant information obtained from official publications on the site concerned has high weight. Relevant information obtained from informal sources on the site concerned or official publications on another site has moderate weight. Information collected from informal sources on another site has low weight.

(2) Adjust the weight of the relevant information to the weight of the evidence according to the accuracy of the analysis method used in the evidence. The analysis method used to obtain the prior uncertain estimate in the evidence can be categorized into two types: qualitative analysis and quantitative analysis. The accuracy of qualitative analysis is considered relatively poor compared with that of quantitative analysis. When qualitative analysis is used in the evidence, the weight of the evidence is obtained by decreasing the weight of the corresponding relevant information by one level. When quantitative analysis is used in the evidence, adjustment of the weight of the relevant information depends on the quantity of data used in the analysis. If there is a

relatively large number of data used in the analysis, the weight of the evidence is obtained by increasing the weight of the corresponding relevant information by one level. If there are relatively limited data, the weight of the evidence is obtained by decreasing the weight of the corresponding relevant information by one level.

For the evidence in which the relevant information is completely equivalent to the prior uncertain estimate, the weight of the evidence is determined by adjusting the weight of the relevant information according to the quantity of data contained in the relevant information. Note that when the weight of the relevant information is already high and there exists a need of increasing it to obtain the weight of the evidence, the weight of the evidence is still high. Similarly, when weight of the relevant information is already low and there exists a need of decreasing it to obtain the weight of the evidence, the weight of the evidence is still low.

When the weight of all the evidence in the evidence list is determined, engineers are suggested to intuitively check the weight of all the evidence in the list. This can be implemented by intuitively thinking about how reliable the evidence is. The outcomes of intuitively weighing the evidence can be divided into three levels: highly, moderately, and lowly reliable, which are corresponding to high, moderate, and low weight, respectively. If the weight of the evidence obtained from intuitively weighing the evidence is inconsistent with the weight of the evidence obtained previously, engineers are suggested to cautiously examine the inconsistency and try to find out the reasons resulting in the inconsistency. The weight of the evidence, sometimes, needs to be properly adjusted according to the causes that lead to the inconsistency.

4.6.3 Assembling the Evidence and Statistical Analysis

After the strength and weight of all the evidence are obtained, the next step is to assemble the evidence about the same variable X (i.e., x or $\theta_i, i = 1, 2, \ldots, n_m$) together. For each variable X, the evidence can be categorized into several groups by strength and weight, and the evidence in each group has the same strength and weight. Because both strength and weight have three possible levels (see Sects. 4.6.1 and 4.6.2), there are 9 possible evidence groups: (1) group with weak strength and low weight; (2) group with weak strength and moderate weight; (3) group with weak strength and high weight; (4) group with moderate strength and low weight; (5) group with moderate strength and moderate weight; (6) group with moderate strength and high weight; (7) group with strong strength and low weight; (8) group with strong strength and moderate weight; and (9) group with strong strength and high weight. For each evidence group, conventional statistical equations (e.g., Eqs. (4.1)–(4.4)) can be used to analyze the information on the variable X (i.e., x or $\theta_i, i = 1, 2, \ldots, n_m$) provided by the evidence. By this means, some estimates of statistics of X are obtained. The procedure described above is

repeatedly performed for each variable involved in the subjective probability assessment objectives, including x in the general assessment objective and $\theta_i, i = 1, 2, \ldots, n_m$, in sub-objectives.

4.6.4 Reassembling the Relevant Evidence for Each Sub-objective

Evidence with regard to the soil property x provides information on different statistics $\theta_i, i = 1, 2, \ldots, n_m$, of x. In other words, estimates from the evidence on x might be related to different sub-objectives since each sub-objective involves only one statistic of x. For the convenience of subjective probability assessment, the relevant evidence (or evidence groups) about the same sub-objective shall be assembled together and be written down with the strength and weight of the evidence. After that, engineers can examine cautiously the relevant evidence on each sub-objective and make their engineering judgments on the sub-objective internally based on the evidence.

It is worthwhile to point out that the evidence group with limited evidence shall be used with caution when formulating engineering judgments. In addition, when using the relevant evidence to make engineering judgments on a sub-objective, the strength and weight of the evidence need to be considered. The relevant evidence with strong strength and high weight is more persuasive and reliable than that with relatively weak strength and relatively low weight. Convincingness and reliability of the evidence decrease as the levels of strength and weight decrease.

Based on the relevant evidence, engineers have formulated their engineering judgments on statistics $\theta_i, i = 1, 2, \ldots, n_m$, in sub-objectives internally. The next step is to elicit engineering judgments on $\theta_i, i = 1, 2, \ldots, n_m$, from engineers and to express the engineering judgments through numerical values. Engineers are, however, not used to thinking in terms of probability due to relatively limited training in probability theory and statistics (El-Ramly et al. 2002; Vick 2002; Baecher and Christian 2003). In the next section, the equivalent lottery method and verbal descriptors of the likelihood (or plausibility) are used to assist engineers in assigning numerical values (i.e., subjective probability) to their engineering judgments on $\theta_i, i = 1, 2, \ldots, n_m$, in sub-objectives.

4.7 Numerical Assignment

4.7.1 Equivalent Lottery Method

Equivalent lottery method (e.g., Clemen 1996; Vick 2002) assists engineers in making decisions by comparing two lotteries. One of the two lotteries involves the

event of interest, and the other one is designed as reference lottery in which the probability information is contained as a reference. The plausibility of the event concerned is equal to the probability in the reference lottery when indifference between two lotteries is achieved by adjusting one of them. For example, two lotteries are used to determine the median value of the statistic $\theta_i, i = 1, 2, \ldots, n_m$, for a given range from the minimum $\theta_{i,\min}$ to the maximum $\theta_{i,\max}$, which are given by

Lottery 1:

Win a prize if $\theta_{i,\min} \leq \theta_i \leq a_s$ occurs, where a_s is a possible value of θ_i falling within the range $[\theta_{i,\min}, \theta_{i,\max}]$.
Win nothing if $a_s < \theta_i \leq \theta_{i,\max}$ occurs.

Lottery 2:

Win a prize with known probability $p = 0.5$.
Win nothing with probability $1 - p = 0.5$.

The second lottery (i.e., lottery 2) is the reference lottery. Engineers can adjust the value of a_s between the minimum and maximum (i.e., $\theta_{i,\min}$ and $\theta_{i,\max}$) of θ_i until they are indifferent between the two lotteries according to the previously obtained relevant evidence on θ_i. The indifference indicates that engineers believe that the two lotteries are equivalent to each other. Since occurrence probabilities of the two choices in lottery 2 are fixed at 0.5, engineers believe that occurrence probabilities of the two choices in lottery 1 are also 0.5 after the indifference is reached. Therefore, when the indifference is reached, engineers believe that the probability of $\theta_{i,\min} \leq \theta_i \leq a_s$ for a given range from $\theta_{i,\min}$ to $\theta_{i,\max}$ is equal to that of $a_s < \theta_i \leq \theta_{i,\max}$, and both of them are equal to 0.5. In other words, a_s is the median value of θ_i for the given range from $\theta_{i,\min}$ to $\theta_{i,\max}$ after the indifference is reached.

The equivalent lottery method described above requires a range of θ_i, i.e., $[\theta_{i,\min}, \theta_{i,\max}]$, as input. Using different ranges of θ_i in the equivalent lottery method leads to different median values. For example, using the range from 1 % percentile (i.e., $\theta_{i,0.01}$) of θ_i to 99 % percentile (i.e., $\theta_{i,0.99}$) of θ_i in the equivalent lottery method leads to a median value of θ_i equivalent to its 50 % percentile (i.e., $\theta_{i,0.5}$). Subsequently, using the range from $\theta_{i,0.01}$ to $\theta_{i,0.5}$ (i.e., $[\theta_{i,0.01}, \theta_{i,0.5}]$) in the equivalent lottery method results in a median value of θ_i equivalent to its 25 % percentile (i.e., $\theta_{i,0.25}$). Similarly, using the range from $\theta_{i,0.5}$ to $\theta_{i,0.99}$ (i.e., $[\theta_{i,0.5}, \theta_{i,0.99}]$) in the equivalent lottery method results in a median value of θ_i equivalent to its 75 % percentile (i.e., $\theta_{i,0.75}$). Then, using ranges of $[\theta_{i,0.01}, \theta_{i,0.25}]$, $[\theta_{i,0.25}, \theta_{i,0.5}]$, $[\theta_{i,0.5}, \theta_{i,0.75}]$, and $[\theta_{i,0.75}, \theta_{i,0.99}]$ in the equivalent lottery method leads to the median values equivalent to its 12.5 % (i.e., $\theta_{i,0.125}$), 37.5 % (i.e., $\theta_{i,0.375}$), 62.5 % (i.e., $\theta_{i,0.625}$), and 87.5 % (i.e., $\theta_{i,0.875}$) percentiles, respectively.

4.7.2 Verbal Descriptors of the Likelihood

To start the equivalent lottery method described above, 1 % and 99 % percentiles (i.e., $\theta_{i,0.01}$ and $\theta_{i,0.99}$) of θ_i should be determined first. Direct elicitation of numerical values of probability from engineers might lead to unstable and incoherent results because engineers are not used to thinking in terms of numerical values of probability (e.g., Baecher and Christian 2003). On the other hand, engineers prefer to express their engineering judgments using words that indicate the likelihood, namely verbal descriptors of the likelihood (Vick 2002). Verbal descriptors can be mapped to numerical values of probability by transformation conventions. For example, Table 4.1 shows a transformation convention between verbal descriptors and numerical values of probability (Vick 2002). By this convention, the words "virtually impossible," "very unlikely," "equally likely," "very likely," and "virtually certain" are equivalent to the probability of 0.01, 0.1, 0.5, 0.9, and 0.99, respectively. Note that in this convention the probability value ranges from 0.01 to 0.99 (see Table 4.1), which happens to be the valid cognitive discrimination range (i.e., from 0.01 to 0.99) of subjective probability (Fischhoff et al. 1977; Hogarth 1975; Vick 1997, 2002).

The probability value in the transformation convention increases from 0.01 to 0.99 monotonically (see Table 4.1). Therefore, the transformation convention corresponds to the cumulative distribution function (CDF) of the variable θ_i concerned, and the words "virtually impossible" and "virtually certain" can be used to determine the 1 % and 99 % percentiles of θ_i, respectively. 1 % and 99 % percentiles are located at the lower and upper tails of probability density function (PDF), respectively. They can be considered as the minimum and maximum possible values of θ_i, respectively. Therefore, in the convention shown in Table 4.1, the words "virtually impossible" and "virtually certain" are actually used to determine the minimum and maximum possible values of θ_i in terms of PDF, respectively. In this chapter, the words "minimum" and "maximum" are directly used to determine the 1 % and 99 % percentiles, respectively. The 1 % and 99 % percentiles of θ_i are then determined by asking "What is the minimum possible value of θ_i?" and "What is the maximum possible value of θ_i?", respectively.

It is also worthwhile to note that the verbal descriptor "equally likely" is equivalent to the probability of 0.5 (see Table 4.1). By this convention, the two lotteries proposed in the previous subsection can be rewritten as follows:

Table 4.1 Verbal descriptors and their probability equivalents (After Vick 2002)

Verbal descriptor	Probability equivalent	Percentile
Virtually impossible	0.01	$\theta_{i,0.01}$
Very unlikely	0.10	$\theta_{i,0.1}$
Equally likely	0.50	$\theta_{i,0.5}$
Very likely	0.90	$\theta_{i,0.9}$
Virtually certain	0.99	$\theta_{i,0.99}$

Lottery 1:

Win a prize if $\theta_{i,\min} \leq \theta_i \leq a_s$ occurs, where a_s is a possible value of θ_i falling within the range $[\theta_{i,\min}, \theta_{i,\max}]$.
Win nothing if $a_s < \theta_i \leq \theta_{i,\max}$ occurs.

Lottery 2:

Win a prize or nothing equally likely.

4.7.3 Implementation of the Equivalent Lottery Method

Using the two lotteries and verbal descriptors, the percentiles of θ_i in each sub-objective can be determined accordingly. A questionnaire is designed in this chapter to implement the equivalent lottery method, as shown in Appendix 4.1. When answering the questions in the questionnaire, engineers might revisit the relevant evidence on θ_i collected before.

The questionnaire starts with a question (i.e., Q1) that is used to determine a reference prize for the lottery 1, followed by the second and third questions (i.e., Q2 and Q3) for determining $\theta_{i,0.01}$ and $\theta_{i,0.99}$, respectively. Then, the equivalent lottery method can be used to estimate the median value (i.e., $\theta_{i,0.5}$) for the given range from $\theta_{i,0.01}$ and $\theta_{i,0.99}$ in Q4 if there is sufficient information provided by the relevant evidence on θ_i. Such a procedure can be repeatedly performed to determine the percentiles of θ_i progressively using different ranges of θ_i in the equivalent lottery method, as described in Sect. 4.7.1. The questionnaire shall be stopped when engineers believe that there is no sufficient information on θ_i to balance the two lotteries in the equivalent lottery method for a given range of θ_i.

For example, if the information on θ_i is very sparse, it might be too difficult for engineers to estimate 50 %, 25 %, 75 %, 12.5 %, 37.5 %, 62.5 %, and 87.5 % percentiles (i.e., $\theta_{i,0.5}, \theta_{i,0.25}, \theta_{i,0.75}, \theta_{i,0.125}, \theta_{i,0.375}, \theta_{i,0.625}$, and $\theta_{i,0.875}$) of θ_i. In such cases, the questionnaire is stopped after $\theta_{i,0.01}$ and $\theta_{i,0.99}$ are obtained from Q2 and Q3. On the other hand, if there is a large number of information on θ_i, the questionnaire can be continued to obtain more percentiles of θ_i after 12.5 %, 37.5 %, 62.5 %, and 87.5 % percentiles are obtained.

The questionnaire is repeated n_m times for the n_m sub-objectives. After that, the percentiles of the statistics $\theta_i, i = 1, 2, \ldots, n_m$, of x are obtained. The prior distribution of θ_i is then estimated from its percentiles, as discussed in the next subsection.

4.7.4 Prior Distribution

After the percentiles of θ_i are obtained, its cumulative distribution function (CDF) and probability density function (PDF) can be estimated from its percentiles through two methods: a simplified method and a least squares regression method.

4.7.4.1 A Simplified Method

The range of θ_i from $\theta_{i,0.01}$ to $\theta_{i,0.99}$ is divided into several intervals by its percentiles. Consider, for example, that θ_i is uniformly distributed within each interval. Then, an empirical CDF of θ_i is obtained by plotting a line through the points at percentiles (i.e., data pairs of the percentiles of θ_i and their respective cumulative probability levels, such as ($\theta_{i,0.01}$, 1 %), ($\theta_{i,0.5}$, 50 %), and ($\theta_{i,0.99}$, 99 %)). The PDF of θ_i is estimated by constructing a histogram with bins equal to the intervals of θ_i between adjacent percentiles. In each bin, the PDF value of θ_i is calculated as the ratio of the increase in cumulative probability level in this bin over the length of the bin. For example, the PDF value of θ_i in the bin from $\theta_{i,0.5}$ to $\theta_{i,0.625}$ is calculated as $(0.625 - 0.5)/(\theta_{i,0.625} - \theta_{i,0.5})$. The PDF of θ_i is then taken as the prior distribution of θ_i in the Bayesian framework formulated in Chap. 3.

4.7.4.2 A Least Squares Regression Method

The CDF of θ_i can also be obtained by fitting a probability distribution with assessment results (i.e., data pairs of the percentiles of θ_i and their respective cumulative probability levels) using the least squares regression method (e.g., Baecher and Christian 2003; Ang and Tang 2007). The least squares regression method requires a probability distribution as the model function for data fitting. Consider, for example, the Gaussian CDF as the model function. The least squares regression method provides a Gaussian CDF of θ_i as the best fit of the assessment results and, simultaneously, gives the values of the mean and standard deviation of the Gaussian distribution. Using the mean and standard deviation, the PDF of θ_i is determined, which is then taken as the prior distribution of θ_i in the Bayesian framework formulated in Chap. 3. Note that the least squares regression method can be achieved using commercial software packages. For example, MATLAB (Mathworks Inc. 2010) provides a built-in function "nlinfit" for the least squares regression method.

4.8 Confirmation of Assessment Outcomes

Because of cognitive biases and limitations, the assessment outcomes (e.g., the percentiles and probability distributions of $\theta_i, i = 1, 2, \ldots, n_m$) might violate the basic probability axioms and deviate from the actual beliefs of engineers (Vick

2002). Several suggestions are provided herein to help engineers check the assessment outcomes, such as

(1) Check the coherence between the assessment outcomes and the basic probability axioms (e.g., probability falls within the range from 0 to 1, and integration on a PDF is equal to unity) (e.g., Ang and Tang 2007; Ross 2007). The assessment outcomes (the percentiles and probability distributions of $\theta_i, i = 1, 2, \ldots, n_m$) obtained from the proposed SPAF have to conform to the basic probability axioms.
(2) Examine biases arising from cognitive heuristics. This can be carried out by reviewing all the evidence carefully and checking that "is there any evidence that is overlooked or underemphasized" and "is there any evidence that is overemphasized". The careful examination of the evidence reduces the overconfidence bias arising from overemphasis on the supportive evidence and ignorance of disconfirming evidence (Vick 2002). In addition, the attempts to find out the evidence that is overlooked or underemphasized reduce the availability bias.
(3) Engineers are suggested to interpret the assessment outcomes to check whether or not the outcomes are reasonable in reality according to their expertise and reflect their actual beliefs.

If there is any inconsistency or any evidence that is misused, engineers need to adjust properly the percentiles obtained from the SPAF and to reevaluate the prior distributions accordingly, and they are suggested to write down the reasons for the adjustment. This provides an opportunity to examine the adjustment and to reduce the hindsight bias (Vick 2002). The confirmation-reevaluation process might be iterated several times until engineers believe that the assessment outcomes are reasonable in reality and reflect their actual beliefs according to the prior knowledge, and all the evidence has been taken into account properly. After the final confirmation of the assessment outcomes, probability distributions of $\theta_i, i = 1, 2, \ldots, n_m$, quantify their respective plausibility according to the prior knowledge. In the next section, the proposed SPAF is applied to characterize probabilistically soil properties at the sand site of US NGES at Texas A&M University (TAMU) (Briaud 2000), and it is illustrated under two scenarios: scenario I with uninformative prior knowledge and scenario II with a reasonable amount of prior knowledge, as discussed in the following two sections.

4.9 Scenario I: Uninformative Prior Knowledge

4.9.1 Assessment Objectives

The sand site of US National Geotechnical Experimentation Site (NGES) at Texas A&M University is comprised of a top layer of sands to about 12.5 m deep and a

stiff clay layer thereafter (see Fig. 2.5 in Chap. 2). Consider, for example, the sand effective friction angle ϕ' of interest, i.e., $x = \phi'$. The general assessment objective is, therefore, defined as "probabilistic characterization of effective friction angle ϕ' at the sand site." The sand effective friction angle ϕ' within a statistically homogenous soil layer can be probabilistically characterized by the random field theory (Vanmarcke 1977, 1983), in which three model parameters are required, i.e., mean μ, standard deviation σ, and correlation length λ of ϕ'. The statistics of interest are μ, σ, and λ, i.e., $\Theta = [\mu, \sigma, \lambda]$. The general assessment objective is then decomposed into three sub-objectives: "evaluating probability of μ," "evaluating probability of σ," and "evaluating probability of λ."

4.9.2 Relevant Information and Prior Uncertain Estimates

For illustration, suppose that only one piece of relevant information is obtained according to previous engineering experience at this site (e.g., Briaud 2000), and it indicates that the site is underlain by sand layers. The piece of relevant information leads to three pieces of evidence, as shown in Table 4.2. For sands, the typical value of ϕ' falls within the range from 27.5° to 50.0° by Terzaghi and Peck (1967) and Kulhawy and Mayne (1990) (see Table 2.11), i.e., evidence (1). The respective typical ranges of σ and λ are from 3.7° to 5.5° (i.e., evidence (2)) and from 2.0 m to 6.0 m (i.e., evidence (3)) by Phoon and Kulhawy (1999a, 1999b).

4.9.3 Strength and Weight of the Evidence and Statistical Analysis

4.9.3.1 Strength and Weight of the Evidence

Table 4.3 summarizes the strength (i.e., Column 6) and weight (i.e., Column 7) of the 3 pieces of evidence and the procedure of evaluating their strength and weight, including source of the information (i.e., Column 2), procedure of estimation (i.e., Column 3), type of analysis (i.e., Column 4), and type of correlation (i.e., Column 5).

Table 4.2 Summary of relevant information and prior uncertain estimates for scenario I

Type	Relevant information	Correlations	Prior uncertain estimates		No. of evidence
Geotechnical properties	Sands (Briaud 2000)	Table 2.11 after Kulhawy and Mayne (1990)	ϕ'	27.5°–50.0°	(1)
		Phoon and Kulhawy (1999b)	σ	3.7°–5.5°	(2)
		Phoon and Kulhawy (1999a)	λ	2.0–6.0 m	(3)

Table 4.3 Summary of strength and weight of the evidence for scenario I

No. of evidence	Source of information	Procedure of estimation	Type of analysis	Type of correlation	Strength	Weight
(1)	An official report of the sand site	Soil type —range of ϕ'	Qualitative analysis	Empirical correlation	Strong	Moderate
(2)	An official report of the sand site	Soil type —range of σ	Qualitative analysis	Empirical correlation	Strong	Moderate
(3)	An official report of the sand site	Soil type —range of λ	Qualitative analysis	Empirical correlation and Intuitive inference	Moderate	Low

In evidence (1), the range of ϕ' is estimated from the relevant information (i.e., the site is underlain by sands) by an empirical correlation (Kulhawy and Mayne 1990). Thus, evidence (1) has a strong strength. The relevant information is obtained from an official report (Briaud 2000). Thus, the weight of the information is high. The range of ϕ' in evidence (1) is qualitatively estimated from the relevant information, so that the weight of the evidence is obtained through decreasing the level of the weight of the relevant information by one level, i.e., moderate.

In evidence (2), the relevant information is related to the range of σ by an empirical correlation (Phoon and Kulhawy 1999b). Thus, evidence (2) has a strong strength. The information is obtained from an official report of the sand site (Briaud 2000). Thus, the weight of the relevant information is high. The range of σ is qualitatively estimated from the relevant information, so that the weight of the evidence is obtained through decreasing the level of the weight of the relevant information by one level, i.e., moderate.

In evidence (3), the relevant information is related to the correlation length of soil properties by an empirical correlation (Phoon and Kulhawy 1999b). The empirical correlation does not directly give the range of correlation length λ of ϕ', but provides the correlation length of other soil properties (e.g., standard penetration test (SPT) N-value, cone tip resistance obtained from cone penetration test (CPT)) of sands. The range of λ of ϕ' is intuitively inferred from the range of correlation length of other soil properties (e.g., SPT N-value) of sands. The empirical correlation and intuitive inference are sequentially used in evidence (3). Therefore, the strength of the evidence is moderate. The relevant information in evidence (3) is collected from an official report of the sand site (Briaud 2000). Thus, the weight of the relevant information is high. The range of λ is qualitatively estimated from the relevant information, so the weight of the evidence is obtained through decreasing the level of the weight of the relevant information by one level, i.e., moderate. However, the assessor believes that the intuitive inference on the correlation length λ of ϕ' from that of other soil properties is not very reliable. Thus, the weight of the evidence is further decreased to the third level, i.e., low.

4.9.3.2 Assembling Evidence and Statistical Analysis

There are only three pieces of evidence available. Evidence (1) gives a possible range of ϕ' with strong strength and moderate weight. The range of ϕ' in evidence (1) provides some information on the mean μ of ϕ'. Evidence (2) gives a possible range of σ with strong strength and moderate weight. Evidence (3) gives a possible range of λ with moderate strength and low weight. For each sub-objective, there is only one piece of evidence available, i.e., evidence (1) for evaluating the probability of μ, evidence (2) for evaluating the probability of σ, and evidence (3) for evaluating the probability of λ.

4.9.4 Results of Subjective Probability Assessment

Based on the evidence on each sub-objective, the percentiles of μ, σ, and λ are elicited from the assessor using the questionnaire shown in Appendix 4.1. Because there is only one piece of evidence for each sub-objective, only the 1 % and 99 % percentiles of μ, σ, and λ are evaluated (i.e., only Q1 to Q3 in the questionnaire (see Appendix 4.1) are answered). As shown in Table 4.4, the 1 % and 99 % percentiles of μ, σ, and λ are $\mu_{0.01} = 27.5°, \mu_{0.99} = 50.0°, \sigma_{0.01} = 3.7°, \sigma_{0.99} = 5.5°, \lambda_{0.01} = 2.0\,\text{m}$, and $\lambda_{0.99} = 6.0\,\text{m}$. Using the simplified method described in Sect. 4.7.4.1, prior distributions of μ, σ, and λ are obtained from their respective percentiles, as discussed in the following three subsections.

4.9.4.1 Prior Distribution of the Mean μ

Figure 4.3a shows the CDF of μ obtained from the simplified method by a solid line with open circles. The CDF value of μ increases linearly from 0.01 to 0.99 as μ increases from 27.5° to 50.0°. Figure 4.3b shows the PDF of μ obtained from the simplified method by a histogram with only one bin (i.e., a uniform distribution with a range from 27.5° to 50.0°), and the PDF value of μ is about 0.044. The uniform PDF of μ (see Fig. 4.3b) can be taken as the prior distribution of μ in the Bayesian framework developed in Chap. 3.

Table 4.4 Summary of percentiles of the mean, standard deviation, and correlation length for scenario I

Cumulative probability	0.01	0.99
Mean μ (°)	27.5	50
Standard deviation σ (°)	3.7	5.5
Correlation length λ (m)	2.0	6.0

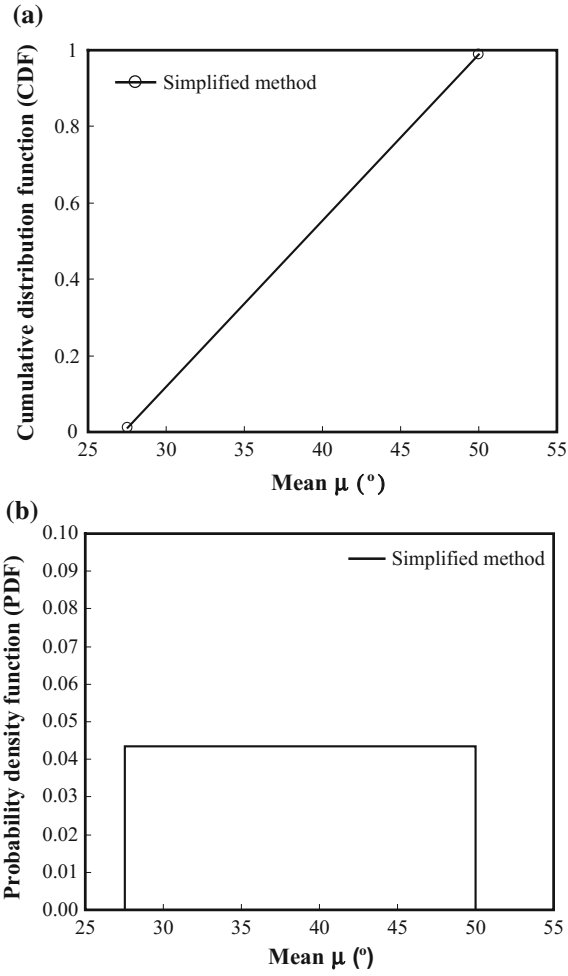

Fig. 4.3 Prior distribution of the mean, μ, in scenario I. **a** Cumulative distribution function (CDF) of the mean, μ. **b** Probability density function of the mean, μ

4.9.4.2 Prior Distribution of the Standard Deviation σ

Figure 4.4a shows the CDF of σ obtained from the simplified method by a solid line with open circles. The CDF value of σ increases linearly from 0.01 to 0.99 as σ increases from 3.7° to 5.5°. Figure 4.4b shows the PDF of σ obtained from the simplified method by a histogram with only one bin (i.e., a uniform distribution with a range from 3.7° to 5.5°), and the PDF value of σ is about 0.54. The uniform PDF of σ (see Fig. 4.4b) can be taken as the prior distribution of σ in the Bayesian framework developed in Chap. 3.

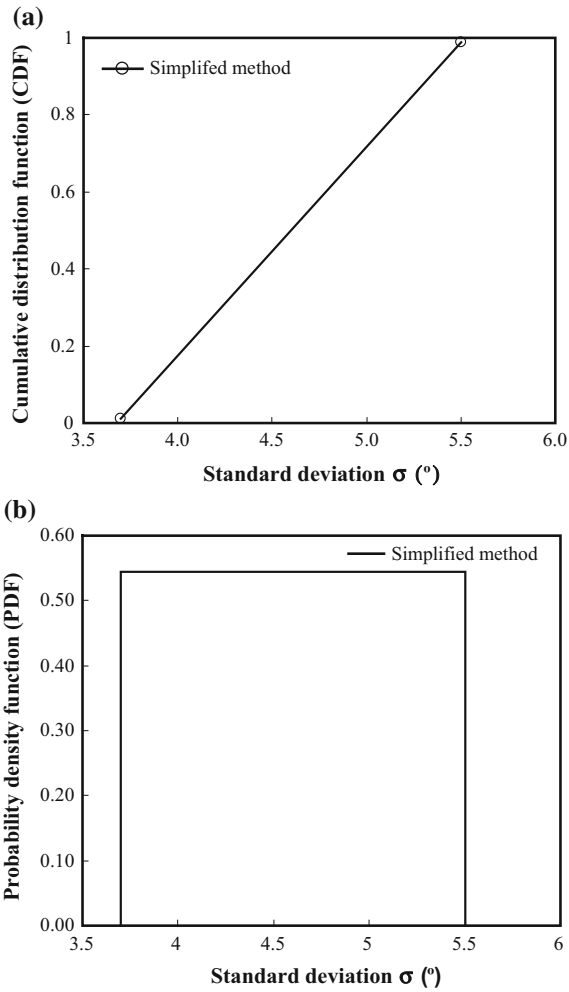

Fig. 4.4 Prior distribution of the standard deviation, σ, in scenario I. **a** Cumulative distribution function (CDF) of the standard deviation, σ. **b** Probability density function (PDF) of the standard deviation, σ

4.9.4.3 Prior Distribution of the Correlation Length λ

Figure 4.5a shows the CDF of λ obtained from the simplified method by a solid line with open circles. The CDF value of λ increases linearly from 0.01 to 0.99 as λ increases from 2.0 to 6.0 m. Figure 4.5b shows the PDF of λ obtained from the simplified method by a histogram with only one bin (i.e., a uniform distribution with a range from 2.0 to 6.0 m), and the PDF value of λ is about 0.25. The uniform PDF of λ (see Fig. 4.5b) can be taken as the prior distribution of λ in the Bayesian framework developed in Chap. 3.

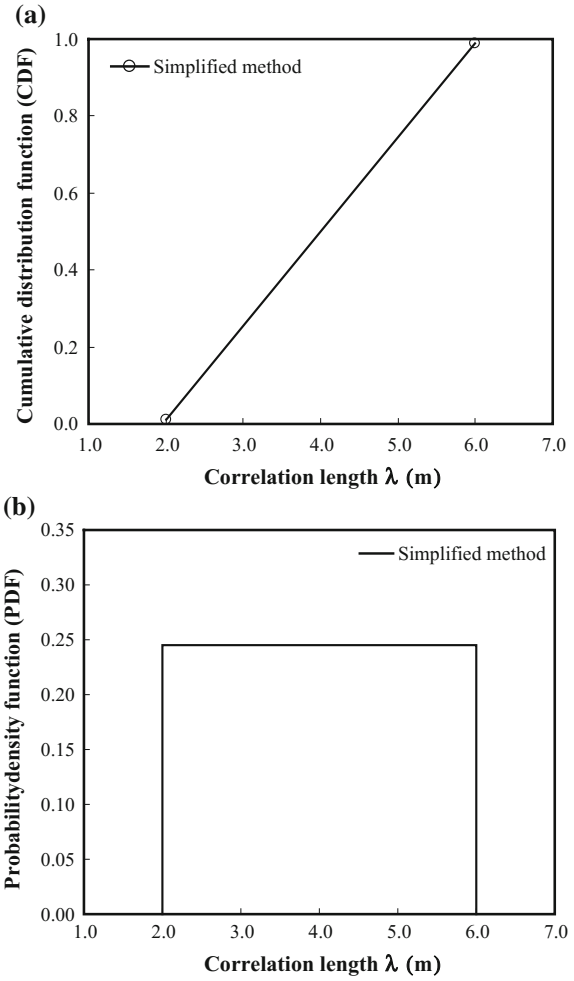

Fig. 4.5 Prior distribution of the correlation length, λ, in scenario I. **a** Cumulative distribution function (CDF) of the correlation length, λ. **b** Probability density function (PDF) of the correlation length, λ

4.9.5 Final Confirmation

All the areas under the respective PDFs (see Figs. 4.3b, 4.4b, and 4.5b) of μ, σ, and λ are summed up to unity. This is consistent with the basic probability axiom that integration on a PDF is unity. The prior distributions of μ, σ, and λ are consistent with the information on them provided by evidence (1), (2), and (3), respectively. All the three pieces of evidence are taken into account properly. Because the information on μ, σ, and λ is very sparse in this scenario, the prior distributions of μ, σ, and λ obtained from the SPAF are uninformative (i.e., uniform distributions). The prior distributions of μ, σ, and λ reflect properly the prior knowledge. The

assessment outcomes are then confirmed. In the next section, the proposed SPAF is further illustrated under another scenario that has a reasonable amount of prior knowledge.

4.10 Scenario II: Informative Prior Knowledge

4.10.1 Assessment Objectives

The sand effective friction angle ϕ' at the sand site of NGES at Texas A&M university is still of interest under this scenario. The general assessment objective remains unchanged, i.e., "probabilistic characterization of effective friction angle ϕ' at the sand site." Similar to scenario I, it is then decomposed into three sub-objectives: "evaluating probability of μ," "evaluating probability of σ," and "evaluating probability of λ."

4.10.2 Relevant Information and Prior Uncertain Estimates

In this scenario, geological information and soil classification information are obtained from Briaud (2000). Table 4.5 summarizes the relevant information (i.e., Column 2) on geology and soil classification, available correlations (i.e., Column 3) between the geology and soil classification information and ϕ', μ, σ, and λ; their prior uncertain estimates (i.e., Column 4). As shown in Table 4.5, a total of 11 pieces of evidence are obtained from geological information and soil classification information.

Evidence (1), (2), and (3) are obtained from geological information. The sand site is underlain by fluvial and overbank deposits (Briaud 2000), which can be categorized as alluvium deposits (Heim 1990). Alluvium deposits usually have relatively low in-situ densities (e.g., loose or medium) (Heim 1990). For loose and medium sands, ϕ' varies from 28° to 40° (i.e., evidence (1)) or varies from 30° to 40° (i.e., evidence (2)) (Kulhawy and Mayne 1990). In addition, a textbook (Rollings and Rollings 1996) provides consistent values (i.e., from 30° to 40°) of ϕ' of alluvium deposits, i.e., evidence (3).

The sands underlying the site include silty sand, clean sand, and clayey sand (Briaud 2000). Two peer-reviewed academic papers (i.e., Phoon and Kulhawy 1999a, 1999b) provided six pieces of evidence (i.e., evidence (4)–(9)) on ϕ', μ, σ, and λ of sands. Evidence (4) and (5) give the two possible ranges of ϕ', i.e., from 35° to 41° and from 33° to 43° (Phoon and Kulhawy 1999a), respectively. Evidence (6) and (7) provide two possible values of μ, i.e., 37.6° or 36.7° (Phoon and Kulhawy 1999a), respectively. Evidence (8) and (9) provide the respective ranges of σ (i.e., from 3.7° to 5.5°) and λ (i.e., from 2 to 6 m) (Phoon and Kulhawy 1999a).

Table 4.5 Summary of relevant information and prior uncertain estimates for scenario II

Type	Relevant information	Correlations		Prior uncertain estimates		No. of evidence
Geology	Fluvial and overbank deposits (Briaud 2000)	Alluvium deposit—relatively low in-situ density: loose or medium sand (Heim 1990)	Table 2.8 after Kulhawy and Mayne (1990)	ϕ'	28°–40°	(1)
			Table 2.9 after Kulhawy and Mayne (1990)	ϕ'	30°–40°	(2)
		Alluvium Deposit (Heim 1990)	Rollings and Rollings (1996)	ϕ'	30°–40°	(3)
Geotechnical properties	Classification: silty sand, clean sand, and clayey sand (Briaud 2000)	Sand	Phoon and Kulhawy (1999a)	ϕ'	35°–41°	(4)
					33°–43°	(5)
				μ	37.6°	(6)
					36.7°	(7)
			Phoon and Kulhawy (1999b)	σ	3.7°–5.5°	(8)
			Phoon and Kulhawy (1999a)	λ	2–6 m	(9)
		Dry unit weight: 13.3–21.7 kN/m^3 (Table 2.10 after Kulhawy and Mayne (1990))	Figure 2.7 after Kulhawy and Mayne (1990)	ϕ'	27.0°–37.0°	(10)
		Sand or silty sand	Table 2.11 after Kulhawy and Mayne (1990)	ϕ'	28°–45°	(11)

Note that evidence (8) and (9) in this scenario are the same as evidence (2) and (3) in scenario I (see Table 4.2), respectively. In addition, the dry unit weight of sands usually varies from 13.3 to 21.7 kN/m^3, and it is also related to ϕ' (Kulhawy

and Mayne 1990). This leads to evidence (10), i.e., a possible range of ϕ' from 27.0° to 37.0°. Kulhawy and Mayne (1990) also reported that the effective friction angle of sand or silty sand ranges from 28° to 45°, i.e., evidence (11).

4.10.3 Strength and Weight of the Evidence and Statistical Analysis

4.10.3.1 Strength and Weight of the Evidence

Table 4.6 summarizes the strength (i.e., Column 7) and weight (i.e., Column 8) of the 11 pieces of evidence and the procedure of evaluating their strength and weight, including source of the information (i.e., Column 2), quantity of data (i.e., Column 3), procedure of estimation (i.e., Column 4), type of analysis (i.e., Column 5), and type of correlation (i.e., Column 6). As mentioned above, evidence (8) and (9) in this scenario are the same as evidence (2) and (3) in scenario I (see Table 4.2), respectively, and the procedures of evaluating their strength and weight have been described in Sect. 4.9.3.1. For further illustration, procedures of evaluating the strength and weight of evidence (3) and (11) in this scenario are described below.

In evidence (3), the type of deposits underlying the sand site is intuitively inferred from the geological information, and the range of ϕ' is then intuitively estimated from the deposit type. Only the intuitive inference is used to estimate the range of ϕ' in evidence (3). Thus, the strength of the evidence is weak. The geological information in evidence (3) is obtained from an official report of the sand site (Briaud 2000). Thus, the weight of the geological information is high. The range of ϕ' in evidence (3) is qualitatively estimated from the geological information, so that the weight of the evidence is obtained through decreasing the level of the weight of the relevant information by one level, i.e., moderate.

In evidence (11), the range of ϕ' is estimated from the soil classification information by an empirical correlation (Kulhawy and Mayne 1990). Thus, the strength of the evidence is strong. The soil classification information in evidence (11) is obtained from an official report of the sand site (Briaud 2000). Thus, the weight of the soil classification information is high. The range of ϕ' in evidence (11) is qualitatively estimated from the geological information, so the weight of the evidence is obtained through decreasing the level of the weight of the relevant information by one level, i.e., moderate.

4.10.3.2 Assembling Evidence and Statistical Analysis

Table 4.7 summarizes the strength and weight of evidence with regard to ϕ', μ, σ, and λ, respectively. Six evidence groups (i.e., evidence groups (I)–(VI)) are obtained with their respective strength and weight.

Table 4.6 Summary of strength and weight of the evidence for scenario II

No. of evidence	Source of information	Quantity	Procedure of estimation	Type of analysis	Type of correlation	Strength	Weight
(1)	An official report of the sand site	N/A	Geological information—type of deposit—geotechnical characteristics—range of ϕ'	Qualitative analysis	Intuitive inference and empirical correlation	Moderate	Moderate
(2)	An official report of the sand site	N/A	Geological information—type of deposit—geotechnical characteristics—range of ϕ'	Qualitative analysis	Intuitive inference and empirical correlation	Moderate	Moderate
(3)	An official report of the sand site	N/A	Geological information—type of deposit—range of ϕ'	Qualitative analysis	Intuitive inference	Weak	Moderate
(4)–(5)	An official report of the sand site	7 data groups and 13 data groups	Soil classification—range of ϕ'	Qualitative analysis	Empirical correlation	Strong	Moderate
(6)–(7)	An official report of the sand site	7 data groups and 13 data groups	Soil classification—values of μ	Qualitative analysis	Empirical correlation	Strong	Moderate
(8)	An official report of the sand site	N/A	Soil classification—range of σ	Qualitative analysis	Empirical correlation	Strong	Moderate
(9)	An official report of the sand site	N/A	Soil classification—range of λ	Qualitative analysis	Empirical correlation and intuitive inference	Moderate	Low
(10)	An official report of the sand site	N/A	Soil classification—dry unit weight—range of ϕ'	Qualitative analysis	Empirical correlation	Moderate	Moderate
(11)	An official report of the sand site	N/A	Soil classification—range of ϕ'	Qualitative analysis	Empirical correlation	Strong	Moderate

Table 4.7 Summary of the evidence for scenario II

Variable	No. of evidence	Prior uncertain estimates	Strength	Weight	No. of evidence group
ϕ'	(3)	30°–40°	Weak	Moderate	(I)
	(1)	28°–40°	Moderate	Moderate	(II)
	(2)	30°–40°	Moderate	Moderate	
	(10)	27°–37°	Moderate	Moderate	
	(4)	35°–41°	Strong	Moderate	(III)
	(5)	33°–43°	Strong	Moderate	
	(11)	28°–45°	Strong	Moderate	
μ	(6)	37.6°	Strong	Moderate	(IV)
	(7)	36.7°	Strong	Moderate	
σ	(8)	3.7°–5.5°	Strong	Moderate	(V)
λ	(9)	2–6 m	Moderate	Low	(VI)

For ϕ', there are in total 7 pieces of relevant evidence that are assembled into evidence groups (I)–(III) by their strength and weight. Evidence group (I) has one piece of evidence with weak strength and moderate weight, i.e., evidence (3). Evidence group (II) consists of 3 pieces of evidence with moderate strength and moderate weight, i.e., evidence (1), (2), and (10). Evidence group (III) is comprised of 3 pieces of evidence with strong strength and moderate weight, i.e., evidence (4), (5), and (11).

Using Eqs. (4.3) and (4.4), the range of ϕ' from 30° to 40° in evidence (3) (i.e., evidence group (I)) leads to $\mu = 35.0°$ and $\sigma = 1.7°$, respectively. In evidence group (II), the 3 possible ranges of ϕ' (i.e., evidence (1), (2), and (10)) provide 3 possible values of μ (i.e., 34.0°, 35.0°, and 32.0°) and σ (i.e., 2.0°, 1.7°, and 1.7°) by Eqs. (4.3) and (4.4), respectively. In evidence group (III), the 3 possible ranges of ϕ' (i.e., evidence (4), (5), and (11)) provide 3 possible values of μ (i.e., 38.0°, 38.0°, and 36.5°) and σ (i.e., 1.0°, 1.7°, and 2.8°) by Eqs. (4.3) and (4.4), respectively. Note that each range of ϕ' in evidence group (I), (II), and (III) leads to a pair of estimates of μ and σ. These estimates of μ and σ should be used with caution during subjective probability assessment since they are obtained from only one piece of evidence.

There are 2 pieces of evidence (i.e., evidence (6) and (7)) about the mean value μ of ϕ' in the evidence list, which suggest that μ is equal to 37.6° or 36.7°, i.e., evidence group (IV). For the standard deviation σ of ϕ', there is a possible range (i.e., from 3.7° to 5.5° in evidence (8)) in the evidence list. In addition, there is a possible range (i.e., from 2.0 to 6.0 m in evidence (9)) of λ in the evidence list.

4.10.3.3 Reassembling the Relevant Evidence for Each sub-objective

Table 4.8 summarizes the relevant evidence (i.e., Column 3) for each assessment sub-objective (i.e., Column 1) together with the strength (i.e., Column 4) and

Table 4.8 Summary of relevant evidence for each sub-objective of scenario II

sub-objective	No. of evidence group	No. of Evidence	Strength of the evidence	Weight of the evidence
Evaluating probability of μ	(I)	(3)	Weak	Moderate
	(II)	(1), (2), (10)	Moderate	Moderate
	(III)	(4), (5), (11)	Strong	Moderate
	(IV)	(6), (7)	Strong	Moderate
Evaluating probability of σ	(I)	(3)	Weak	Moderate
	(II)	(1), (2), (10)	Moderate	Moderate
	(III)	(4), (5), (11)	Strong	Moderate
	(V)	(8)	Strong	Moderate
Evaluating probability of λ	(VI)	(9)	Moderate	Low

weight (i.e., Column 5) of the evidence. There are a total of 9 pieces of evidence on evaluating probability of μ, including evidence (3) with weak strength and moderate weight, evidence (1), (2), and (10) with moderate strength and moderate weight, and evidence (4), (5), (6), (7), and (11) with strong strength and moderate weight. 8 pieces of evidence are obtained for evaluating probability of σ, including evidence (3) with weak strength and moderate weight, evidence (1), (2), and (10) with moderate strength and moderate weight, and evidence (4), (5), (8), and (11) with strong strength and moderate weight. Only one piece of evidence is obtained for evaluating probability of λ, i.e., evidence (9), with moderate strength and low weight.

4.10.4 Results of Subjective Probability Assessment

Based on the relevant evidence on each sub-objective (see Tables 4.7 and 4.8), percentiles of μ, σ, and λ are elicited from the assessor using the equivalent lottery method with the aid of the questionnaire shown in Appendix 4.1. Table 4.9 summarizes the percentiles of μ, σ, and λ obtained from the equivalent lottery method in Rows 2, 3, and 4, respectively. For the mean μ, 1 %, 25 %, 50 %, 75 % and 99 % percentiles are obtained from the equivalent lottery method according to the nine pieces of evidence shown in Table 4.8, and they are $\mu_{0.01} = 28.0^\circ, \mu_{0.25} = 33.0^\circ, \mu_{0.5} = 36.0^\circ, \mu_{0.75} = 38.0^\circ$, and $\mu_{0.99} = 45.0^\circ$. For the standard deviation σ, 1 %, 50 %, and 99 % percentiles are evaluated using the eight pieces of evidence shown in Table 4.8, and they are $\sigma_{0.01} = 1.0^\circ, \sigma_{0.5} = 2.5^\circ$, and $\sigma_{0.99} = 5.5^\circ$. The information on λ is much less than that of μ and σ (see Table 4.8). Therefore, only

Table 4.9 Summary of percentiles of the mean, standard deviation, and correlation length for scenario II

Cumulative probability	0.01	0.25	0.5	0.75	0.99
Mean μ (°)	28.0	33.0	36.0	38.0	45.0
Standard deviation σ (°)	1.0	N/A	2.5	N/A	5.5
Correlation length λ (m)	2.0	N/A	N/A	N/A	6.0

1 % and 99 % percentiles of λ are evaluated, and they are $\mu_{0.01} = 2.0\,\text{m}$ and $\mu_{0.99} = 6.0\,\text{m}$. Using the simplified method and the least squares regression method described in Sect. 4.7.4.1, prior distributions of μ, σ, and λ are obtained from their respective percentiles, as discussed in the following three subsections.

4.10.4.1 Prior Distribution of the Mean μ

Figure 4.6a shows the CDF of μ obtained from the simplified method and the least squares regression method by a solid line with open circles and a dark solid line, respectively. By the simplified method, the CDF of μ increases linearly between the adjacent percentiles (i.e., adjacent open circles). By the least squares regression method, a Gaussian CDF with a mean of 35.7° and standard deviation of 3.7° is obtained, and it is in good agreement with the CDF (i.e., the line with open circles) obtained from the simplified method. Figure 4.6a also includes the 95 % confidence interval of the CDF obtained from the least squares regression method by dashed lines. The five percentiles of μ obtained from the SPAF fall within the 95 % confidence interval of the Gaussian CDF. Therefore, the Gaussian CDF represents the assessment outcomes (i.e., percentiles of μ) from the SPAF reasonably well. Figure 4.6b shows the PDF of μ obtained from the simplified method and the least squares regression method by a histogram with four bins and a dark solid line, respectively. The Gaussian PDF of μ obtained from the least squares regression method compares favorably with the histogram of μ obtained from the simplified method. Both can be used as the prior distribution of μ in the Bayesian framework developed in Chap. 3.

4.10.4.2 Prior Distribution of the Standard Deviation σ

Figure 4.7a shows the CDF of σ obtained from the simplified method by a solid line with open circles. The CDF value of σ increases linearly from 0.01 to 0.5 as σ increases from 1.0° to 2.5° and then increases linearly from 0.5 to 0.99 as σ increases from 2.5° to 5.0°. Figure 4.7b shows the PDF of σ obtained from the simplified method by a histogram with two bins (i.e., from 1.0° to 2.5° and from 2.5° to 5.5°), and the PDF values of σ in the two bins are about 0.33 and 0.16,

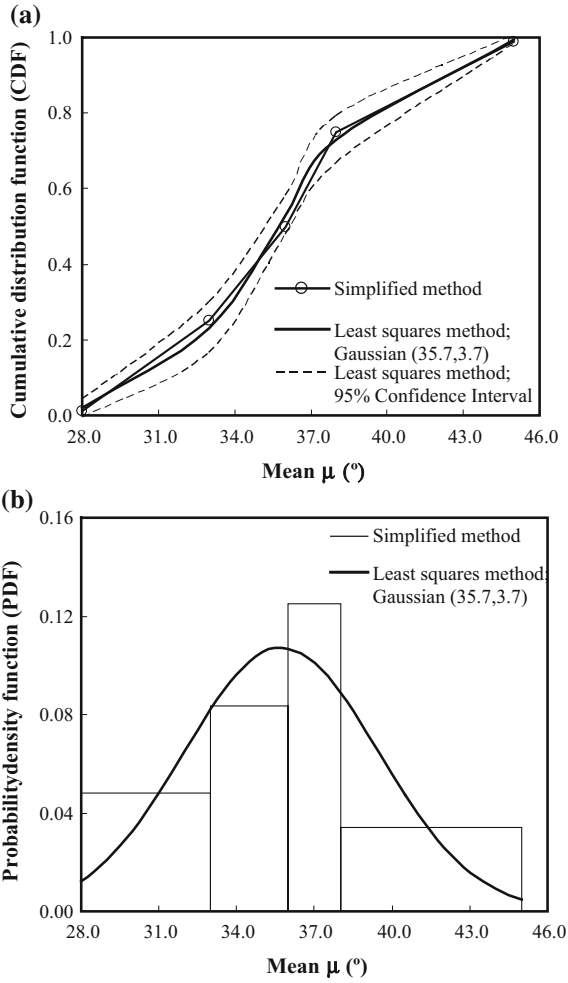

Fig. 4.6 Prior distribution of the mean, μ, in scenario II. **a** Cumulative distribution function (CDF) of the mean, μ. **b** Probability density function of the mean, μ

respectively. The PDF of σ (see Fig. 4.7b) can be taken as the prior distribution of σ in the Bayesian framework developed in Chap. 3.

4.10.4.3 Prior Distribution of the Correlation Length λ

Figure 4.8a shows the CDF of λ obtained from the simplified method by a solid line with open circles. The CDF value of λ increases linearly from 0.01 to 0.99 as λ increases from 2.0 to 6.0 m. Figure 4.8b shows the PDF of λ obtained from the simplified method by a histogram with only one bin (i.e., a uniform distribution with a range from 2.0 to 6.0 m), and the PDF value of λ is about 0.25. The probability distribution of λ obtained in this scenario remains the same as that

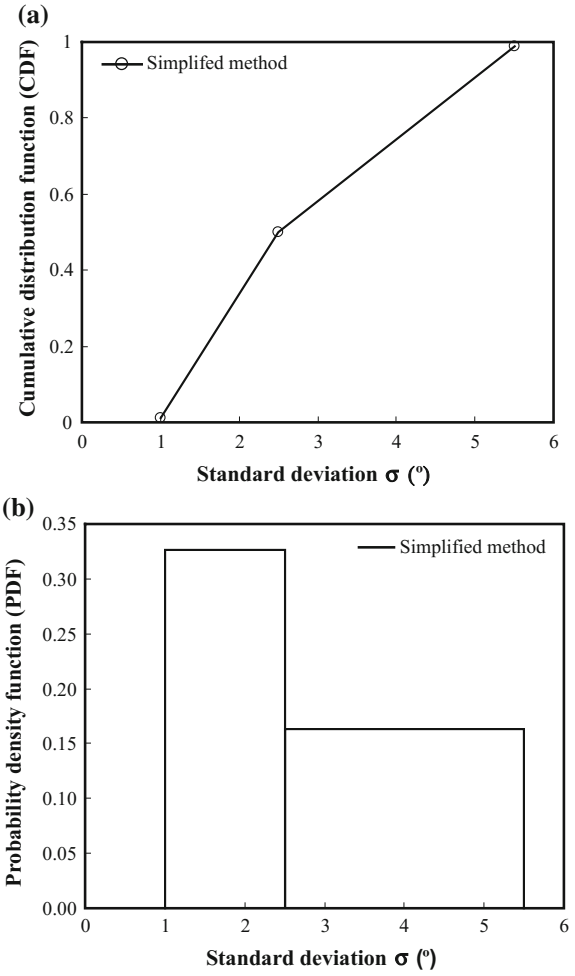

Fig. 4.7 Prior distribution of the standard deviation, σ, in scenario II. **a** Cumulative distribution function (CDF) of the standard deviation, σ. **b** Probability density function (PDF) of the standard deviation, σ

obtained in scenario I. It is not surprising to see this because the same information (i.e., a possible range of λ from 2.0 to 6.0 m) on λ is used in both scenarios. Similar to scenario I, the uniform PDF of λ (see Fig. 4.8b) can be taken as the prior distribution of λ in the Bayesian framework developed in Chap. 3.

4.10.5 Final Confirmation

All the areas under the respective PDFs (see Figs. 4.6b, 4.7b, and 4.8b) of μ, σ, and λ are summed up to unity. This is consistent with the basic probability axiom that the integration on a PDF is unity. The PDF value of μ in the bin from 36.0° to 38.0° is

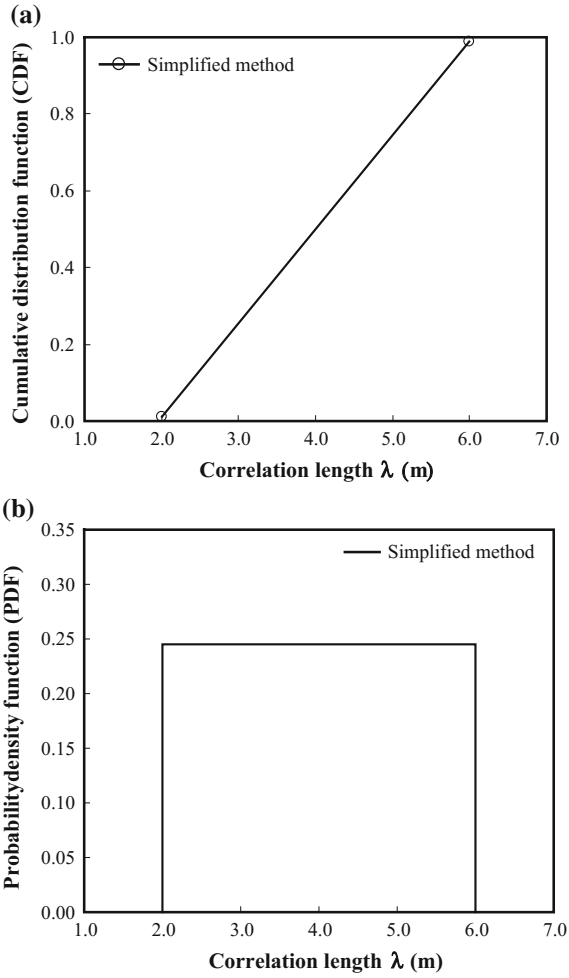

Fig. 4.8 Prior distribution of the correlation length, λ, in scenario II. **a** Cumulative distribution function (CDF) of the correlation length, λ. **b** Probability density function (PDF) of the correlation length, λ

greater than that of μ in the other bins, as shown in Fig. 4.6b. This is consistent with the information provided by evidence groups (III) and (IV) (see Tables 4.7 and 4.8), both of which have strong strength and moderate weight. Although the information provided by evidence groups (I) and (II) suggests that μ is 35.0° or varies from 32.0° to 35.0° (see Sect. 4.10.3.2), they have relatively weak strength (i.e., weak and moderate) compared with evidence groups (III) and (IV) (see Table 4.8). The PDF of μ reflects properly the information provided by prior knowledge.

The PDF value of σ in the bin from 1.0° to 2.5° is greater than that of σ in the bin from 2.5° to 5.5°. This is consistent with the information provided by evidence groups (I), (II), and (III) (see Sect. 4.10.3.2). Although the evidence group (V) suggests strongly that σ varies from 3.7° to 5.5°, the evidence group (V) only contains one piece of evidence (see Table 4.7) and should not be overemphasized.

The PDF of σ reflects properly the information provided by prior knowledge. Examination of the evidence is performed cautiously. It is found that no evidence is overlooked or overemphasized and the weight and strength of the evidence are properly taken into account when determining the percentiles of μ, σ, and λ.

It is also noted that the prior distributions of μ and σ (Figs. 4.6 and 4.7) obtained in this scenario are more informative than those obtained in scenario I (Figs. 4.3 and 4.4). This is reasonable in the sense that more information on μ and σ is used in this scenario (see Tables 4.7 and 4.8). In addition, the ranges of μ (i.e., from 28.0° to 45.0°), σ (i.e., from 1.0° to 5.5°), and λ (i.e., from 2.0 to 6.0 m) obtained from the SPAF are generally consistent with the actual belief of the assessor. The outcomes obtained from the SPAF are then confirmed. The probability distributions (see Figs. 4.6, 4.7 and 4.8) of μ, σ, and λ reflect the confidence levels of prior knowledge on them, respectively, and quantify properly the information provided by the prior knowledge.

4.11 Summary and Conclusions

This chapter proposed a subjective probability assessment framework (SPAF) based on a stage cognitive model of engineers' cognitive process. The SPAF assists engineers in utilizing prior knowledge in a relatively rational way and expressing quantitatively their engineering judgments in a probabilistic manner. The assessment outcomes (e.g., probability distributions) obtained from the SPAF are then taken as the prior distribution in the Bayesian framework developed in Chap. 3.

The SPAF consists of five steps: specification of assessment objectives (i.e., the soil property and its statistics of interest), collection of relevant information and preliminary estimation, synthesis of the evidence, numerical assignment, and confirmation of assessment outcomes. The steps of the proposed SPAF are corresponding to the stages of cognitive process of engineers. By this means, engineers can formulate their engineering judgments naturally using prior knowledge and express quantitatively the engineering judgments using subjective probability with relative ease. Several suggestions were provided for each step to assist engineers in utilizing prior knowledge in a relatively rational way and reducing the effects of cognitive biases and limitations during subjective probability assessment.

The proposed SPAF is applied to characterize probabilistically the sand effective friction angle at a US National Geotechnical Experimentation Site (NGES) at Texas A&M University, and it is illustrated under two scenarios: one with sparse prior knowledge and the other with a reasonable amount of prior knowledge. It is shown that the SPAF is applicable for both scenarios. When the prior knowledge is sparse, the prior distribution obtained from the proposed approach is relatively uninformative (e.g., uniform distributions). As the information provided by the prior knowledge improves, the proposed approach provides informative prior

distribution. The prior distribution obtained from the SPAF quantifies properly the information provided by the prior knowledge.

Appendix 4.1: Questionnaire for Implementing the Equivalent Lottery Method

This appendix provides a questionnaire for implementing the equivalent lottery method. The questionnaire starts with a question (i.e., Q1), that is used to determine a reference prize for the equivalent lottery method, followed by the second and third questions (i.e., Q2 and Q3) for determining 1 % and 99 % percentiles (i.e., $\theta_{i,0.01}$ and $\theta_{i,0.99}$) of the variable θ_i concerned, respectively. Then, the fourth question (i.e., Q4) can be used to estimate the 50 % percentile (i.e., $\theta_{i,0.5}$) of θ_i if sufficient information on θ_i is available. The questionnaire can be continued to determine percentiles of θ_i progressively until engineers believe that there is no sufficient information on θ_i to balance the two lotteries in the equivalent lottery method for a given range of θ_i.

Questionnaire

Q1: What is the prize that you want recently? Please write it down.
Answer: A_1

Q2: What is the minimum possible value of θ_i?
Answer: A_2

Q3: What is the maximum possible value of θ_i?
Answer: A_3

Q4: There are two lotteries as follows.

Lottery 1:

Win A_1 if $A_2 \leq \theta_i \leq a_s$ occurs.
Win nothing if $a_s < \theta_i \leq A_3$ occurs.

Lottery 2:

Win A_1 or nothing equally likely.

Please adjust the value a_s from A_3 to A_2 gradually until you feel indifferent between the two lotteries. Please write down the resulting value of a_s and denote it by A_4.

Note that the questionnaire shall be continued to determine percentiles of θ_i progressively using different ranges of θ_i in the equivalent lottery method if there is sufficient information on θ_i to balance the two lotteries for a given range of θ_i.

References

Ang, A.H.S., and W.H. Tang. 2007. *Probability concepts in engineering: emphasis on applications to civil and environmental engineering*. New York: Wiley.

Baecher, G.B., and J.T. Christian. 2003. *Reliability and statistics in geotechnical engineering*, 605 pp. Hoboken, New Jersey: Wiley.

Briaud, J.L. 2000. The national geotechnical experimentation sites at Texas A&M University: clay and sand. A summary. *National Geotechnical Experimentation Sites, Geotechnical Special Publication* 93: 26–51.

Cao, Z., Y. Wang, and D. Li. 2016. Quantification of prior knowledge in geotechnical site characterization. *Engineering Geology* 203: 107–116.

Clayton, C.R.I., M.C. Matthews, and N.E. Simons. 1995. *Site investigation*. Cambridge, MA, USA: Blackwell Science.

Clemen, R.T. 1996. *Making hard decisions: An introduction to decision analysis*. Pacific Grove: Duxbury Press.

Duncan, J.M. 2000. Factors of safety and reliability in geotechnical engineering. *Journal Geotechnical and Geoenvironmental Engineering* 126(4): 307–316.

El-Ramly, H., N.R. Morgenstern, and D.M. Cruden. 2002. Probabilistic slope stability analysis for practice. *Canadian Geotechnical Journal* 39: 665–683.

Fischhoff, B., P. Slovic, and S. Lichtenstein. 1977. Knowing with certainty: The appropriateness of extreme confidence. *Journal of Experimental Psychology: Human Perception and Performance* 3(4): 552–564.

Griffin, D., and A. Tversky. 1992. The weighing of evidence and the determinants of confidence. *Cognitive Psychology* 24(3): 411–435.

Heim, G.E. 1990. Knowledge of the origin of soil deposits is of primary importance to understanding the nature of the deposit. *Bulletin of the Association of Engineering Geologists* 27(1): 109–112.

Hogarth, R.M. 1975. Cognitive processes and the assessment of subjective probability distributions. *Journal of the American Statistical Association* 70(350): 271–289.

Kulhawy, F.H., and P.W. Mayne. 1990. *Manual on Estimating Soil Properties for Foundation Design*, Report EL 6800, 360 pp. Palo Alto: Electric Power Research Inst.

Mathworks, Inc. 2010. MATLAB—the language of technical computing. http://www.mathworks.com/products/matlab/, 9 Mar 2009.

Mayne, P.W., B.R. Christopher, and J. DeJong. 2002. *Subsurface investigations—geotechnical site characterization*, No. FHWA NHI-01-031. Washington D.C.: Federal Highway Administration, U. S. Department of Transportation.

Phoon, K.K., and F.H. Kulhawy. 1999a. Characterization of geotechnical variability. *Canadian Geotechnical Journal* 36(4): 612–624.

Phoon, K.K., and F.H. Kulhawy. 1999b. Evaluation of geotechnical property variability. *Canadian Geotechnical Journal* 36(4): 625–639.

Rollings, M.P., and R.S. Rollings. 1996. *Geotechnical materials in construction*. New York: McGraw-Hill.

Ross, S.M. 2007. *Introduction to probability models*. California, USA: Academic Press.

Terzaghi, K., and Peck, R.B. 1967. *Soil mechanics in engineering practice*, 729 pp. New York: Wiley.

Vanmarcke, E.H. 1977. Probabilistic modeling of soil profiles. *Journal of Geotechnical Engineering* 103(11): 1127–1246.

Vanmarcke, E.H. 1983. *Random fields: Analysis and synthesis*. Cambridge: MIT Press.

Vick, S.G. 2002. *Degrees of belief: Subjective probability and engineering judgment*. Reston, Virginia: ASCE Press.

Vick, S.G. 1997. Dam safety risk assessment: New directions. *Water Power and Dam Construction* 49(6).

Chapter 5
Probabilistic Characterization of Young's Modulus of Soils Using Standard Penetration Tests

5.1 Introduction

The subjective probability approach developed in the previous chapter quantifies probabilistically the information provided by prior knowledge that is collected during the preliminary stages (i.e., desk study and site reconnaissance) of geotechnical site characterization. The prior knowledge is of great significance in geotechnical site characterization (Clayton et al. 1995), particularly when only limited project-specific test results are obtained from test boring, in situ testing (e.g., standard penetration tests (SPTs)), and laboratory testing. For example, in projects with medium or relatively small sizes, the number of SPT results is generally too sparse to generate meaningful statistics (e.g., mean, standard deviation, and other high-order moments) of soil properties. Such information is, however, required in probabilistic analysis and/or designs of geotechnical structures. To address this problem, this chapter develops a Markov Chain Monte Carlo simulation (MCMCS)-based approach that utilizes both prior knowledge and project-specific SPT results to generate a large number of equivalent samples of the soil property of interest for its probabilistic characterization. The proposed approach takes advantage of prior knowledge in a rational way and integrates systematically the prior knowledge and project-specific test results under the Bayesian framework developed in Chap. 3. The proposed approach is formulated for the undrained Young's modulus E_u estimated from SPT, but it is equally applicable for other soil properties and other in situ or laboratory tests.

This chapter starts with probabilistic modeling of the inherent variability of E_u and the transformation uncertainty associated with the regression between E_u and SPT N-values (i.e., N_{SPT}), followed by integration of the prior knowledge and project-specific SPT data under the Bayesian framework and derivation of the probability density function (PDF) of E_u. Then, a large number of equivalent samples of E_u are generated from the PDF of E_u using MCMCS. Conventional statistical analysis of the equivalent examples is subsequently carried out to

Z. Cao et al., *Probabilistic Approaches for Geotechnical Site Characterization and Slope Stability Analysis*, DOI 10.1007/978-3-662-52914-0_5

determine the statistics of E_u. Implementation procedure of the proposed equivalent sample approach is described. As an illustration, the proposed approach is applied to characterizing probabilistically the E_u at the clay site of the US National Geotechnical Experimentation Sites (NGES) at Texas A&M University. In addition, sensitivity studies are performed to explore effects of the number of project-specific test data and prior knowledge on the probabilistic characterization of soil properties.

5.2 Uncertainty Modeling

5.2.1 Inherent Variability

Geotechnical materials are natural materials, and their properties are affected by various factors during their formation process, such as properties of their parent materials, weathering and erosion processes, transportation agents, and conditions of sedimentation (Vanmarcke 1977; Phoon and Kulhawy 1999a; Baecher and Christian 2003; Mitchell and Soga 2005). Properties of geotechnical materials therefore vary spatially, and such inherent variability is independent of the state of knowledge about geotechnical properties and cannot be reduced as the knowledge improves (Baecher and Christian 2003). Consider, for example, undrained Young's modulus, E_u, within a clay layer. To model explicitly the inherent variability, E_u is represented by a lognormal random variable with a mean μ and standard deviation σ, and it is defined as (e.g., Ang and Tang 2007; Au et al. 2010)

$$E_u = \exp\left(\mu_N + \sigma_N z\right) \tag{5.1}$$

in which z is a standard Gaussian random variable; $\mu_N = \ln \mu - \frac{1}{2}\sigma_N^2$ and $\sigma_N = \sqrt{\ln\left(1 + (\sigma/\mu)^2\right)}$ are the mean and standard deviation of the logarithm (i.e., $\ln(E_u)$) of E_u, respectively. $\ln(E_u)$ is normally distributed, and it is expressed as

$$\ln(E_u) = \mu_N + \sigma_N z \tag{5.2}$$

Note that both the σ of E_u and the σ_N of $\ln(E_u)$ represent the inherent variability of the undrained Young's modulus within the clay layer.

5.2.2 Transformation Uncertainty

The undrained Young's modulus of clays can be measured directly using pressuremeter tests, which are generally considered as one of the most accurate measurements for E_u, but are certainly expensive and time consuming (Mair and Wood

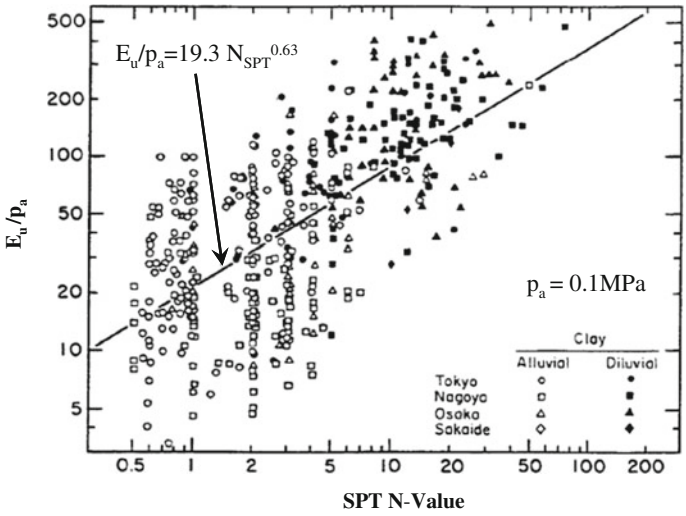

Fig. 5.1 Regression between SPT *N*-value and undrained Young's modulus of clay (After Ohya et al. 1982; Kulhawy and Mayne 1990; Phoon and Kulhawy 1999b; Wang and Cao 2013)

1987; Briaud 1992; Wang and O'Rourke 2007). More frequently and particularly for projects with medium or relatively small sizes, the E_u is usually estimated indirectly from other in situ tests, such as SPTs (Kulhawy and Mayne 1990; Clayton 1995; Mayne et al. 2002). The E_u value of the tested soil is obtained by means of regression between the E_u and the *N*-values (i.e., N_{SPT}) obtained by SPTs. Figure 5.1 shows a regression model between the E_u measured by pressuremeter tests and SPT *N*-values (Kulhawy and Mayne 1990; Phoon and Kulhawy 1999b)

$$E_u/p_a = 19.3N_{SPT}^{0.63} \tag{5.3}$$

in which p_a is the atmospheric pressure (i.e., 0.1 MPa). Equation (5.3) can be rewritten in a log-log scale as

$$\xi = \ln(N_{SPT}) = a\ln(E_u) + b + \varepsilon \tag{5.4}$$

in which $\xi = \ln(N_{SPT})$ denotes the SPT *N*-value in a log scale; $a = 1.587$, $b = -1.044$, and ε is a Gaussian random variable with a zero mean and a standard deviation $\sigma_\varepsilon = 1.352$ (Ohya et al. 1982; Kulhawy and Mayne 1990; Phoon and Kulhawy 1999b). The last term ε represents a modeling scatterness or transformation uncertainty associated with the regression equation. Combining Eqs. (5.2) and (5.4) leads to

$$\xi = \ln(N_{SPT}) = (a\mu_N + b) + a\sigma_N z + \varepsilon \tag{5.5}$$

When the inherent variability is assumed to be independent of the transformation uncertainty (i.e., z is independent of ε), ξ is a Gaussian random variable with a mean of $(a\mu_N + b)$ and standard deviation of $\sqrt{(a\sigma_N)^2 + (\sigma_\varepsilon)^2}$.

Information provided by SPT data ξ is quantified by its probability distribution. For completely defining the probability distribution of ξ, the information on μ_N and σ_N (or μ and σ, see Eq. (5.1)) is needed. Such information is unknown and needs to be determined during site characterization. In the next section, the Bayesian framework, developed in Chap. 3, is applied to updating the knowledge of model parameters μ and σ based on prior knowledge and project-specific SPT N-values.

5.3 Bayesian Framework

Under a Bayesian framework, the updated knowledge about μ and σ is reflected by their joint posterior distributions based on prior knowledge and site observation data (e.g., Ang and Tang 2007; Wang et al. 2010)

$$P(\mu, \sigma \mid Data) = KP(Data \mid \mu, \sigma)P(\mu, \sigma) \tag{5.6}$$

in which $K = (\int_{\mu,\sigma} P(Data \mid \mu, \sigma)P(\mu, \sigma)d\mu\, d\sigma)^{-1}$ is a normalizing constant that does not depend on μ and σ; $Data = \{\xi_i = \ln(N_{\mathrm{SPT},i}), i = 1, 2, \ldots, n_s\}$ is a set of SPT data with totally n_s $\ln(N_{\mathrm{SPT}})$ values obtained within a clay layer; $P(Data \mid \mu, \sigma)$ is the likelihood function reflecting the likelihood of obtaining the *Data* for a given set of μ and σ; $P(\mu, \sigma)$ is the prior distribution of μ and σ that reflects the prior knowledge on μ and σ in the absence of *Data*.

As described in the Sect. 5.2.2, $\xi = \ln(N_{\mathrm{SPT}})$ is a Gaussian random variable with a mean of $(a\mu_N + b)$ and standard deviation of $\sqrt{(a\sigma_N)^2 + (\sigma_\varepsilon)^2}$. The project-specific SPT data (i.e., $Data = \{\xi_i = \ln(N_{\mathrm{SPT},i}), i = 1, 2, \ldots, n_s\}$) can be considered as n_s independent realizations of the Gaussian random variable ξ. The likelihood function for the project-specific SPT data is therefore expressed as (e.g., Ang and Tang 2007)

$$P(Data \mid \mu, \sigma) = \prod_{i=1}^{n_s} \frac{1}{\sqrt{2\pi}\sqrt{(a\sigma_N)^2 + (\sigma_\varepsilon)^2}} \exp\{-\frac{1}{2}[\frac{\xi_i - (a\mu_N + b)}{\sqrt{(a\sigma_N)^2 + (\sigma_\varepsilon)^2}}]^2\} \tag{5.7}$$

The prior distribution can be simply assumed as a joint uniform distribution of μ and σ with respective minimum values of $\mu_{\min}$ and $\sigma_{\min}$ and respective maximum values of $\mu_{\max}$ and $\sigma_{\max}$, and it is expressed as (e.g., Ang and Tang 2007)

$$P(\mu,\sigma)=\begin{cases}\frac{1}{\mu_{\max}-\mu_{\min}}\times\frac{1}{\sigma_{\max}-\sigma_{\min}} & \text{for } \mu\in[\mu_{\min},\mu_{\max}] \text{ and } \sigma\in[\sigma_{\min},\sigma_{\max}]\\ 0 & \text{otherwise}\end{cases} \tag{5.8}$$

Note that only the possible ranges (i.e., $\mu_{\min}$ and $\mu_{\max}$, $\sigma_{\min}$ and $\sigma_{\max}$) of model parameters are needed to completely define a uniform prior distribution herein. This requires relatively limited prior knowledge (e.g., reasonable ranges of soil properties of interest), which is commonly available in geotechnical literature (e.g., Kulhawy and Mayne 1990; Phoon and Kulhawy 1999a, b). The approach proposed in this chapter is general and equally applicable for more sophisticated types of prior distributions, which of course require relatively informative prior knowledge as justifications. The effect of different prior knowledge is further discussed in Sect. 5.9.

The posterior distribution in Eq. (5.6) is a joint distribution of μ and σ, and it represents the updated knowledge of μ and σ based on prior knowledge and project-specific SPT data (i.e., *Data*). In the next section, the updated knowledge of μ and σ is applied to determine the probabilistic density function (PDF) of the undrained Young's modulus E_u.

5.4 Probability Density Function of Undrained Young's Modulus

As defined by Eq. (5.1) or (5.2), the undrained Young's modulus is modeled by a random variable E_u which follows a lognormal distribution with a mean μ and standard deviation σ. Both prior knowledge and project-specific test data (e.g., SPT *N*-values) are used to estimate the distribution model parameters μ and σ in geotechnical site characterization. For a given set of prior knowledge and project-specific SPT data, there are many sets of possible values of μ and σ. Each set of μ and σ has its corresponding plausibility (or occurrence probability), which is defined by a joint conditional PDF $P(\mu,\sigma\,|\,Data,Prior)$. Using the conventional notation of Bayesian framework, $P(\mu,\sigma\,|\,Data,Prior)$ is simplified as $P(\mu,\sigma\,|\,Data)$ and is given by Eq. (5.6). Using the Theorem of Total Probability (e.g., Ang and Tang 2007), the PDF of the undrained Young's modulus E_u for a given set of prior knowledge and project-specific SPT data is expressed as

$$P(E_u\,|\,Data,Prior)=\int_{\mu,\sigma}P(E_u\,|\,\mu,\sigma)P(\mu,\sigma\,|\,Data,Prior)d\mu\,d\sigma \tag{5.9}$$

where *Prior* and *Data* denote prior knowledge and project-specific SPT data, respectively; $P(E_u\,|\,\mu,\sigma)$ is conditional PDF of E_u for a given set of model parameters (i.e., μ and σ). Because E_u is lognormally distributed, $P(E_u\,|\,\mu,\sigma)$ is expressed as (e.g., Ang and Tang 2007)

$$P(E_u \mid \mu, \sigma) = \frac{1}{\sqrt{2\pi}\sigma_N E_u} \exp\{-\frac{1}{2}[\frac{\ln(E_u) - \mu_N}{\sigma_N}]^2\} \tag{5.10}$$

where both μ_N and σ_N are functions of μ and σ (see Sect. 5.2.1). Combining Eqs. (5.6) and (5.9), the PDF of undrained Young's modulus E_u (i.e., Eq. (5.9)) is rewritten as

$$P(E_u \mid Data, Prior) = K \int_{\mu,\sigma} P(E_u \mid \mu, \sigma) P(Data \mid \mu, \sigma) P(\mu, \sigma) d\mu \, d\sigma \tag{5.11}$$

Equation (5.11) is a product of the normalizing constant K and the integral term $I = \int_{\mu,\sigma} P(E_u \mid \mu, \sigma) P(Data \mid \mu, \sigma) P(\mu, \sigma) d\mu \, d\sigma$, and it gives the PDF of E_u for a given set of prior knowledge (i.e., $P(\mu, \sigma)$) and project-specific SPT data (i.e., *Data*). In the next section, Markov Chain Monte Carlo simulation (MCMCS) method (e.g., Beck and Au 2002; Robert and Casella 2004) is used to generate a sequence of E_u samples whose limiting stationary distribution tends to be the PDF of E_u (i.e., Eq. (5.11)).

5.5 Markov Chain Monte Carlo Simulation and Equivalent Samples

MCMCS method is a numerical process that simulates a sequence of samples of a random variable (e.g., E_u) as a Markov Chain with the PDF of the random variable (e.g., Eq. (5.11) for E_u) as the Markov Chain's limiting stationary distribution (e.g., Beck and Au 2002; Robert and Casella 2004). The states of the Markov Chain after it reaches stationary condition are then used as samples of the random variable with the target PDF. It provides a feasible way to generate samples from an arbitrary PDF, particularly when the PDF is complicated and is difficult to be expressed analytically and explicitly.

5.5.1 Metropolis–Hastings (MH) Algorithm

In this chapter, the Metropolis–Hastings (MH) algorithm (Metropolis et al. 1953; Hastings 1970; Beck and Au 2002) is used in MCMCS to generate totally n_{MCMC} number of the E_u samples from Eq. (5.11). The E_u Markov Chain starts with an arbitrary initial state, $E_{u,1}$. Then, the jth state of the E_u Markov Chain, $E_{u,j}$, $j = 2, 3, \ldots, n_{MCMC}$, (e.g., $E_{u,2}$ for the second state) is generated from its previous state (j-1)th, $E_{u,j-1}$ (e.g., the initial state $E_{u,1}$ for $E_{u,2}$). A candidate sample, $E^*_{u,j}$, $j = 2, 3, \ldots, n_{MCMC}$, for the jth state is generated from the proposal PDF $f(E^*_{u,j} \mid E_{u,j-1})$. The proposal PDF $f(E^*_{u,j} \mid E_{u,j-1})$ herein is taken as a Gaussian PDF,

which is centered at the previous state $E_{u,j-1}$, $j = 2, 3, \ldots, n_{MCMC}$, and has a COV equal to the mean COV of the prior knowledge (e.g., $COV = [0.5(\sigma_{\max} + \sigma_{\min})] / [0.5(\mu_{\max} + \mu_{\min})] = (\sigma_{\max} + \sigma_{\min}) / (\mu_{\max} + \mu_{\min})$ for the uniform prior μ given in Eq. (5.8)). For example, $E^*_{u,2}$ is simulated from a Gaussian PDF with a mean of $E_{u,1}$ and $COV = (\sigma_{\max} + \sigma_{\min}) / (\mu_{\max} + \mu_{\min})$. The candidate sample $E^*_{u,j}$ is, however, not necessarily to be accepted as the jth state of the E_u Markov Chain (i.e., $E_{u,j}$). The chance to accept the candidate sample $E^*_{u,j}$ as the $E_{u,j}$ depends on the "acceptance ratio," r_a, which is calculated as

$$r_a = \frac{P(E^*_{u,j} \mid Data, Prior)}{P(E_{u,j-1} \mid Data, Prior)} \times \frac{f(E_{u,j-1} \mid E^*_{u,j})}{f(E^*_{u,j} \mid E_{u,j-1})} \quad for \quad j = 2, 3, \ldots, n_{MCMC} \tag{5.12}$$

in which $P(E^*_{u,j} \mid Data, Prior)$ and $P(E_{u,j-1} \mid Data, Prior)$ are respective PDF values of $E^*_{u,j}$ and $E_{u,j-1}$, and they are calculated from Eq. (5.11); $f(E^*_{u,j} \mid E_{u,j-1})$ is the conditional PDF value of $E^*_{u,j}$ given $E_{u,j-1}$; $f(E_{u,j-1} \mid E^*_{u,j})$ is the conditional PDF value of $E_{u,j-1}$ given $E^*_{u,j}$. In this chapter, $f(E^*_{u,j} \mid E_{u,j-1})$ and $f(E_{u,j-1} \mid E^*_{u,j})$ are calculated from the Gaussian PDF with respective mean values of $E_{u,j-1}$ and $E^*_{u,j}$. Combining Eqs. (5.11) and (5.12) leads to

$$r_a = \frac{I(E^*_{u,j})}{I(E_{u,j-1})} \times \frac{f(E_{u,j-1} \mid E^*_{u,j})}{f(E^*_{u,j} \mid E_{u,j-1})} \quad for \quad j = 2, 3, \ldots, n_{MCMC} \tag{5.13}$$

in which $I(E^*_{u,j})$ and $I(E_{u,j-1})$ are respective values of the integral term I in Eq. (5.11) at $E^*_{u,j}$ and $E_{u,j-1}$. Note that there is no need to calculate the K term during the MCMCS because it is canceled out when calculating the r_a value (see Eqs. (5.12) and (5.13)). The integral term I is still needed for the r_a calculation (see Eq. (5.13)), and it can be calculated numerically using a two-dimensional grid over the space of μ and σ as follows:

$$I = \sum_{j_\mu=1}^{n_\mu} \sum_{j_\sigma=1}^{n_\sigma} P(E_u \mid \mu_{j_\mu}, \sigma_{j_\sigma}) P(Data \mid \mu_{j_\mu}, \sigma_{j_\sigma}) P(\mu_{j_\mu}, \sigma_{j_\sigma}) \Delta\mu \, \Delta\sigma \tag{5.14}$$

in which $\Delta\mu$ and $\Delta\sigma$ are respective intervals of μ and σ used in the two-dimensional grid; $n_\mu = (\mu_{\max} - \mu_{\min}) / \Delta\mu$ and $n_\sigma = (\sigma_{\max} - \sigma_{\min}) / \Delta\sigma$ are the respective numbers of intervals of μ and σ in the two-dimensional grid; $\mu_{j_\mu} = \mu_{\min} + (2j_\mu - 1)\Delta\mu / 2$, $j_\mu = 1, 2, \ldots n_\mu$, is the average value of μ in j_μth interval of μ; $\sigma_{j_\sigma} = \sigma_{\min} + (2j_\sigma - 1)\Delta\sigma/2$, $j_\sigma = 1, 2, \ldots n_\sigma$, is the average value of σ in j_σth interval of σ. $P(Data \mid \mu_{j_\mu}, \sigma_{j_\sigma})$, $P(\mu_{j_\mu}, \sigma_{j_\sigma})$, and $P(E_u \mid \mu_{j_\mu}, \sigma_{j_\sigma})$ are calculated from Eqs. (5.7), (5.8), and (5.10) at μ_{j_μ} and σ_{j_σ}, respectively. Among these three terms, only $P(E_u \mid \mu_{j_\mu}, \sigma_{j_\sigma})$ needs to be calculated repeatedly for different

samples of E_u during MCMCS, because $P(Data \mid \mu_{j_\mu}, \sigma_{j_\sigma})$ and $P(\mu_{j_\mu}, \sigma_{j_\sigma})$ are independent of E_u and remain unchanged during MCMCS.

When r_a is greater than unity, the candidate sample $E^*_{u,j}$ is accepted as the jth state of the E_u Markov Chain (i.e., $E_{u,j}$). When r_a falls within [0, 1], the probability to accept $E^*_{u,j}$ as $E_{u,j}$ is r_a. In implementation, a random number u is generated from a uniform distribution with a range from zero to one. If u is less than r_a, $E^*_{u,j}$ is accepted as $E_{u,j}$, i.e., $E_{u,j} = E^*_{u,j}$. Otherwise, $E^*_{u,j}$ is rejected, and $E_{u,j}$ is taken as the previous state $E_{u,j-1}$, i.e., $E_{u,j} = E_{u,j-1}$. For example, the r_a value for the candidate sample $E^*_{u,2}$ is calculated from Eqs. (5.13) and (5.14) using $E_{u,1}$ and $E^*_{u,2}$, and the second state $E_{u,2}$ is then determined accordingly by comparing the values of r_a and u. Starting from the initial sample $E_{u,1}$, the procedure described above is repeated $n_{MCMC} - 1$ times to generate $n_{MCMC} - 1$ samples of E_u, i.e., $E_{u,j}$, $j = 2, 3, \ldots, n_{MCMC}$. This leads to a Markov Chain that is comprised of n_{MCMC} E_u samples (including the initial sample). Finally, the E_u samples obtained after the Markov Chain reaches its stationary condition are considered as appropriate samples for probabilistic characterization of E_u. Note that, because the Markov Chain at its stationary condition is independent of the initial state, the arbitrary value of $E_{u,1}$ taken as the initial state of the Markov Chain has no effect on the E_u samples adopted herein.

5.5.2 Equivalent Samples

Equation (5.11) shows that the PDF of E_u contains information from both project-specific test data (i.e., *Data*) and prior knowledge (i.e., *Prior*). The information from these two different sources is integrated probabilistically in a rational manner. The MCMCS samples that are drawn from the E_u PDF, therefore, contain the integrated information of both project-specific site observation data and prior knowledge. When the project-specific data are limited, the MCMCS samples mainly reflect the prior knowledge. As the number of project-specific data increases, the effect of the project-specific data on the MCMCS samples gradually increases.

More importantly, a large number of E_u samples can be generated conveniently by MCMCS. From a statistical point of view, these MCMCS samples are equivalent to those E_u data that are measured physically from laboratory or in situ tests (e.g., pressuremeter tests). Therefore, this large number of equivalent samples can be analyzed statistically, using conventional statistical methods, to estimate the required statistics (e.g., mean and standard deviation) of E_u, and they can also be used to construct histogram and cumulative frequency diagram for proper estimations of the PDF and cumulative distribution function (CDF) of E_u. This allows a proper characterization of the statistical distribution of E_u, and subsequently a proper selection of the characteristic value of E_u for the implementation of the recent design codes, such as Eurocode 7 (BSI 2010).

In summary, the approach proposed in this chapter integrates probabilistically the prior knowledge (e.g., previous engineering experience) and project-specific test data (e.g., SPT data) and transforms the integrated information into a large number, as many as needed, of equivalent samples. This allows meaningful statistics of soil properties to be obtained using conventional statistical analysis, leading to a proper selection of the characteristic value (e.g., mean or lower 5 % percentile) of soil properties for probabilistic geotechnical analysis and/or designs. The proposed approach effectively tackles the difficulty in generating meaningful statistics from the usually limited number of soil property data obtained during geotechnical site characterization.

5.6 Implementation Procedures

Figure 5.2 shows a flowchart for the implementation of the equivalent sample approach schematically. In general, the implementation procedure involves 5 steps. Details of each step and its associated equations are summarized as follows:

(1) Obtain n_s SPT N-values from SPTs and convert them to $Data = \{\xi_i = \ln(N_{\mathrm{SPT},i}),\ i = 1, 2, \ldots, n_s\}$;
(2) Obtain an appropriate prior knowledge on the mean μ and standard deviation σ, such as reasonable ranges of μ and σ with respective minimum values $\mu_{\min}$ and $\sigma_{\min}$ and respective maximum values of $\mu_{\max}$ and $\sigma_{\max}$;
(3) Choose an appropriate two-dimensional grid over the space of μ and σ to calculate $P(Data \,|\, \mu_{j_\mu}, \sigma_{j_\sigma})$ and $P(\mu_{j_\mu}, \sigma_{j_\sigma})$ at μ_{j_μ} and σ_{j_σ} for each interval of μ and σ according to Eqs. (5.7) and (5.8), respectively;
(4) Choose an initial state for the Markov Chain of E_u, such as the mean of the prior knowledge of μ (e.g., $(\mu_{\max} + \mu_{\min}) / 2$ for the uniform prior μ given in Eq. (5.8)), and use the MH algorithm to generate a large number of the E_u samples using Eqs. (5.9) and (5.11), as illustrated by the textboxes with dashed lines in Fig. 5.2;
(5) Estimate μ and σ (or μ_N and σ_N) using the large number of equivalent E_u samples and/or estimate the PDF and CDF of E_u from the histogram and cumulative frequency diagram of the equivalent samples, respectively.

These five steps can be readily programmed as a user function or toolbox in commonly available commercial software packages, e.g., MATLAB (Mathworks Inc. 2010) or Microsoft Excel (Microsoft Corporation 2012). Geotechnical practitioners only need to provide prior knowledge (e.g., reasonable ranges of soil properties) and project-specific test data (e.g., SPT N-values) as input, and the user function or toolbox will return a large number, as many as needed, of equivalent samples that can be analyzed using conventional statistical analysis. The equivalent sample approach and implement procedure described above are illustrated through a real example in the next section.

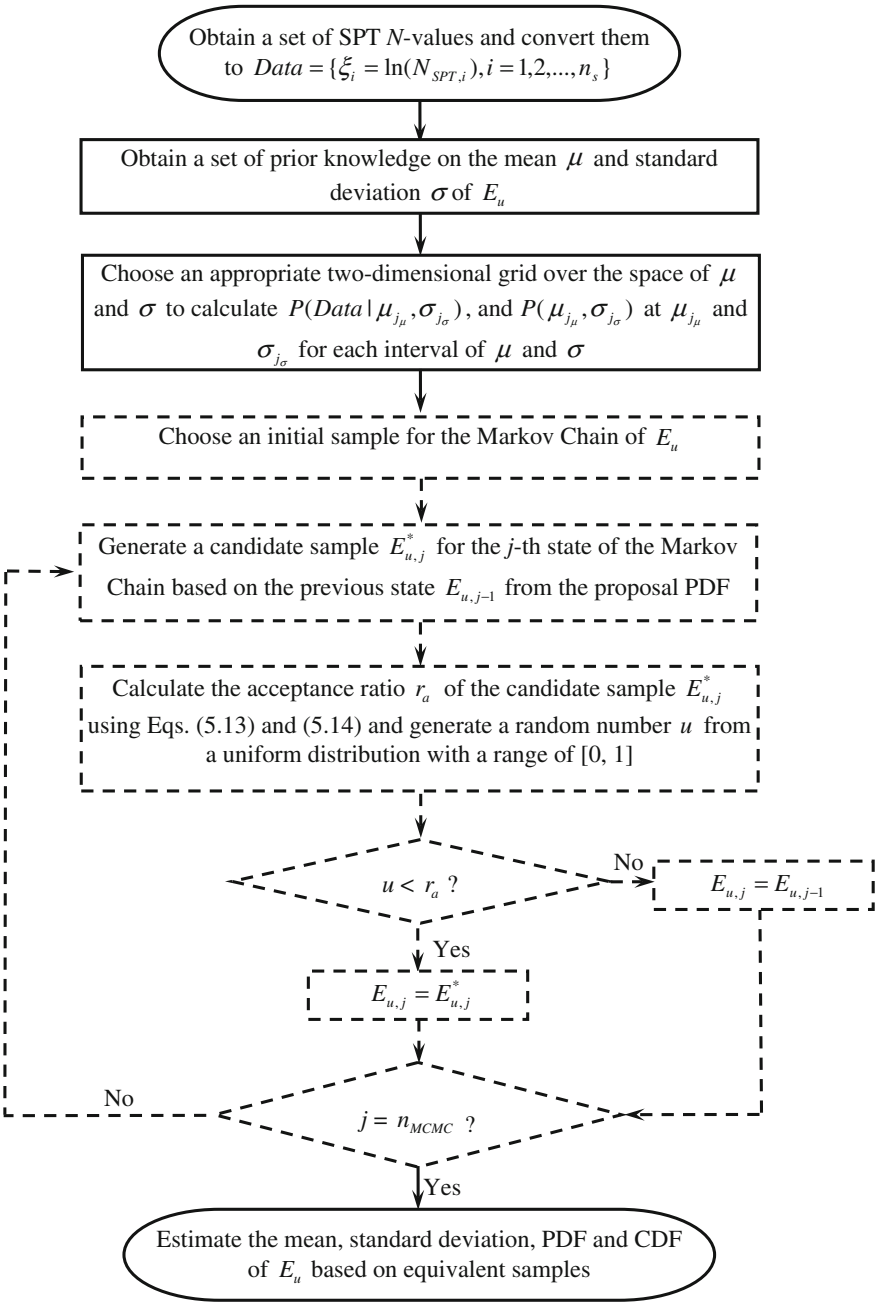

Fig. 5.2 Flowchart for the implementation of the equivalent sample approach (After Wang and Cao 2013)

5.7 Illustrative Example

The proposed equivalent sample approach is applied to characterize probabilistically the undrained Young's modulus using SPT *N*-values obtained from the clay site of the NGES at Texas A&M University (Briaud 2000). The site is comprised of a top stiff clay layer extending from the ground surface to a depth of 5.5 m, a thin sand layer from the depth of 5.5 m to the depth of 6.5 m, another stiff clay layer down to 12.5 m deep, and a hard clay layer thereafter (see Fig. 2.5 in Chap. 2). Figure 5.3a shows 5 SPT *N*-values versus depth obtained from the SPTs performed within the top stiff clay layer (Briaud 2000). Pressuremeter tests were also carried out in the top clay layer (Briaud 2000). Figure 5.3b shows totally 42 measurements of the undrained Young's modulus from pressuremeter tests performed at different depths of the top clay layer (Briaud 2000), which yield a mean of about 13.5 MPa and standard deviation of about 7.5 MPa.

The equivalent sample approach is illustrated using the 5 SPT *N*-values shown in Fig. 5.3a for probabilistic characterization of the undrained Young's modulus in the clay layer. Consider, for example, a set of prior knowledge in which μ is uniformly distributed between 5.0 and 15.0 MPa (i.e., $\mu_{\min} = 5.0$ MPa and $\mu_{\max} = 15.0$ MPa) and σ is uniformly distributed between 0.5 and 13.5 MPa (i.e., $\sigma_{\min} = 0.5$ MPa and

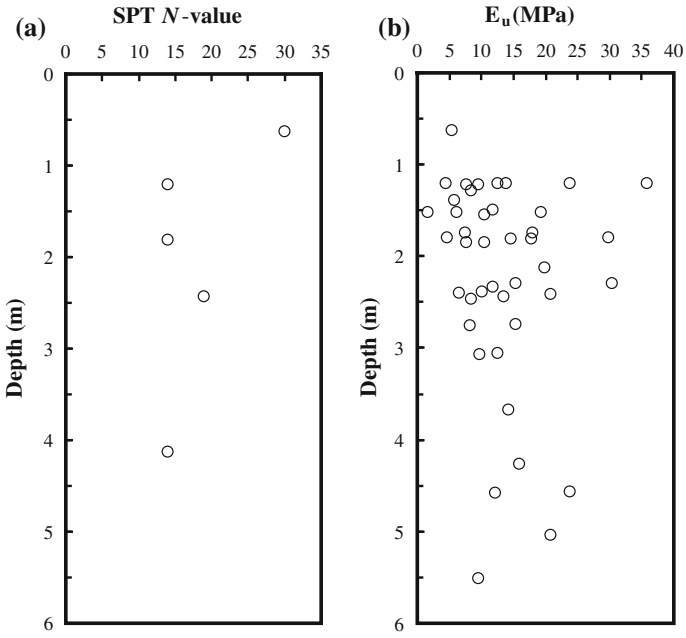

Fig. 5.3 Standard penetration test (SPT) *N*-values and undrained Young's modulus measured by pressuremeter tests at the clay site of the NGES at Texas A&M University (After Briaud 2000; Wang and Cao 2013). **a** SPT *N*-values. **b** Undrained Young' modulus

$\sigma_{max} = 13.5$ MPa). This set of prior knowledge is consistent with the typical ranges of undrained Young's modulus reported in the literature (e.g., Kulhawy and Mayne 1990; Phoon and Kulhawy 1999a, b). Using the prior knowledge and the SPT results shown in Fig. 5.3a, a MCMCS run is performed to simulate 30,000 equivalent samples of E_u together with a two-dimensional grid over the space of μ and σ that has intervals (i.e., $\Delta\mu = \Delta\sigma = 0.1$ MPa) of 0.1 MPa in both directions of μ and σ.

5.7.1 Equivalent Samples

Figure 5.4 shows a scatter plot for the 30,000 equivalent samples of E_u. 28,167 equivalent samples (i.e., around 94 % of the 30,000 equivalent samples) are less than 20.0 MPa. The equivalent samples become growingly sparse when $E_u > 20.0$ MPa. To examine the statistical distribution of the equivalent samples, the corresponding histogram is constructed, as shown in Fig. 5.5. The histogram peaks at a E_u value of around 12.0 MPa, and 26,947 equivalent samples (i.e., around 90 % of the 30,000 equivalent samples) fall within the range of [4.0–20.0 MPa]. 1,220 equivalent samples (i.e., slightly over 4 % of the 30,000 equivalent samples) are less than 4.0 MPa, and 1,833 equivalent samples (i.e., around 6 % of the 30,000 equivalent samples) are greater than 20.0 MPa. Therefore, the 90 % interpercentile range (i.e., the range from 5 % percentile to 95 % percentile) of E_u is around [4.0 MPa, 20.0 MPa].

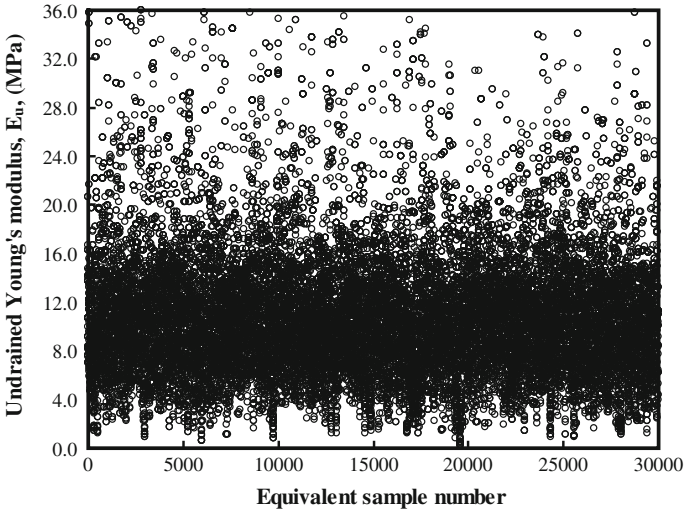

Fig. 5.4 Scatter plot of the equivalent samples for undrained Young's modulus (After Wang and Cao 2013)

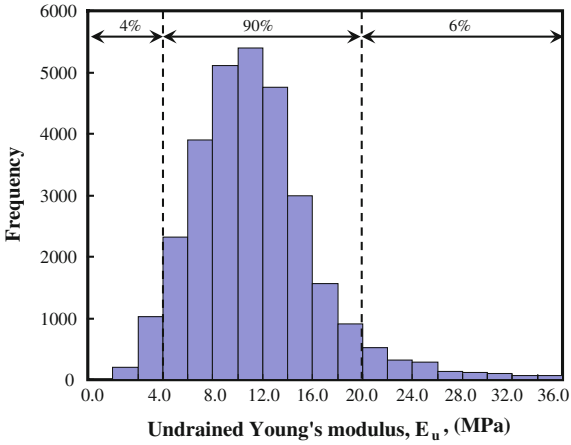

Fig. 5.5 Histogram of the equivalent samples for undrained Young's modulus (After Wang and Cao 2013)

5.7.2 *Probability Distribution of Undrained Young's Modulus*

Figure 5.6 shows the PDF of E_u estimated from the histogram (see Fig. 5.5) of the equivalent samples by a dashed line with open triangles. For validation, numerical integration is also performed to calculate directly the E_u PDF using Eq. (5.11), in which both the normalizing constant K and the integral term I are calculated numerically and repeatedly. The PDF of E_u obtained from the numerical integration is included in Fig. 5.6 by a solid line. The solid line plots closely to the dashed line with open triangles. The PDF of E_u estimated from the equivalent samples is in good agreement with that obtained from the numerical integration. Such agreement indicates that the 30,000 equivalent samples portray the E_u PDF reasonably well and the PDF of E_u estimated from the equivalent samples is reasonably accurate.

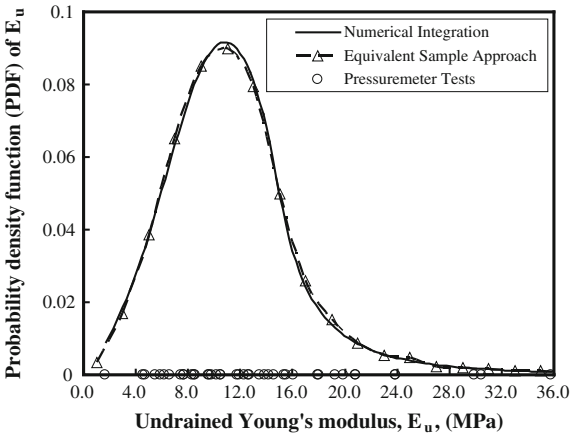

Fig. 5.6 Probability density function (PDF) for undrained Young's modulus (After Wang and Cao 2013)

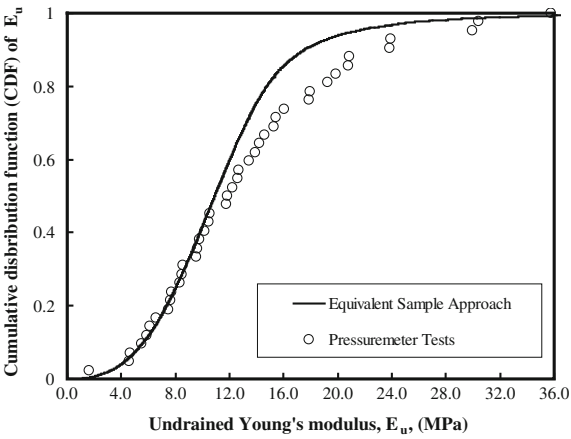

Fig. 5.7 Validation of the probability distribution for undrained Young's modulus estimated from equivalent samples (After Wang and Cao 2013)

Figure 5.6 also includes the values of E_u obtained from the pressuremeter tests by open circles. 34 out of the 42 values of E_u provided by the pressuremeter tests fall within the range of [4.0–20.0 MPa], i.e., the 90 % interpercentile range of E_u estimated from the equivalent samples. Figure 5.7 plots the CDFs of E_u estimated from the cumulative frequency diagrams of the 30,000 equivalent samples (see Fig. 5.4) and the 42 pressuremeter test results (see Fig. 5.3b) by a solid lines and open circles, respectively. The open circles plot closely to the solid line. The CDF of E_u estimated from the equivalent samples compares favorably with that obtained from the 42 pressuremeter tests. Such agreement suggests that based on the limited SPT data (i.e., 5 SPT N-values) and relatively uninformative prior knowledge (i.e., reasonable ranges of model parameters reported in the literature), the equivalent sample approach provides a reasonable estimate of the statistical distribution of E_u. Such probabilistic characterization used to require a large number of data from laboratory and/or in situ tests (e.g., 42 pressuremeter tests in this illustrative example), which of course involves significant commitment of cost, man power, and time.

5.7.3 *Estimates of the Mean, Standard Deviation, and Characteristic Value*

Table 5.1 summarizes the estimates of the mean μ and standard deviation σ of E_u obtained from the 30,000 equivalent samples (see Fig. 5.4) in the second column. Using conventional mean and standard deviation equations, the mean and standard deviation of E_u from equivalent samples are calculated as 11.6 MPa and 6.0 MPa, respectively. Table 5.1 also includes μ and σ values (i.e., 13.5 MPa and 7.5 MPa) estimated from the pressuremeter test results (see Fig. 5.3b) in the third column.

Table 5.1 Summary of the estimated statistics of undrained Young's modulus (After Wang and Cao 2013)

Approaches	Equivalent sample approach	Pressuremeter tests	Difference (MPa)
Estimates of the mean μ^* (MPa)	11.6	13.5	1.9
Estimates of the standard deviation σ^* (MPa)	6.0	7.5	1.5

The difference between the μ values estimated from the equivalent samples and pressuremeter test results is 1.9 MPa, and the difference between their σ values is 1.5 MPa. Compared with the σ value (e.g., 7.5 MPa from the pressuremeter test results), the difference (i.e., 1.9 MPa) between the μ values and the difference (i.e., 1.5 MPa) between the σ values resulted from these two approaches are relatively small. This subsequently leads to consistent estimation of the characteristic value of E_u. For example, if the characteristic value is defined as the mean value; then, it is 11.6 MPa and 13.5 MPa, respectively.

With a proper selection of the characteristic values for soil properties, design calculations can be carried out in accordance with those probabilistic design codes (e.g., Eurocode 7). In addition, the probabilistic characterization of soil properties is also one key input information for evaluating risk and reliability related issues in geotechnical engineering (Hicks 2005), such as probabilistic analysis of slope stability (e.g., Wang et al. 2009) and foundations under ultimate limit state (e.g., Soubra and Massih 2010) or serviceability limit state (e.g., Wang and Kulhawy 2008). It is also worthwhile to note that the equivalent samples generated in this chapter can be used directly in the probabilistic analysis and/or designs that are based on Monte Carlo simulation (e.g., Wang 2011; Wang et al. 2011). This will be further discussed in Chaps. 7 and 8.

5.8 Sensitivity Study on Project-Specific Test Data

The equivalent samples reflect the integrated knowledge of both prior knowledge and project-specific test data (see Eq. (5.11)). The probabilistic characterization of soil properties using the equivalent samples is therefore affected by both prior knowledge and project-specific test data. A sensitivity study is carried out in this section to explore the effect of the quantity of project-specific test data. In addition, the effect of the prior knowledge is explored in the next section.

The sensitivity study is performed using simulated SPT data, which are simulated using the uncertainty model given by Eq. (5.5) with $\mu_N = 2.23$ and $\sigma_N = 0.39$ (i.e., $\mu = 10.0$ MPa and $\sigma = 4.0$ MPa). For example, Fig. 5.8 shows 10 sets of the simulated SPT data with 10 SPT N-values in each data set (i.e., data quantity $n_s = 10$ in each data set). Note that in practice the actual values of soil properties are unknown, and they are estimated through prior knowledge and project-specific

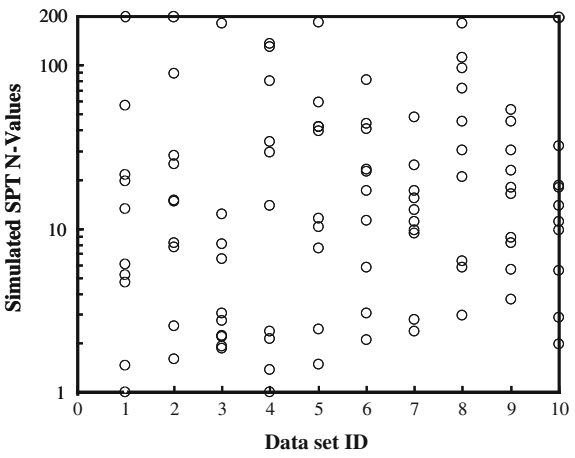

Fig. 5.8 Ten sets of simulated SPT data (After Wang and Cao 2013)

test results. To explore the effect of n_s, another 10 sets of SPT data are simulated, respectively, for n_s = 3, 20, and 30, resulting in a total of 40 sets of SPT data with 10 sets for each n_s.

Then, using each set of these 40 sets of simulated SPT data as project-specific test data and the prior knowledge that corresponds to the typical ranges of undrained Young's modulus reported in the literature (i.e., a uniform prior distribution with $\mu_{\min} = 5.0$ MPa, $\mu_{\max} = 15.0$ MPa, $\sigma_{\min} = 0.5$ MPa, and $\sigma_{\max} = 13.5$ MPa used in the previous section), 30,000 equivalent samples of E_u are generated for each of the 40 data sets, respectively. This leads to 40 sets of the probabilistic characterization of E_u, including estimations (i.e., μ_N^* and σ_N^*) of μ_N and σ_N. In addition, for each set of the simulated SPT data, the E_u values are also directly calculated using the regression model given by Eq. (5.3) in the absence of prior knowledge. This leads to another 40 sets of μ_N^* and σ_N^*.

The results of μ_N^* and σ_N^* from both the equivalent sample approach and direct calculation of Eq. (5.3) are evaluated through hypothesis tests. In the hypothesis tests, the respective acceptance regions of μ_N^* and σ_N^* at a significance level of α are formulated as (e.g., Ang and Tang 2007)

$$\mu_N + \frac{\sigma_N}{\sqrt{n_s}}\Phi_{\alpha/2}^{-1} < \mu_N^* \le \mu_N + \frac{\sigma_N}{\sqrt{n_s}}\Phi_{1-\alpha/2}^{-1} \text{ and } \sqrt{\frac{c_{\alpha/2,n_s-1}}{n_s-1}}\sigma_N < \sigma_N^* \le \sqrt{\frac{c_{1-\alpha/2,n_s-1}}{n_s-1}}\sigma_N \tag{5.15}$$

in which $\Phi_{\alpha/2}^{-1}$ and $\Phi_{1-\alpha/2}^{-1}$ are the values of an inverse standard Gaussian CDF at $\alpha/2$ and $1-\alpha/2$, respectively; $c_{\alpha/2,n_s-1}$ and $c_{1-\alpha/2,n_s-1}$ are the values of a chi-squared statistic with $n_s - 1$ degrees of freedom at the levels of $\alpha/2$ and $1-\alpha/2$, respectively. Note that the acceptance regions of μ_N^* and σ_N^* decrease as n_s increases (see Eq. (5.15)). In other words, the criteria to accept μ_N^* and σ_N^* at a given α level become more and more stringent as n_s increases.

5.8.1 *Effect of Data Quantity on the Mean of ln(E_u)*

Figure 5.9a shows the values of μ_N^* versus the number n_s of the SPT data in each data set. The μ_N^* values calculated from the equivalent samples and directly estimated from the regression model in the absence of prior knowledge are plotted by open triangles and circles, respectively. Figure 5.9a also includes the true value (i.e., 2.23) of μ_N and the acceptance region of μ_N^* at 5 % significance level by a dashed line and solid lines, respectively. In general, open triangles plot more closely to the dashed line than open circles. The μ_N^* values estimated from the equivalent samples are generally better estimations of the true value than those directly estimated from the regression model without prior knowledge. By incorporating

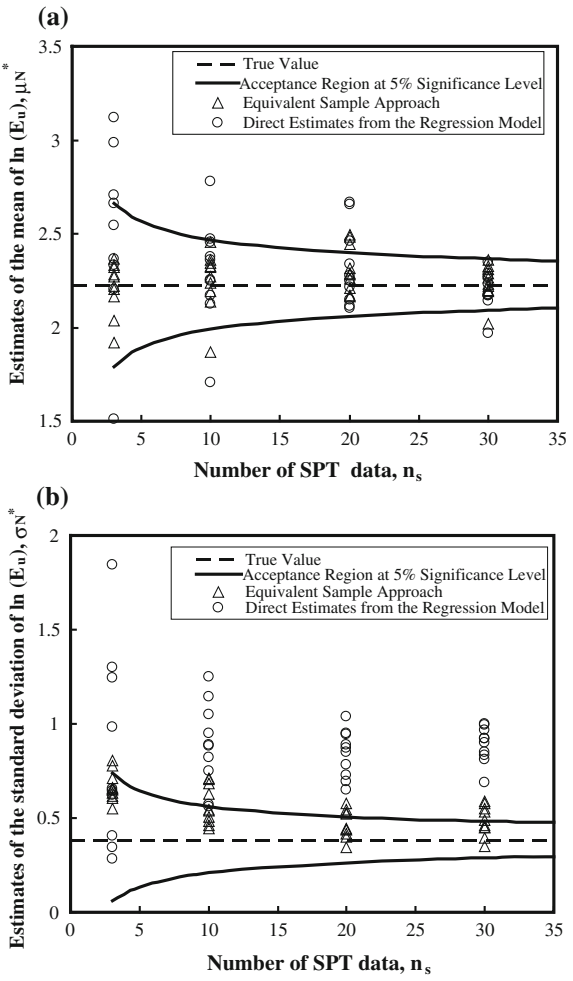

Fig. 5.9 Effects of the project-specific test data (After Wang and Cao 2013). **a** Estimates of the mean of $\ln(E_u)$. **b** Estimates of the standard deviation of $\ln(E_u)$

relatively limited and commonly available prior knowledge (i.e., the typical ranges of model parameters reported in the literature), the equivalent sample approach significantly improves the estimation of μ_N.

Figure 5.9a also shows that the scatterness of the μ_N^* diminishes significantly as the value of n_s increases. As the number of SPT data increases, the statistical uncertainty that arises from incomplete statistical information tends to diminish. In addition, as the value of n_s increases, the difference between the range of μ_N^* obtained from the equivalent sample approach and that from direct estimate is reduced. Such difference becomes relatively minor when $n_s = 30$, which happens to be the "rule-of-thumb" minimum number of data suggested in conventional statistical analysis (e.g., Walpole et al. 1998). The proposed approach combines the prior knowledge and project-specific test data and transforms them into equivalent samples. When the quantity of project-specific test data is limited (e.g., $n_s = 3$) and its statistical uncertainty is substantial, the equivalent samples are affected significantly by the prior knowledge, resulting in significant improvement on the estimation of μ_N. The prior knowledge adopted in the proposed approach effectively reduces the substantial statistical uncertainty that raises from a small number of project-specific test data, and it enables a proper estimation of μ_N at a small n_s value (e.g., $n_s = 3$). This is particularly beneficial in geotechnical practice where the number of soil property data obtained during site characterization is generally small and its statistical uncertainty is substantial. On the other hand, when there is a large number of project-specific test data (e.g., $n_s = 30$), the equivalent samples are dominated by the project-specific test data, and the μ_N^* values estimated from the equivalent samples converge to those estimated directly from regression.

5.8.2 *Effect of Data Quantity on the Standard Deviation of ln($\mathbf{E_u}$)*

Figure 5.9b shows the values of σ_N^* versus the number n_s of the SPT data in each data set. The σ_N^* values calculated from the equivalent samples and directly estimated from the regression model without prior knowledge are plotted by open triangles and circles, respectively. Figure 5.9b also includes the true value (i.e., 0.39) of σ_N and the acceptance region of σ_N^* at 5 % significance level by a dashed line and solid lines, respectively. Similar to μ_N^*, the σ_N^* values (i.e., open triangles) estimated from the equivalent samples generally plot more closely to the true values (i.e., the dashed line) than those (i.e., open circles) directly estimated from the regression model without prior knowledge. The equivalent sample approach provides better estimation of σ_N than direct estimation using regression model, because the prior knowledge is incorporated in the equivalent sample approach. The improvement on the estimation of σ_N is more significant when the n_s value is small (e.g., $n_s = 3$).

Figure 5.9b also shows that the σ_N^* values estimated from the equivalent samples gradually approach the true value of σ_N as n_s increases (see Fig. 5.9b). On the other hand, the σ_N^* values estimated directly from the regression model are much larger than the true value of σ_N even when the n_s value is large (i.e., n_s = 30). It is worthwhile to note that the SPT data are simulated using Eq. (5.5), which contains both inherent variability and transformation uncertainty. These uncertainties propagate from the SPT N-values to the E_u values through Eq. (5.3), when the E_u values are estimated directly using regression. The corresponding σ_N^* values therefore contain both inherent variability and transformation uncertainty, and they are obviously larger than the inherent variability itself (i.e., the true value of σ_N). In contrast, the transformation uncertainty is formulated and considered explicitly in the equivalent sample approach, and its corresponding σ_N^* values mainly reflect the inherent variability itself.

5.9 Sensitivity Study on Prior Knowledge

To explore the effect of prior knowledge, a sensitivity study is performed in this section using four different sets (i.e., prior knowledge I, II, III, and IV) of prior knowledge shown in Fig. 5.10, together with the 10 sets of SPT data shown in Fig. 5.8. Note that each of the SPT data set includes 10 SPT N-values, i.e., $n_s = 10$. Figure 5.10 also includes the true values of μ (i.e., 10.0 MPa) and σ (i.e., 4.0 MPa) that have been used to generate the SPT data in Fig. 5.8.

The prior knowledge I in Fig. 5.10a has been used in the previous section, and it is used as the baseline case in this sensitivity study. The prior knowledge II in Fig. 5.10b follows a uniform distribution, but the ranges of both μ and σ values are much smaller than the prior knowledge I. The prior knowledge II is, therefore, much more informative and confident than the prior knowledge I, and it is more consistent with the true values of μ and σ. The prior knowledge III in Fig. 5.10c has the same ranges of both μ and σ values as the prior knowledge I, but it follows an arbitrary histogram type of distribution with relatively large PDF values allocated close to the true values of μ and σ. Therefore, the prior knowledge III is slightly more informative and confident than the prior knowledge I, and it is slightly more consistent with the true values of μ and σ. The prior knowledge IV in Fig. 5.10d is the Gaussian best fit of the prior knowledge III, and information provided by the prior knowledge III and IV is more or less the same.

For each set of the SPT data and prior knowledge, a MCMCS run is performed to generate 30,000 equivalent samples of E_u. Then, conventional statistical analysis is performed to estimate μ_N^* and σ_N^*. Effects of the ranges of the uniform prior distributions and effects of different types of the prior distributions are discussed in the following two subsections.

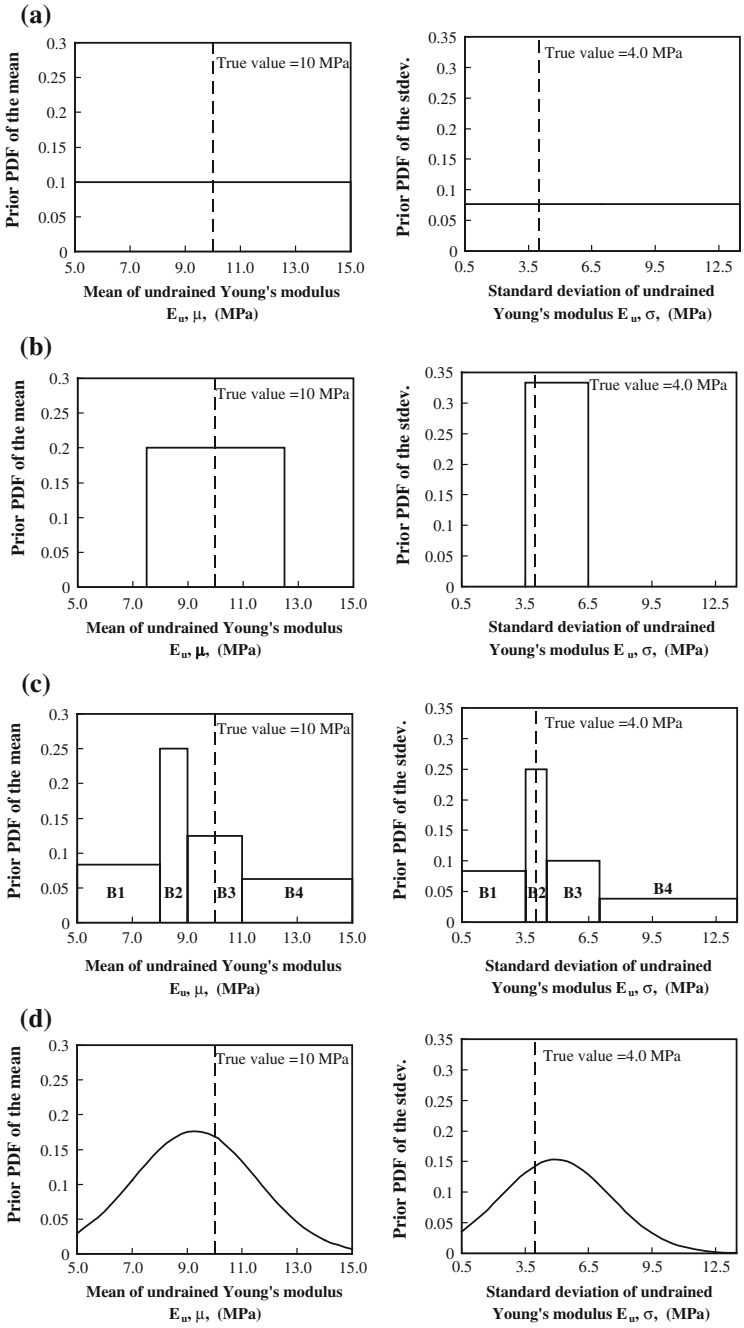

Fig. 5.10 Summary of prior knowledge used in the sensitivity study (After Wang and Cao 2013). **a** Prior knowledge I. **b** Prior knowledge II. **c** Prior knowledge III. **d** Prior knowledge IV

5.9.1 *Effect of the Ranges of Uniform Prior Distributions*

Figure 5.11a shows values of μ_N^* obtained from the equivalent sample approach using prior knowledge I and II by open squares and triangles, respectively. Figure 5.11a also includes the acceptance region of μ_N^* at 5 % significance level for $n_s = 10$ and the true value (i.e., 2.23) of μ_N by solid lines and a dashed line, respectively. For a given set of SPT data, the μ_N^* value (i.e., the open triangle) obtained using prior knowledge II plots more closely to the true value (i.e., the dashed line) of μ_N than that (i.e., the open square) obtained using prior knowledge I. For the third set of SPT data, using prior knowledge I leads to a μ_N^* value that plots outside the acceptance region and hence is rejected at 5 % significance level. In contrast, using prior knowledge II results in a μ_N^* value that falls within the

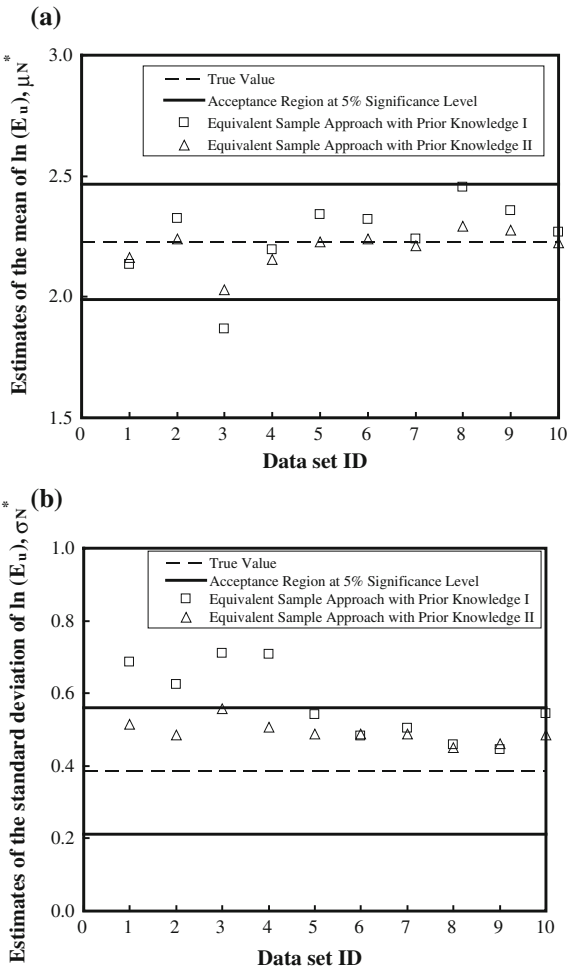

Fig. 5.11 Effects of the ranges of uniform prior distribution on estimates of the mean and standard deviation of $\ln(E_u)$ (After Wang and Cao 2013). **a** Estimates of the mean of $\ln(E_u)$. **b** Estimates of the standard deviation of $\ln(E_u)$

acceptance region and is therefore accepted at 5 % significance level. It is obvious that informative and consistent prior knowledge improves the estimation of μ_N^*.

Figure 5.11b shows the σ_N^* values obtained using prior knowledge I and II by open squares and triangles, respectively. It also includes the acceptance region of σ_N^* at 5 % significance level for $n_s = 10$ and the true value (i.e., 0.39) of σ_N by solid lines and a dashed line, respectively. Similar to μ_N^*, the σ_N^* values (i.e., the open triangles) obtained using prior knowledge II plot more closely to the true value (i.e., the dashed line) of σ_N than those (i.e., the open squares) obtained using prior knowledge I. Using relatively informative and consistent prior knowledge improves the estimation of σ_N^*.

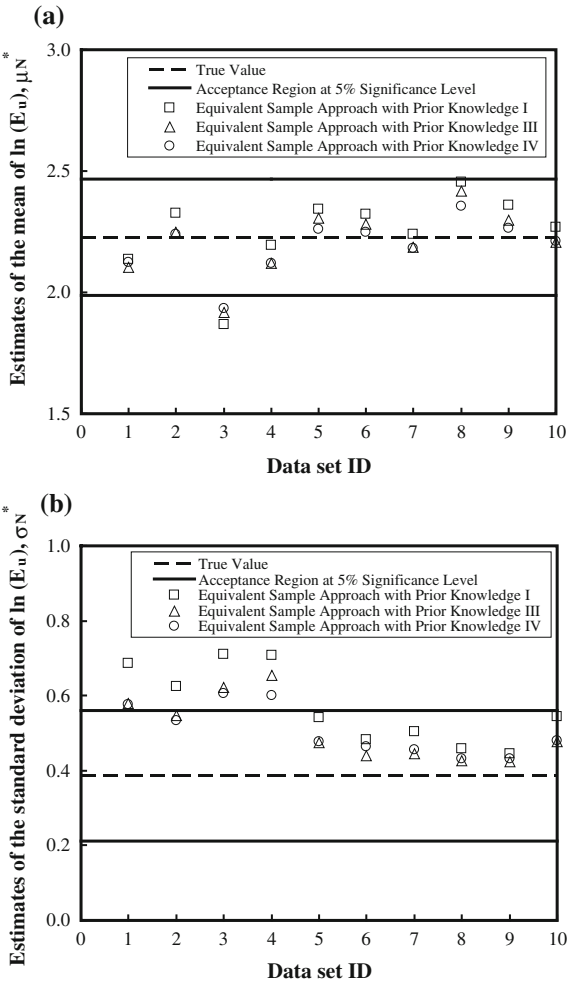

Fig. 5.12 Effects of different types of prior distributions on estimates of the mean and standard deviation of $\ln(E_u)$ (After Wang and Cao 2013). **a** Estimates of the mean of $\ln(E_u)$. **b** Estimates of the standard deviation of $\ln(E_u)$

5.9.2 *Effect of Different Types of Prior Distributions*

Although the prior knowledge defined by Eq. (5.8) is a uniform distribution, the equivalent sample approach developed in this chapter is general and equally applicable for more sophisticated types of prior distributions. Figure 5.12a shows the values of μ_N^* obtained using the prior knowledge I, III (i.e., an arbitrary histogram type of distribution), and IV (i.e., a truncated Gaussian distribution) by open squares, triangles, and circles, respectively. Figure 5.12a also includes the acceptance region of μ_N^* at 5 % significance level and the true value (i.e., 2.23) of μ_N by solids lines and a dashed line, respectively. Figure 5.12b shows the corresponding values of σ_N^* using similar symbols. Because the prior knowledge III and IV are slightly more informative and consistent than the prior knowledge I, the estimation of μ_N^* and σ_N^* is slightly better when using the prior knowledge III and IV. In addition, because the information provided by the prior knowledge III and IV is more or less the same, their estimation of μ_N^* and σ_N^* is also more or less the same.

5.10 Summary and Conclusions

This chapter developed a Markov Chain Monte Carlo simulation (MCMCS)-based approach for probabilistic characterization of undrained Young's modulus, E_u, of clay using standard penetration tests (SPTs). Prior knowledge (e.g., previous engineering experience) and project-specific test data (e.g., SPT data) are integrated probabilistically under the Bayesian framework developed in this book and transformed into a large number, as many as needed, of equivalent samples of E_u. Then, conventional statistical analysis is carried out to estimate statistics of E_u. This allows a proper selection of characteristic value of the soil property in the implementation of probabilistic design codes (e.g., Eurocode 7) and reliability analysis in geotechnical engineering practice. The proposed approach effectively tackles the difficulty in generating meaningful statistics from the usually limited number of soil property data obtained during geotechnical site characterization.

Equations were derived for the proposed equivalent sample approach, and it was illustrated and validated using real SPT and pressuremeter test data at the clay site of the US National Geotechnical Experimentation Sites (NGES) at Texas A&M University. It has been shown that based on the limited SPT data (i.e., 5 SPT N-values) and relatively uninformative prior knowledge (i.e., reasonable ranges of soil parameters reported in the literature), the equivalent sample approach provides a reasonable estimate of the statistical distribution of E_u. Such probabilistic characterization is used to require a large number of data from laboratory and/or in situ tests (e.g., 42 pressuremeter tests in this illustrative example), which of course involves significant commitment of cost, man power, and time.

A sensitivity study was performed to explore the effect of the number of project-specific test data. It has been shown that when only limited project-specific

test data are available, the equivalent sample approach improves significantly the probabilistic characterization of soil properties and reduces the effect of statistical uncertainty by incorporating reasonable ranges of soil parameters as prior knowledge. As the number of project-specific test data increases, the standard deviation of soil properties estimated from the equivalent sample approach gradually approaches its true value and mainly reflects inherent variability itself. In addition, a sensitivity study was performed to explore the effect of prior knowledge. It has been shown that the proposed approach is general and equally applicable for different types of prior knowledge, although using relatively informative and consistent prior knowledge does improve probabilistic characterization of soil properties.

References

Ang, A.H.S., and W.H. Tang. 2007. *Probability concepts in engineering: emphasis on applications to civil and environmental engineering*. New York: Wiley.

Au, S.K., Z. Cao, and Y. Wang. 2010. Implementing advanced Monte Carlo simulation under spreadsheet environment. *Structural Safety* 32(5): 281–292.

Baecher, G.B., and J.T. Christian. 2003. *Reliability and statistics in geotechnical engineering*, 605 pp. Hoboken, New Jersey: Wiley.

Beck, J.L., and S.K. Au. 2002. Bayesian updating of structural models and reliability using Markov chain Monte Carlo simulation. *Journal of Engineering Mechanics* 128(4): 380–391.

Briaud, J.L. 2000. The National Geotechnical Experimentation Sites at Texas A&M University: Clay and sand. A Summary. *National Geotechnical Experimentation Sites, Geotechnical Special Publication No. 93*, 26–51.

Briaud, J.L. 1992. *The pressuremeter*. London, UK: Taylor & Francis.

BSI 2010. Eurocode 7: Geotechnical Design—Part 1: General Rules.

Clayton, C.R.I. 1995. *The Standard Penetration Test (SPT): Methods and Use*, Report 143, Construction Industry Research and Information Association, UK.

Clayton, C.R.I., M.C. Matthews, and N.E. Simons. 1995. *Site investigation*. Cambridge, Mass., USA: Blackwell Science.

Hastings, W.K. 1970. Monte Carlo sampling methods using Markov chains and their applications. *Biometrika* 57: 97–109.

Hicks, M.A. 2005. Risk and variability in geotechnical engineering. *Geotechnique* 55(1): 1–2.

Kulhawy, F.H., and P.W. Mayne. 1990. *Manual on estimating soil properties for foundation design*, Report EL 6800, 306 pp. Palo Alto: Electric Power Research Inst.

Mair, R.J., and D.M. Wood. 1987. *Pressuremeter testing: Methods and interpretation*. London: Ciria.

Mathworks, Inc. 2010. MATLAB—the language of technical computing. http://www.mathworks.com/products/matlab/. Accessed 9 Mar 2009.

Mayne, P.W., B.R. Christopher, and J. DeJong. 2002. *Subsurface Investigations—Geotechnical Site Characterization*, No. FHWA NHI-01-031, Federal Highway Administration, U. S. Department of Transportation, Washington D. C.

Metropolis, N., A. Rosenbluth, M. Rosenbluth, and A. Teller. 1953. Equations of state calculations by fast computing machines. *Journal of Chemical Physics* 21(6): 1087–1092.

Mitchell, J.K., and K. Soga. 2005. *Fundamentals of soil behavior*. Hoboken, New Jersey: Wiley.

Microsoft Corporation. 2012. Microsoft Office EXCEL 2010. http://www.microsoft.com/en-us/default.aspx.

Ohya, S., T. Imai, and M. Matsubara. 1982. Relationships between N value by SPT and LLT pressuremeter results. In *Proceedings of 2nd European Symposium on Penetration Testing* Vol. 1, Amsterdam, 125–130.

Phoon, K.K., and F.H. Kulhawy. 1999a. Characterization of geotechnical variability. *Canadian Geotechnical Journal* 36(4): 612–624.

Phoon, K.K., and F.H. Kulhawy. 1999b. Evaluation of geotechnical property variability. *Canadian Geotechnical Journal* 36(4): 625–639.

Robert, C., and G. Casella. 2004. *Monte Carlo statistical methods*. Springer.

Soubra, A.-H., and D.S.Y.A. Massih. 2010. Probabilistic analysis and design at the ultimate limit state of obliquely loaded strip footings. *Geotechnique* 60(4): 275–285.

Vanmarcke, E.H. 1977. Probabilistic modeling of soil profiles. *Journal of Geotechnical Engineering* 103(11): 1127–1246.

Walpole, R.E., R.H. Myers, and S.L. Myers. 1998. *Probability and statistics for engineers and scientists*. Upper Saddle River, New Jersey: Prentice Hall.

Wang, Y. 2011. Reliability-based design of spread foundations by Monte Carlo simulations. *Geotechnique* 61(8): 677–685.

Wang, Y., S.K. Au, and F.H. Kulhawy. 2011. Expanded reliability-based design approach for drilled shafts. *Journal of Geotechnical and Geoenvironmental Engineering* 137(2): 140–149.

Wang, Y., and Z. Cao. 2013. Probabilistic characterization of Young's modulus of soil using equivalent samples. *Engineering Geology* 159(12): 106–118.

Wang, Y., S.K. Au, and Z. Cao. 2010. Bayesian approach for probabilistic characterization of sand friction angles. *Engineering Geology* 114(3–4): 354–363.

Wang, Y., Z. Cao, S.K. Au, and Q. Wang. 2009. Reliability analysis of a benchmark problem for slope stability. In *Proceedings of the Second International Symposium on Geotechnical Safety and Risk*, Gifu Japan, June 2009, 89–93.

Wang, Y., and F.H. Kulhawy. 2008. Reliability index for serviceability limit state of building foundations. *Journal of Geotechnical and Geoenvironmental Engineering* 134(11): 1587–1594.

Wang, Y., and T.D. O'Rourke. 2007. Interpretation of secant shear modulus degradation characteristics from pressuremeter tests. *Journal of Geotechnical and Geoenvironmental Engineering* 133(12): 1556–1566.

Chapter 6
Probabilistic Site Characterization Using Cone Penetration Tests

6.1 Introduction

In the previous chapter, an equivalent sample approach is developed for probabilistic site characterization using standard penetration test (SPT) results. SPTs provide soil samples that can be used to determine the underground stratigraphy (i.e., the number and thicknesses of soil layers). On the other hand, it is a challenging task to characterize probabilistically the underground stratigraphy for those tests that do not allow retrieving of soil samples for visual inspection to assist in soil classification, such as cone penetration test (CPT) (e.g., Lunne 1997; Phoon et al. 2003). However, CPTs provide a relatively large number of project-specific test data (i.e., almost continuous measurements during a CPT) compared with SPTs. This allows an explicit modeling of the inherent spatial variability of soil properties using random field theory (e.g., Vanmarcke 1977).

This chapter develops a Bayesian approach for probability site characterization based on the Bayesian framework developed in Chap. 3 and random field theory. The Bayesian approach integrates systematically prior knowledge with project-specific CPT data under the Bayesian framework to describe the underground stratigraphy and to estimate probabilistically the effective friction angle of soil simultaneously. It addresses explicitly and directly the inherent spatial variability of effective friction angle using random field theory. The proposed approach contains two major components: a Bayesian model class selection method to identify the most probable number of statistically homogenous soil layers and a Bayesian system identification method to estimate the most probable layer thicknesses/boundaries and soil properties probabilistically.

This chapter starts with random field modeling of the inherent spatial variability of the effective friction angle in a soil profile with multiple sand layers and a regression between cone tip resistance and effective friction angle of sand, followed by the development of the proposed Bayesian system identification and model class selection approach. Then, the implementation procedure for the Bayesian approach

Z. Cao et al., *Probabilistic Approaches for Geotechnical Site Characterization and Slope Stability Analysis*, DOI 10.1007/978-3-662-52914-0_6

is described. The proposed approach is illustrated using a set of real CPT data obtained from a site in the Netherlands. Finally, a sensitivity study is performed to explore the effect of prior knowledge on the identification of statistically homogenous soil layers and probabilistic characterization of the effective friction angle.

6.2 Random Field Modeling of Inherent Spatial Variability

Random field theory (Vanmarcke 1977, 1983) is applied in this chapter to model the inherent spatial variability of effective friction angle, ϕ', in a soil profile containing N_L statistically homogenous sand layers. The number N_L in the first part of this chapter (i.e., before Sect. 6.6 "The Most Probable Number of Soil Layers") is considered as a given value. It is then determined among several possible values by a Bayesian model class selection approach proposed in Sect. 6.6. As shown in Fig. 6.1, the inherent spatial variability of ϕ' within the N_L layers of sand is modeled by N_L one-dimensional (i.e., along the vertical direction) and mutually independent Gaussian random fields (i.e., $\phi'_n(D)$, $n = 1, 2, \ldots, N_L$), in which the subscript n denotes the layer number (i.e., the nth layer of sand) and D is the depth. The mean and standard deviation of ϕ'_n are μ_n and σ_n, respectively. The correlation structure of ϕ_n' (i.e., the correlation structure within the nth layer of sand) follows

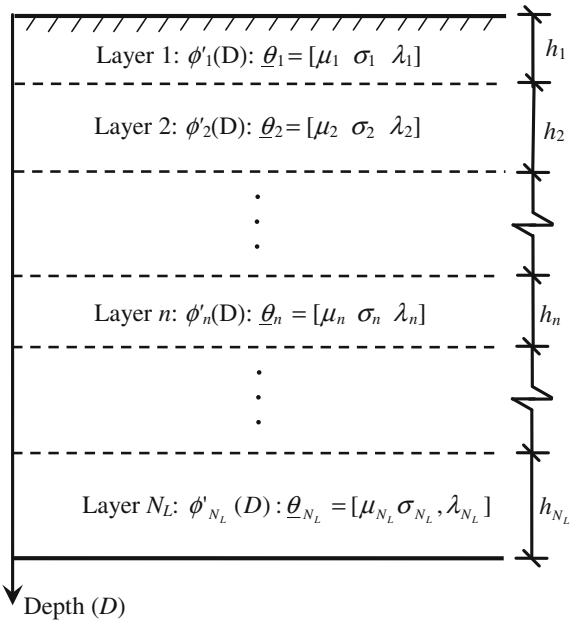

Fig. 6.1 An illustration of random field model (After Cao and Wang 2013)

an exponential correlation function r_n (Fenton 1999a, b; Wang et al. 2010; Cao and Wang 2013)

$$r_n\left[\varphi_n^{'}(D_i),\varphi_n^{'}(D_j)\right]=\exp\left(-\frac{2\left|d_{i,j}\right|}{\lambda_n}\right),n=1,2,\ldots,N_L \tag{6.1}$$

where λ_n is the correlation length, also sometimes known as scale of fluctuation, of ϕ'_n in the nth layer, and it is a separation distance within which the soil property shows a relatively strong correlation from point to point (Vanmarcke 1977, 1983; Fenton and Griffiths 2008); $d_{i,j}=\left|D_i-D_j\right|$ is the distance between depths D_i and D_j within the nth layer.

Let $\underline{\phi}'_n=[\phi'_n(D_1),\phi'_n(D_2),\ldots,\phi'_n(D_{k_n})]^T$ be a vector of effective friction angles at depths $D_1,D_2,\ldots,D_{k_n}$ within the nth layer. In the context of a Gaussian random field, $\underline{\phi}'_n$ has the following representation in terms of a sequence of independent and identically distributed random variables

$$\underline{\phi}'_n=\mu_n\underline{l}_n+\sigma_n\underline{L}_n^T\underline{Z}_n,n=1,2,\ldots,N_L \tag{6.2}$$

where $\underline{l}_n$ is a vector with k_n components that are all equal to one; $\underline{Z}_n=[Z_1,\ldots,Z_{k_n}]^T$ is a standard Gaussian vector with k_n independent components; $\underline{L}_n$ is a k_n-by-k_n upper triangular matrix obtained by Cholesky decomposition of the correlation matrix $\underline{R}_n$ satisfying

$$\underline{R}_n=\underline{L}_n^T\underline{L}_n,n=1,2,\ldots,N_L \tag{6.3}$$

and the (i, j)th entry of $\underline{R}_n$ is given by Eq. (6.1). Note that the second term in Eq. (6.2) represents inherent spatial variability of the effective friction angle of the nth sand layer. Let h_n, n = 1, 2, …, N_L, denote the thickness of the nth sand layer (see Fig. 6.1), then the N_L Gaussian random fields are uniquely represented by a thickness vector $\underline{h}_{N_L}=[h_1,h_2,\ldots,h_{N_L}]^T$ and a model parameter matrix Θ_{N_L} that consists of N_L model parameter vectors $\underline{\theta}_n=[\,\mu_n\quad\sigma_n\quad\lambda_n\,]$ and N_L correlation matrices $\underline{R}_n$.

Although in this chapter one-dimensional Gaussian random fields with an exponential correlation structure (see Eq. (6.1)) are used for the development of the method, the Bayesian approach is general and applicable for two- or three-dimensional random fields and for other distribution types of random variables or different correlation structures. For example, two- or three-dimensional random fields can be applied in the Bayesian approach to account for the anisotropy in inherent spatial variability, provided that a large number of measurement data are available for each direction. It is also worthwhile to note that the model parameters $\underline{\theta}_n=[\,\mu_n\quad\sigma_n\quad\lambda_n\,]$ of ϕ'_n within the nth sand layer are considered spatially constant within the nth sand layer in this chapter. There is therefore no need to remove the spatial trend (i.e., perform detrending) for the parameters. For some soil

properties (e.g., undrained shear strength) that exhibit obvious spatial trend, however, detrending should be performed before using statistically homogenous random fields to model the inherent spatial variability (e.g., Lumb 1966; Jaksa 1995; Fenton 1999a, b; Phoon et al. 2003).

6.3 Regression Between Cone Tip Resistance and Effective Friction Angle

The effective friction angle ϕ' of soil can be estimated from CPTs using a regression between ϕ' and the cone tip resistance q_c that is measured at the cone tip during the CPT. Figure 6.2 shows an empirical model developed by Kulhawy and Mayne (1990), which is a semilog regression equation

$$\xi = \ln q = a\phi' + b + \varepsilon_{T\phi'} \tag{6.4}$$

where ξ represents the measured data in a log scale; $q = (q_c/p_a)/(\sigma'_{v0}/p_a)^{0.5}$ is the normalized cone tip resistance; σ'_{v0} and p_a are vertical effective stress and standard atmospheric pressure (i.e., 0.1 MPa), respectively; a = 0.209, b = −3.684, and $\varepsilon_{T\phi'}$

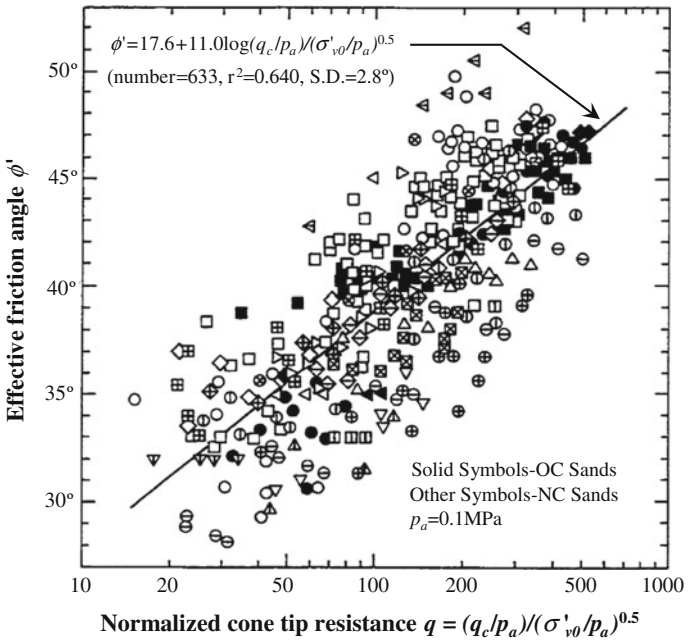

Fig. 6.2 Regression between effective friction angle and normalized cone tip resistance (After Kulhawy and Mayne 1990; Cao and Wang 2013)

is a Gaussian random variable with a mean $\mu_{\varepsilon T} = 0$ and standard deviation $\sigma_{\varepsilon T} = 0.586$ (Kulhawy and Mayne 1990; Phoon and Kulhawy 1999b; Wang et al. 2010). $\varepsilon_{T\varphi'}$ represents the transformation uncertainty (i.e., modeling scatterness) associated with the regression model. It should be noted that the original equation in Kulhawy and Mayne (1990) expresses ϕ' in term of ξ; it is inverted here to facilitate development in this chapter.

Let $\underline{\xi} = [\underline{\xi}_1, \underline{\xi}_2, \ldots, \underline{\xi}_{N_L}]^T$ be a set of ln$q$ data at different depths obtained from a CPT in a soil profile with N_L statistically homogenous layers of sand, in which $\underline{\xi}_n = [\xi_{n1}(D_1), \xi_{n2}(D_2), \ldots, \xi_{nk_n}(D_{k_n})]^T, n = 1, 2, \ldots, N$, is a set of ln$q$ that are measured at the k_n depths $D_1, D_2, \ldots, D_{k_n}$ within the nth sand layer. Using Eqs. (6.2) and (6.4) gives

$$\underline{\xi}_n = (a\mu_n + b)\underline{l}_n + (a\sigma_n \underline{L}_n^T \underline{Z}_n + \underline{\varepsilon}_{T\phi'}), n = 1, 2, \ldots, N_L \tag{6.5}$$

When inherent spatial variability is assumed to be independent of model uncertainty, i.e., $\underline{Z}_n$ and $\underline{\varepsilon}_{T\phi'}$ are independent, it can be readily reasoned that $\underline{\xi}_n$ measured within the nth sand layer is a Gaussian vector with a mean $(a\mu_n + b)\underline{l}_n$ and covariance matrix $\underline{C}_n = a^2\sigma_n^2\underline{R}_n + \sigma_{\varepsilon T}^2\underline{I}_n$ (Wang et al. 2010; Cao et al. 2011), where $\underline{I}_n$ is a k_n-by-k_n identity matrix.

It is worthwhile to point out that dividing the CPT data $\underline{\xi}$ into different sand layers (i.e., dividing $\underline{\xi}$ into $\underline{\xi}_n$, $n = 1, 2, \ldots, N_L$) requires information on the boundaries that separate the various statistically homogenous layers of soil. Such information is unknown and needs to be determined in geotechnical site characterization. In the next section, a Bayesian system identification approach is developed to determine the thicknesses/boundaries of various sand layers for a given layer number N_L and to update, simultaneously, knowledge on model parameters of sand properties using prior knowledge and site observation data $\underline{\xi}$.

6.4 Bayesian System Identification

Within the Bayesian framework, the updated knowledge on model parameters Θ_{N_L} of soil properties in the N_L statistically homogenous layers of soil is represented by their joint posterior distribution (e.g., Ang and Tang 2007)

$$P(\Theta_{N_L}|\underline{\xi}, N_L) = K_{N_L} P(\underline{\xi}|\Theta_{N_L}, N_L) P(\Theta_{N_L}|N_L) \tag{6.6}$$

where $K_{N_L} = 1/P(\underline{\xi}|N_L)$ is a normalizing constant for a given N_L value; $P(\underline{\xi}|\Theta_{N_L}, N_L)$ is the likelihood function that reflects the model fit with site observation data $\underline{\xi}$ within the N_L layers of sand; $P(\Theta_{N_L}|N_L)$ is the prior distribution of model parameters in the N_L layers of sand that reflects prior knowledge about Θ_{N_L} in the absence of data.

Since the N_L Gaussian random fields are mutually independent, the likelihood function $P(\underline{\xi}|\Theta_{N_L}, N_L)$ is given by

$$P(\underline{\xi}|\Theta_{N_L}, N_L) = \prod_{n=1}^{N_L} P(\underline{\xi}_n|\underline{\theta}_n, N_L) \tag{6.7}$$

where $P(\underline{\xi}_n|\underline{\theta}_n, N_L), n = 1, 2, \ldots, N_L$, is the likelihood function for the nth sand layer, since $\underline{\xi}_n$ is a Gaussian vector with a mean $(a\mu_n + b)\underline{l}_n$ and covariance matrix $\underline{C}_n = a^2\sigma_n^2\underline{R}_n + \sigma_{\varepsilon T}^2\underline{I}_n, P(\underline{\xi}_n|\underline{\theta}_n, N_L)$ is expressed as

$$P(\underline{\xi}_n|\underline{\theta}_n, N_L) = (2\pi)^{-k_n/2}|\det \underline{C}_n|^{-1/2}\exp\left\{-\frac{1}{2}[\underline{\xi}_n - (a\mu_n + b)\underline{l}_n]^T\underline{C}_n^{-1}\left[\underline{\xi}_n - (a\mu_n + b)\underline{l}_n\right]\right\} \tag{6.8}$$

Note that as the boundaries (or thickness $\underline{h}_{N_L}$) of sand layers change, the division of CPT data $\underline{\xi}$ into $\underline{\xi}_n$ also changes. In other words, $\underline{\xi}_n$ is a function of $\underline{h}_{N_L}$. Because $P(\underline{\xi}_n|\underline{\theta}_n, N_L)$ is a function of $\underline{\xi}_n$ (see Eq. (6.8)), $P(\underline{\xi}_n|\underline{\theta}_n, N_L)$ is also a function of $\underline{h}_{N_L}$. Therefore, although $\underline{h}_{N_L}$ does not explicitly appears in Eqs. (6.7) or (6.8), the likelihood function $P(\underline{\xi}|\Theta_{N_L}, N_L)$ is a function of the thickness vector $\underline{h}_{N_L}$. This is very important for determining thicknesses of the N_L statistically homogenous sand layers, as further illustrated in the next section.

Similar to the likelihood function, the prior distribution $P(\Theta_{N_L}|N_L)$ is expressed as

$$P(\Theta_{N_L}|N_L) = \prod_{n=1}^{N_L} P(\underline{\theta}_n|N_L) \tag{6.9}$$

where $P(\underline{\theta}_n|N_L)$, n = 1, 2,…, N_L, is the prior distribution of model parameters $\underline{\theta}_n = [\,\mu_n \quad \sigma_n \quad \lambda_n\,]$ of the nth sand layer. Assuming that $P(\underline{\theta}_n|N_L)$ is a Gaussian distribution with the mean $\overline{\theta}_n = [\,\overline{\mu}_n \quad \overline{\sigma}_n \quad \overline{\lambda}_n\,]$ and standard deviation $\underline{w}_n = [\,w_{\mu n} \quad w_{\sigma n} \quad w_{\lambda n}\,]$, it is then expressed as

$$\begin{aligned} P(\underline{\theta}_n|N_L) = {} & \frac{1}{(2\pi)^{3/2}w_{\mu n}w_{\sigma n}w_{\lambda n}}\exp\{-\frac{1}{2w_{\mu n}^2}(\mu_n - \overline{\mu}_n)^2 \\ & - \frac{1}{2w_{\sigma n}^2}(\sigma_n - \overline{\sigma}_n)^2 - \frac{1}{2w_{\lambda n}^2}(\lambda_n - \overline{\lambda}_n)^2\}, n = 1, 2, \ldots, N_L \end{aligned} \tag{6.10}$$

The posterior distribution $P(\Theta_{N_L}|\underline{\xi}, N_L)$ in Eq. (6.6) is a joint distribution of model parameters Θ_{N_L}. To obtain the posterior marginal probability density function (PDF) for one parameter among Θ_{N_L}, integration on Eq. (6.6) over the space of the other parameters is needed. Since the integrand is complicated, analytical integration is often infeasible. For the posterior PDF of one parameter among Θ_{N_L},

numerical integration may be performed using a multidimensional grid on the space of the other parameters, but it must be performed repeatedly for a number of values of the model parameter so as to yield information about the whole marginal distribution. To bypass the computational complexity of repetitive integration in high dimensions which has been recognized as one key limitation of the Bayesian approach in the literature (e.g., Zhang et al. 2009), an asymptotic technique is applied in the next section to provide an approximation of the posterior PDF of model parameters and the most probable thicknesses of the N_L sand layers.

6.5 Posterior Knowledge and Boundaries of Statistically Homogenous Layers

6.5.1 Posterior Knowledge on Model Parameters

The asymptotic technique involves approximating the posterior PDF as a Gaussian PDF, which is in the same spirit of Laplace asymptotic approximation of integrals (Bleisten and Handelsman 1986). By this approximation, the posterior PDF of the model parameters is a joint Gaussian PDF with a mean matrix equal to the most probable values (MPVs) of the posterior PDF. The MPV, denoted by $\Theta^*_{N_L}$, maximizes the posterior PDF. Note that $\Theta^*_{N_L}$ consists of N_L model parameter MPV vectors, i.e., $\underline{\theta}^*_n = [\,\mu^*_n \quad \sigma^*_n \quad \lambda^*_n\,]$, $n = 1, 2, \ldots, N_L$, where μ^*_n, σ^*_n, and λ^*_n are the respective MPV of μ_n, σ_n, and λ_n of the nth sand layer. Under this approximation, the determination of the posterior mean for Θ_{N_L} reduces to finding the MPV $\Theta^*_{N_L}$ by maximizing $P(\Theta_{N_L}|\underline{\xi}, N_L)$ or, for numerical convenience, minimizing an objective function $f_{obj} = -\ln[P(\Theta_{N_L}|\underline{\xi}, N_L)]$. Using Eqs. (6.6)–(6.10), f_{obj} is given by

$$f_{obj} = \sum_{n=1}^{N_L} \{\frac{1}{2}\ln|\det \underline{C}_n| + \frac{1}{2}[\underline{\xi}_n - (a\mu_n + b)\underline{l}_n]^T \underline{C}_n^{-1}[\underline{\xi}_n - (a\mu_n + b)\underline{l}_n\} + \sum_{n=1}^{N_L} \{\frac{1}{2w^2_{\mu n}}(\mu_n - \overline{\mu}_n)^2 + \frac{1}{2w^2_{\sigma n}}(\sigma_n - \overline{\sigma}_n)^2 + \frac{1}{2w^2_{\lambda n}}(\lambda_n - \overline{\lambda}_n)^2\} + Con_{N_L} \tag{6.11}$$

in which Con_{N_L} is a constant for a given N_L statistically homogenous soil layers.

Under the Laplace asymptotic approximation of integrals (Bleisten and Handelsman 1986), the covariance matrix $\underline{G}$ of the Gaussian PDF that approximates $P(\Theta_{N_L}|\underline{\xi}, N_L)$ is given by the inverse of the Hessian matrix $\underline{H}$ of $f_{obj} = -\ln[P(\Theta_{N_L}|\underline{\xi}, N_L)]$ evaluated at the MPV, i.e., $\underline{G} = \underline{H}^{-1}(\Theta^*_{N_L})$. Since the N_L random fields are assumed to be mutually independent, the model parameters of different sand layers are uncorrelated. The Hessian matrix of $f_{obj} = -\ln[P(\Theta_{N_L}|\underline{\xi}, N_L)]$

is given by a diagonal matrix $\underline{H} = \text{diag}(\underline{H}_1, \underline{H}_2, \ldots, \underline{H}_{N_L})$ with main diagonal terms of $\underline{H}_n, n = 1, 2, \ldots, N_L$ which are expressed as

$$\underline{H}_n = \begin{bmatrix} \dfrac{\partial^2 f_{obj}}{\partial \mu_n^2} & \dfrac{\partial^2 f_{obj}}{\partial \mu_n \partial \sigma_n} & \dfrac{\partial^2 f_{obj}}{\partial \mu_n \partial \lambda_n} \\ & \dfrac{\partial^2 f_{obj}}{\partial \sigma_n^2} & \dfrac{\partial^2 f_{obj}}{\partial \sigma_n \partial \lambda_n} \\ \text{sym.} & & \dfrac{\partial^2 f_{obj}}{\partial \lambda_n^2} \end{bmatrix}, n = 1, 2, \ldots, N_L \tag{6.12}$$

The covariance matrix $\underline{G}$ is therefore given by a diagonal matrix $\underline{H}^{-1} = \text{diag}(\underline{H}_1^{-1}, \underline{H}_2^{-1}, \ldots, \underline{H}_{N_L}^{-1})$ with main diagonal terms of $\underline{H}_n^{-1}$, n = 1, 2, …, N_L, where $\underline{H}_n^{-1}$ is the inverse of $\underline{H}_n$ and provides the covariance matrix of model parameters of the nth sand layer. Therefore, the main diagonal terms of $\underline{H}_n^{-1}$ give the posterior variance of μ_n, σ_n, and λ_n, while the off-diagonal terms give their covariance, i.e., $s_{\mu n}^2 = \underline{H}_n^{-1}(1,1)$, $s_{\sigma n}^2 = \underline{H}_n^{-1}(2,2)$, and $s_{\lambda n}^2 = \underline{H}_n^{-1}(3,3)$. Note that the Laplace asymptotic approach described above has been successfully applied to obtain the posterior distribution of random field model parameters using CPT data by Wang et al. (2010), and they showed that the results obtained from the Laplace asymptotic approach are in good agreement with those obtained from numerical integration.

6.5.2 The Most Probable Thicknesses and Boundaries of Statistically Homogenous Layers

As mentioned before, the likelihood function $P(\underline{\xi}|\Theta_{N_L}, N_L)$ is a function of thicknesses $\underline{h}_{N_L}$ of statistically homogenous layers. Thus, both the posterior distribution $P(\Theta_{N_L}|\underline{\xi}, N_L)$ and the objective function $f_{obj} = -\ln[P(\Theta_{N_L}|\underline{\xi}, N_L)]$ are functions of $\underline{h}_{N_L}$. Maximizing the posterior distribution $P(\Theta_{N_L}|\underline{\xi}, N_L)$, i.e., minimizing $f_{obj} = -\ln[P(\Theta_{N_L}|\underline{\xi}, N_L)]$, provides not only the MPV of model parameters $\Theta_{N_L}^*$ but also the MPV of thicknesses $\underline{h}_{N_L}^* = [h_1^*, h_2^*, \ldots, h_{N_L}^*]^T$ for the statistically homogenous layers, in which h_n^*, n = 1, 2, …, N_L, represents the most probable thickness of the nth sand layer. This delineates the boundaries that separate the N_L statistically homogenous layers of sand.

6.6 The Most Probable Number of Layers

The number N_L of the statistically homogenous layers is considered as a given value in the previous sections. This section considers the number of statistically homogenous layers as a variable k and utilizes a Bayesian model class selection

approach (Beck and Yuen 2004; Yan et al. 2009; Yuen 2010) to determine the most probable value k^* (or the most probable model class) among a pool of candidate model classes. A model class herein is referred to a family of stratification models that share the same number (e.g., k) of statistically homogenous soil layers but have different model parameters (e.g., layer thickness $\underline{h}_N$ and the model parameter matrix Θ_N). Let N_{Lmax} denote the maximum possible number of sand layers within the depth of which CPT is performed. Then, the model class number k is a positive integer varying from 1 to N_{Lmax}. Subsequently, there are N_{Lmax} candidate model classes M_k, $k = 1, 2, \ldots, N_{\text{Lmax}}$, and the kth model class M_k has k statistically homogenous layers. The most probable model class M_k^* is the model class that has the maximum plausibility (or occurrence probability), among all candidate model classes, given that a set of CPT data $\underline{\xi}$ is observed. The most probable layer number k^* therefore can be determined by comparing the conditional probabilities $P(M_k|\underline{\xi})$ for all candidate model classes (i.e., $k = 1, 2, \ldots, N_{Lmax}$) and selecting the one with the maximum value of $P(M_k|\underline{\xi})$.

According to Bayes' theorem, $P(M_k|\underline{\xi})$ is written as (Beck and Yuen 2004; Yan et al. 2009; Yuen 2010)

$$P(M_k|\underline{\xi}) = P(\underline{\xi}|M_k)P(M_k)/P(\underline{\xi}), k = 1, 2, \ldots, N_{Lmax} \tag{6.13}$$

where $P(\underline{\xi})$ is the PDF of $\underline{\xi}$, and it is constant and independent of M_k; $P(\underline{\xi}|M_k)$ is the conditional PDF of $\underline{\xi}$ for a given the model class M_k; $P(M_k)$ is the prior probability of the model class M_k, which reflects the prior knowledge on the number of sand layers. $P(\underline{\xi}|M_k)$ is frequently referred to as the "evidence" for the model class M_k provided by the CPT data $\underline{\xi}$, and it increases as the plausibility of $\underline{\xi}$ conditional on M_k increases. In the case of no prevailing prior knowledge on the number of sand layers (i.e., uniformly distributed prior), the N_{Lmax} candidate model classes have the same prior probability, and hence, $P(M_k)$ can be taken as a constant $1/N_{\text{Lmax}}$. Then, based on Eq. (6.13), $P(M_k|\underline{\xi})$ is proportional to $P(\underline{\xi}|M_k)$. Since the most probable model class M_k^* corresponds to the maximum value of $P(M_k|\underline{\xi})$, it also has the maximum value of $P(\underline{\xi}|M_k)$. In other words, the most probable model class M_k^* can be selected by comparing the values of $P(\underline{\xi}|M_k)$ among N_{Lmax} candidate model classes. The model class that has the maximum value of $P(\underline{\xi}|M_k)$ is taken as the most probable class M_k^* among the N_{Lmax} candidates. The calculation of $P(\underline{\xi}|M_k)$ is discussed in the next subsection.

6.6.1 Calculation of the Evidence for Each Model Class

By the Theorem of Total Probability, the evidence $P(\underline{\xi}|M_k)$ for model class M_k can be expressed as

$$P(\underline{\xi}|M_k) = \int P(\underline{\xi}|\Theta_k, M_k)P(\Theta_k|M_k)d\Theta_k, k = 1, 2, \ldots, N_{Lmax} \tag{6.14}$$

Equation (6.14) involves integration over the multidimensional space of model parameters Θ_k for model class M_k (Beck and Yuen 2004). To avoid the computational complexity of multidimensional integration, the asymptotic technique described in the Sect. 6.5 "Posterior Knowledge and Boundaries of Statistically Homogenous Layers" is also adopted, and $P(\underline{\xi}|M_k)$ in Eq. (6.14) can be approximated as (Papadimitriou et al. 1997; Beck and Katafygiotis 1998; Beck and Yuen 2004)

$$P(\underline{\xi}|M_k) \approx P(\underline{\xi}|\Theta_k^*, M_k)P(\Theta_k^*|M_k)(2\pi)^{j_k/2}\left|\det \underline{H}(\Theta_k^*)\right|^{-1/2}, k = 1, 2, \ldots, N_{Lmax} \tag{6.15}$$

where Θ_k^* is the MPV of model parameters for model class M_k; $P(\underline{\xi}|\Theta_k^*, M_k)$ is the likelihood function of M_k evaluated at Θ_k^*, and it is given by Eqs. (6.7) and (6.8); $P(\Theta_k^*|M_k)$ is the prior distribution of M_k evaluated at Θ_k^*, and it is calculated using Eqs. (6.9) and (6.10); $\underline{H}(\Theta_k^*)$ is the Hessian matrix of M_k evaluated at Θ_k^*; $j_k = 3k$ is the number of model parameters of M_k. $P(\Theta_k^*|M_k)(2\pi)^{j_k/2}\left|\det \underline{H}(\Theta_k^*)\right|^{-1/2}$ is called the Ockham factor Ock_{Mk} that serves as a measure of the robustness of M_k (Gull 1988). The Ockham factor decreases exponentially as the number (i.e., j_k) of uncertain model parameters increases, and it represents a penalty against parameterization (Gull 1988; Mackay 1992, Beck and Yuen 2004; Yan et al. 2009; Yuen 2010). It is worthwhile to note that the value of $P(\underline{\xi}|\Theta_k^*, M_k)$ tends to increase as the number k of soil layers or the number (i.e., j_k) of uncertain model parameters increases. The evidence $P(\underline{\xi}|M_k)$ in Eq. (6.15) therefore is a result of two contradicting factors: $P(\underline{\xi}|\Theta_k^*, M_k)$ that increases as k increases and the Ockham factor (i.e., $P(\Theta_k^*|M_k)(2\pi)^{j_k/2}\left|\det \underline{H}(\Theta_k^*)\right|^{-1/2}$) that decreases as k increases. The maximum value of $P(\underline{\xi}|M_k)$ is obtained when a balance between these two contradicting factors is achieved, and the corresponding k^* value represents the most probable number of soil layers.

The evidence $P(\underline{\xi}|M_k)$ is calculated repeatedly for k = 1, 2, …, N_{Lmax}. In each repeated calculation, the value of k or the number of soil layers is constant. The Bayesian system identification method developed in Sects. 6.2−6.5 for a soil profile with given N_L layers of soil can be applied directly by setting $N_L = k$. The Bayesian system identification approach leads to $\Theta_k^*, \underline{H}(\Theta_k^*)$ and its inverse $\underline{H}^{-1}(\Theta_k^*)$, and the most probable thicknesses $\underline{h}_k^*$ for the model class M_k. The evidence $P(\underline{\xi}|M_k)$ is then obtained using Eqs. (6.7)−(6.10) and (6.15). The calculation is repeated N_{Lmax} times for the N_{Lmax} candidate model classes, and the values of $P(\underline{\xi}|M_k)$ for the N_{Lmax} model classes are obtained. By comparing these $P(\underline{\xi}|M_k)$ values, the most probable model class M_k^* and the most probable number k^* of soil layers are determined. Note that the most probable thicknesses $\underline{h}_{k^*}^*$ and other MPVs of model

parameters $\Theta_{k^*}^*$ have been determined in the previous repeated calculation for Bayesian system identification. Therefore, the determination of the most probable number k^* of soil layers simultaneously leads to the determination of the most probable thicknesses $\underline{h}_{k^*}^*$ and other MPV of model parameters $\Theta_{k^*}^*$ for each soil layer in M_k^*.

6.7 Implementation Procedure

The implementation of the Bayesian approach involves 8 steps. Details of each step and their associated equations are summarized as follows:

(1) Obtain a set of cone tip resistance q_c versus depth data from CPTs and convert them to a vector $\underline{\xi}$ at different depths using Eq. (6.4);
(2) Choose an appropriate maximum number N_{Lmax} of sand layers for the CPT data $\underline{\xi}$, resulting in N_{Lmax} candidate model classes and the k value varying from 1 to N_{Lmax};
(3) Obtain appropriate prior knowledge including the mean $\overline{\theta}_n = [\,\overline{\mu}_n \quad \overline{\sigma}_n \quad \overline{\lambda}_n\,]$ and standard deviation $\underline{w}_n = [\,w_{\mu n} \quad w_{\sigma n} \quad w_{\lambda n}\,], n = 1, 2, \ldots, k$, for the kth model class;
(4) Construct the objective function $f_{obj} = -\ln[P(\Theta_k|\underline{\xi}, k)]$ using Eqs. (6.6) −(6.10) for the kth model class;
(5) Minimize the objective function $f_{obj} = -\ln[P(\Theta_k|\underline{\xi}, k)]$ and determine its corresponding MPV (i.e., Θ_k^*) as posterior mean and the most probable thicknesses $\underline{h}_k^* = [h_1^*, h_2^*, \ldots, h_k^*]$ for the kth model class;
(6) Calculate the inverse of the Hessian matrix of the objective function evaluated at Θ_k^* (i.e., $\underline{H}^{-1}(\Theta_k^*)$) to obtain posterior variance $s_{\mu n}^2, s_{\sigma n}^2$ and $s_{\lambda n}^2, n = 1, 2, \ldots, k$, for the kth model class. Each term in the Hessian matrix given by Eq. (6.12) is calculated using finite difference methods;
(7) Calculate the conditional probability $P(\underline{\xi}|M_k)$ of $\underline{\xi}$ given the kth model class using Eqs. (6.7)−(6.10) and (6.15);
(8) Repeat steps (3)−(7) N_{Lmax} times to calculate $\Theta_k^*, \underline{H}^{-1}(\Theta_k^*), \underline{h}_k^*$ and $P(\underline{\xi}|M_k)$ for the N_{Lmax} candidate model classes, respectively. The model class with the maximum value of $P(\underline{\xi}|M_k)$ is selected as the most probable model class M_k^*, and the corresponding $k^*, \underline{h}_{k^*}^*, \Theta_{k^*}^*$ and $\underline{H}^{-1}(\Theta_{k^*}^*)$ are obtained.

Note that the minimization of the objective function $f_{obj} = -\ln[P(\Theta_k|\underline{\xi}, k)]$ in step (5) can be readily implemented by conventional optimization algorithm, e.g., the function "fminsearch" in MATLAB (Mathworks 2010). The differentiation of $f_{obj} = -\ln[P(\Theta_k|\underline{\xi}, k)]$ for constructing the Hessian matrix in step (6) can be evaluated numerically in MATLAB using finite difference method. The proposed approach and the implementation procedure described above will be illustrated through a real example in the next section.

6.8 Illustrative Example

The proposed Bayesian system identification and model class selection approach are illustrated using a set of real CPT data obtained from a site at Eemshaven, the Netherlands (Niazi and Mayne 2010). The site is comprised of a sequence of loose to very dense sand layers with occasional clay and silt inclusions extending from a depth of 1.5 m to a depth of about 50 m. The groundwater table is at about 1.5 m below ground surface. As shown in Fig. 6.3a, there are two relatively clean sand layers between 22.5 m and 37.5 m below ground surface, including a medium to dense sand layer from 22.5 m to about 29.1 m and a very dense sand layer from about 29.1 m to 37.5 m. Note that the boundary at a depth of 29.1 m given in the original data is based on relative density (Holtz 1973, Niazi and Mayne 2010). As shown in Fig. 6.3a, the thickness and the total unit weight (i.e., γ_{t1} and γ_{t2}) of the two layers are 6.6 and 8.4 m, 17.9 and 18.9 kN/m^3, respectively. Figure 6.3a also includes the cone tip resistance measured from a CPT at this site (Fugro 2004; Niazi and Mayne 2010). As a reference, the sand effective friction angle ϕ' can be estimated directly using the regression between cone tip resistance and ϕ' (i.e., Eq. (6.4)). As shown in Fig. 6.3b, the resulting ϕ' profiles in these two layers are

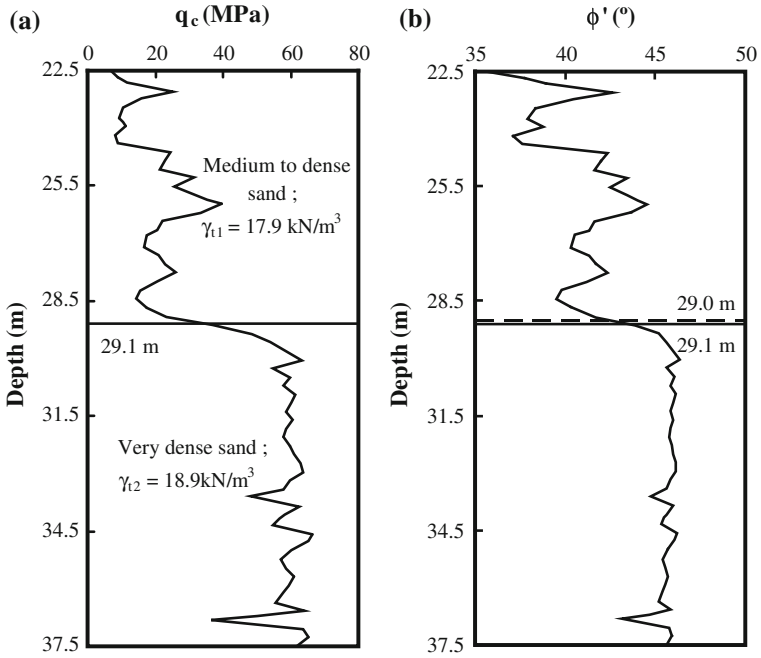

Fig. 6.3 An illustrative example with a set of real CPT results at Eemshaven, the Netherlands (After Niazi and Mayne 2010 and Cao and Wang 2013), **a** cone tip resistance, **b** sand effective friction angle

quite different, with their respective means of 40.9° and 45.6°, and respective standard deviations of 2.1° and 0.6°.

Consider, for example, five candidate model classes (i.e., the maximum number of sand layers, $N_{\mathrm{Lmax}} = 5$). The possible numbers (i.e., k) of sand layers therefore are 1, 2, 3, 4, and 5. Since the number and thicknesses of sand layers are unknown, the prior knowledge is assumed identical for all sand layers. For the kth model class, prior knowledge of the nth sand layer is taken as follows: the mean $\overline{\mu}_n = 40^\circ, \overline{\sigma}_n = 4.0^\circ, \overline{\lambda}_n = 1.5\,\mathrm{m}$ and standard deviation $w_{\mu n} = 16^\circ, w_{\sigma n} = 1.6^\circ, w_{\lambda n} = 0.6\,\mathrm{m}$, $n = 1, 2, \ldots, k$. This prior knowledge falls within the typical ranges of sand effective friction angles reported in the literature (e.g., Kulhawy and Mayne 1990; Phoon and Kulhawy 1999a). Note that the ratio of standard deviation over mean (i.e., the coefficient of variation (COV), $w_{\mu n}/\overline{\mu}_n, w_{\sigma n}/\overline{\sigma}_n$, and $w_{\lambda n}/\overline{\lambda}_n$) of model parameters in prior knowledge is taken as 40 % in this example. This COV of model parameters in the adopted prior knowledge is relatively large, and thus, the confidence level of the adopted prior knowledge is relatively low, and the prior knowledge is relatively uninformative. Effects of the confidence level of prior knowledge will be explored further in the next section. Using the prior knowledge and the CPT data shown in Fig. 6.3a, the proposed Bayesian approach provides the most probable number of statistically homogenous sand layers, the most probable boundaries (or thicknesses) of the layers, and posterior knowledge of model parameters in each layer, as discussed in the following three subsections.

6.8.1 The Most Probable Number of Sand Layers

Table 6.1 summarizes the logarithm of evidence (i.e., $\ln\left[P(\underline{\xi}|M_k)\right]$) in the second column for five candidate model classes. The value of $\ln\left[P(\underline{\xi}|M_k)\right]$ increases from −93.7 to −85.8 as k increases from 1 to 2, and it then decreases from −85.8 to −97.5 as k further increases from 2 to 5. The model class with two sand layers, i.e., M_2, has the largest value of $\ln\left[P(\underline{\xi}|M_k)\right]$ (i.e.,−85.8) among all five model classes. Therefore, the most probable number of statistically homogenous sand layers is two, i.e., $k^* = 2$. This is consistent with the ground condition given in the original

Table 6.1 Results of the Bayesian model class selection approach (After Cao and Wang 2013)

Model class M_k	$\ln[P(\underline{\xi}\|M_k)]$	$\ln(Ock_{Mk})$	The most probable thicknesses $\underline{h}_k^*$ (m)				
			h_1^*	h_2^*	h_3^*	h_4^*	h_5^*
M_1	−93.7	−7.2	15	–	–	–	–
M_2^*	−85.8	−14.3	6.5	8.5	–	–	–
M_3	−86.7	−19.1	1.9	4.7	8.4	–	–
M_4	−90.2	−22.4	2.0	3.4	1.2	8.4	–
M_5	−97.5	−28.7	1.9	2.9	1.9	2.9	5.4

data and shown in Fig. 6.3. Table 6.1 also summarizes the logarithm of Ockham factor (i.e., ln (Ock_{Mk})) in the third column. As k increases and the number of model parameters increases, the logarithm of Ockham factor decreases monotonically from −7.2 to −28.7. This is consistent with the results of the previous studies on model class selection which have shown that the Ockham factor decreases exponentially as the number of model parameters increases for the same set of data (Beck and Yuen 2004; Yuen 2010). The Ockham factor therefore assures that the observed data are not overfitted by a model class with a large number of model parameters (e.g., a large k value in this chapter) or the most probable model class is not biased to favor a model class with a large k value.

6.8.2 The Most Probable Thicknesses or Boundaries

Table 6.1 also summarizes the most probable thicknesses (i.e., $\underline{h}_k^*$ in Column 4) of sand layers for the five candidate model classes. Using $\underline{h}_k^*, k = 1, 2, \ldots, 5$, the most probable boundaries of statistically homogeneous layers are delineated accordingly for the five model classes. Figure 6.4 shows the most probable boundaries for the five model classes and the boundary (i.e., 29.1 m) of the two sand layers defined in the original data by dashed lines and solid lines, respectively. For the most probable model class M_2, the most probable thicknesses of these two layers are 6.5 m and

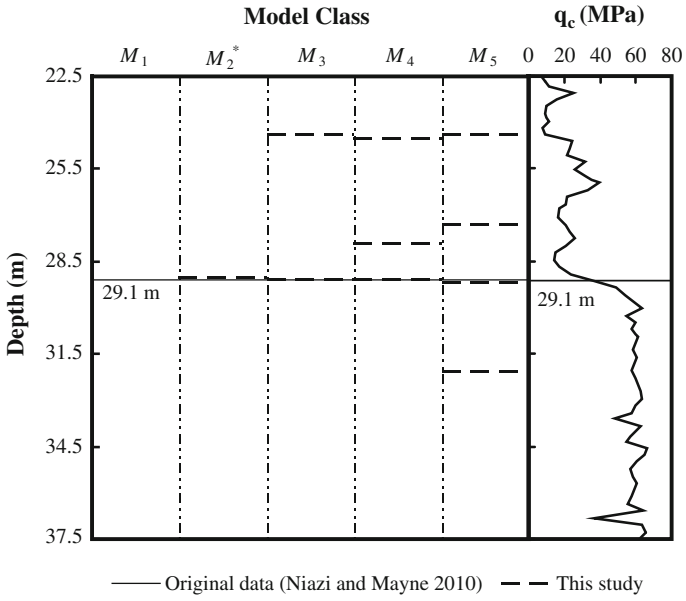

Fig. 6.4 The most probable boundaries of statistically homogenous layers for different model classes (After Cao and Wang 2013)

8.5 m, respectively. The most probable boundary for M_2 is thus at the depth of 22.5 m + 6.5 m = 29.0 m, and it is in good agreement with the one (i.e., 29.1 m) defined in the original data.

Figure 6.4 also shows an evolution of layer identification as the model class varies from M_1 to M_5 (i.e., the number of layers increases from 1 to 5). Model class M_1 only has one layer, and hence, it does not have any internal boundary. The number of internal boundaries increases from 1 for M_2 to 4 for M_5. All model classes M_2 to M_5 share a common internal boundary at a depth of about 29.1 m. In addition, model classes M_3, M_4, and M_5 share one more common internal boundary at a depth of about 24.4 m, and model classes M_4 and M_5 share another common one at a depth of about 27.6 m. The first layer in M_2 is further divided into two new layers in M_3; the second layer in M_3 is further divided into two new layers in M_4; and the fourth layer in M_4 is further divided into two new layers in M_5. The most probable boundaries in a model class M_k include those identified in the previous model class M_{k-1} and one additional internal boundary that divides one layer in M_{k-1} into two new layers in M_k. As the value of k increases, the Bayesian approach developed in this chapter identifies the statistically homogenous layers progressively, starting from the most statistically significant boundary (e.g., at a depth of 29.1 m in this example) and gradually "zooming" into local differences with improved "resolution." Such improved "resolution," of course, comes with an expense of an increasing number of model parameters (e.g., j_k in Eq. (6.15) increases as k increases). As the number of model parameters increases, the value of evidence (i.e., $\ln[P(\underline{\xi}|M_k)]$, see Table 6.1) first increases, before the most probable model class (e.g., M_2 in this example), and then decreases after the most probably model class. The "zooming" therefore should be stopped when the maximum value of $\ln[P(\underline{\xi}|M_k)]$ is obtained or the most probable model class is identified. As discussed in Sect. 6.6.1 "Calculation of the evidence for each model class," the Ockham factor in Eq. (6.15) decreases exponentially as the number (i.e., j_k) of model parameters increases, and it assures that the most probable model class is not biased to favor a model class with a large k value. The Bayesian approach not only provides a means to identify the statistically homogenous layers progressively by gradually "zooming" into local difference with improved "resolution," but also contains a mechanism to determine when to stop such "zooming."

6.8.3 The Posterior Knowledge on Model Parameters

Table 6.2 summarizes the posterior knowledge on model parameters for the most probable model class M_2, including their posterior MPV (or mean) $\underline{\theta}_n^* = [\,\mu_n^* \quad \sigma_n^* \quad \lambda_n^*\,]$, n = 1, 2, in the third column and posterior standard deviation $\underline{s}_n = [\,s_{\mu n} \quad s_{\sigma n} \quad s_{\lambda n}\,]$, $n = 1, 2$, in the fourth column. The posterior MPVs of mean values (i.e., $\mu_n^*, n = 1, 2$) of the medium to dense sand layer and very dense sand layer are 40.9° and 45.7°, respectively. These values are almost identical to their respective values (i.e., 40.9° and 45.6°) that are directly estimated from the CPT

Table 6.2 Posterior knowledge on model parameters of the most probable model class (After Cao and Wang 2013)

The most probable model class	Sand layer	Posterior MPV (or mean) of $\underline{\theta}_n$			Posterior standard deviation of $\underline{\theta}_n$			Posterior standard deviation of ϕ'_n
M_k^*	n	μ_n^* (°)	σ_n^* (°)	λ_n^* (m)	$s_{\mu n}$ (°)	$s_{\sigma n}$ (°)	$s_{\lambda n}$ (m)	$s_{\phi n}$ (°)
M_2	1	40.9	1.4	1.6	0.7	0.5	0.5	1.6
	2	45.7	0.2	1.5	0.3	0.3	0.6	0.5

data (i.e., without any prior knowledge or consideration of inherent spatial variability). The posterior MPVs of standard deviations (i.e., $\sigma_n^*, n = 1, 2$) of the two sand layers are 1.4° and 0.2°, respectively. The posterior standard deviations $s_{\mu 1}, s_{\sigma 1}, s_{\mu 2}$, and $s_{\sigma 2}$ of model parameters $\mu_1, \sigma_1, \mu_2, \sigma_2$ are 0.7°, 0.5°, 0.3°, and 0.3°, respectively. Then, the posterior standard deviation (i.e., $s_{\varphi n}$) of ϕ_n', n = 1, 2, is estimated as $\sqrt{\sigma_n^{*2} + s_{\mu n}^2 + s_{\sigma n}^2}$ (Wang et al. 2010) and shown in the fifth column. The respective values of $s_{\varphi 1}$ and $s_{\varphi 2}$ are 1.6° and 0.5°, and they compare favorably with those (i.e., 2.1° and 0.6°, respectively) directly estimated from the CPT data. The results on μ_n^* and $s_{\varphi n}$ imply that the information provided by CPT data dominates the estimates of μ_n^* and $s_{\varphi n}$, and the effect of the prior knowledge adopted in this example is rather minor. It is not surprising to see such results because the prior knowledge used in this example is relatively uninformative. Effects of prior knowledge are further explored in the next section.

6.9 Sensitivity Study on Confidence Level of Prior Knowledge

Prior knowledge on model parameters includes the mean (i.e., $\overline{\theta}_n = [\overline{\mu}_n \quad \overline{\sigma}_n \quad \overline{\lambda}_n]$, $n = 1, 2, \ldots, k$) and standard deviation (i.e., $\underline{w}_n = [w_{\mu n} \quad w_{\sigma n} \quad w_{\lambda n}]$, $n = 1, 2, \ldots, k$). The ratio of standard deviation over mean (i.e., COV) reflects the confidence level of the prior knowledge on model parameters. When the COV in prior knowledge is relatively small, the confidence level of prior knowledge is relatively high, and the prior knowledge is informative. The confidence level decreases as the COV increases. To illustrate the effects of confidence level of prior knowledge, a sensitivity study is performed with a set of CPT data that are simulated from a soil profile with three layers of sand, as shown in Fig. 6.5. The effective friction angles in these three sand layers are represented by three Gaussian random fields with respective thicknesses of 4 m, 6 m, and 5 m. The CPT data are simulated using the random fields and the regression model described in this chapter with $\mu_1 = 30.0^\circ, \sigma_1 = 1.5^\circ$, and $\lambda_1 = 1.5\,\text{m}; \mu_2 = 40.0^\circ, \sigma_2 = 2.0^\circ$, and $\lambda_2 = 2.0\,\text{m}; \mu_3 =$

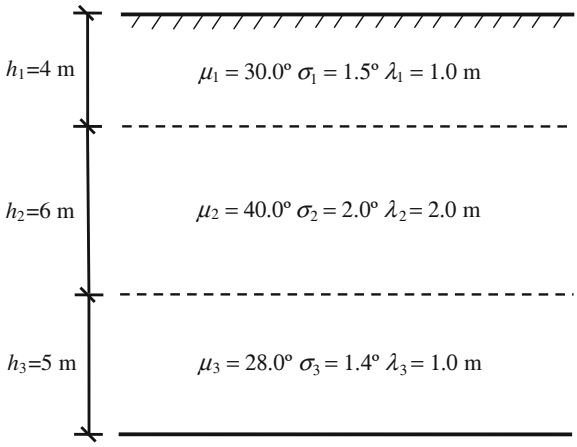

Fig. 6.5 A soil profile with three layers of sand (After Cao and Wang 2013)

28.0°, $\sigma_3 = 1.4^{\circ}$, and $\lambda_3 = 1.0$ m, respectively. Note that in practice both the true boundaries of soil layers and the actual values of soil properties are unknown, and they are estimated through prior knowledge and project-specific test results.

Figure 6.6 shows a set of normalized cone tip resistance q data from simulation for a cone penetration depth up to 15.0 m with a depth interval of 0.1 m. Subsequently, the CPT data are integrated with seven different sets of prior

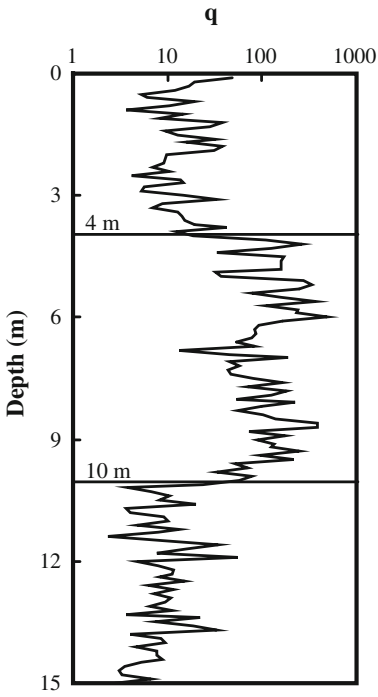

Fig. 6.6 A set of simulated CPT results from three soil layers (After Cao and Wang 2013)

Table 6.3 Summary of prior knowledge used in sensitivity study (After Cao and Wang 2013)

Case ID	Prior mean			Coefficient of variation (%)	Prior standard deviation		
	$\overline{\mu}_n$ (°)	$\overline{\sigma}_n$ (°)	$\overline{\lambda}_n$ (m)		$w_{\mu n}$ (°)	$w_{\sigma n}$ (°)	$w_{\lambda n}$ (m)
I	30.0	3.0	1.5	5	1.5	0.15	0.075
II	30.0	3.0	1.5	10	3.0	0.3	0.15
III	30.0	3.0	1.5	20	6.0	0.6	0.3
IV	30.0	3.0	1.5	40	12.0	1.2	0.6
V	30.0	3.0	1.5	60	18.0	1.8	0.9
VI	30.0	3.0	1.5	80	24.0	2.4	1.2
VII	30.0	3.0	1.5	100	30.0	3.0	1.5

knowledge to estimate the most probable number and boundaries of sand layers and their posterior knowledge on soil properties. Table 6.3 summarizes seven sets of prior knowledge used in the sensitivity study. The prior mean of model parameters is all taken as $\overline{\mu}_n = 30.0^{\circ}, \overline{\sigma}_n = 3.0^{\circ}, \overline{\lambda}_n = 1.5\,\text{m}, n = 1, 2, \ldots k,$, and the prior COV increases from 5 to 100 % (i.e., $w_{\mu n}, w_{\sigma n}$, and $w_{\lambda n}$ range from 1.5° to 30.0°, from 0.15° to 3.0°, and from 0.075 m to 1.5 m, respectively).

6.9.1 *Effect on the Most Probable Number of Sand Layers*

Table 6.4 summarizes the most probable model classes M_k^* (i.e., the most probable number of sand layers) obtained from the Bayesian approach using different sets of prior knowledge. The most probable number of sand layers is 3 when using the prior knowledge IV, V, VI, or VII which is relatively uninformative (i.e., with relatively low confidence level and large prior COV of 40 %, 60 %, 80 %, and 100 %, respectively). The true sand layer number of 3 is identified correctly. In

Table 6.4 Summary of the most probable model classes and most probable thicknesses in sensitivity study (After Cao and Wang 2013)

Case ID	Coefficient of variation (%)	The most probable model class M_k^*	The most probable thicknesses $\underline{h}_{k^*}^*$ (m)				
			h_1^*	h_2^*	h_3^*	h_4^*	h_5^*
I	5	M_5	2.0	2.0	6.0	1.9	3.1
II	10	M_5	2.0	2.0	6.1	1.8	3.1
III	20	M_4	1.9	2.1	6.1	4.9	–
IV	40	M_3	4.0	6.1	4.9	–	–
V	60	M_3	4.0	6.1	4.9	–	–
VI	80	M_3	4.0	6.1	4.9	–	–
VII	100	M_3	4.0	6.1	4.9	–	–

contrast, the most probable number of sand layers is 5, 5, or 4, respectively, when using the prior knowledge I, II, or III which is relatively informative (i.e., with relatively high confidence level and small prior COV of 5 %, 10 %, and 20 %, respectively). This is obviously incorrect because the true number of sand layers is 3 (see Fig. 6.5). Note that the same prior mean values of model parameters are adopted for all sand layers (see Table 6.3), and some of them are quite different from the actual soil properties in the soil layer (see Fig. 6.5). If the adopted prior knowledge is very confident and very informative, it carries a relatively heavy weight in the Bayesian approach and affects its results significantly. The most probable layer number obtained for prior knowledge case I, II, or III is affected significantly by their inconsistent prior knowledge, and therefore, it is incorrect. The Bayesian approach provides a formal and rational framework to integrate prior knowledge and project-specific test data together. Its results are therefore affected by the quality of both prior knowledge and project-specific test data. It is always prudent to rely more on the high-quality project-specific test data, if available, and to start the Bayesian approach with relatively uninformative prior knowledge (i.e., large COV and low confidence level), particularly when the prior knowledge is not well justified.

6.9.2 *Effect on the Most Probable Thicknesses or Boundaries*

Table 6.4 also includes the most probable thicknesses $\underline{h}^*_{k^*}$ of the statistically homogenous sand layers when using different sets of prior knowledge. The most probable boundaries for all seven cases are then delineated accordingly in Fig. 6.7 by dashed lines. All seven cases correctly locate the true boundaries (i.e., the solid line in Fig. 6.7) of the soil profile. On the other hand, when the prior knowledge is inconsistent with the actual soil properties but with high confidence level (e.g., low COV for case I, II, or III), the Bayesian approach provides incorrect results by further dividing some layers into sublayers. This again suggests that it is a good idea to start the Bayesian approach with a relatively uninformative prior knowledge (i.e., large COV and low confidence level).

6.9.3 *Effect on Posterior Knowledge on Model Parameters*

As the true number of sand layers in the soil profile is 3 (see Fig. 6.5), the cases I, II, and III in the sensitivity study are re-evaluated with a deterministic sand layer number of 3 (i.e., M_3). It is found that the most probable thicknesses and boundaries are all identical to their true values or those obtained from cases IV, V, VI, or VII

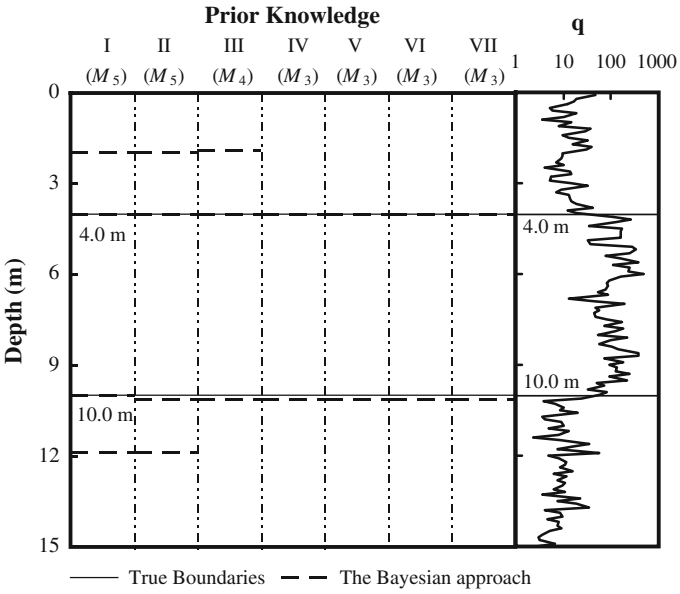

Fig. 6.7 The most probable boundaries for different prior knowledge (After Cao and Wang 2013)

(see Table 6.4). The resulting posterior MPVs of mean $\mu_n^*, n = 1, 2, 3$, and standard deviation $\sigma_n^*, n = 1, 2, 3$, for these seven cases of M_3 are shown in Fig. 6.8.

Figure 6.8a plots a variation of the posterior MPV of mean $\mu_n^*, n = 1, 2, 3$, as a function of prior COV of mean by solid lines with open circles, squares, and triangles, respectively. Figure 6.8a also shows the true values of mean, i.e., $\mu_1 = 30^\circ, \mu_2 = 40^\circ$, and $\mu_3 = 28^\circ$, by solid lines. As the value of COV increases (i.e., confidence level decreases), the posterior MPVs of means in three layers all approach their respective true values. It is also obvious that when the prior knowledge is inconsistent with the actual soil properties but with low COV value (i.e., high confidence level), such as $\mu_2^* = 35^\circ$ at COV = 5 %, the posterior MPV of mean (i.e., 35º) deviates significantly from its true value of 40º. This underscores the negative effect of overconfident prior knowledge.

Figure 6.8b shows a variation of posterior MPV of standard deviation $\sigma_n^*, n = 1, 2, 3$, as a function of prior COV of standard deviation by solid lines with open circles, squares, and triangles, respectively. Figure 6.8b also includes the true values of standard deviation, i.e., $\sigma_1 = 1.5^\circ, \sigma_2 = 2.0^\circ$, and $\sigma_3 = 1.4^\circ$ by solid lines. Similar to Fig. 6.8a, as the value of COV increases, the posterior MPVs of standard deviations in three layers all approach their respective true values. When the prior knowledge is inconsistent with the actual soil properties but is

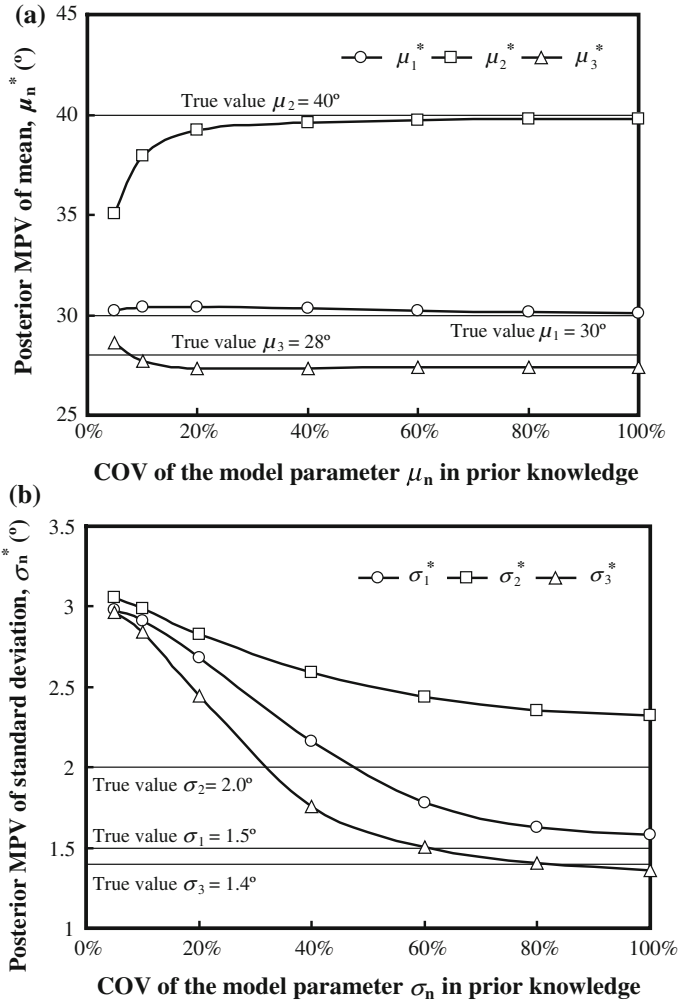

Fig. 6.8 Posterior most probable values (MPVs) of mean and standard deviation for different prior knowledge of M_3 (After Cao and Wang 2013), **a** posterior MPV of mean, **b** posterior MPV of standard deviations

overconfident, the posterior MPV of standard deviation deviates significantly from its true value. On the other hand, prior knowledge with large COV values generally results in consistent posterior MPV of standard deviation.

6.10 Summary and Conclusions

This chapter developed a Bayesian approach for probabilistic site characterization using cone penetration test (CPT). Prior knowledge and results of project-specific CPTs are integrated properly under the Bayesian framework developed in this book to identify the most probable number and thicknesses/boundaries of statistically homogenous layers of soil and to estimate probabilistically the soil effective friction angle simultaneously. The Bayesian approach has been developed in conjunction with random field theory to model explicitly the inherent spatial variability and regression between CPT measurement and soil properties. It contains two major components: a Bayesian model class selection method to identify the most probable number of statistically homogenous layers of soil and a Bayesian system identification method to estimate the most probable layer thicknesses and soil properties probabilistically.

Equations were derived for the Bayesian approach, and the proposed approach was illustrated using a set of real CPT data obtained from a site in the Netherlands. It has been shown that the proposed approach correctly identifies the number and thicknesses/boundaries of the statistically homogenous layers of soil and provides proper probabilistic characterization of soil properties. In addition, as the number of model classes increases, the Bayesian model class selection approach identifies the statistically homogenous layers progressively, starting from the most statistically significant boundary and gradually "zooming" into local difference with improved "resolution." The Bayesian approach also contains a mechanism to determine when to stop further increasing the number of model class (i.e., the "zooming").

A sensitivity study was performed to explore the effect of prior knowledge on identification of statistically homogenous soil layers and probabilistic characterization of soil properties. It is found that the results of Bayesian approach are affected by the quality of both prior knowledge and project-specific test data. It is always prudent to rely more on the high-quality project-specific test data, if available, and to start the Bayesian approach with relatively uninformative prior knowledge (i.e., large COV and low confidence level), particularly when the prior knowledge is not well justified.

References

Ang, A.H.S., and W.H. Tang. 2007. *Probability concepts in engineering: Emphasis on applications to civil and environmental engineering*. New York: John Wiley and Sons.

Beck, J.L., and L.S. Katafygiotis. 1998. Updating models and their uncertainties. I: Bayesian statistical framework. *Journal of Engineering Mechanics* 124(4): 455–461.

Beck, J.L., and K.V. Yuen. 2004. Model selection using response measurements: Bayesian probabilistic approach. *Journal of Engineering Mechanics* 130(2): 192–203.

Bleisten, N., and R. Handelsman. 1986. *Asymptotic expansions of integrals*. New York: Dover.

Cao, Z., and Y. Wang. 2013. Bayesian approach for probabilistic site characterization using cone penetration tests. *Journal of Geotechnical and Geoenvironmental Engineering* 139(2): 267–276.

Cao, Z., Y. Wang, and S.K. Au. 2011. CPT-Based probabilistic characterization of effective friction angle of sand. *Geotechnical Risk Assessment and Management, Geotechnical Special Publication* 224: 403–410.

Fenton, G. 1999a. Estimation for stochastic soil models. *Journal of Geotechnical and Geoenvironmental Engineering* 125(6): 470–485.

Fenton, G. 1999b. Random field modeling of CPT data. *Journal of Geotechnical and Geoenvironmental Engineering* 125(6): 486–498.

Fenton, G., and D.V. Griffiths. 2008. *Risk assessment in geotechnical engineering*. Hoboken, New Jersey: John Wiley and Sons.

Fugro. 2004. *Axial pile capacity design method for offshore driven piles in sand.* Report to American Petroleum Institute, No. P1003, Issue 3, Houston, Texas. 122p.

Gull, S.F. 1988. Bayesian inductive inference and maximum entropy. In *Maximum entropy and Bayesian methods*, ed. J. Skilling. 53−74. Boston: Kulwer Academic.

Holtz, W.G. 1973. The relative density approach—uses, testing requirements, reliability, and shortcomings. In *Proceedings of Symposium on Evaluation of Relative Density and Its Role in Geotechnical Projects Involving Cohesionless Soils*, American Society for Testing and Materials, Special Technical Publication 523, Philadelphia, 5–17.

Jaksa, M.B. 1995. The Influence of Spatial Variability on the Geotechnical Design Properties of a Stiff, Overconsolidated Clay. Ph.D. thesis, University of Adelaide.

Kulhawy, F.H., and P.W. Mayne. 1990. *Manual on estimating soil properties for foundation design, Report EL 6800*. Palo Alto: Electric Power Research Inst. 306p.

Lumb, P. 1966. The variability of natural soils. *Canadian Geotehcnial Journal* 3(2): 74–97.

Lunne, T., P.K. Robertson, and J.J.M. Powell. 1997. *Cone penetration testing in geotechnical practice*. London, U.K.: Blackie-Academic Publishing. 317p.

MacKay, D.J.C. 1992. Bayesian interpolation. *Neural computation* 4(3): 415–447.

Mathworks, Inc. 2010. MATLAB—the language of technical computing. http://www.mathworks.com/products/matlab/. Accessed 09 Mar 2009.

Niazi, F.S., and P.W. Mayne. 2010. Evaluation of EURIPIDES pile load tests response from CPT data. *International Journal of Geoengineering Case Histories* 1(4): 367–386.

Papadimitriou, C., J.L. Beck, and L.S. Katafygiotis. 1997. Asymptotic expansions for reliability and moments of uncertain systems. *Journal of Engineering Mechanics* 123(12): 1219–1229.

Phoon, K.K., and F.H. Kulhawy. 1999a. Characterization of geotechnical variability. *Canadian Geotechnical Journal* 36(4): 612–624.

Phoon, K.K., and F.H. Kulhawy. 1999b. Evaluation of geotechnical property variability. *Canadian Geotechnical Journal* 36(4): 625–639.

Phoon, K.K., S.T. Quek, and P. An. 2003. Identification of statistically homogeneous soil layers using modified Bartlett statistics. *Journal of Geotechnical and Geoenviornmental Engineering* 129(7): 649–659.

Vanmarcke, E.H. 1977. Probabilistic modeling of soil profiles. *Journal of Geotechnical Engineering* 103(11): 1127–1246.

Vanmarcke, E.H. 1983. *Random fields: Analysis and synthesis*. Cambridge: MIT Press.

Wang, Y., S.K. Au, and Z. Cao. 2010. Bayesian approach for probabilistic characterization of sand friction angles. *Engineering Geology* 114(3–4): 354–363.

Yan, W.M., K.V. Yuen, and G.L. Yoon. 2009. Bayesian probabilistic approach for the correlations of compression index for marine clays. *Journal of Geotechnical and Geoenvironmental Engineering* 135(12): 1932–1940.

Yuen, K.V. 2010. Recent development of Bayesian model class selection and applications in civil engineering. *Structural Safety* 32(5): 338–346.

Zhang, J., L.M. Zhang, and W.H. Tang. 2009. Bayesian framework for characterizing geotechnical model uncertainty. *Journal of Geotechnical and Geoenvironmental Engineering* 135(7): 932–940.

Chapter 7
Practical Reliability Analysis of Slope Stability by Advanced Monte Carlo Simulations in a Spreadsheet

7.1 Introduction

The previous chapters developed several probabilistic approaches for geotechnical site characterization. These probabilistic approaches provide probabilistic characterization of soil properties and underground stratigraphy and account rationally for inherent spatial variability of soils and various uncertainties (i.e., statistical uncertainties, measurement errors, and transformation uncertainties) that arise during site characterization. The uncertainties (including inherent spatial variability of soils) obviously affect probabilistic estimations of soil properties and underground stratigraphy, which are key input information in probabilistic analysis and/or designs of geotechnical structures. Therefore, the uncertainties subsequently influence probabilistic analysis and/or designs of geotechnical structures. Consider, for example, probabilistic slope stability analysis. Various uncertainties can be taken into account rationally in probabilistic slope stability analysis through Monte Carlo simulation (MCS). MCS method provides a robust and conceptually simple way to estimate the "reliability index" β or slope failure probability P_f (e.g., El-Ramly et al. 2002; Griffiths and Fenton 2004; El-Ramly et al. 2005). Direct MCS, however, suffers from a lack of efficiency and resolution at small probability levels that are of great interest to geotechnical practitioners (see Chap. 2).

In addition, it has been recognized that a slope may fail along an unlimited number of potential slip surfaces, although evaluating the total failure probability along all potential slip surfaces is considered a mathematically formidable task (El-Ramly et al. 2002). The value of β for slope stability therefore is frequently determined only for one or a limited number of slip surfaces (e.g., Tang et al. 1976; Hassan and Wolff 1999; El-Ramly et al. 2002). A few exceptions are the recent work by Griffiths and Fenton (2004), Xu and Low (2006), and Hong and Roh (2008) that utilize direct MCS and finite element analysis to search for the critical slip surfaces. Nevertheless, the effect of critical slip surface uncertainty has not been explored systematically.

Z. Cao et al., *Probabilistic Approaches for Geotechnical Site Characterization and Slope Stability Analysis*, DOI 10.1007/978-3-662-52914-0_7

This chapter presents a practical approach of slope stability–reliability analysis that implements an advanced MCS method called "subset simulation" in a spreadsheet environment for improving the efficiency and resolution of MCS at relatively small probability levels and for exploring the effect of critical slip surface uncertainty. MCS and subset simulation are operationally decoupled from deterministic slope stability analysis and implemented using a commonly available spreadsheet software, Microsoft Excel. The proposed methodology is illustrated through application to a cohesive slope and validated against results from other reliability solution methods and commercial software. With the aid of improved computational efficiency and resolution at relatively small probability levels offered by the proposed methodology, the effects of inherent spatial variability of soil property and critical slip surface uncertainty will be explored.

7.2 Monte Carlo Simulation of Slope Stability

Figure 7.1 shows a flowchart for MCS of slope stability analysis schematically. The MCS starts with characterization of probability distributions of uncertainties concerned, as well as slope geometry and other necessary information, followed by the generation of n_{MC} sets of random samples according to the prescribed probability distributions. Note that the input information required (e.g., probability distributions of soil properties) in MCS can be obtained from probabilistic approaches developed for geotechnical site characterization in the previous four chapters. For each set of random samples, limit equilibrium methods are utilized, and the critical slip surface is searched for obtaining the minimum FS, resulting in totally n_{MC} sets of minimum FS. Then, statistical analysis is performed to estimate P_f or β, with the slope failure defined as the minimum $FS < 1$. To ensure a desired level of accuracy in P_f, the number of samples in direct MCS should be at least ten times greater than the reciprocal of the probability level of interest (Robert and Casella 2004). For a P_f level of 0.001 that corresponds to an expected performance level of "above average" (see Table 2.7 in Chap. 2), the sample sizes of direct MCS should be greater than 10,000. As the deterministic slope stability analysis explicitly searches a wide range of potential slip surfaces to obtain the minimum FS, direct MCS takes considerable amount of time. This further calls for improvement of computational efficiency via advanced Monte Carlo procedures as presented in the following section.

7.3 Subset Simulation

Subset simulation (Au and Beck 2001, 2003) stems from the idea that a small failure probability can be expressed as a product of larger conditional failure probabilities for some intermediate failure events, thereby converting a rare event

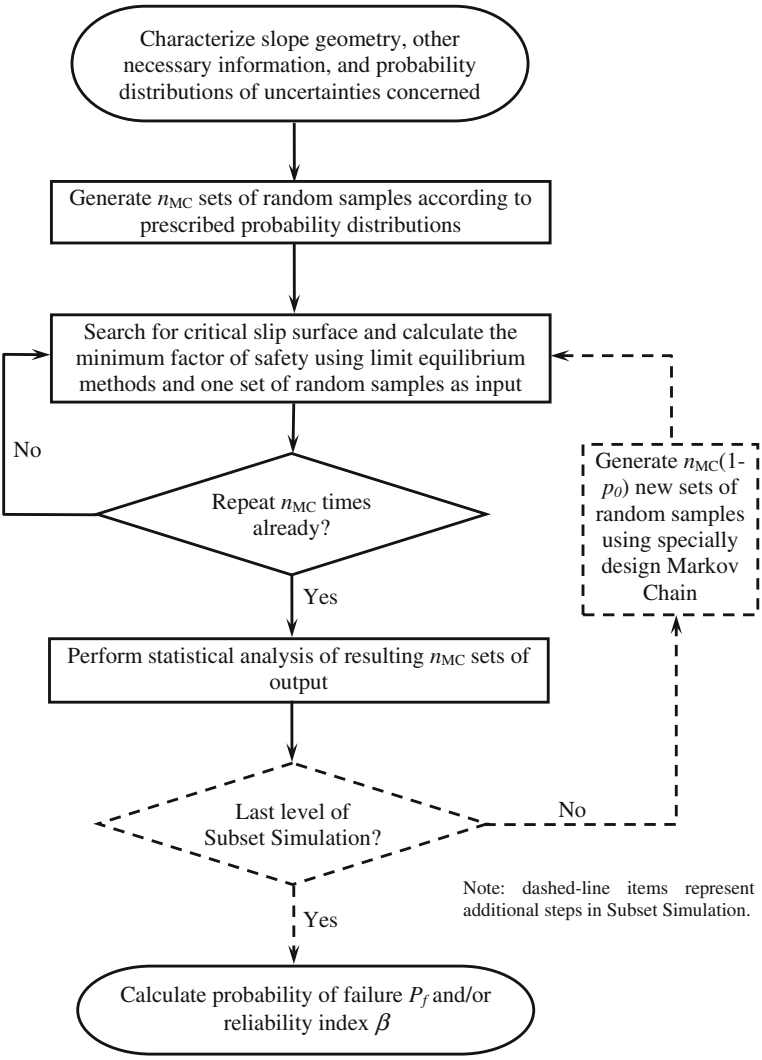

Fig. 7.1 Flowchart for Monte Carlo simulation of slope stability analysis (after Wang et al. 2011)

(small probability levels) simulation problem into a sequence of more frequent ones. Consider the slope stability problem where FS is the critical response and the probability of FS smaller than a given value "fs" (i.e., $P(FS < fs)$) is of interest. Let $fs = fs_m < fs_{m-1} < \cdots fs_2 < fs_1$ be an increasing sequence of m intermediate threshold values. By sequentially conditioning on the event $\{F_i = FS < fs_i, i = 1, 2, \ldots, m\}$, the probability $P(FS < fs)$ can be written as

$$P(FS < fs) = P(FS < fs_1)P(FS < fs_2 | FS < fs_1) \times \cdots \times P(FS < fs_m | FS < fs_{m-1}) \tag{7.1}$$

In implementation, $fs_1, \ldots, fs_m$ are determined adaptively based on the statistical analysis of simulation output (as shown by the dashed-line items in Fig. 7.1) so that the sample estimates of $P(FS < fs_1)$ and $\{P(FS < fs_i | FS < fs_{i-1}),\ i = 2, \ldots, m\}$ always correspond to a common specified value of the conditional probability p_0 ($p_0 = 0.1$ is found to be a good choice) (Au et al. 2009 and 2010).

The efficient generation of conditional samples is pivotal in the success of subset simulation, and it is made possible through the machinery of Markov Chain Monte Carlo simulation (MCMCS). MCMCS uses a modified version of the Metropolis algorithm (Metropolis et al. 1953) that is applicable for high-dimensional problems. Successive samples are generated from a specially designed Markov Chain whose limiting stationary distribution tends to the target probability distribution function (PDF) as the length of the Markov Chain increases. Details of the modified Metropolis algorithm of MCMCS are referred to Au and Beck (2001 and 2003) and Au et al. (2007).

7.4 Implementation of Subset Simulation in a Spreadsheet Environment

The subset simulation described above has been implemented in a commonly available spreadsheet environment by a package of worksheets and functions/Add-In in Excel with the aid of Visual Basic for Application (VBA) (Au et al. 2009; Au et al. 2010; Wang et al. 2011). It is of particular interest to decouple the development of Excel worksheets and VBA functions/Add-In for deterministic slope stability analysis and those for reliability analysis (e.g., random sample generations and statistical analysis) so that the reliability analysis can proceed as an extension of deterministic analysis in a non-intrusive manner. This allows the deterministic analysis of slope stability and reliability analysis to be performed separately by personnel with different expertise and in a parallel fashion. This alleviates the geotechnical practitioners from performing reliability computational algorithms so that they can focus on the slope stability problem itself. The software package developed in this chapter therefore is divided into three parts: deterministic model worksheet for deterministic analysis of slope stability, uncertainty model worksheet for generating random samples, and subset simulation Add-In for uncertainty propagation, which are described in the following three subsections, respectively.

7.4.1 Deterministic Model Worksheet

For a slope stability problem, deterministic model analysis is the process of calculating factor of safety (i.e., *FS*) for a given nominal set of values of system parameters. The system parameters include the geometry information of the slope and the slip surface, soil properties, and profile of soil layers. In this chapter, limit equilibrium methods (e.g., Swedish circle method, simplified Bishop method, and Spencer method) (Duncan and Wright 2005) are employed to calculate the factor of safety for the critical slip surface. The calculation process of deterministic analysis is implemented in a series of worksheets assisted by some VBA functions/Add-In. Figure 7.2 illustrates an example of deterministic model worksheet which is modified after Low (2003) and uses Ordinary Method of Slices. The worksheet is

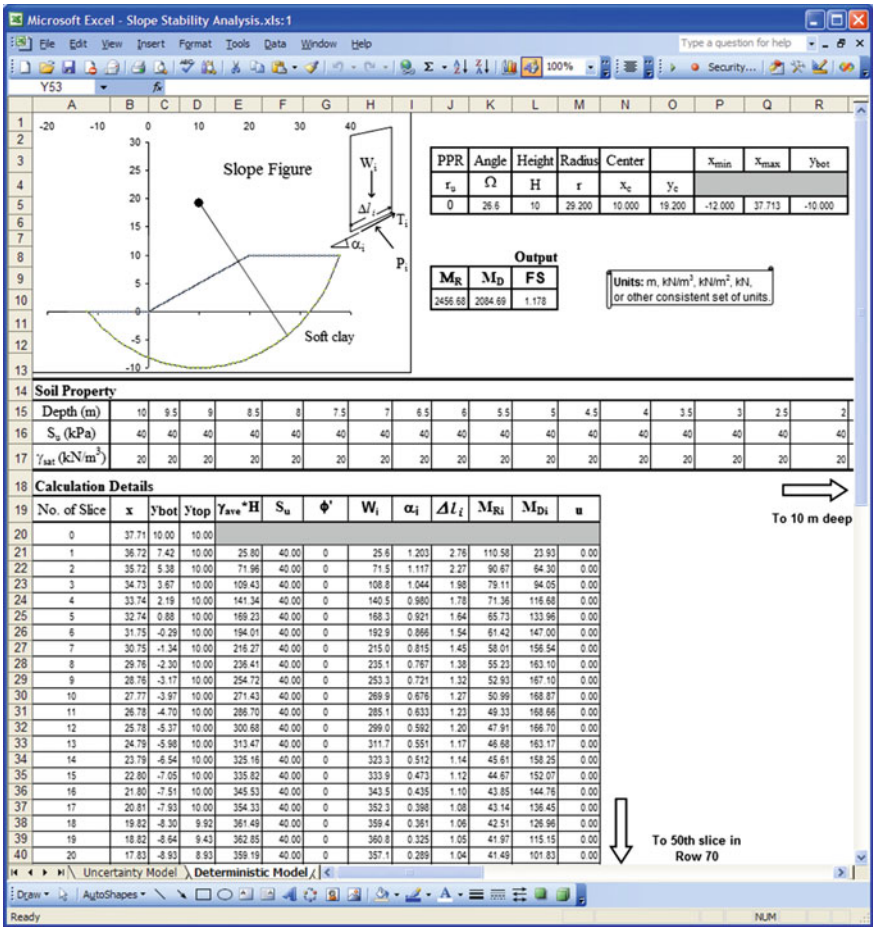

Fig. 7.2 Deterministic model worksheet for slope stability analysis (after Au et al. 2010)

divided into three parts: slope geometry and *FS* calculation (i.e., Rows 1–13), soil property profiles (Rows 14–17), and calculation details for each slice (Rows 18–70). For a given slip surface defined by radius (i.e., Cell M5) and center coordinates (i.e., Cell N5 and Cell O5), a *FS* (i.e., Cell L10) can be calculated accordingly. A wide range of combinations of slip surface radius and center coordinates are then searched explicitly to obtain the minimum *FS* and its corresponding critical slip surface. From an input–output perspective, the deterministic analysis worksheets take a given set of values (e.g., Row 16 in Fig. 7.2) as input, calculate the factor of safety, and return the factor of safety as an output.

7.4.2 Uncertainty Model Worksheet

An uncertainty model worksheet is developed to generate random samples of uncertain system parameters that are treated as random variables in the analysis. The uncertain worksheet includes detailed information of random variables, such as statistics, distribution type, and correlation information. The generation of random samples starts with an Excel built-in function "RAND()" for generating uniform random samples, which are then transformed to random samples of the target distribution type (e.g., normal distribution or lognormal distribution). If the random variables are considered correlated, Cholesky factorization of the correlation matrix is performed to obtain a lower triangular matrix, which is used in the transformation to generate correlated random samples. Figure 7.3 shows an example of uncertainty model worksheet, which consists of three parts: a variable description zone (i.e., Rows 2–5), a random sample generation zone (i.e., Rows 6–13), and a zone showing a lower triangular matrix obtained from Cholesky factorization of the correlation matrix (i.e., Rows 14–54). From the input–output perspective, the uncertainty model worksheet takes no input but returns a set of random samples (e.g., Row 13 in Fig. 7.3) of the uncertain system parameters as its output.

When deterministic model worksheet and uncertainty model worksheet are developed, they are linked together through their input/output cells (e.g., Row 16 in Fig. 7.2 and Row 13 in Fig. 7.3) to execute probabilistic analysis of slope stability. The connection is carried out by simply setting the cell references for nominal values of uncertain parameters in deterministic model worksheet to be the cell references for the random samples in the uncertainty model worksheet in Excel. After this task, the values of uncertain system parameters shown in the deterministic model worksheet are equal to that generated in the uncertainty model worksheet, and so the values of the safety factor calculated in the deterministic model worksheet are random.

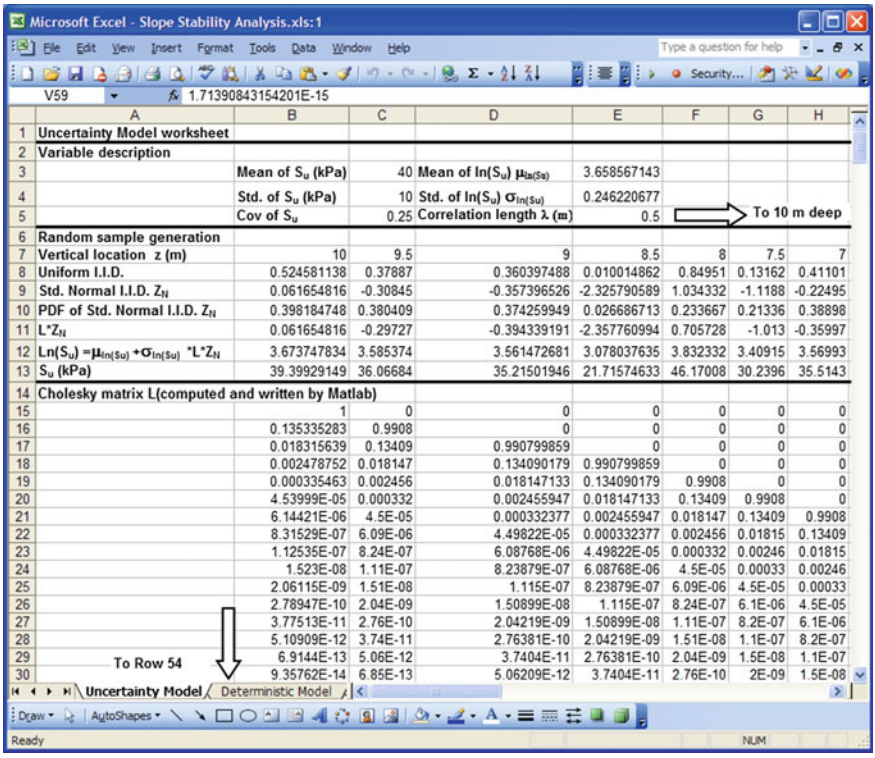

	A	B	C	D	E	F	G	H
1	Uncertainty Model worksheet							
2	Variable description							
3		Mean of S_u (kPa)	40	Mean of ln(S_u) $\mu_{ln(Su)}$	3.658567143			
4		Std. of S_u (kPa)	10	Std. of ln(S_u) $\sigma_{ln(Su)}$	0.246220677			
5		Cov of S_u	0.25	Correlation length λ (m)	0.5			
6	Random sample generation							
7	Vertical location z (m)	10	9.5	9	8.5	8	7.5	7
8	Uniform I.I.D.	0.524581138	0.37887	0.360397488	0.010014862	0.84951	0.13162	0.41101
9	Std. Normal I.I.D. Z_N	0.061654816	-0.30845	-0.357396526	-2.325790589	1.034332	-1.1188	-0.22495
10	PDF of Std. Normal I.I.D. Z_N	0.398184748	0.380409	0.374259949	0.026686713	0.233667	0.21336	0.38898
11	L*Z_N	0.061654816	-0.29727	-0.394339191	-2.357760994	0.705728	-1.013	-0.35997
12	Ln(S_u) =$\mu_{ln(Su)}$ +$\sigma_{ln(Su)}$ *L*Z_N	3.673747834	3.585374	3.561472681	3.078037635	3.832332	3.40915	3.56993
13	S_u (kPa)	39.39929149	36.06684	35.21501946	21.71574633	46.17008	30.2396	35.5143
14	Cholesky matrix L(computed and written by Matlab)							
15		1	0	0	0	0	0	0
16		0.135335283	0.9908	0	0	0	0	0
17		0.018315639	0.13409	0.990799859	0	0	0	0
18		0.002478752	0.018147	0.134090179	0.990799859	0	0	0
19		0.000335463	0.002456	0.018147133	0.134090179	0.9908	0	0
20		4.53999E-05	0.000332	0.002455947	0.018147133	0.13409	0.9908	0
21		6.14421E-06	4.5E-05	0.000332377	0.002455947	0.018147	0.13409	0.9908
22		8.31529E-07	6.09E-06	4.49822E-05	0.000332377	0.002456	0.01815	0.13409
23		1.12535E-07	8.24E-07	6.08768E-06	4.49822E-05	0.000332	0.00246	0.01815
24		1.523E-08	1.11E-07	8.23879E-07	6.08768E-06	4.5E-05	0.00033	0.00246
25		2.06115E-09	1.51E-08	1.115E-07	8.23879E-07	6.09E-06	4.5E-05	0.00033
26		2.78947E-10	2.04E-09	1.50899E-08	1.115E-07	8.24E-07	6.1E-06	4.5E-05
27		3.77513E-11	2.76E-10	2.04219E-09	1.50899E-08	1.11E-07	8.2E-07	6.1E-06
28		5.10909E-12	3.74E-11	2.76381E-10	2.04219E-09	1.51E-08	1.1E-07	8.2E-07
29		6.9144E-13	5.06E-12	3.7404E-11	2.76381E-10	2.04E-09	1.5E-08	1.1E-07
30		9.35762E-14	6.85E-13	5.06209E-12	3.7404E-11	2.76E-10	2E-09	1.5E-08

Fig. 7.3 Uncertainty model worksheet (after Au et al. 2010)

7.4.3 Subset Simulation Add-In

When the deterministic analysis and uncertainty model worksheets are completed and linked together, subset simulation procedure is invoked for uncertainty propagation. In this chapter, subset simulation is implemented as an Add-In in Excel (Au et al. 2009, 2010). The userform of the Add-In is shown in Fig. 7.4. The upper four input fields of the userform (i.e., number of subset simulation runs, number of samples per level N, conditional probability from one level to next p_0, and the highest subset simulation level m) control the number of samples generated by subset simulation. The total number of samples per subset simulation run is equal to $N + mN\ (1 - p_0)$. The lower four input fields of the userform record the cell references of the random variables, their PDF values, and the cell references of the system response (e.g., $Y = 1/FS$) and other variables V (e.g., random samples) of interest, respectively.

After each simulation run, the Add-In provides the complementary cumulative density function (CDF) of the driving variable versus the threshold level, i.e.,

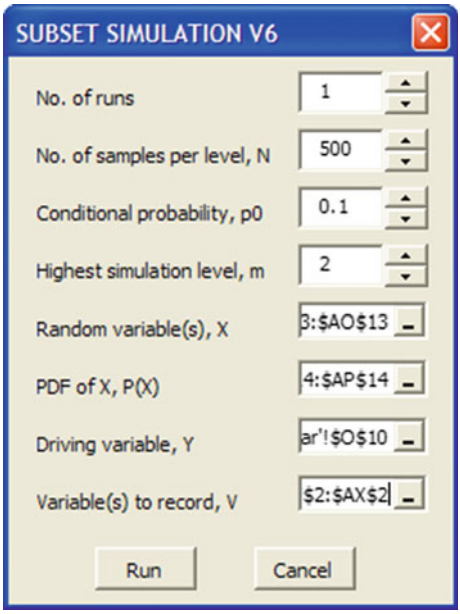

Fig. 7.4 The userform of subset simulation Add-In (after Au et al. 2010; Wang and Cao 2013)

estimate for *P(Y > 1/fs)* versus *1/fs*, into a new spreadsheet and produces a plot of it. Then, the CDF, histograms, or conditional counterparts of uncertain parameters of interest can be calculated using the output information obtained.

7.5 Illustrative Example

The proposed methodology and Excel spreadsheet package developed are applied to assess the reliability of short-term stability of a cohesive soil slope as shown in Fig. 7.5. The cohesive soil slope has a height H = 10 m and slope angle of 26.6º, corresponding to an inclination ratio of 1:2. The cohesive soil is underlain by a firm stratum at 20 m below top of the slope. Short-term shear strength of the cohesive soil is characterized by undrained shear strength S_u, and the saturated unit weight of soil is γ_{sat}. Short-term stability of the slope is assessed using Ordinary Method of Slices under undrained condition (Duncan and Wright 2005). The factor of safety FS is defined as the minimum ratio of resisting moment over the overturning moment, and the slip surface is assumed to be a circular arc centered at coordinate (x_c, y_c) and with radius r. As shown in Fig. 7.5, the soil mass above the slip surface is divided into a number of vertical slices, each of which has a weight W_i, circular slip segment length Δl_i, undrained shear strength S_{ui} along the slip segment, and an angle α_i between the base of the slice and the horizontal. The FS is then given by

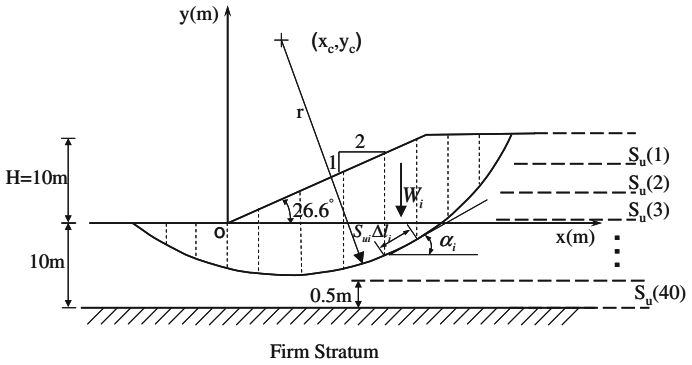

Fig. 7.5 A cohesive soil slope example (after Wang et al. 2011)

$$FS = \min_{x_c, y_c, r} \frac{\sum S_{ui} \Delta l_i}{\sum W_i \sin \alpha_i} \tag{7.2}$$

where the minimum is taken over all possible slip circles, i.e., all possible choices of (x_c, y_c) and r. Note that Δl_i, W_i, and α_i change as (x_c, y_c) and/or r change (i.e., geometry of the ith slice changes). In addition, the W_i is a function of the soil saturated unit weight γ_{sat}. FS therefore depends on geometry of slip surface (i.e., (x_c, y_c) and r) and soil properties (i.e., S_u and γ_{sat}), and S_{ui} and γ_{sat} are key input variables as described in the following subsection.

7.5.1 Input Variables

The undrained shear strength S_u of soil is modeled by a one-dimensional random field spatially varying along the vertical direction. The value of S_u at the same depth is assumed to be fully correlated. The inherent spatial variability with depth is modeled by a homogeneous lognormal random field with an exponentially decaying correlation structure. Let $S_u(D_i)$ be the value of undrained shear strength at depth D_i. The correlation R_{ij} between $\ln[S_u(D_i)]$ and $\ln[S_u(D_j)]$ at respective depths D_i and D_j is given by

$$R_{ij} = \exp(-2|\mathrm{D_i} - \mathrm{D_j}|/\lambda) \tag{7.3}$$

where λ is the effective correlation length. As implied by this correlation function, when $|D_i - D_j| \geq \lambda$, $\ln[S_u(D_i)]$ and $\ln[S_u(D_j)]$ are effectively uncorrelated (Vanmarcke 1977, 1983). When $|D_i - \mathrm{D_j}|$ is much smaller than λ, $\ln[S_u(D_i)]$ and $\ln[S_u(D_j)]$ are highly correlated. In this example, the value of λ varies from 0.5 m to infinity for consideration of different spatial correlations. As shown in Fig. 7.5, the

Table 7.1 The values and distributions of the input variables (after Wang et al. 2011)

Variable	Distribution	Statistics
$\underline{S_u}$	Lognormal (a vector with a length of 40)	Mean = 40 kPa COV[a] = 25 % λ varies from 0.5 m to $+\infty$
γ_{sat}	Deterministic	20 kN/m^3

[a] "COV" stands for coefficient of variation

20-m-thick cohesive soil layer is divided into forty 0.5-m-thick sublayers, and S_u at each sublayer is represented by an entry in a $\underline{S_u}$ vector with a length of 40. Table 7.1 summarizes the material parameters and their variability used in the analysis. The mean and standard deviation of S_u are approximately equal to 40 and 10 kPa (i.e., 25 % coefficient of variation (COV)), respectively. The saturated unit weight of cohesive soil γ_{sat} is taken as deterministic with a value of 20 kN/m^3. As a reference, the nominal value of FS that corresponds to the case where all S_u values equal to their mean values of 40 kPa is equal to 1.178.

7.5.2 Simulation Results

Table 7.2 summarizes the results of both direct MCS and subset simulation for $\lambda = +\infty$ and 0.5 m, respectively. When $\lambda = +\infty$, all 40 entries in the $\underline{S_u}$ vector are fully correlated, and they are equivalent to a single random variable. Both direct MCS and subset simulation provide a consistent P_f value of about 30 %, which compares well with the P_f value given by Griffiths and Fenton (2004) for cohesive slopes with similar geometry and soil properties. When $\lambda = 0.5$ m, all 40 entries in the $\underline{S_u}$ vector can be approximated as 40 independent and identically distributed random variables. Direct MCS and subset simulation provide a consistent P_f value of about 0.9 %, which is significantly smaller than the one for $\lambda = +\infty$. This is

Table 7.2 Summary of simulation results (after Wang et al. 2011)

Effective correlation length λ (m)	Simulation method	Number of samples	Reliability index β[a]	Probability of failure P_f (%)
$+\infty$	Direct MCS	1000	0.52	30
$+\infty$	Subset simulation	200 + 180 + 180 = 560	0.55	29
0.5	Direct MCS	2000	2.35	0.95
0.5	Subset simulation	500 + 450 + 450 = 1400	2.36	0.92

[a]Equivalent reliability index $\beta = \Phi^{-1}(1 - P_f)$ where Φ = standard normal cumulative distribution function

consistent with the observation by Hong and Roh (2008) that P_f decreases if spatial correlation is ignored (i.e., as λ decreases). The effect of inherent spatial variability is discussed further in a later section of this chapter.

As the value of P_f decreases to a relatively small level (e.g., around 0.9 % for λ = 0.5 m), the number of samples required in direct MCS increases significantly and efficiency of direct MCS decreases dramatically. Figure 7.6 shows a histogram of the *FS* from 2000 direct MCS samples, among which 19 samples have a $FS < 1$. The efficiency of simulating failure events (i.e., $FS < 1$) is relatively low. The resolution of P_f is 1/2000 = 0.05 %, and this resolution might not be sufficient for a P_f value of 0.95 %.

In contrast, Fig. 7.7 shows histograms of the *FS* from three levels of subset simulation with a p_0 value of 0.1. The first level of subset simulation is equivalent to a direct MCS with a sample number of 500, and only 2 samples have a $FS < 1$, as shown in Fig. 7.7a. All 500 *FS* values are then sorted in a decreasing order, and 50 samples (i.e., 10 % (or $p_0 = 0.1$) of 500 samples) with the lowest *FS* are used to generate 450 samples in the second level of subset simulation, as illustrated by the dashed-line items in Fig. 7.1. As shown in Fig. 7.7b, the samples at the second level fall into the region of $FS < 1.06$ and have relatively small *FS* values. Forty-four samples out of 450 samples have a $FS < 1$, and the efficiency of simulating failure events improves significantly when compared with direct MCS. As shown in Fig. 7.7c, the samples at the third level move further to the lower *FS* region, and 413 samples out of 450 samples have a $FS < 1$. The P_f is calculated as $0.1 \times 0.1 \times 413/450 = 0.92$ %, and the resolution of P_f is $0.1 \times 0.1 \times 1/450 = 0.002$ %. Subset simulation significantly improves efficiency and resolution of simulations at small probability levels. Such improvement becomes increasingly substantial and necessary as the probability level of interest decreases (e.g., P_f further decreases to 0.1 % or 0.003 % for expected performance levels of "above

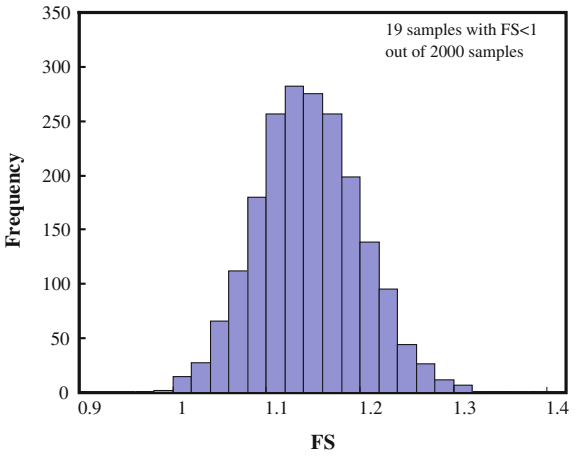

Fig. 7.6 *FS* histogram from direct Monte Carlo simulation (after Wang et al. 2011)

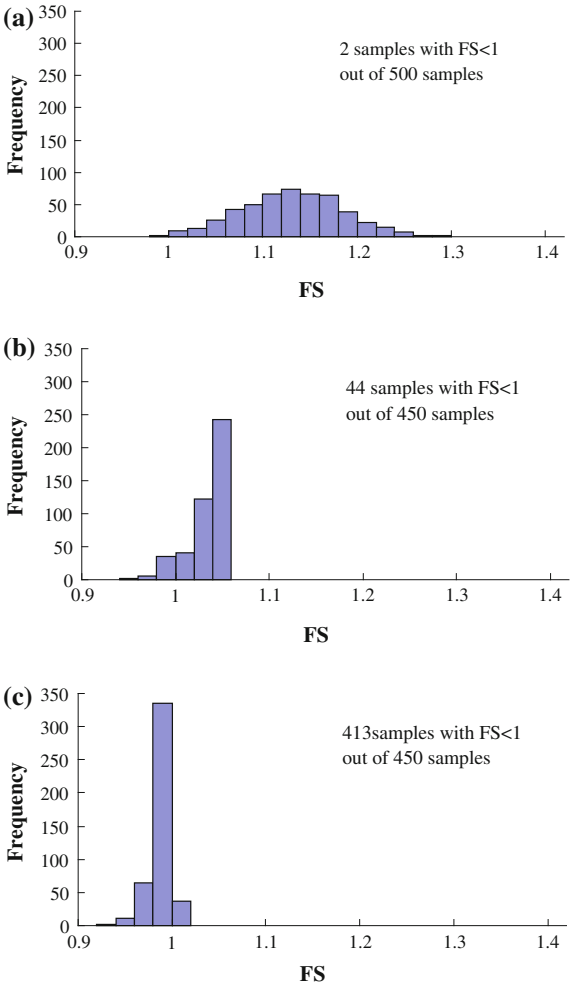

Fig. 7.7 *FS* histogram from subset simulation (after Wang et al. 2011). **a** First level. **b** Second level. **c** Third level

average" or "good" (see Table 2.7 in Chap. 2), respectively, as direct MCS is increasingly inefficient).

7.5.3 Comparison with Other Reliability Analysis Methods

The analysis results are compared with those from other reliability analysis methods, including the first-order second-moment method (FOSM), first-order reliability method (FORM), and direct MCS using commercial software Slope/W (GEO-SLOPE International Ltd. 2008). Table 7.3 summarizes analysis results from different reliability methods with $\lambda = +\infty$. The value of P_f varies from about 27 to 30 % with a maximum relative difference of 10 % among difference methods.

Table 7.3 Summary of analysis results from different reliability methods ($\lambda = +\infty$) (after Wang et al. 2011)

Reliability method	Reliability index β	Probability of failure P_f (%)	Relative difference in P_f (%)
FOSM	0.61	27	−10
FORM	0.55	29	−3
Direct MCS with Slope/W	0.55	29	−3
Direct MCS with Excel	0.52	30	N/A
Subset simulation with Excel	0.55	29	−3

Table 7.4 Summary of analysis results from different reliability methods ($\lambda = 0.5$ m) (after Wang et al. 2011)

Reliability method	Reliability index β	Probability of failure P_f (%)	Relative difference in P_f (%)
FOSM	2.53	0.57	−40
FORM	2.61	0.45	−53
Direct MCS with Slope/W	2.80	0.26	−73
Direct MCS with Excel	2.35	0.95	N/A
Subset simulation with Excel	2.36	0.92	−3

The results from direct MCS or subset simulations compare favorably with those from FOSM, FORM, or direct MCS using Slope/W. Table 7.4 summarizes similar results for $\lambda = 0.5$ m. The value of P_f varies from 0.26 to 0.95 %, which is significantly smaller than those for $\lambda = +\infty$. The maximum relative difference among different methods for $\lambda = 0.5$ m is about 73 %, which is significantly larger than that for $\lambda = +\infty$. These differences can be attributed to calculation details of each reliability analysis method, inherent spatial variability of soil property, and critical slip surface uncertainty, which are discussed in the following several sections.

7.6 Calculation Details of Other Reliability Analysis Methods

7.6.1 First-Order Second-Moment Method (FOSM)

FOSM uses the first-order terms of a Taylor series expansion of *FS* with respect to the random variables, and it is frequently performed with a fixed critical slip surface (e.g., Ang and Tang 1984; Tang et al. 1976; Wu 2008). Consistent with the previous studies, the critical slip surface here is determined by setting all $\underline{S_u}$ values

equal to their mean values of 40 kPa and searching for the minimum FS. The resulting critical slip surface has an r = 29.2 m and (x_c, y_c) = (10.0 m, 19.2 m), and the corresponding FS is 1.178. The mean and standard deviation of FS are then estimated for both cases of λ =+∞ and λ = 0.5 m. Note that, when λ =+∞, all 40 entries in the $\underline{S_u}$ vector are fully correlated, and all S_{ui} behave as a single random variable S_u. Equation (7.2) then can be rewritten as

$$FS = \min_{x_c,y_c,r} \frac{\sum S_{ui}\Delta l_i}{\sum W_i \sin\alpha_i} = \min_{x_c,y_c,r} \frac{S_u \sum \Delta l_i}{\sum W_i \sin\alpha_i} = S_u \min_{x_c,y_c,r} \frac{\sum \Delta l_i}{\sum W_i \sin\alpha_i} \tag{7.4}$$

As the geometry and soil unit weight are considered deterministic, $\min_{x_c,y_c,r} \frac{\sum \Delta l_i}{\sum W_i \sin\alpha_i}$ is deterministic. Equation (7.4) implies that when λ = +∞ (i.e., inherent spatial variability is ignored or perfect correlation), location of critical slip surface (i.e., x_c, y_c, and r) is independent of the value of S_u, although the value of minimum FS does vary as the S_u value changes. In this case, it is theoretically appropriate that FOSM method only uses a given slip surface in the analysis. In contrast, when λ = 0.5 m (i.e., inherent spatial variability is considered), all 40 S_{ui} are random variables. Critical slip surface (i.e., x_c, y_c, and r) varies spatially and is uncertain, depending on the value of S_{ui}. Using only one given critical slip surface in FOSM method therefore underestimates the uncertainty of failure. This results in significant increase of relative difference in P_f between FOSM method and direct MCS with Excel from Table 7.3 (i.e., −10 % for λ = +∞) to Table 7.4 (i.e., −40 % for λ = 0.5 m). The effect of critical slip surface uncertainty is discussed further under the Sect. 7.8 "Effect of Critical Slip Surface Uncertainty".

7.6.2 *First-Order Reliability Method (FORM)*

The reliability index β for FORM in Tables 7.3 and 7.4 is calculated using an Excel spreadsheet with its built-in optimization tool "Solver" to obtain the minimum distance of interest as β (Low and Tang 2007; Low 2003). Although this FORM approach is mathematically sound, its successful application relies on a robust optimization algorithm for multidimensional minimization. Similar to other optimization algorithm, the generalized reduced gradient algorithm used in the Excel "Solver" might not result in a global minimum but a local minimum, particularly when the function of interest is complex and dimension of the space is high. One frequently used heuristic for checking if the global minimum is obtained is simply repeating the optimization with widely varying starting points. The β values for FORM in Tables 7.3 and 7.4 are obtained with a starting point that corresponds to the critical slip surface obtained from a deterministic slope stability analysis with all soil properties equal to their respective mean values (Low 2003). When the optimization is repeated with a slightly different starting point (e.g., different slip surface parameters or soil properties), the Excel "Solver" gives significantly

different β value, or even fails to converge. The value of β given by the Excel "Solver" should, therefore, be treated with caution, and it may correspond to a local minimum that is larger than the global minimum (i.e., the true β value). In other words, the FORM overestimates the β value or underestimates the P_f value, which is unconservative and undesirable. This observation is consistent with the results summarized in Tables 7.3 and 7.4. The β values for both cases of $\lambda = +\infty$ and $\lambda = 0.5$ m are larger than those from direct MCS with Excel. Note that FORM's overestimation of β is not unique for slope stability problem. Similar observations are also reported by Ching et al. (2009) for consolidation problem.

7.6.3 *Monte Carlo Simulations Using Commercial Software Slope/W*

The commercial software Slope/W (GEO-SLOPE International Ltd. 2008) is first used to perform a deterministic slope stability analysis with all $\underline{S_u}$ values equal to their mean values of 40 kPa. The resulting minimum *FS* (i.e., 1.178) and critical slip surface (i.e., $r = 29.0$ m and $(x_c, y_c) = (9.9$ m, 19.0 m)) are virtually identical to those obtained from the Excel spreadsheet. Monte Carlo simulations are then performed using Slope/W for both cases of $\lambda = +\infty$ and $\lambda = 0.5$ m. When $\lambda = +\infty$, the relative difference in P_f between direct MCS from Slope/W and Excel is within 3 % (see Table 7.3). When λ decreases to 0.5 m, the relative difference in P_f increases to 73 % (see Table 7.4). The relatively large difference can be attributed to the way that Slope/W handles the critical slip surface in direct MCS. Slope/W uses only one given critical slip surface in direct MCS, and the given slip surface is determined based on a deterministic slope stability analysis with all random variables equal to their respective mean values. Figure 7.8 shows the critical slip surface obtained in Slope/W using the mean values of $\underline{S_u}$. As discussed under the Sect. 7.6.1 "first-order second-moment method (FOSM)," when $\lambda = +\infty$ (i.e., inherent spatial variability is ignored), it is theoretically appropriate to use only one given critical slip surface. The direct MCS in Slope/W therefore gives reasonable result, and the relative difference in P_f between direct MCS from Slope/W and Excel is small. When $\lambda = 0.5$ m (i.e., inherent spatial variability is considered), the critical slip surface itself varies spatially. Using only one given critical slip surface in direct MCS with Slope/W therefore underestimates the P_f, and the relative difference in P_f between direct MCS from Slope/W and Excel increases significantly (see Table 7.4). The effects of inherent spatial variability of soil property and critical slip surface uncertainty are discussed in two following sections, respectively.

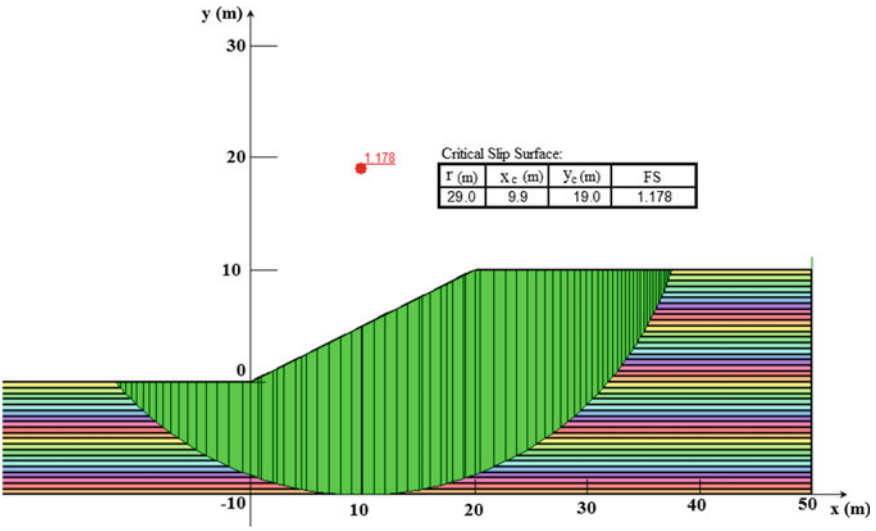

Fig. 7.8 Critical slip surface in Slope/W (after Wang et al. 2011)

7.7 Effect of Inherent Spatial Variability of Soil Property

A series of direct MCS and subset simulations with different λ values are performed using the Excel spreadsheet package developed in this chapter. Figure 7.9 summarizes the results in a plot of P_f versus normalized correlation length (λ/H). As λ/H increases from 0.05 to 1 (or λ increases from 0.5 to 10 m for H = 10 m), the value of P_f increases significantly from about 0.9 to 26 %. When $\lambda/H > 1$ or λ is larger than the slope height H, the effect of λ on P_f begins to diminish, and P_f varies slightly as λ/H further increases. If the soil properties (e.g., S_u) are characterized by a single random variable or the inherent spatial variability is ignored, the value of P_f is overestimated significantly, particularly when the effective correlation length is smaller than the slope height.

Note that FS is defined as the minimum ratio of summation of resisting moments over the summation of overturning moments (see Eq. (7.2)) and slope failure occurs when $FS < 1$. Let M_R be a summation of n_R resisting moments $\Delta l_i S_{ui}$ (i.e., $M_R = \sum_{i=1}^{n_R} \Delta l_i S_{ui}$) and variance of M_R then can be expressed as

$$Var(M_R) = \sum_{i=1}^{n_R} \Delta l_i^2 \sigma_{S_{ui}}^2 + \sum_{i,j=1}^{n_R} \sum_{i \neq j}^{n_R} \rho_{ij} \Delta l_i \Delta l_j \sigma_{S_{ui}} \sigma_{S_{uj}} \tag{7.5}$$

where $\sigma_{S_{ui}}^2$ is variance of S_{ui} and ρ_{ij} is correlation coefficient between S_{ui} and S_{uj}. The effect of inherent spatial variability is reflected by the variation of ρ_{ij} (i.e., between 0 and 1) and the second term at the right-hand side of Eq. (7.5), i.e., $\sum_{i,j=1}^{n_R} \sum_{i \neq j}^{n_R} \rho_{ij} \Delta l_i \Delta l_j \sigma_{S_{ui}} \sigma_{S_{uj}}$. When S_{ui} and S_{uj} are uncorrelated, $\rho_{ij} = 0$ and

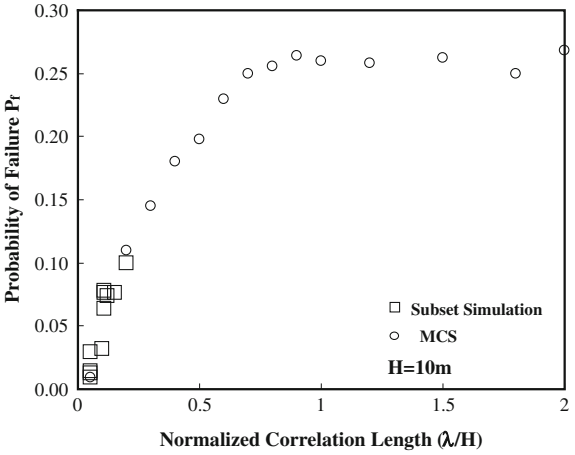

Fig. 7.9 Effect of spatial variability of soil property (after Wang et al. 2011)

$Var(M_R)$ is equal to $\sum_{i=1}^{n_R} \Delta l_i^2 \sigma_{S_{ui}}^2$. When the inherent spatial variability is ignored by assuming perfect correlation, $\rho_{ij} = 1$ and $Var(M_R)$ is equal to $\sum_{i=1}^{n_R} \Delta l_i^2 \sigma_{S_{ui}}^2 + \sum_{i,j=1}^{n_R} \sum_{i \neq j}^{n_R} \Delta l_i \Delta l_j \sigma_{S_{ui}} \sigma_{S_{uj}}$. This leads to overestimation of $Var(M_R)$ and, hence, overestimation of the FS variance.

It is important to note that overestimation of the FS variance may result in either overestimation (conservative) or underestimation (unconservative) of P_f (i.e., probability of $FS < 1$). If $FS = 1$ occurs at the lower tail of the FS probability distribution, overestimation of the FS variance leads to overestimation of P_f, and it is therefore conservative. Figure 7.9 illustrates such case, and similar results have also been reported by Sivakumar Babu and Mukesh (2004) and Hong and Roh (2008). If the location of $FS = 1$ approaches the center, or even the upper tail, of the FS probability distribution (i.e., FS is relatively low), overestimation of the FS variance leads to underestimation of P_f, and it is therefore unconservative. Griffiths and Fenton (2004) reported that when FS is relatively low and the inherent spatial variability is ignored by assuming perfect correlation, the value of P_f is underestimated and unconservative. Depending on the location of $FS = 1$ in the FS probability distribution, the overestimation of FS variance may result in contradicting results, as reported in the literature.

7.8 Effect of Critical Slip Surface Uncertainty

The discussions above show that different reliability methods deal with the critical slip surface differently. FOSM and direct MCS with Slope/W use a given slip surface and do not account for critical slip surface uncertainty. The FORM proposed by Low (2003) includes center coordinates and radius of slip surface as

additional optimization variables, and variation of potential critical slip surfaces is implicitly factored in the analysis. However, because of limitation of the optimization tool used, it tends to overestimate β and underestimate P_f.

The direct MCS and subset simulation with Excel package developed in this chapter explicitly search a wide range of potential slip surfaces for obtaining the minimum FS in each random sample of $\underline{S_u}$. Figure 7.10 shows examples of different critical slip surfaces obtained from different random samples of $\underline{S_u}$ when $\lambda = 0.5$ m. It is obvious that the critical slip surface varies spatially as the spatial distribution of $\underline{S_u}$ changes among different random samples. As a reference, the critical slip surface highlighted by a thick line in Fig. 7.10 is the one used in the FOSM method and direct MCS with Slope/W. Table 7.5 summarizes ranges of (x_c, y_c) and r for critical slip surfaces obtained from direct MCS with Excel. The r varies from 21.0 to 29.8 m and has a range of 8.8 m. When inherent spatial variability of soil property and critical slip surface uncertainty are considered explicitly in the simulation, the value of P_f from direct MCS and subset simulation with Excel is about 40–70 % larger than that from FOSM and direct MCS with Slope/W which use only one given critical slip surface.

To further illustrate the effect of critical slip surface uncertainty on P_f, direct MCS and subset simulation are also performed in Excel with the fixed critical slip surface highlighted by thick line in Fig. 7.10, which is the same one used in the direct MCS with Slope/W. As shown in Table 7.6, the resulting P_f value decreases to 0.1–0.2 % and compares well with that from Slope/W which uses the same critical slip surface. The comparison summarized in Table 7.6 confirms that when

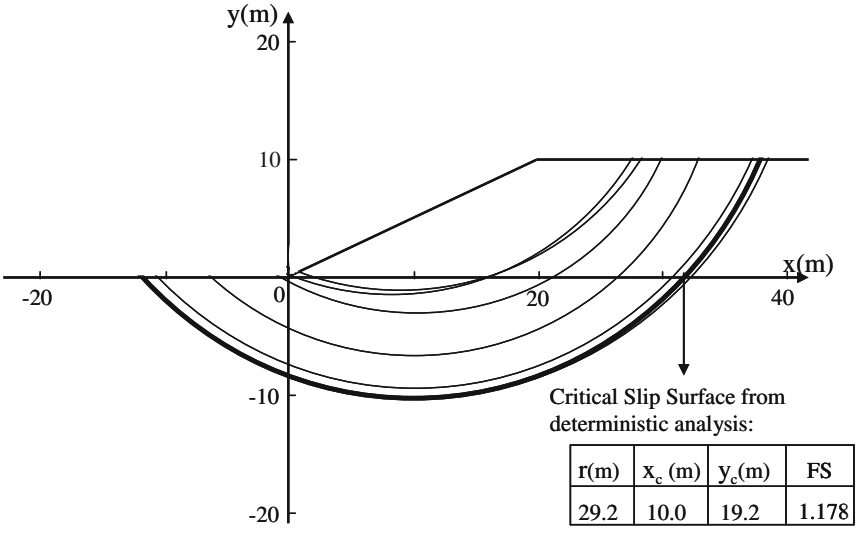

r(m)	x_c (m)	y_c(m)	FS
29.2	10.0	19.2	1.178

Fig. 7.10 Examples of critical slip surfaces obtained from direct MSC with Excel (after Wang et al. 2011)

Table 7.5 Ranges of center coordinates and radius of critical slip surfaces obtained from MCS with Excel (after Wang et al. 2011)

Parameter	Minimum	Maximum	Range
Coordinate x_c (m)	8.0	10.4	2.4
Coordinate y_c (m)	17.6	22.0	4.4
Radius r (m)	21.0	29.8	8.8

Table 7.6 Comparison of simulation results with different critical slip surfaces (after Wang et al. 2011)

Reliability method	Reliability index β	Probability of failure P_f (%)	Relative difference in P_f (%)
MCS with Slope/W and fixed critical slip surface	2.80	0.26	−73
MCS with Excel and fixed critical slip surface	2.95	0.16	−83
Subset simulation with Excel and fixed critical slip surface	3.00	0.13	−86
MCS with Excel and changing critical slip surface	2.35	0.95	N/A
Subset simulation with Excel and changing critical slip surface	2.36	0.92	−3

inherent spatial variability of soil property is considered, the substantial difference among P_f from different reliability methods is mainly attributed to the effect of critical slip surface uncertainty, and using only one given critical slip surface results in underestimation (or unconservative) of P_f. Thus, when inherent spatial variability of soil property is considered, the critical slip surface uncertainty should be properly accounted for.

7.9 Summary and Conclusions

This chapter developed a Monte Carlo simulation (MCS)-based practical reliability analysis approach for slope stability problem and implemented an advanced MCS method called subset simulation in a commonly available spreadsheet environment, Microsoft Excel. The Excel spreadsheet package developed was used to assess reliability of short-term stability of a cohesive soil slope, followed by a comparative study on different reliability methods, including the FOSM, FORM, direct MCS using commercial software Slope/W, and direct MCS and subset simulation using the Excel package. Subset simulation was shown to significantly improve efficiency and resolution of simulations at small probability levels. Such improvement

becomes increasingly substantial and necessary as the probability level of interest decreases (e.g., the failure probability further decreases to 0.1 % or 0.003 % for expected performance levels of "above average" or "good," respectively, as direct MCS is increasingly inefficient).

Effect of inherent spatial variability of soil property was explored using the Excel spreadsheet package developed in this chapter. It is found that when inherent spatial variability of soil property is ignored by assuming perfect correlation, the variance of FS is overestimated. However, the overestimation of the FS variance may result in either overestimation (conservative) or underestimation (unconservative) of P_f. If $FS = 1$ occurs at the lower tail of the FS probability distribution, overestimation of the FS variance leads to overestimation of P_f, and it is therefore conservative. If the location of $FS = 1$ approaches the center, or even the upper tail, of the FS probability distribution (i.e., FS is relatively low), overestimation of the FS variance leads to underestimation of P_f, and it is therefore unconservative.

The effect of critical slip surface uncertainty was also examined. When the inherent spatial variability of soil property is ignored or soil property is characterized by a single random variable, the location of critical slip surface is deterministic. It is therefore theoretically appropriate to use only one given slip surface in the analysis, as what FOSM method or direct MCS with Slope/W does. When the inherent spatial variability of soil property is considered, the critical slip surface varies spatially. Using only one given critical slip surface significantly underestimates P_f, and it is unconservative. Thus, when the inherent spatial variability of soil property is considered, the critical slip surface uncertainty should be properly accounted for.

It is worthwhile to note that although the proposed practical reliability analysis approach was illustrated through a cohesive soil slope example with Ordinary Method of Slices, the approach is general and can be readily adapted to frictional slopes and more sophisticated limit equilibrium methods (e.g., Spencer, Morgenstern, and Price methods). Usage of these more sophisticated methods may be more appropriate for general slopes, although their FS equations and associated discussions may not be as explicit as those (e.g., Eq. (7.4) and its relevant discussions) shown in the chapter.

References

Ang, A.H.S., and W.H. Tang. 1984. *Probability concepts in engineering planning and design*, vol. II. New York: Wiley.

Au, S.K., and J.L. Beck. 2001. Estimation of small failure probabilities in high dimensions by subset simulation. *Probabilistic Engineering Mechanics* 16(4): 263–277.

Au, S.K., and J.L. Beck. 2003. Subset simulation and its applications to seismic risk based on dynamic analysis. *Journal of Engineering Mechanics* 129(8): 1–17.

Au, S.K., Z. Cao, and Y. Wang. 2010. Implementing advanced Monte Carlo simulation under spreadsheet environment. *Structural Safety* 32(5): 281–292.

Au, S.K., J. Ching, and J.L. Beck. 2007. Application of subset simulation methods to reliability benchmark problems. *Structural Safety* 29(3): 183–193.

Au, S.K., Y. Wang, and Z. Cao. 2009. Reliability analysis of slope stability by advanced simulation with spreadsheet. In *Proceedings of the Second International Symposium on Geotechnical Safety and Risk*. Gifu, Japan, June 2009, 275–280.

Ching, J.Y., K.K. Phoon, and Y.H. Hsieh. 2009. Reliability analysis of a benchmark problem for 1-D consolidation. In *Proceeding of the 2nd International Symposium on Geo-technical Safety and Risk (IS-Gifu2009)*, June 2009, Gifu, Japan, 69–74.

Duncan, J.M. and S.G. Wright. 2005. *Soil strength and slope stability*. New Jersey: Wiley.

El-Ramly, H., N.R. Morgenstern, and D.M. Cruden. 2002. Probabilistic slope stability analysis for practice. *Canadian Geotechnical Journal* 39: 665–683.

El-Ramly, H., N.R. Morgenstern, and D.M. Cruden. 2005. Probabilistic assessment of stability of a cut slope in residual soil. *Geotechnique* 55(1): 77–84.

GEO-SLOPE International Ltd. 2008. *Stability modeling with slope/W 2007 version*. Calgary, Alberta, Canada: GEO-SLOPE International Ltd.

Griffiths, D.V., and G.A. Fenton. 2004. Probabilistic slope stability analysis by finite elements. *Journal of Geotechnical and Geoenvironmental Engineering* 130(5): 507–518.

Hassan, A.M., and T.F. Wolff. 1999. Search algorithm for minimum reliability index of earth slopes. *Journal of Geotechnical and Geoenvironmental Engineering* 125(4): 301–308.

Hong, H.P., and G. Roh. 2008. Reliability evaluation of earth slopes. *Journal of Geotechnical and Geoenvironmental Engineering* 134(12): 1700–1705.

Low, B.K. 2003. Practical probabilistic slope stability analysis. In *Proceeding of 12th Panamerican Conference on Soil Mechanics and Geotechnical Engineering and 39th U.S. Rock Mechanics Symposium*, 2777–2784. Cambridge, Massachusetts: MIT Press, Verlag Gluckauf Gmbh Essen.

Low, B.K., and W.H. Tang. 2007. Efficient spreadsheet algorithm for first-order reliability method. *Journal of Engineering Mechanics* 133(2): 1378–1387.

Metropolis, N., A. Rosenbluth, M. Rosenbluth, and A. Teller. 1953. Equations of state calculations by fast computing machines. *Journal of Chemical Physics* 21(6): 1087–1092.

Robert, C. and G. Casella. 2004. *Monte Carlo Statistical Methods*. Springer.

Sivakumar Babu, G.L., and M.D. Mukesh. 2004. Effect of soil variability on reliability of soil slopes. *Geotechnique* 54(5): 335–337.

Tang, W.H., M.S. Yucemen, and A.H.S. Ang. 1976. Probability based short-term design of slope. *Canadian Geotechnical Journal* 13: 201–215.

Vanmarcke, E.H. 1977. Probabilistic modeling of soil profiles. *Journal of Geotechnical Engineering* 103(11): 1127–1246.

Vanmarcke, E.H. 1983. *Random fields: analysis and synthesis*. Cambridge: MIT Press.

Wang, Y., and Z. Cao. 2013. Probabilistic characterization of Young's modulus of soil using equivalent samples. *Engineering Geology* 159(12): 106–118.

Wang, Y., Z. Cao, and S.K. Au. 2011. Practical analysis of slope stability by advanced Monte Carlo Simulation in spreadsheet. *Canadian Geotechnical Journal* 48(1): 162–172.

Wu, T.H. 2008. Reliability analysis of slopes. In *Reliability-based design in geotechnical engineering: computations and applications*, Chapter 11, ed. Phoon, 413–447. Taylor and Francis.

Xu, B., and B.K. Low. 2006. Probabilistic stability analyses of embankments based on finite-element method. *Journal of Geotechnical and Geoenvironmental Engineering* 132(11): 1444–1454.

Chapter 8
Efficient Monte Carlo Simulation of Parameter Sensitivity in Probabilistic Slope Stability Analysis

8.1 Introduction

In the previous chapter, Monte Carlo simulation (MCS) method has been applied to probabilistic slope stability analysis and an advanced MCS method (i.e., subset simulation) is used to improve the resolution and efficiency at small probability levels. MCS method provides a robust and conceptually simple way to account rationally for various uncertainties (e.g., inherent spatial variability of soil properties and uncertainties in subsurface stratigraphy) in slope engineering when calculating slope failure probability. However, as pointed out by Baecher and Christian (2003), MCS does not offer insight into the relative contributions of various uncertainties to the failure probability.

This chapter develops a probabilistic failure analysis approach that makes use of failure samples generated in the MCS and analyzes these failure samples to assess the effects of various uncertainties on slope failure probability. Subset simulation (Au and Beck 2001 and 2003) is, again, employed to improve efficiency of generating failure samples in MCS and resolution of calculating failure probability at small failure probability levels. This chapter starts with mathematical formulation of the approach, including hypothesis tests for prioritizing the effects of various uncertainties and Bayesian analysis for further quantifying their effects. The software package of probabilistic slope stability analysis developed in the previous chapter is applied to generate failure samples for the probabilistic failure analysis. As an illustration, the proposed approach is applied to study a design scenario of the James Bay Dyke (Christian et al. 1994; El-Ramly 2001; Xu and Low 2006).

Z. Cao et al., *Probabilistic Approaches for Geotechnical Site Characterization and Slope Stability Analysis*, DOI 10.1007/978-3-662-52914-0_8

8.2 Probabilistic Failure Analysis Approach

Probabilistic failure analysis is similar to back analysis (Luckman et al. 1987; Gilbert et al. 1998; Zhang et al. 2010), which is a common analysis procedure in geotechnical engineering. The back analysis intends to find a set of model parameters that would result in the observed performance of geostructures. Similarly, probabilistic failure analysis aims to identify a group of uncertain parameters that would significantly affect the slope performance (i.e., the probability of slope failure). The back analysis, however, relies on the observed performance and it is inapplicable when observed performance of the geostructures of interest is unavailable (e.g., during design analysis of a new geostructure). On the other hand, probabilistic failure analysis makes use of failure samples generated in the MCS, and it is readily applicable in design analysis for evaluating the effects of various uncertainties. The proposed probabilistic failure analysis approach contains two major components: hypothesis tests for prioritizing the effects of various uncertainties and Bayesian analysis for further quantifying their effects, which are described in the following two subsections, respectively.

8.2.1 Hypothesis Tests

The effects of various uncertainties on the probability of slope failure are prioritized by comparing, statistically, failure samples with their respective nominal (unconditional) samples. When the uncertainty of an uncertain system parameter has a significant effect on the probability of slope failure, the mean μ of failure samples of the parameter differs significantly from the mean μ_0 of its unconditional samples. The statistical difference between μ and μ_0 is evaluated by hypothesis tests. A null hypothesis H_0 and alternative hypothesis H_A are defined as (Walpole et al. 1998; Wang et al. 2010)

$$\begin{aligned} H_0 &: \mu = \mu_0 \\ H_A &: \mu \neq \mu_0 \end{aligned} \tag{8.1}$$

Then, a hypothesis test statistic Z_H of the parameter is formulated as

$$Z_H = \frac{\mu - \mu_0}{\sigma/\sqrt{n_f}} \tag{8.2}$$

where σ is standard deviation of the uncertain parameter; and n_f is the number of failure samples. Based on central limit theorem, Z_H follows the standard normal distribution when n_f is large (e.g., $n_f \geq 30$) (Walpole et al. 1998). When the failure sample mean μ deviates statistically from the unconditional mean μ_0 of the parameter, the absolute value of Z_H is relatively large. As the absolute value of Z_H

increases, the statistical difference between μ and μ_0 becomes growingly significant, and the effect of the uncertain parameter on failure probability also becomes growingly significant. The absolute value of Z_H is therefore formulated in this chapter as an index to measure the effects of the uncertain parameters on failure probability and to prioritize their relative effects on failure probability. Using the absolute value of Z_H, the uncertain parameters that have significant effects on failure probability are selected, and their effects are further quantified using a Bayesian analysis approach described in the next subsection.

8.2.2 Bayesian Analysis

The failure samples generated in the MCS are further analyzed by a Bayesian analysis to quantify the effects of various uncertainties. Let θ denote an uncertain parameter selected based on hypothesis tests. In the context of the Bayes' theorem (e.g., Au 2005; Ang and Tang 2007),

$$P(F|\theta) = P(\theta|F)P_f/P(\theta) \tag{8.3}$$

where $P(F|\theta)$ is the conditional probability density function (PDF) of slope failure for a given θ value; $P(\theta|F)$ is the conditional PDF of θ given that the slope has failed; P_f is the failure probability of slope stability; and $P(\theta)$ is the unconditional PDF of θ. As both $P(\theta|F)$ and P_f are estimated from failure samples of MCS and $P(\theta)$ is given before MCS, Eq. (8.3) can be used to estimate $P(F|\theta)$ using $P(\theta)$ and $P(\theta|F)$ obtained from analysis of failure samples. Note that $P(F|\theta)$ is a variation of failure probability as a function of θ, and it can be considered as results of a sensitivity study of θ on slope failure probability. In other words, the probabilistic failure analysis approach presented in this chapter, which makes use of failure samples generated in a single run of MCS for assessment of failure probability, provides results that are equivalent to those from a sensitivity study, which frequently includes many repeated runs of MCS with different given values of θ in each run. Additional computational time and efforts for repeated runs of MCS in the sensitivity study can be avoided using the probabilistic failure analysis approach described herein.

In addition, Eq. (8.3) implies that comparison between the conditional probability $P(\theta|F)$ and its unconditional one $P(\theta)$ provides an indication of the effect of the uncertain parameter θ on failure probability. In general, $P(F|\theta)$ changes as the values of the uncertain parameter θ changes. However, when $P(\theta|F)$ is similar to $P(\theta)$, $P(F|\theta)$ remains more or less constant regardless of the values of θ. This implies that the effect of θ on the slope failure probability is minimal. Such implication can be used to validate the prioritization obtained from hypothesis tests, as shown in the example of the James Bay Dyke later.

The resolution of P_f and $P(\theta|F)$ is pivotal to obtain $P(F|\theta)$, and it depends on the number of failure samples generated in MCS. As the number of failure samples

increases, the resolution improves. For a given slope stability problem, the value of P_f is constant, although unknown before MCS. In this case, increasing the number of failure samples necessitates an increase in the total number of samples in MCS. One possible way to improve the resolution is, therefore, to increase the total number of samples in MCS at the expense of computational time. Alternatively, advanced MCS methods can be employed to improve efficiency and resolution at small failure probability levels. Subset simulation (Au and Beck 2001, 2003; Au et al. 2009, 2010) is used in this chapter to calculate the failure probability and generate failure samples efficiently for the probabilistic failure analysis.

8.3 Subset Simulation

Subset simulation is an adaptive stochastic simulation procedure for efficiently generating failure samples and computing small tail probability (Au and Beck 2001, 2003). It expresses a small probability event as a sequence of intermediate events $\{F_1, F_2, \ldots, F_m\}$ with larger conditional probability and employs specially designed Markov Chains to generate conditional samples of these intermediate events until the final target failure region is achieved, as discussed in Sect. 7.3 in Chap. 7. "Subset simulation". For the slope stability problem, factor of safety (FS) is the critical response, and the probability of FS smaller than a given value "fs" (i.e., $P(FS<fs)$) is of interest.

Subset simulation provides much more failure samples than direct MCS under the same total number of samples, especially when the failure probability is relatively small. When compared with failure samples generated in direct MCS where each sample carries equal weight in the calculation of P_f and $P(\theta|F)$, the samples generated by subset simulation are conditional samples and carry different weights for different intermediate events F_m. Thus, when using these conditional failure samples collected from subset simulation to construct the conditional PDF $P(\theta|F)$ required in Eq. (8.3), a weighted summation by the total probability theorem (e.g., Au 2005; Ang and Tang 2007) is necessary, which is described in the following subsection.

8.3.1 *Estimation of* $\mathbf{P(\theta|F)}$ *Based on Conditional Failure Samples*

Consider a subset simulation that performs $m + 1$ levels of simulations. The first level of subset simulation is direct MCS, and samples of the next level are generated conditional on the samples collected from the previous level. The intermediate threshold values $\{fs_i,\ i = 1, 2, \ldots, m\}$ divide the sample space Ω of an uncertain parameter θ into m individual sets $\{\Omega_i, i = 0, 1, 2, \ldots, m\}$ (see Sect. 7.3 in

Chap. 7 "subset simulation"). According to the total probability theorem (e.g., Ang and Tang 2007), the failure probability can be written as

$$P_f = \sum_{i=0}^{m} P(F|\Omega_i)P(\Omega_i) \tag{8.4}$$

where $\Omega_0 = \{FS \geq fs_1\}$; Ω_i, $i = 1, \ldots, m-1$ is equal to $F_i - F_{i+1}$ (i.e., $\Omega_i = \{fs_{i+1} \leq FS < fs_i\}$); Ω_m is equal to F_m (i.e., $\Omega_m = \{FS < fs_m\}$); $P(F|\Omega_i)$ is the conditional failure probability given sampling in Ω_i; and $P(\Omega_i)$ is the probability of the event Ω_i. $P(F|\Omega_i)$ is estimated as the fraction of the failure samples in Ω_i. The failure samples are collected from samples generated by subset simulation and are based on the performance failure criteria (i.e., $FS < 1$ for a slope stability problem). $P(\Omega_i)$ is calculated as

$$\begin{aligned} P(\Omega_0) &= 1 - p_0 \\ P(\Omega_i) &= p_0^i - p_0^{i+1}, i = 1, \ldots, m-1 \\ P(\Omega_m) &= p_0^m \end{aligned} \tag{8.5}$$

Note that $P(\Omega_i \cap \Omega_j) = 0$ for $i \neq j$ and $\sum_{i=0}^{m} P(\Omega_i) = 1$. When P_f, $P(F|\Omega_i)$, and $P(\Omega_i)$ are obtained, the conditional probability $P(\Omega_i|F)$ is calculated using the Bayes' theorem

$$P(\Omega_i|F) = P(F|\Omega_i)P(\Omega_i)/P_f \tag{8.6}$$

Then, the conditional PDF $P(\theta|F)$ of an uncertain parameter θ is given by the total probability theorem as

$$P(\theta|F) = \sum_{i=0}^{m} P(\theta|\Omega_i \cap F)P(\Omega_i|F) \tag{8.7}$$

where $P(\theta|\Omega_i \cap F)$ is the conditional probability of θ estimated from failure samples that lie in Ω_i. In this chapter, $P(\theta|\Omega_i \cap F)$ is estimated from the failure sample histogram in Ω_i. The number of bins k_{Bin} in the failure sample histogram is estimated as (Sturges 1926)

$$k_{Bin} = 1 + \log_2^{n_i} \tag{8.8}$$

where n_i is the number of the failure samples in Ω_i. Using Eqs. (8.4) and (8.7), P_f and $P(\theta|F)$ can be, respectively, calculated from the samples generated by subset simulation, and subsequently $P(F|\theta)$ is calculated using Eq. (8.3) accordingly.

The probabilistic failure analysis approach proposed in this chapter requires failure samples as input. The software package of probabilistic slope stability analysis developed in the previous chapter is readily used to generate failure samples for the probabilistic failure analysis of slope stability in this chapter.

8.4 The James Bay Dyke Case History

As an illustration, the probabilistic failure analysis approach is applied to analyze a design scenario of the James Bay Dyke. The James Bay Dyke is a 50-km-long earth dyke of the James Bay hydroelectric project in Canada. Soil properties and various design scenarios of the dyke were studied by Ladd et al. (1983), Soulié et al. (1990), Christian et al. (1994), El-Ramly (2001), El-Ramly et al. (2002), and Xu and Low (2006). As shown in Fig. 8.1, the embankment is 12.0 m high with a 56.0-m-wide berm at mid-height. The slope angle of the embankment is about 18.4° (3H:1V). The embankment is overlying on a clay crust with a thickness T_{cr}. The clay crust is underlain by a layer of 8.0-m-thick sensitive marine clay and a layer of lacustrine clay with a thickness T_L. The undrained shear strength (i.e., S_{uM} and S_{uL}) of the marine clay and the lacustrine clay were measured by field vane tests (Ladd et al. 1983; Soulié et al. 1990; Christian et al. 1994; El-Ramly 2001). The lacustrine clay is overlying on a stiff till layer, and the depth to the top of the stiff till layer is D_{Till}.

Six uncertain system parameters have been considered in the literature (e.g., El-Ramly 2001; El-Ramly et al. 2002; and Xu and Low 2006), including the friction angle ϕ_{Fill}, the unit weight γ_{Fill} of the embankment material, the thickness T_{cr} of clay crust, the undrained shear strength S_{uM} of the marine clay, the undrained shear strength S_{uL} of the lacustrine clay, and the depth of the till layer D_{Till}. During the probabilistic failure analysis of the dyke, the six uncertain parameters are represented by six independent Gaussian random variables (El-Ramly 2001), respectively. Table 8.1 summarizes the statistics (i.e., mean, standard deviation, and coefficient of variation (COV)) of these six random variables. These statistics are used to generate random samples for each random variable in uncertain model worksheet. Note that the thickness of the lacustrine clay T_L is an uncertain variable that depends on T_{cr} and D_{Till} and has a mean of about 6.5 m (see Fig. 8.1). In addition to these uncertain parameters, other system parameters are considered deterministic, including an undrained shear strength of 41 kPa for the clay crust and unit weights of 19, 19, and 20.5 kN/m^3 for the clay crust, marine clay, and lacustrine clay (El-Ramly 2001), respectively.

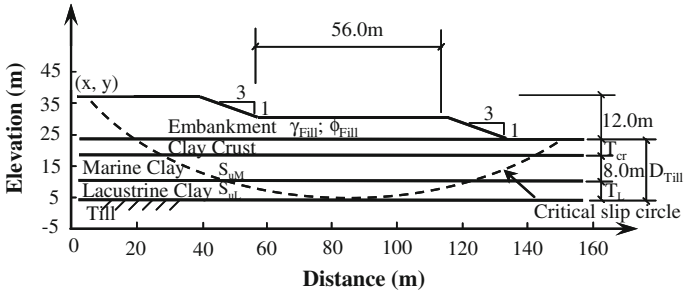

Fig. 8.1 The James Bay Dyke (After El-Ramly 2001; Wang et al. 2010)

Table 8.1 Soil properties of the James Bay Dyke (After El-Ramly 2001; Wang et al. 2010)

Soil layers	Uncertain system parameters[a]	Mean	Standard deviation	Coefficient of variation (%)
Embankment	ϕ_{Fill} (°)	30.0	1.79	6.0
	γ_{Fill} (kN/m^3)	20.0	1.10	5.5
Clay crust	T_{cr} (m)	4.0	0.48	12.0
Marine clay	S_{uM} (kN/m^2)	34.5	3.95	11.5
Lacustrine clay	S_{uL} (kN/m^2)	31.2	6.31	20.2
Till	D_{Till} (m)	18.5	1.00	5.4

[a]All parameters are modeled as Gaussian random variables. Thickness of the lacustrine clay layer T_L is an uncertain variable that depends on T_{cr} and D_{Till} and has a mean of about 6.5 m

Using the soil properties described above, El-Ramly (2001) and Xu and Low (2006) employed direct MCS methods to evaluate failure probability of the dyke together with limit equilibrium methods and response surface method, respectively. To enable a consistent comparison with the analyses by El-Ramly (2001), the critical slip surfaces recommended by El-Ramly (2001) are adopted in this chapter, which are circular and always tangential to top of the till layer and pass through the point (x = 4.9 m, y = 36.0 m). The x-coordinate of the center is fixed at 85.9 m. For each set of random samples, the critical slip surface is specified uniquely by the value of D_{Till}. In this chapter, the safety factor of the critical slip surface is calculated by simplified Bishop method, and two subset simulation runs are performed using the software package developed in the previous chapter. One has the highest simulation level m = 3 and sample number N = 1000 per each level, as opposed to m = 4 and N = 10000 per each level in the other run.

8.4.1 Simulation Results

Figure 8.2 shows a typical cumulative distribution function (CDF) of FS (i.e., $P(FS < fs)$ versus fs) from two subset simulation runs with a total sample number $N_T = 1000 + 3 \cdot 1000 \cdot (1 - 0.1) = 3700$ (i.e., subset simulation Run 1) and $N_T = 10000 + 4 \cdot 10000 \cdot (1 - 0.1) = 46000$ (i.e., subset simulation Run 2), respectively. For comparison, the result from a direct MCS with 20000 samples is also plotted. Three consistent failure probabilities $P(FS < 1) = 0.22$, 0.23, and 0.25 % are estimated from direct MCS and two runs of subset simulations, respectively. In addition, the two runs of subset simulations provide results that are consistent even at low probability levels (e.g., $P(FS < fs) = 0.01$ %) where the CDF curve from direct MCS becomes erratic.

Table 8.2 compares the simulation results with those reported by El-Ramly (2001) and Xu and Low (2006). El-Ramly (2001) performed direct MCS with the simplified Bishop method (i.e., the same limit equilibrium method used in this

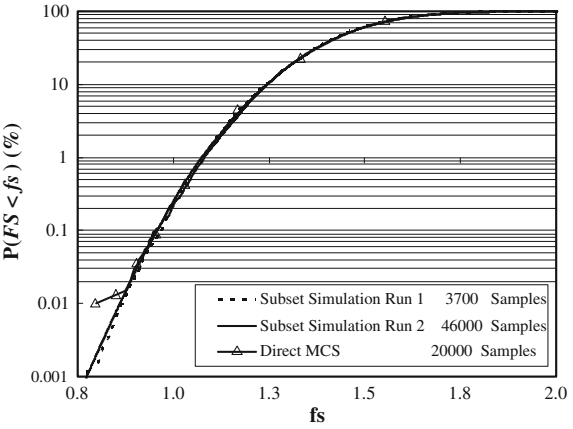

Fig. 8.2 Cumulative distribution function (CDF) from simulations (After Wang et al. 2010)

Table 8.2 Comparison of simulation results (After Wang et al. 2010)

Simulation results	El-Ramly (2001)	Xu and Low (2006)	Direct MCS with Excel	Subset simulation with Excel Run 1	Subset simulation with Excel Run 2
Failure probability P_f (%)	0.24[a]	0.33[b]	0.22[a]	0.23[a]	0.25[a]
Number of failure samples N_F	48	N/A	44	1128	20482
Number of total samples N_T	20000	N/A	20000	3700	46000
Percentage of failure samples N_F/N_T (%)	0.24	N/A	0.22	30.5	44.5

[a] P_f is calculated by MCS methods integrating with the simplified Bishop method
[b] P_f is calculated by MCS methods integrating with the response surface method

chapter) and obtained a $P_f = 0.24$ %. This P_f value is almost identical to the average of the three P_f values obtained in this chapter (i.e., 0.22, 0.23, and 0.25 % in Column 4–6 of Table 8.2). In addition, Xu and Low (2006) combined MCS with response surface method to estimate the P_f of the James Bay Dyke and obtained a P_f value of 0.33 %. Although different deterministic slope stability analysis methods were used, the obtained P_f values compare favorably with each other. This implies that the probabilistic analysis models for the James Bay Dyke presented in this chapter work properly.

Table 8.2 also compares the number of failure samples in direct MCS (e.g., Column 2 or 4) with that in subset simulations (e.g., Column 5 or 6). For a total sample number $N_T = 20000$, direct MCS leads to only 48 or 44 failure samples. In

contrast, subset simulations with $m = 3$ and $N_T = 3700$ (i.e., Run 1 in Column 5) or $m = 4$ and $N_T = 46000$ (i.e., Run 2 in Column 6) result in a failure sample number of 1128 and 20482, respectively. This comparison clearly shows that subset simulations significantly improve the efficiency of generating failure samples, which enables generation of a large number of failure samples with relative ease and makes the probabilistic failure analysis feasible. Table 8.2 also shows that as the value of m increases (e.g., from 3 in Column 5−4 in Column 6), the efficiency increases as well (e.g., the percentage of failure sample increases from 30.5 to 44.5 %).

8.5 Probabilistic Failure Analysis Results

With the large number of failure samples generated from subset simulations, probabilistic failure analysis are performed for the James Bay Dyke, including hypothesis tests for identifying key uncertainties that have significant effects on slope failure probability and Bayesian analysis for further quantifying their effects.

8.5.1 Hypothesis Test Results

Based on the failure samples generated from subset simulation Run 1, the hypothesis test statistics Z_H defined by Eq. (8.2) are calculated and shown in Fig. 8.3 for all uncertain parameters. The absolute values of Z_H varies from less than 2 for the thickness of clay crust T_{cr} to about 95 for undrained shear strength of the lacustrine clay S_{uL}. The decreasing order of the Z_H absolute values is S_{uL}, D_{Till},

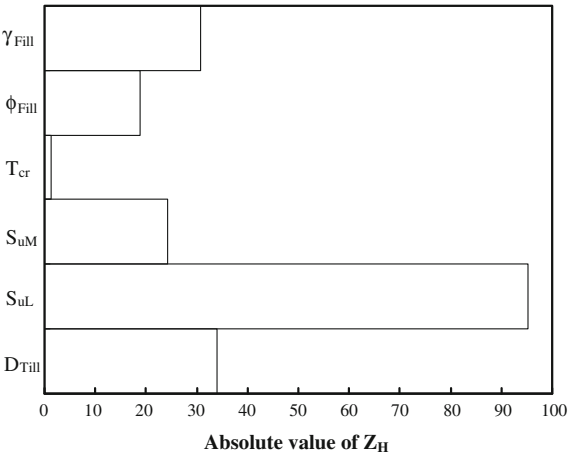

Fig. 8.3 Summary of absolute values of Z_H (After Wang et al. 2010)

γ_{Fill}, S_{uM}, ϕ_{Fill}, and T_{cr}. This implies that the uncertainty of S_{uL} has the most significant effects on the slope failure probability, while the uncertainty of T_{cr} contributes the least to the failure probability. This result is consistent with that reported by El-Ramly (2001) who employed an Excel spreadsheet-based MCS program @RISK (Palisade Corporation 2010) and compared the spearman's rank correlation coefficients for various uncertain parameters. El-Ramly (2001) showed that S_{uL} and T_{cr} are the most and least influential parameters, respectively. The results can be validated by an independent sensitivity studies on S_{uL} and T_{cr}, which are described in next subsection.

8.5.2 Validation of Hypothesis Test Results

Sensitivity studies are performed to further explore the effect of S_{uL} and T_{cr} uncertainties on slope failure probability. The respective values of the coefficient of variation (COV) of S_{uL} and T_{cr} vary from 0.15 to 0.50 and from 0.05 to 0.25 in the sensitivity studies. The range of S_{uL} COV adopted in this chapter follows the typical range of COV of undrained shear strength of clay measured by vane shear tests (Phoon and Kulhawy 1999), and the COV of T_{cr} varies from half to about twice of the value reported by El-Ramly (2001). Other parameters (including the mean values of S_{uL} and T_{cr}) remain unchanged in the sensitivity studies. About 40 additional subset simulation runs are performed to validate the hypothesis test results, and their results are shown in Fig. 8.4a, b for T_{cr} and S_{uL}, respectively. In addition, sensitivity studies on COVs of T_{cr} and S_{uL} are also carried out using the Excel spreadsheet-based MCS program @RISK (Palisade Corporation 2010) and a first-order reliability method (FORM) calculation spreadsheet developed by Low and his coworkers (Low and Tang 1997; Low et al. 1998; Low 2003; Low and Tang 2007). Figure 8.4 also includes the results from @RISK and FORM for comparison.

Figure 8.4a shows that when the COV of T_{cr} varies from 0.05 to 0.25, the slope failure probability fluctuates between 0.19 % and 0.43 %. For comparison, the baseline failure probability (i.e., about 0.24 % corresponding to the values summarized in Table 8.2) is also included in the figure. The failure probabilities from sensitivity study using subset simulations fall around the horizontal line of 0.24 %, and the failure probability is insensitive to the uncertainty on T_{cr}. The results from subset simulations are in good agreement with those from @RISK and FORM. This validates the results from hypothesis tests that the T_{cr} uncertainty has the least effect on the failure probability. It is interesting to note that the probability of slope failure should, theoretically, increase as the COV of T_{cr} increases from 0.05 to 0.25, as shown by the FORM results (i.e., a rather slight increase of the P_f values shown by the open circles in Fig. 8.4a when the COV of T_{cr} increases from 0.05 to 0.25). The effect is, however, so minimal that it is dominated by the MCS "noise" (i.e., the random fluctuations of the P_f values obtained from subset simulations and @RISK).

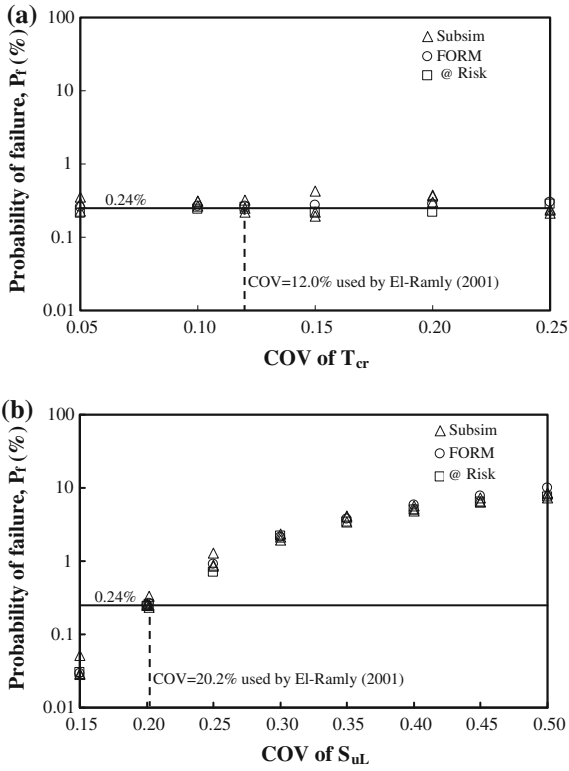

Fig. 8.4 Effects of coefficient of variation (COV) for different system parameters (After Wang et al. 2010), **a** Thickness of clay crust, T_{cr}, **b** Undrained shear strength of the lacustrine clay, S_{uL}

On the other hand, Fig. 8.4b shows that the slope failure probability increases as the COV of S_{uL} increases. The results from subset simulations are in good agreement with those from @RISK and FORM. When the COV of S_{uL} is 0.15, the probability is less than 0.1 %. When the COV of S_{uL} increases to 0.50, the slope failure probability increases by two orders of magnitude (i.e., increases to about 10 %). The failure probability varies significantly with the change of the S_{uL} COV. This agrees well with the results from hypothesis tests that the uncertainty of S_{uL} has significant effects on the slope failure probability. Such agreement further validates that the hypothesis test procedure proposed in this chapter prioritizes the effects of various uncertainties on failure probability properly.

8.5.3 Bayesian Analysis Results

Based on the failure samples generated from subset simulation Run 2, a Bayesian analysis is performed using Eqs. (8.3), (8.6), and (8.7) accordingly. Figure 8.5 shows the Bayesian analysis results by open circles for S_u and D_{Till}, which have been identified from the hypothesis tests (see Sect. 8.5.1 "Hypothesis Test

Results") as the two most influential uncertain parameters. Note that the conditional probability (i.e., $P(F|S_{uL})$ in Fig. 8.5a and $P(F|D_{\text{Till}})$ in Fig. 8.5b) obtained from the Bayesian analysis is a variation of failure probability as a function of S_{uL} or D_{Till}. Figure 8.5a shows that as S_{uL} increases from 12 to 24 kPa, the slope failure probability decreases from more than 10 % to less than 0.1 %. Similarly, Fig. 8.5b shows that as D_{Till} increases from about 18 to 23 m, the slope failure probability increases from about 0.1 % to about 10 %. It is obvious that the values of S_{uL} and D_{Till} have significant effects on slope failure probability, and such effects can be quantified explicitly from the Bayesian analysis of failure samples.

8.5.4 Validation of Bayesian Analysis Results

Note that the variations of failure probability as a function of S_{uL} or D_{Till} shown in Fig. 8.5 can also be obtained from sensitivity studies on S_{uL} or D_{Till}, which frequently include many repeated runs of MCS with different given values of S_{uL} or D_{Till} in each run. Therefore, to validate the Bayesian analysis results, about 40

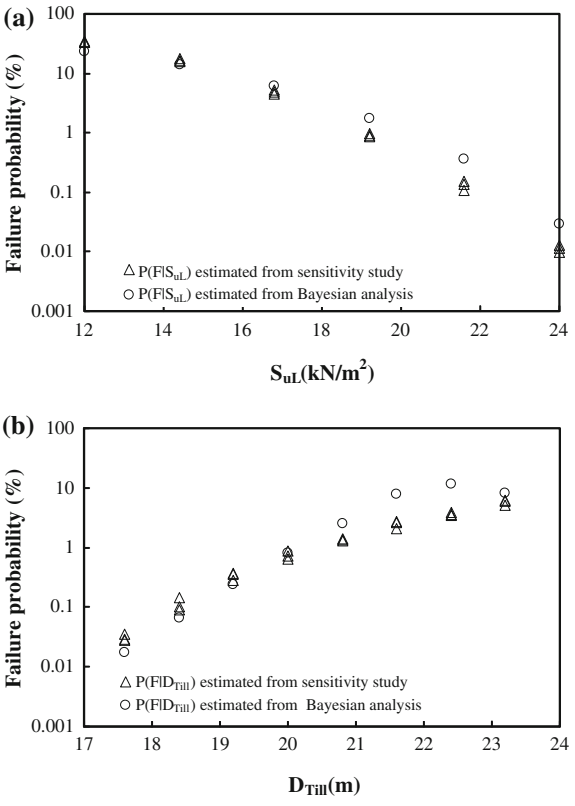

Fig. 8.5 Bayesian analysis results for different system parameters θ (After Wang et al. 2010), **a** θ = undrained shear strength of the lacustrine clay, S_{uL}, **b** θ = depth of the till layer, D_{Till}

additional subset simulation runs are performed with different given values of S_{uL} or D_{Till} in each run. Figure 8.5 also includes the results from these additional sensitivity runs by open triangles. The open triangles follow trends similar to the open circles (i.e., the Bayesian analysis results) and plot closely to the open circles as well. This validates that a Bayesian analysis of failure samples generated in MCS or subset simulations provides results equivalent to those from additional sensitivity

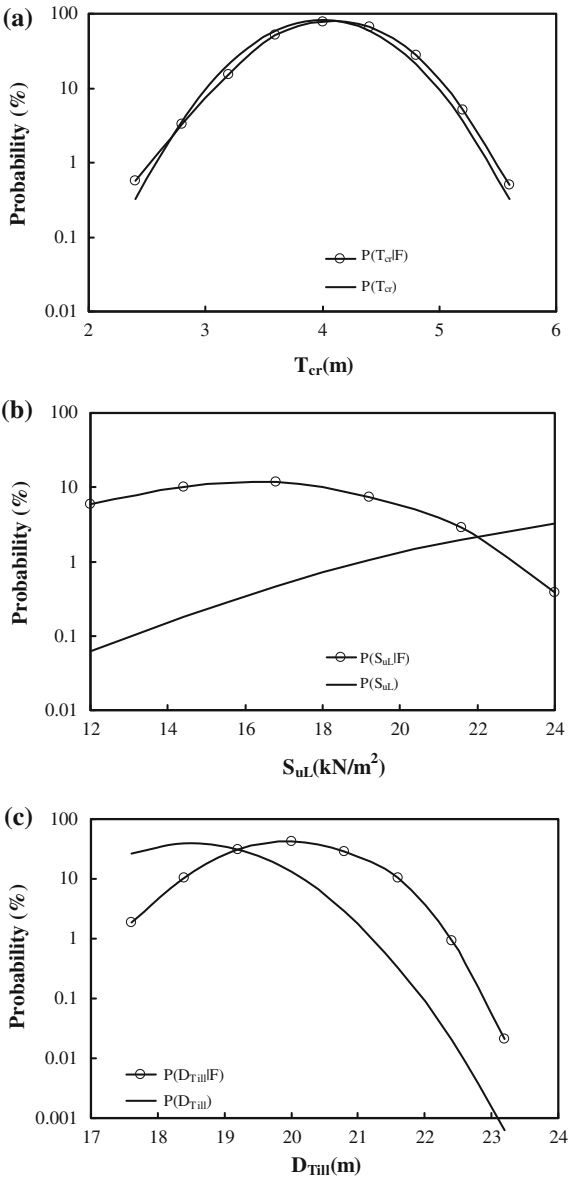

Fig. 8.6 Conditional probability density function (PDF) ($P(\theta|F)$) for different system parameters θ (After Wang et al. 2010), **a** θ = thickness of clay crust, T_{cr}, **b** θ = undrained shear strength of the lacustrine clay, S_{uL}, **c** θ = depth of the till layer, D_{Till}

studies. In addition, the Bayesian analysis has the advantage of avoiding additional computational time and efforts for repeated runs of MCS or subset simulations in the sensitivity studies.

As mentioned before, Eq. (8.3) implies that comparison between the conditional probability $P(\theta|F)$ and its unconditional one $P(\theta)$ provides an indication of the effect of the uncertain parameter θ on failure probability. This offers a means to check the Bayesian analysis results with those from hypothesis tests. Figure 8.6 compares the conditional probabilities (i.e., $P(T_{cr}|F)$, $P(S_{uL}|F)$, and $P(D_{\text{Till}}|F)$) of T_{cr}, S_{uL}, and D_{Till} and their unconditional ones (i.e., $P(T_{cr})$, $P(S_{uL})$, and $P(D_{\text{Till}})$). Figure 8.6a shows that $P(T_{cr}|F)$ and $P(T_{cr})$ are almost identical for different T_{cr} values, which is consistent with the hypothesis test results that T_{cr} has the least effect on failure probability. In contrast, the hypothesis tests show that S_{uL} and D_{Till} are the two most influential uncertain parameters. Figure 8.6b, c show that $P(S_{uL}|F)$ and $P(D_{\text{Till}}|F)$ differ significantly from their respective unconditional one (i.e., $P(S_{uL})$ and $P(D_{\text{Till}})$). The Bayesian analysis results agree well with the hypothesis test results.

8.6 Summary and Conclusions

This chapter developed a probabilistic failure analysis approach that makes use of failure samples generated in the MCS and analyzes these failure samples to assess the effects of various uncertainties on slope failure probability. The approach contains two major components: hypothesis tests for prioritizing the effects of various uncertainties and Bayesian analysis for further quantifying their effects.

A hypothesis test statistic Z_H was formulated to evaluate the statistical difference of failure samples with their respective nominal (unconditional) samples. As the absolute value of Z_H increases, the statistical difference between failure samples and their respective nominal samples becomes growingly significant, and the effect of the uncertain parameter on failure probability also becomes growingly significant. Therefore, the absolute value of Z_H is used as an index to measure the effects of the uncertain parameters on failure probability and to prioritize their relative effects on failure probability.

A Bayesian analysis approach was developed to further quantify the effects of the uncertain parameters that have been identified from the hypothesis tests as influential parameters. Equations were derived for estimating conditional PDF (i.e., $P(F|\theta)$) of slope failure for a given value of uncertain parameter θ. Because $P(F|\theta)$ is a variation of failure probability as a function of θ, it can be considered as results of a sensitivity study of θ on slope failure probability. In other words, a Bayesian analysis of the failure samples provides results that are equivalent to those from additional sensitivity studies. In addition, it has the advantage of avoiding additional computational time and efforts for repeated runs of MCS or subset simulations in the sensitivity studies. Furthermore, it was shown that comparison between the conditional probability $P(\theta|F)$ and its unconditional one $P(\theta)$ provides an

indication of the effect of the uncertain parameter θ on failure probability. This offers a means to check the Bayesian analysis results with those from hypothesis tests.

The resolution of P_f and $P(\theta|F)$ is pivotal to obtain $P(F|\theta)$, and it depends on the number of failure samples generated in MCS. An advanced Monte Carlo simulation called "subset simulation" that has been implemented in Excel spreadsheet environment in the previous chapter was employed to improve efficiency of generating failure samples in MCS and resolution at small failure probability levels.

As an illustration, the proposed probabilistic failure analysis approach was applied to study a design scenario of the James Bay Dyke. The hypothesis tests show that the uncertainty of S_{uL} has the most significant effect on the slope failure probability, while the uncertainty of T_{cr} contributes the least to the failure probability. The hypothesis test results are very consistent with results from independent sensitivity studies. Such agreement validates that the hypothesis test procedure proposed in this chapter properly prioritizes the effects of various uncertainties on failure probability.

A Bayesian analysis was performed to quantify explicitly the effects of S_{uL} and D_{Till}, which have been identified from the hypothesis tests as the two most influential uncertain parameters. It is shown that the slope failure probability changes significantly as the values of S_{uL} and D_{Till} change. The Bayesian analysis results have also been validated against those from independent sensitivity studies. In addition, a cross-check between the hypothesis test results and the Bayesian analysis results shows that they agree well with each other.

It is worthwhile to note that although the proposed approach was developed together with a slope stability analysis problem, the approach is general and applicable for other types of geotechnical analyses and engineering problems.

References

Ang, A.H.S., and W.H. Tang. 2007. *Probability concepts in engineering: Emphasis on applications to civil and environmental engineering*. New York: John Wiley and Sons.

Au, S.K. 2005. Reliability-based design sensitivity by efficient simulation. *Computers & Structures* 83(14): 1048–1061.

Au, S.K., and J.L. Beck. 2001. Estimation of small failure probabilities in high dimensions by subset simulation. *Probabilistic Engineering Mechanics* 16(4): 263–277.

Au, S.K., and J.L. Beck. 2003. Subset simulation and its applications to seismic risk based on dynamic analysis. *Journal of Engineering Mechanics* 129(8): 1–17.

Au, S.K., Y. Wang, and Z. Cao. 2009. Reliability analysis of slope stability by advanced simulation with spreadsheet. In *Proceedings of the Second International Symposium on Geotechnical Safety and Risk*. Gifu, Japan, June 2009. pp. 275–280.

Au, S.K., Z. Cao, and Y. Wang. 2010. Implementing advanced Monte Carlo simulation under spreadsheet environment. *Structural Safety* 32(5): 281–292.

Baecher, G.B., and J.T. Christian. 2003. *Reliability and statistics in geotechnical engineering*. Hoboken, New Jersey: John Wiley & Sons. 605p.

Christian, J.T., C.C. Ladd, and G.B. Baecher. 1994. Reliability applied to slope stability analysis. *Journal of Geotechnical Engineering* 120(12): 2180–2207.

El-Ramly, H. 2001. Probabilistic analysis of landslide hazards and risks bridging theory and practice. Ph.D. thesis, University of Alberta, Canada.

El-Ramly, H., N.R. Morgenstern, and D.M. Cruden. 2002. Probabilistic slope stability analysis for practice. *Canadian Geotechnical Journal* 39: 665–683.

Gilbert, R.B., S.G. Wright, and E. Liedtke. 1998. Uncertainty in back-analysis of slopes: Kettleman Hills case history. *Journal of Geotechnical and Geoenvironmental Engineering* 124 (12): 1167–1176.

Ladd, C.C., O. Dascal, K.T. Law, G. Lefebrve, G. Lessard, G. Mesri, and F. Tavenas. 1983. In *Report of the subcommittee on embankment stability—annex II*. Committee of Specialists on Sensitive Clays on the NBR Complex. Société d'Energie de la BaieJames, Montréal, Que.

Low, B.K. (2003). Practical probabilistic slope stability analysis. In *Proceeding of 12th Panamerican Conference on Soil Mechanics and Geotechnical Engineering and 39th U.S. Rock Mechanics Symposium*. M.I.T., Cambridge, Massachusetts. Verlag Gluckauf Gmbh Essen, 2003. pp. 2777−2784.

Low, B.K., and W.H. Tang. 1997. Reliability analysis of reinforced embankments on soft ground. *Canadian Geotechnical Journal* 34(5): 672–685.

Low, B.K., and W.H. Tang. 2007. Efficient spreadsheet algorithm for first-order reliability method. *Journal of Engineering Mechanics* 133(2): 1378–1387.

Low, B.K., R.B. Gilbert, and S.G. Wright. 1998. Slope reliability analysis using generalized method of slices. *Journal of Geotechnical and Geoenvironmental Engineering* 124(4): 350–362.

Luckman, P.G., K.A. Der, and N. Sitar. 1987. Use of stochastic stability analysis for Bayesian back calculation of pore pressures acting in a cut at failure. In *Proceeding of 5th International Conference on Application of Statistics and Probability in Soil and Structure Engineering.* Vancouver, Canada: University of British Columbia.

Palisade Corporation. 2010. @Risk and the Decision Tools Suite Version 5.5.1. http://www.palisade.com.

Phoon, K.K., and F.H. Kulhawy. 1999. Evaluation of geotechnical property variability. *Canadian Geotechnical Journal* 36(4): 625–639.

Soulié, M., P. Montes, and V. Silvestri. 1990. Modeling spatial variability of soil parameters. *Canadian Geotechnical Journal* 27: 617–630.

Sturges, H. 1926. The choice of a class-interval. *Journal of American Statistical Association* 21: 65–66.

Walpole, R.E., R.H. Myers, and S.L. Myers. 1998. *Probability and Statistics for Engineers and Scientists*. Upper Saddle River, New Jersey: Prentice Hall.

Wang, Y., Z. Cao, and S.K. Au. 2010. Efficient Monte Carlo Simulation of parameter sensitivity in probabilistic slope stability analysis. *Computers and Geotechnics* 37(7–8): 1015–1022.

Xu, B., and B.K. Low. 2006. Probabilistic stability analyses of embankments based on finite-element method. *Journal of Geotechnical and Geoenvironmental Engineering* 132(11): 1444–1454.

Zhang, J., W.H. Tang, and L.M. Zhang. 2010. Efficient probabilistic back-analysis of slope stability model parameters. *Journal of Geotechnical and Geoenvironmental Engineering* 136 (1): 99–109.

Chapter 9
Summary and Concluding Remarks

9.1 Introduction

The previous chapters have developed several probabilistic approaches for geotechnical site characterization and slope stability analysis, including a general Bayesian framework for geotechnical site characterization, a subjective probability assessment approach for determining prior distribution, an equivalent sample approach using limited site observation data, a Bayesian approach using a relatively large number of test data, a probabilistic slope stability analysis approach, and a probabilistic failure analysis approach. This chapter summarizes the major conclusions drawn from previous chapters and provides some recommendations for future studies.

9.2 Uncertainty Propagation During Geotechnical Site Characterization

This book revisited geotechnical site characterization from an uncertainty propagation point of view. Geotechnical site characterization was divided into six stages as follows: desk study, site reconnaissance, in situ investigation, laboratory testing, interpretation of site observation data, and inferring soil properties and underground stratigraphy. Desk study and site reconnaissance provide prior knowledge (i.e., site information available prior to the project) about the site. The prior knowledge is not perfect information but is combined with some uncertainties, such as inherent spatial variability and measurement errors in existing data and uncertainties in engineers' expertise. Then, project-specific test data can be obtained from in situ investigation work and laboratory testing but it fluctuates because of inherent spatial variability of soils, statistical uncertainty, and measurement errors. These uncertainties together with the transformation uncertainty are incorporated into the

Z. Cao et al., *Probabilistic Approaches for Geotechnical Site Characterization and Slope Stability Analysis*, DOI 10.1007/978-3-662-52914-0_9

interpretation outcomes obtained from site observation data using a transformation model. Geotechnical engineers use both interpretation outcomes of site observation data and prior knowledge to estimate soil properties and underground stratigraphy for geotechnical analysis and/or designs. Estimations of soil properties and underground stratigraphy are, therefore, affected by both uncertainties in prior knowledge and uncertainties (i.e., inherent spatial variability of soils, statistical uncertainty, measurement errors, and transformation uncertainty) in interpretation outcomes of project-specific test data. These uncertainties are taken into account rationally by the Bayesian framework developed in this book, as discussed in the next section.

9.3 Bayesian Framework for Geotechnical Site Characterization

A Bayesian framework was developed for geotechnical site characterization, which integrates systematically prior knowledge and site observation data to characterize probabilistically soil properties and boundaries of statistically homogenous soil layers. The Bayesian framework addresses directly the inherent spatial variability of the design soil property and models explicitly the transformation uncertainty associated with the transformation model. In addition, statistical uncertainty and measurement errors are incorporated into the Bayesian framework through site observation data. Based on the Bayesian framework, the most probable number of statistically homogenous soil layers is then determined through a Bayesian model class selection method. It is also noted that the Bayesian framework provides a rational vehicle to accumulate the knowledge of soil properties progressively as the site observation data increase.

The proposed Bayesian framework is general and equally applicable for different types of prior knowledge and different numbers of site observation data. It was applied to combine prior knowledge and sparse standard penetration test (SPT) data for probabilistic characterization of Young's modulus and to integrate prior knowledge with a relatively large number of cone penetration test (CPT) data for probabilistic characterization of effective friction angle, as discussed in Sects. 9.5 and 9.6, respectively.

9.4 Prior Knowledge and Prior Distribution

Under the Bayesian framework, the information provided by prior knowledge is quantitatively reflected by prior distribution in a probabilistic manner. As mentioned above, the Bayesian framework is equally applicable for different types of prior knowledge. When only a typical range of the soil parameter concerned is

available as prior knowledge, a uniform prior distribution of the soil parameter that covers the typical range can be used in the Bayesian framework. As the information provided by prior knowledge improves, a more sophisticated and informative prior distribution can be estimated from the prior knowledge.

Based on a stage cognitive model of engineers' cognitive process, a subjective probability assessment approach was developed to estimate prior distribution from prior knowledge. The subjective probability assessment approach assists engineers in utilizing prior knowledge in a relatively rational way and expressing quantitatively their engineering judgments in a probabilistic manner. The assessment outcomes obtained from the proposed approach are then taken as the prior distribution in the Bayesian framework. The proposed subjective probability assessment approach consists of five steps as follows: specification of assessment objectives, collection of relevant information and preliminary estimation, synthesis of the evidence, numerical assignment, and confirmation of assessment outcomes. Several suggestions were provided for each step to assist engineers in reducing the effects of cognitive biases and limitations during subjective probability assessment.

The proposed subjective probability assessment approach was illustrated under two scenarios as follows: one with sparse prior knowledge and the other with a reasonable amount of prior knowledge. When prior knowledge is sparse, the prior distribution obtained from the proposed approach is relatively uninformative (e.g., uniform distributions). As the information provided by prior knowledge improves, the proposed approach provides informative prior distribution. The prior distribution obtained from the subjective probability assessment approach quantifies properly the information provided by prior knowledge and is readily used in the Bayesian framework.

9.5 Probabilistic Characterization of Young's Modulus Using SPT

The number of project-specific test results is generally too sparse to generate meaningful statistics (i.e., mean, standard deviation, and other high order statistics) of soil properties, particularly in projects with medium or relatively small sizes. For this case, a Markov Chain Monte Carlo simulation (MCMCS)-based approach (i.e., the equivalent sample approach) was developed for probabilistic characterization of soil properties. The proposed approach is equally applicable for various soil properties and different types of in situ or laboratory tests. As an illustration, the proposed approach was formulated for probabilistic characterization of the undrained Young's modulus E_u using SPT. Project-specific SPT data and prior knowledge are integrated probabilistically under the Bayesian framework developed in this book and are transformed into a large number, as many as needed, of equivalent samples of E_u. Then, conventional statistical analysis is carried out to estimate statistics of E_u. This allows a proper selection of characteristic value of the

soil property in implementation of probabilistic design codes (e.g., Eurocode 7) and reliability analysis in geotechnical engineering practice. The equivalent sample approach effectively tackles the difficulty in generating meaningful statistics from the usually limited number of soil property data obtained during geotechnical site characterization.

Equations were derived for the proposed equivalent sample approach, and the proposed approach was illustrated and validated using real SPT data and simulated SPT data. It has been shown that based on the limited SPT data and relatively uninformative prior knowledge (i.e., reasonable ranges of soil parameters reported in the literature), the equivalent sample approach provides reasonable estimates of statistics and probability distribution of E_u. Such probabilistic characterization is used to require a large number of data from laboratory and/or in situ tests (e.g., pressure meter tests), which of course involve significant commitment of cost, man power, and time.

It is also noted that results of the equivalent sample approach are affected by both the number of project-specific test results and prior knowledge. When only limited project-specific test data is available, the equivalent sample approach improves significantly the probabilistic characterization of soil properties and reduces the effects of statistical uncertainty by incorporating reasonable ranges of soil parameters as prior knowledge. As the number of project-specific test data increases, the standard deviation of soil properties estimated from the equivalent sample approach gradually approaches its true value and mainly reflects the inherent variability itself. The proposed approach is general and applicable for different types of prior knowledge, although using relatively informative and consistent prior knowledge does improve the probabilistic characterization of soil properties.

9.6 Probabilistic Site Characterization Using CPT

When a large number of site observation data can be obtained directly from project-specific tests (e.g., near-continuous measurements during a cone penetration test (CPT)), the inherent spatial variability of soil properties can be explicitly modeled using the random field theory. In such a case, a Bayesian approach was proposed for probabilistic site characterization using the Bayesian framework developed in this book and the random field theory. The proposed Bayesian approach was formulated for probabilistic characterization of effective friction angle ϕ' using CPT. Project-specific CPT data and prior knowledge are integrated probabilistically under the Bayesian framework. The Bayesian approach addresses explicitly the inherent spatial variability of ϕ' using random field theory. It contains two major components as follows: a Bayesian model class selection method to identify the most probable number of soil layers and a Bayesian system

identification method to estimate the most probable layer thicknesses/boundaries and soil properties simultaneously.

Equations were derived for the Bayesian approach, and the proposed approach was illustrated and validated using real CPT data and simulated CPT data. It has been shown that the proposed Bayesian approach correctly identifies the number and thicknesses/boundaries of the statistically homogenous soil layers and provides proper probabilistic characterization of soil properties. In addition, as the number of model classes increases, the Bayesian model class selection method identifies the statistically homogenous layers progressively, starting from the most statistically significant boundary and gradually "zooming" into local difference with improved "resolution". The Bayesian approach also contains a mechanism to determine when to stop further increasing the number of model class (i.e., the "zooming").

Furthermore, it is also found that results of the Bayesian approach are affected by the quality of both prior knowledge and project-specific test data. It is always prudent to rely more on the high quality project-specific test data, if available, and to start the Bayesian approach with relatively uninformative prior knowledge (i.e., low confidence level), particularly when the prior knowledge is not well justified.

9.7 Probabilistic Slope Stability Analysis

Inherent spatial variability of soils and various uncertainties arising during geotechnical site characterization affect probabilistic estimations of soil properties and underground stratigraphy, which subsequently influence probabilistic analysis and/or designs of geotechnical structures, such as probabilistic slope stability analysis. Monte Carlo simulation (MCS) provides a robust and conceptually simple way to account rationally for these uncertainties (including inherent spatial variability of soils).

A MCS-based probabilistic slope stability analysis approach was developed using an advanced MCS method called "subset simulation" in a commonly available spreadsheet environment, Microsoft Excel, with the aid of Visual Basic for Application (VBA). Excel worksheets and VBA functions/Add-In for deterministic slope stability analysis are deliberately decoupled from those for reliability analysis (e.g., random sample generations and statistical analysis) so that the reliability analysis can proceed as an extension of deterministic analysis in a non-intrusive manner. The Excel spreadsheet package was used to assess reliability of short-term stability of a cohesive soil slope, followed by a comparative study on different reliability methods, including the first-order second-moment method (FOSM), first-order reliability method (FORM), direct MCS using commercial software Slope/W, and direct MCS and subset simulation using the Excel package.

It has been shown that the MCS-based probabilistic slope stability analysis approach significantly improves the efficiency and resolution at relatively small probability levels. With the aid of improved efficiency, the MCS-based probabilistic slope stability analysis approach was used to explore the effects of inherent spatial

variability of soil properties and the critical slip surface uncertainty. It is found that when the inherent spatial variability of soil properties is ignored by assuming perfect correlation, the variance of factor of safety (*FS*) is overestimated. Such overestimation of the *FS* variance may result in either overestimation (conservative) or underestimation (unconservative) of slope failure probability P_f. It is also noted that when the inherent spatial variability of soil properties is considered, the critical slip surface varies spatially. Using only one given critical slip surface significantly underestimates P_f, and it is unconservative. Thus, when the inherent spatial variability of soil properties is considered, the critical slip surface uncertainty should be properly accounted for.

9.8 Probabilistic Failure Analysis of Slope Stability

Based on failure samples generated in MCS, a probabilistic failure analysis approach was developed to shed light on relative contributions of various uncertainties to slope failure probability. The probabilistic failure analysis approach contains two major components as follows: hypothesis tests for prioritizing effects of various uncertainties and Bayesian analysis for further quantifying their effects.

A hypothesis test statistic was formulated to evaluate the statistical difference between failure samples and their respective nominal (unconditional) samples. The absolute value of the hypothesis test statistic is used as an index to measure the effects of the uncertain parameters on failure probability and to prioritize their relative effects on failure probability. A Bayesian analysis approach was developed to further quantify effects of the uncertain parameters that have been identified from the hypothesis tests as influential parameters. Equations were derived for the Bayesian analysis to estimate conditional failure probability of slope stability for a given value of an uncertain parameter. The resolution of the conditional failure probability obtained from the Bayesian analysis relies on the number of failure samples generated in MCS. Subset simulation was employed to improve efficiency of generating failure samples in MCS and resolution at small failure probability levels.

The probabilistic failure analysis approach was illustrated through a case study, and it was validated by independent sensitivity studies using repeated runs of MCS. It has been shown that the effects of various uncertainties on slope failure probability are properly prioritized and quantified by the proposed approach. The proposed failure analysis approach gives results equivalent to those from sensitivity studies, and hence, saves additional computational time and efforts for sensitivity studies. In addition, a cross-check between the hypothesis test results and the Bayesian analysis results showed that they agree well with each other.